

**THE DESIGN OF UNSURFACED ROADS  
USING GEOSYNTHETICS**

**by**

**Peter H Little B.Eng**



**Thesis submitted to the University of Nottingham  
for the degree of Doctor of Philosophy, August 1993.**

**BEST COPY**

**AVAILABLE**

Poor text in the original  
thesis.

## ACKNOWLEDGEMENTS

The author wishes to acknowledge the following people, companies and institutions:

Professor S F Brown for making available the facilities of the Department of Civil Engineering at the University of Nottingham; the Science and Engineering Research Council for funding the project and for making the Bothkennar Soft Clay Site available; Netlon Limited, Du Pont de Nemours Int. S.A, Rhône-Poulenc Fibres and Polyfelt Ges. m.b.h and their representatives for their industrial sponsorship and technical support; Denny Construction for their careful construction of the full-scale trials; and to Professor Alan McGown for making available the facilities of the Department of Civil Engineering at the University of Strathclyde.

During the course of the last three years I have been greatly aided by many friends and colleagues. Particular thanks are due to Mr A R Dawson, my supervisor, and Professor S F Brown for their advice, suggestions and guidance. I would further like to thank Mr M Langford and Mr D Belcher for their cheerful and enthusiastic assistance that made the long hours spent on-site so enjoyable.

On a more personal note, I would like to thank my wife, Alison, for her constant encouragement and support.

Finally, I wish to thank Glenis Fisher for her patient and efficient typing of this thesis.

## ABSTRACT

Current available methods for the design of unpaved roads, with and without geosynthetics, were used for sixteen full-scale test sections which were constructed at the Bothkennar Soft Clay Site, Airth, Scotland. The full-scale trials consisted of twelve pavements including geosynthetics and four control pavements incorporating two types of aggregate and two design life expectancies.

The test pavements were instrumented to monitor the transient stress and strain distribution, permanent strain distribution, geosynthetic temperature and ground water level during the trafficking operation. Traffic loading was provided in two stages by a standard road-going vehicle. The vehicle used for Phase One applied an 80kN axle load and in Phase Two a 126kN axle load. Failure of the pavements was defined as a rut depth of 150mm. The passage of 2115 axles resulted in failure of three sections and significant deformations in many others.

Back-calculation to compare predicted and measured performance was performed and hence the existing design methods were critically assessed. Where possible the measurements obtained from field trials were used to examine the assumptions made within the design methods.

The existing design methods were found to be essentially static in approach and did not model transient stresses and strains or permanent strain development adequately. Pointers towards a new approach ensuring strain compatibility between the elements of the system are suggested. This should enhance the ability of the engineer to assess the value of differing products used in this application.

If water passes through a road and fill up the native soil, the road whatever may be its thickness, loses support and goes to pieces. The erroneous opinion that by placing a large quantity of stone under roads, a remedy will be found for the sinking into wet clay or other soft soils ... (and) that a road may be made artificially strong to carry heavy carriages ... has produced most of the defects of the roads of Great Britain.

John L McAdam 1820

# CONTENTS

<b>CHAPTER ONE</b>		<b>Page</b>
<b>INTRODUCTION</b>		
1.1	BACKGROUND	1
1.2	THE NEED FOR RESEARCH	2
1.3	OBJECTIVES OF THE RESEARCH	3
1.4	THE RESEARCH	4
1.5	EXTENT AND STRUCTURE OF THE THESIS	6
<b>CHAPTER TWO</b>		
<b>A REVIEW OF EXISTING DESIGN METHODS</b>		
2.1	INTRODUCTION	9
	2.1.1 Basic Definition	9
2.2	UNREINFORCED PAVEMENT DESIGN	9
	2.2.1 Unreinforced Pavement Design - Hammitt (1970) Approach	10
	2.2.2 Unreinforced Pavement Design - Giroud & Noiray (1981) Approach	12
2.3	REINFORCED PAVEMENT DESIGN	14
	2.3.1 Reinforced Pavement Design - The Bidim Approach	14
	2.3.2 Reinforced Pavement Design - The Polyfelt Approach	15
	2.3.3 Reinforced Pavement Design - The Tensar Approach	16
	2.3.3.1 Calculation	16
	2.3.3.2 Unreinforced Static Analysis	17
	2.3.3.3 Reinforced Static Analysis	18
	2.3.4 Reinforced Pavement Design - Typar Approach	20

2.3.5 Reinforced Pavement Design - The Oxford Approach	21
2.3.5.1 Bearing Capacity	22
2.3.5.2 Stress Distribution Through the Granular Layer	23
2.3.6 Reinforced Pavement Design - Tensile Reinforcement Approach	25
2.4 REINFORCED PAVEMENT DESIGN	
- OTHER METHODS (SELLMIEJER 1990)	25
2.4.1 Stress Distribution	26
2.4.4.1 Vertical Stress	26
2.4.1.2 Shear stress	27
2.4.2 Horizontal Stress	27
2.4.3 Strain Compatibility	28
2.5 DISCUSSION OF DESIGN METHODS	28
2.5.1 Unreinforced Pavement Design	29
2.5.2 Reinforced Pavement Design	29
2.5.2.1 Bearing Capacity	29
2.5.2.2 3D/Plane Strain Analysis	31
2.5.2.3 The membrane effect	31
2.5.2.4 Separation	32
2.5.2.5 Aggregate Properties	32
2.5.2.6 Strain Compatibility	33

## **CHAPTER THREE**

### **BOTHKENNAR**

3.1 INTRODUCTION	34
3.2 PURPOSE AND CHOICE OF SITE	34
3.3 GENERAL DESCRIPTION	35
3.4 GEOLOGY	35

3.5	ENGINEERING PROPERTIES OF THE SURFACE DEPOSITS.	36
3.5.1	Samples Recovered from Surface Deposits at Bothkennar	36
3.5.2	Index Testing	38
3.5.3	Other Laboratory Tests	40
3.5.4	In-Situ Testing During Construction	41
3.6	SEASONAL VARIATION IN CRUSTAL UNDRAINED SHEAR STRENGTHS.	42

## CHAPTER FOUR

### FULL-SCALE TRIALS

4.1	INTRODUCTION	43
4.2	DESIGN OF THE FULL-SCALE TRIALS	43
4.3	LAYOUT OF THE SITE	45
4.4	SUMMARY OF DESIGNS USED	45
4.5	CONSTRUCTION OF THE FULL-SCALE TRIALS	47
4.5.1	Construction Method	47
4.5.2	Miscellaneous Observations on the Construction	48
4.6	AGGREGATE PROPERTIES	50
4.6.1	Sampling	50
4.6.2	Index Testing	51
4.6.2.1	Aggregate Particle Size Analysis	51
4.6.2.2	Specific Gravity	52
4.6.3	In Situ Density Measurements	52
4.6.4	Falling Weight Deflectometer (FWD) Testing	55
4.6.5	The ODIN Device (Boyce et al (1989))	57
4.6.6	280mm Diameter Triaxial Testing	58
4.7.	GEOSYNTHETIC PROPERTIES	59

4.7.1 Control Samples	59
4.7.2 Simulated Compaction Damage Samples	60
4.7.3 Traffic Damaged Samples	60
4.7.4 Index Testing	61
4.7.5 Interface Friction Angles	65
4.8 THE VEHICLE AND LOADING ARRANGEMENT	66

**CHAPTER FIVE**  
**INSTRUMENTATION**

5.1 INTRODUCTION	69
5.2 STRAIN MEASUREMENT	69
5.2.1 Instruments used to measure strain	69
5.2.2 Manufacture and Calibration	70
5.2.3 Layout and Objectives of Strain Measurement	71
5.3 STRESS MEASUREMENT	73
5.3.1 Instruments Used to Measure Stress	73
5.3.2 Manufacture and Calibration	74
5.3.3 Objectives and Layout of Stress Measurement	74
5.4 PORE WATER PRESSURE MEASUREMENT	75
5.5 MEASUREMENT OF GEOSYNTHETIC PROFILE	76
5.6 MEASUREMENT OF GEOSYNTHETIC TEMPERATURE	77
5.7 MEASUREMENT OF LATERAL SUBGRADE STRAIN	78
5.8 MEASUREMENT OF AGGREGATE THICKNESS	78
5.9 DATA COLLECTION ARRANGEMENTS	80
5.10 FREQUENCY OF MEASUREMENTS	81

5.11	INSTRUMENT PERFORMANCE	81
5.11.1	General	81
5.11.2	Strain Coils	84
5.11.3	Pressure Cells	84

## **CHAPTER SIX**

### **RESULTS**

6.1	INTRODUCTION	85
6.2	SURFACE RESPONSE UNDER TRAFFICKING	86
6.2.1	General Performance	86
6.2.2	Observations on Surface Movements Prior to Significant Rutting	87
6.2.3	Rut Depth Development	87
6.2.4	Localised Phenomena	88
6.2.5	Vertical Displacement	91
6.3	TRANSIENT STRESS DISTRIBUTION	93
6.4	TRANSIENT STRAINS	95
6.5	PERMANENT STRAINS	97
6.6	EXCAVATED CROSS SECTIONS	98
6.6.1	Loss of Aggregate to the Subgrade	99
6.7	SUBGRADE SHEAR STRENGTH	99
6.8	WATER TABLE	101

## **CHAPTER SEVEN**

### **REVIEW AND COMPARISON OF RESULTS**

7.1	INTRODUCTION	102
7.2	TRANSIENT STRESS	102

7.2.1	Comparison of Stress Readings	102
7.2.2	Stress Distribution	103
7.3	TRANSIENT STRAINS	104
7.3.1	Comparison of Transient Strain Readings	104
7.3.2	Transverse Geosynthetic Strain Profile	106
7.4	PERMANENT DEFORMATION	106
7.4.1	Early Rut Formation	106
7.4.2	Comparison of Ultimate Rut Depth	107
7.4.3	Comparison of Rut Depth and Vertical Displacement	108
7.4.4	Examination and Comparison of the Individual Elements	
7.4.4.1	Constituting a Rut	108
7.4.4.1	Control of Aggregate Deformation	108
7.4.5	Geosynthetic Rupture	110
7.4.6	Transverse Geosynthetic Permanent Strain	111
7.5	THE RELATIONSHIP BETWEEN RUT DEPTH AND SUBGRADE STRESSES	111
7.6	RUT DEPTH DEVELOPMENT AND GEOSYNTHETIC STIFFNESS	111
7.7	RELATIONSHIP BETWEEN PERMANENT AND TRANSIENT STRAINS	112
7.8	NON LINEAR BEHAVIOUR	112
7.9	LOAD EQUIVALENCY	115
7.9.1	Common Assumptions	115
7.9.2	Examination of Assumptions	115

## CHAPTER EIGHT

### EVALUATION OF DESIGN METHODS

8.1	INTRODUCTION	117
-----	--------------	-----

8.2	UNREINFORCED PAVEMENTS (SECTIONS D, H & K)	117
8.2.1	Unreinforced Pavement Design After Hammitt (1970)	117
	8.2.1.1 Summary of design method	117
	8.2.1.2 Back analysis	117
	8.2.2 Unreinforced Pavement Design After Giroud and Noiray (1981)	119
	8.2.2.1 Summary of design	119
	8.2.2.2 Back analysis	119
8.3	"BIDIM" REINFORCED PAVEMENTS (SECTIONS C & L)	120
	8.3.1 Summary of design for Section L	120
	8.3.2 Back-Analysis of Section L	121
8.4	"POLYFELT" REINFORCED PAVEMENT (SECTION P)	121
	8.4.1 Summary of Design	121
	8.4.2 Back analysis of Design	122
8.5	TYPAR REINFORCED PAVEMENT (SECTIONS B & M)	122
	8.5.1 Summary of Design for Section M	122
	8.5.2 Back Analysis of Section M	123
8.6	TENSAR REINFROCED PAVEMENTS (SECTIONS A & N)	124
	8.6.1 Summary of Design of Section N	124
	8.6.2 Back Analysis for Section N	125
	8.6.2.1 Static Analysis - Unreinforced Case	125
	8.6.2.2 Static Analysis - Reinforced Case	125
	8.6.2.3 Aggregate Saving	130
	8.6.2.4 Comparison of Design and Performance	130
	8.6.2.5 Comments on the Design Method	131
8.7	BAMBOO REINFROCED PAVEMENT (SECTION O)	132
	8.7.1 Summary of Design	132
	8.7.2 Back analysis	133

8.8	REINFORCE PAVEMENT ANALYSIS AFTER MILLIGAN ET AL (1989 a & b) (SECTIONS F & I)	134
8.8.1	Summary of Design for Section I	134
8.8.2	Back analysis of Section I	134
8.8.3	Observations on the Design Method	137

## **CHAPTER NINE**

### **DISCUSSION**

9.1	INTRODUCTION	138
9.2	RUT DEPTH DEVELOPMENT	138
9.3	DAMAGE FACTORS	140
9.4	MEMBRANE EFFECT	141
9.5	SLAB EFFECT	142
9.6	AGGREGATE BASE RESTRAINT	143
9.6	ESTIMATING TRANSIENT GEOSYNTHETIC STRAIN	144
9.7	ESTIMATE OF GEOSYNTHETIC TENSILE FORCES	145
9.8	PARTIAL REINFORCEMENT	146
9.9	SEPARATION	147

## **CHAPTER TEN**

### **CONCLUSIONS & RECOMMENDATIONS FOR FUTURE WORK**

10.1	THE TRIALS AT BOTHKENNAR	149
10.2	RUT DEPTH DEVELOPMENT	149
10.3	MECHANISMS	151
10.4	RECOMMENDATIONS FOR FUTURE WORK	152

## LIST OF PLATES

- 1.1 The Bothkennar Soft Clay Site
- 3.1 A Split U100 Sample Retrieved from Bothkennar
- 4.1 General View of the Lower-bound Sections
- 4.2 Polyfelt and Bamboo (Section O) General Arrangement
- 4.3 Falling Weight Deflectometer
- 4.4 The ODIN Device
- 4.5 280mm Diameter Triaxial Apparatus - After Cheung & Dawson (1992)
- 4.6 Retrieval of a "Compaction Damaged" Geosynthetic Sample
- 4.7 Recovery of a Post-Trafficking Sample
- 4.8 300mm Shear Box Sample Showing Failure Within the Clay
- 4.9 The Trafficking Vehicle
- 5.1 Strain coil Calibration Rig
- 5.2 Inside a Nottingham University Pressure Cell
- 5.3 Pressure Cell Calibration Rig
- 5.4 Damage to Polyfelt Section (P) Caused by the Vertical Inspection Tubes
- 6.1 Cracks in the Trafficked Pavement
- 6.2 Trafficking of the Localised Pavement Failure Within Section I
- 6.3 Failure of the Geogrid - Tensar SS1 Section I
- 7.1 Pavements After a Few Passes
- 8.1 Bamboo Failure, Excavation after Trafficking
- 8.2 Subgrade Deformation of the Post-Trafficked Polyfelt/Bamboo Section (O)

# CHAPTER ONE

## INTRODUCTION

### 1.1 BACKGROUND

In the design of low volume roads, that is roads whose life expectancy is measured in hundreds or thousands of axle passes, the most economical solution is often a pavement that consists entirely of unbound materials. Such roads are commonly found as forestry and farm access tracks or haul roads. Haul roads are used for large earth moving or quarrying activities and, hence, their economic construction is particularly important as it can dictate the cost of producing the nations raw materials.

The application of repeated axle loadings to these pavements causes permanent surface deformation, rutting, to develop. The permitted rut depth is dependent upon the serviceability requirements of the user but, commonly, falls within the range 75 to 300mm. This serviceability requirement is likely to be dictated by vehicular axle clearance or plant efficiency considerations.

It has been long understood that when roads cross soft ground even large quantities of aggregate are unable to prevent premature pavement disintegration. The Romans used to place brushwood on the surface of soft ground before constructing their roads in order to prevent the stones being lost into the soft foundation. Today, man-made materials are used in place of the brushwood and the general name for such materials used in geotechnical engineering is geosynthetics (from the Greek geo, meaning the Earth, and synthetic, meaning artificially produced). The use of geosynthetics in unpaved roads over soft ground was one of the first applications for these products. The geosynthetic market in Western Europe is growing at 12 to 15 per cent annually and currently stands at 300 million square metres per annum. The application of geosynthetics into the aggregate soil layers of roads accounts for some 40% of the total geosynthetic sales (Jagielski, 1991).

A major problem with unpaved roads over soft ground is that very thick layers of aggregate are required to resist the deformations resulting from trafficking. Low volume roads are often subjected to heavy axle loads and the influence of the axle load upon pavement damage is significant. In these situations geosynthetics are often used in an attempt to reduce the quantity of aggregate required and, hence, the cost of

construction. It is generally believed that geosynthetics contribute by fulfilling one or more of the basic functions of separation, filtration, drainage or reinforcement (Hausmann, 1987).

It is widely accepted that, in certain circumstances, the inclusion of a geosynthetic in an unpaved road can have a beneficial effect on its long-term serviceability. These benefits are generally assumed to increase with decreasing subgrade shear-strength and increasing geosynthetic stiffness (Giroud & Noiray, 1981). For any given design, the economic benefits of including a geosynthetic are normally calculated by comparing the thickness of the aggregate layers required to meet the serviceability criteria for pavements with and without geosynthetics (eg Giroud & Noiray, 1981, Tonus, undated, Houlsby & Jewell, 1989).

## 1.2 THE NEED FOR RESEARCH

A wide variety of geosynthetics are used in the context of unpaved roads. This is due to the range of raw materials and manufacturing methods used to produce geosynthetics. Indeed within each product type several materials with differing polymer contents are available. As a result these materials vary substantially in their physical properties and although some design methods have been proposed which appear to be unified (eg Giroud & Noiray, 1981), design has generally remained product specific (eg Polyfelt (undated)). The use of geosynthetics in unpaved roads has been very much driven by the producers of geosynthetics who have demonstrated the benefit of their individual products. Consequently, most geosynthetic manufacturers have design methods which highlight the performance of their product. Different assumptions and factors of safety within the various methods make it difficult for the consumer to make an engineering judgement as to the suitability of any one product to a given situation or to compare the performance of products A and B.

Unified design methods fail to model the observed behaviour of all geosynthetic reinforced roads which has led to designers using “unified designs” solely for certain product ranges with known past performance. This failure to model observed behaviour may not only be due to different material properties but, at least in part, to a failure to clearly identify the mechanisms involved both within the method and in the field.

Two principal mechanisms are generally assumed to be operating in geosynthetic reinforcement design methods. These are separation (Tonus, undated) as shown in Figure 1.1 and reinforcement (Giroud & Noiray, 1981) as shown in Figure 1.2. However, it is possible that a combination of these two mechanisms is in operation or indeed some other system (Sellmeijer, 1990).

The geosynthetic can be placed either within the aggregate layer or at the interface between this layer and the subgrade. The position of the geosynthetic also influences its performance. To act as a separator it is usually placed at the interface whilst for reinforcement purposes it can be placed either within the layer or at the interface. Obviously the pavement is easier to construct with the reinforcement at the interface.

The concepts behind the design methods currently available for unsurfaced roads with geosynthetic reinforcement are as diverse as the products for which they are intended. Generally, each manufacturer of geosynthetics uses a different design method which highlights the benefits of including their particular product. Such diversity implies that, generally, there is a fundamental lack of understanding of the mechanisms involved in this type of problem which needs further investigation.

### 1.3 OBJECTIVES OF THE RESEARCH

The general objective of the research was to examine, principally by the use of full-scale trials, the behaviour of, and mechanisms at play within, unpaved roads which included geosynthetics at the subgrade-aggregate interface. To aid the understanding of the mechanisms involved, comparisons with unpaved roads not including geosynthetics were required. The general objective was supplemented by examining the critical components of existing design methods and by analysing whether or not the assumed mechanisms within the design methods were observed to occur. The detailed objectives of the research could be described as follows:

- 1 To use measured and predicted transient stresses and strains, surface deformations and permanent deformation for the full scale trials in order to obtain a better understanding of the behaviour of unpaved roads with geosynthetics incorporated.

In common with much pavement engineering there is the necessity of predicting permanent deformation resulting from repeated applied transient loading. This

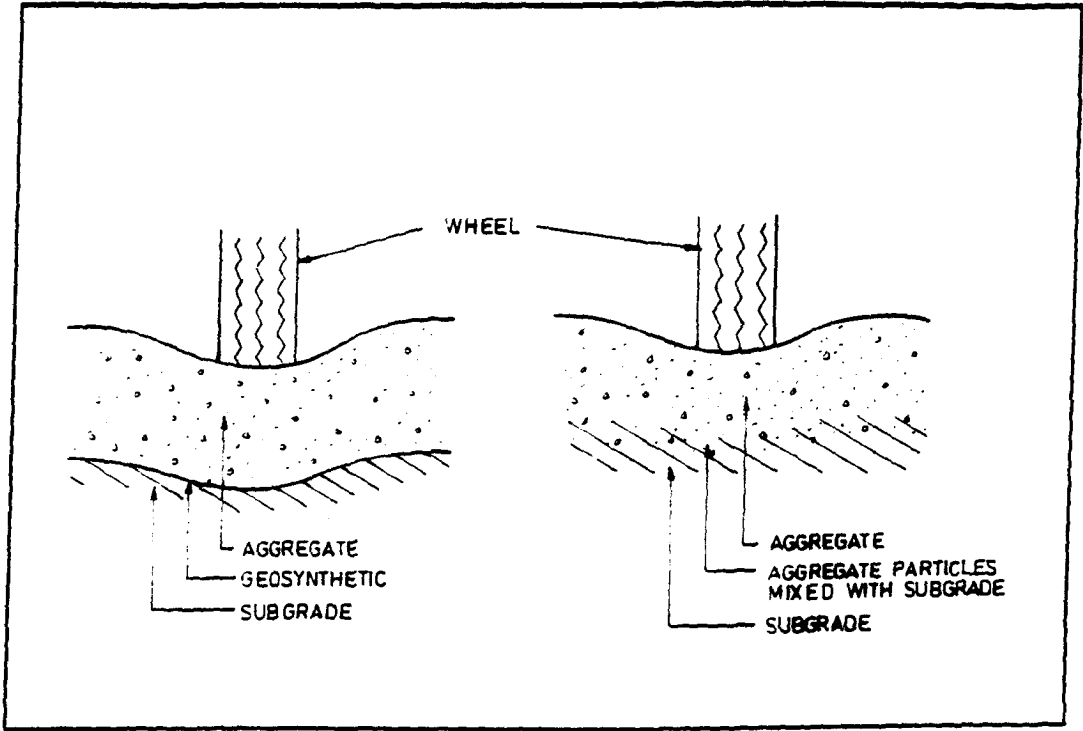


**Figure 1.1 Separation**

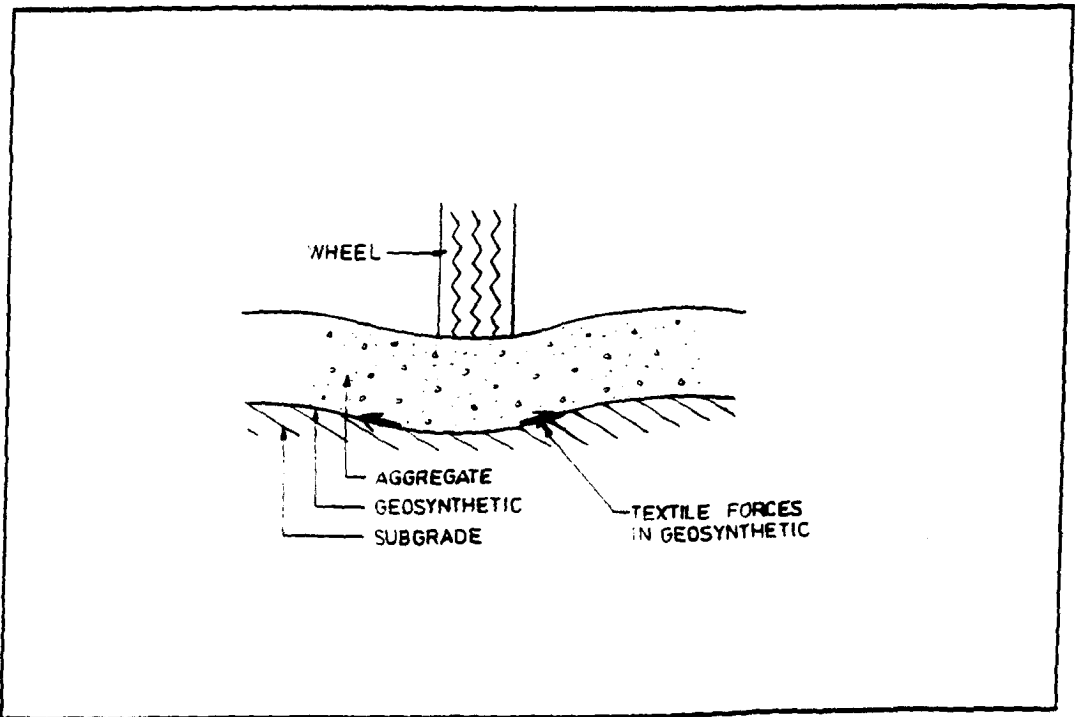


**Figure 1.2 Reinforcement**

transient loading, in any one application, causes very little permanent deformation but is, generally, the basis for design as it most closely represents the static loading models commonly employed in analysis. Thus prior to the trials, the distribution of transient stress and strain within the pavements, resulting from dynamic loading was considered. These transient values could then be critically examined in the light of the existing design methods, and an attempt made to relate them to permanent deformation.

However, pavement performance is measured in terms of permanent deformation. Hence, measurement of permanent strains within the pavement was required, together with the monitoring of surface deformations.

- 2 To determine the engineering properties of the materials used in the trials in order to more fully understand the long-term performance of the pavements. Furthermore, to assess the materials' change of properties with time.
- 3 To use the results of the full-scale trial to build up detailed case studies of the performance of unpaved roads, including and not including geosynthetics, under controlled conditions. These case studies could yield an opportunity to examine critically some of the popular methods of design used in the UK and thereby give some indication as to how a satisfactory unified design method for all types of geosynthetic might be accomplished.

#### 1.4 THE RESEARCH

The full-scale trial involved in the research was based at a site, known as Bothkennar, on the banks of the Forth Estuary and shown in Plate 1.1. The site was purchased by the Science & Engineering Research Council (SERC) in 1988 as a test site for research into the interaction of soft clay with a variety of civil engineering and building operations (Nash et al, 1985). As an access road was to be constructed to enable access to various parts of the site, a proposal was made to SERC that this provided an opportunity to research the performance of unpaved roads using geosynthetics. The proposal was accepted for funding in 1988 and the author was appointed as the research assistant for the project in the Spring of 1989.

The research was sponsored by SERC and by the following manufacturers of geosynthetics: Netlon Limited, Du Pont de Nemours Int. SA, Rhône-Poulenc Fibres



Plate 1.1 - The Bothkennar Soft Clay Site

and Polyfelt Ges. m.b.h. These manufacturers, between them, produce most generic types of geosynthetics.

Involved in the trials were the following geosynthetics: a polypropylene geogrid (Tensar SS2) made by Netlon Ltd; a polypropylene heat-bonded non-woven (Typar 3407) made by Du Pont; a polypropylene needle-punched felt (Polyfelt TS500) made by Polyfelt; a polyester needle-punched felt (Bidim B2) made by Rhone Poulenc; and a polypropylene split film woven geosynthetic.

The industrial sponsorship consisted of a small financial contribution to the cost of the research, a quantity of geosynthetic, a design based on their current method and technical advice and support. None of the sponsors of the project manufactured any woven geosynthetics and, hence, a woven geosynthetic was anonymously purchased and installed in the full-scale trials so that a full range of geosynthetics were represented.

The construction of the full-scale trials pavements was undertaken in the Summer and Autumn of 1989 and they consisted of a loop road comprising sixteen, twenty metre long sections, twelve of which contained geosynthetics and four of which were control sections with no geosynthetics. Two types of aggregate were utilised, a crushed rock and a sand and gravel mixture and six types of geosynthetic were included. Sections were constructed to one of two expected design lives (a thicker “upper-bound” solution and a thinner “lower-bound” one). Loading was provided by a standard road-going, two-axle lorry which imposed 2,115 load repetitions upon the pavements. 1,000 load repetitions were applied in the Spring of 1990 and the remaining loadings were applied in the Spring of 1991. Intervening periods were used to examine the pavement materials’ engineering properties and to analyse the large quantities of data collected from the trials. The loading induced rupture of the geosynthetic in three sections and significant deformations in several of the remaining sections. These sections are summarized in Table 1.1. The terminology used in the table is explained in Chapter 4.4 and a more detailed summary of the sections is shown in Table 4.1.

Section	Geosynthetic type	Manufacturer	Grade of Geosynthetic	Design Solution
A	Geogrid	Netlon	TENSAR SS2	Upper
B	Heat-bonded	Du Pont	TYPAR 3407	Upper
C	Needle-punched	RhonePoulenc	BIDIM B2	Upper
D	none	-	-	Upper
E	Woven	Unspecified	40/45kN	Upper
G	Geogrid	Netlon	TENSAR SS1	Upper
F	none	-	-	Upper
H	none	-	-	Lower
I	Geogrid	Netlon	TENSAR SS1	Lower
J	Woven	Unspecified	40/45kN	Lower
K	none	-	-	Lower
L	Needle-punched	Rhone Poulenc	BIDIM B2	Lower
M	Heat-bonded	Du Pont	TYPAR 3407	Lower
N	Geogrid	Netlon	TENSAR SS2	Lower
O	Needle-punched	Polyfelt	POLYFELT TS 500	Lower
P	Needle-punched	Polyfelt	POLYFELT TS 500	Lower

**Table 1.1 Summary of Sections**

In addition to the work carried out on site at the full scale trial laboratory testing was undertaken at the University of Nottingham to determine the mechanical properties of the aggregate and geosynthetic together with pavement design calculations and data analysis.

The University of Strathclyde provided data to describe the geosynthetic properties for the project. The University of Oxford wished to test a new approach to the mechanisms involved in this type of pavement and provided designs and comments/suggestions for the research.

## 1.5 EXTENT AND STRUCTURE OF THE THESIS

The thesis is concerned principally with the design, construction and subsequent trafficking of the unsurfaced, full-scale trial pavements including geosynthetics at Bothkennar, briefly described above. The structure of the thesis may be summarised as follows:

A review of the design methods used to determine layer thickness for the trial pavement sections is presented in Chapter 2 together with a brief resumé of alternative design methods that are currently available. From this review a summary of the important parameters which may control the performance of the pavements is presented.

The Bothkennar site is described in Chapter 3 both in terms of what was known about the site at the onset of the trials and what was subsequently discovered about the site during the course of the trials.

The details of the full-scale trials are described in Chapter 4. This includes the design of the experiment, the design of the sections, the materials used in the trials and the method of construction.

Many instruments were used in order to determine and measure the important parameters identified in Chapter 2. The layout, calibration, installation and methods of monitoring these instruments is described in Chapter 5 along with the general formats of the measured data.

The results obtained from the instrumentation and from surface deformation monitoring are presented in Chapter 6. The Chapter includes sets of data that enable direct comparison between pavements whilst a further range of data is presented in the appendices and a complete data set is available on IBM compatible data discs (Little 1992).

An analysis of the results is shown in Chapter 7. The analysis is principally concerned with the development of permanent deformation and the position where such deformation is generated. A comparison of the varying pavement performances is also made and some observations on variation in material properties reported.

In the light of the measured performance of each section, an evaluation of each of the design methods is presented in Chapter 8. The strengths and weaknesses of each of the design methods is highlighted and a critical assessment of the presumed important parameters, as indicated in Chapter 2 is presented.

Discussion of, and conclusions drawn from the experiment and the study of the design methods used are presented in Chapters 9 and 10 respectively. These two Chapters

give some pointers to the key elements required for a unified design method and recommendations for further work.

## CHAPTER TWO

### A REVIEW OF EXISTING DESIGN METHODS

#### 2.1 INTRODUCTION

The objective of this chapter is to review the design methods used for the pavements in the full-scale trials and to make a brief examination of some alternative design methods available. The particular features of each design method are highlighted, with an indication of the important implications for the design.

As a result of this review, the chapter concludes with a summary of the parameters that one might wish to measure in an instrumented trial in order to validate the design methods.

##### 2.1.1 Basic Definitions

Design methods are principally based on the prediction of permanent surface deformation. This permanent deformation can be described in two manners, namely rut depth and vertical displacement.

The rut depth ( $r$ ) is defined as the maximum vertical distance to the top of the aggregate surface in the wheel path from a rigid straight 2m long bar placed transversely on the pavements surface.

The vertical displacement ( $s$ ) is defined as the downward movement of the pavement surface layer in the wheel path.

Both of these items are shown in Figure 2.1.

#### 2.2 UNREINFORCED PAVEMENT DESIGN

The design of an unreinforced unsurfaced road requires the thickness of aggregate to be chosen such that the design traffic loading can be carried without either the aggregate undergoing internal deformation or the soil being over stressed and thereby deforming

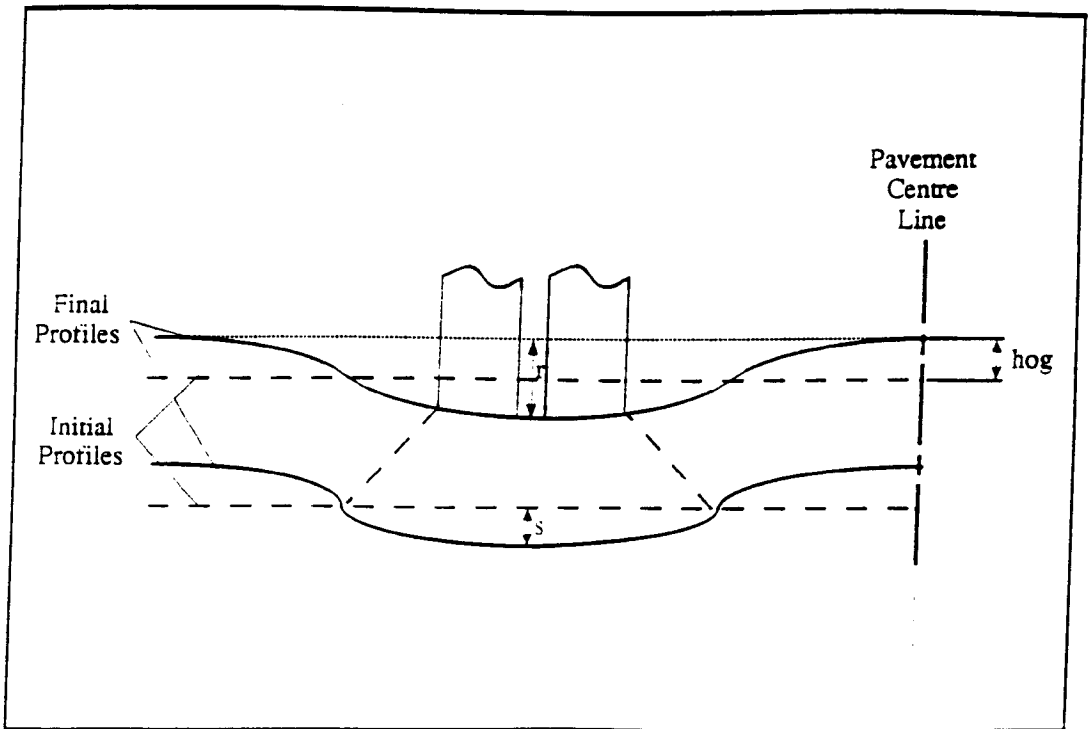


**Figure 2.1 Deformation Geometry**

extensively beneath the aggregate. Both of these failure mechanisms result in a surface rut. The rut depth is the sum of the vertical depression in the wheel path(s) and the hog outside this area as shown in Figure 2.1. This rut or permanent deformation is used as the design criterion by both Hammitt (1970) and Giroud & Noiray (1981) in their design methods.

### 2.2.1 Unreinforced Pavement Design - Hammitt (1970) Approach

Hammitt (1970) reported on extensive trials of unreinforced unpaved roads, where a variety of wheel loads, tyre pressures and subgrade stiffnesses were utilised. Failure of the pavements was defined as the point when the permanent deformation exceeded 0.075m, or the transient deformation exceeded 0.038m, when measured using a 3m straight edge.

The empirical work of Hammitt drew upon, as a starting base, the empirical model developed by Ahlvin (1959) for use with flexible surfaced pavements, namely that:

$$h = f \sqrt{\frac{P}{8.1 \text{ CBR}} - \frac{A}{\pi}} \quad (2.1)$$

where  $h$  = Aggregate thickness (in)  
 $P$  = Single wheel load (lbs)  
 $A$  = Contact area (in<sup>2</sup>)  
 CBR = California Bearing Ratio (%)  
 $f$  = traffic influence factor

Converted to the SI system Equation 2.1 becomes:

$$h = f \sqrt{\frac{P}{\text{CBR}} - 17.8A} \quad (2.2)$$

$h$  is m,  $P$  in kN, and  $A$  in m<sup>2</sup>

It should be noted that the units in Equations 2.1 and 2.2. do not equate.

It should further be noted that in this model the thickness of the granular layer is a function of the square root of the axle load. A 4th power law for non-standard axle

loads is not applied (as is commonly assumed in pavement engineering and by Giroud & Noiray (1981)). For a constant tyre pressure an increase in load will result in an increase in the contact area. Equation 2.2 therefore implies that as the axle load rises, the increase in aggregate layer thickness required is slightly offset by the increase in contact area.

Hammitt (1970) suggested a similar relation for unsurfaced pavements in the form as shown in Equation 2.3.

$$h = f' \sqrt{\frac{P}{\text{CBR}} - 17.8A} \quad (2.3)$$

where a different traffic influence factor,  $f'$ , would apply and would be in the form

$$f' = \log N_{75} + C \quad (2.4)$$

where  $N_{75}$  = Number of axle passes to produce a rut depth of 0.075m and  $C$  = a constant depending on the thickness of the aggregate layer required to resist static deformation failure.

The transference of the general form of the equation, from the flexible surfaced road to the unsurfaced, should be viewed critically. The stress distribution characteristics of the two types of pavement are different, as are the modes of pavement failure. The assumption that the thickness of aggregate required is a function of the logarithm of the number of axle passes is common for surfaced pavements which tend to suffer from fatigue related failure. However, this assumption may be not valid in the case of low volume unpaved roads.

An analysis of 59 test pavements was undertaken by Hammitt (1970). The study included data from a variety of trials where  $P$ ,  $A$ ,  $h$  and  $N_{75}$  were all known. The traffic influence factor,  $f'$ , was plotted against log passes to failure and the results are shown in Figure 2.2. It should be noted that the data exhibits a large degree of scatter. Simple linear regression of the data led Hammitt to suggest that, for unreinforced roads, the traffic influence factor  $f'$  should be determined by Equation 2.5.

$$f' = (0.0236 \log N_{75} + 0.0161) \quad (2.5)$$

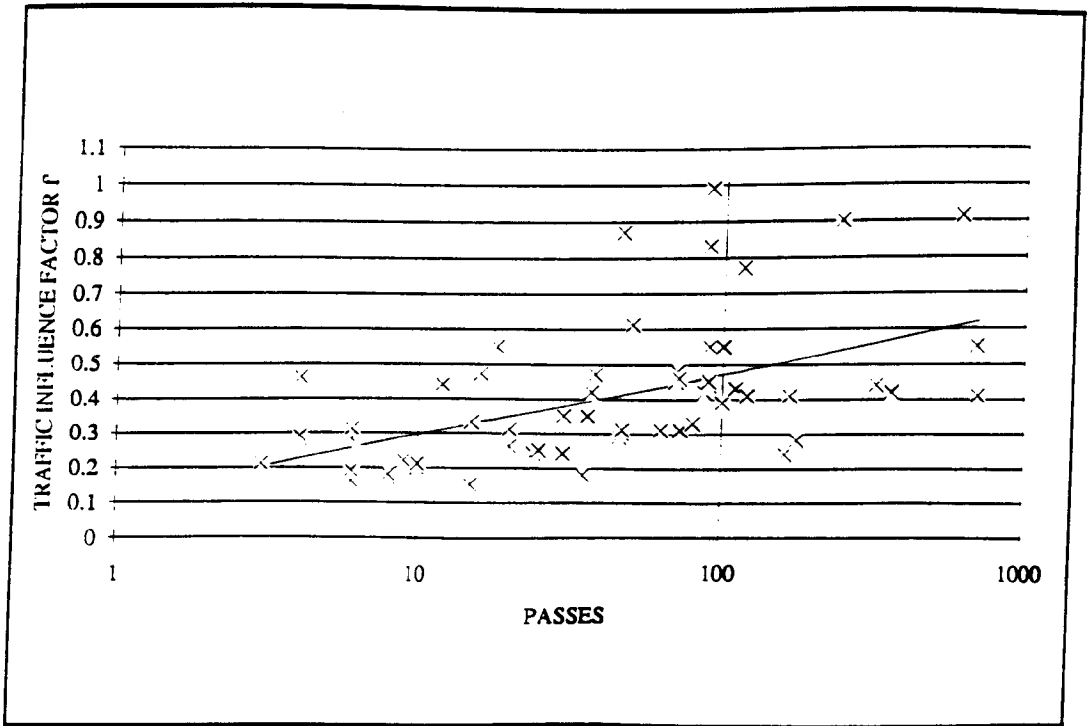


**Figure 2.2 Traffic Influence Factor (f') After Hammitt (1970)**

Hence by combining Equation 2.3 and 2.5 Hammitt (1970) suggested that for a 75mm rut depth

$$h = (0.0236 \log N_{75} + 0.0161) \sqrt{\frac{P}{\text{CBR}} - 17.8A} \quad (2.6)$$

### 2.2.2 Unreinforced Pavement Design - Giroud & Noiray (1981)

#### Approach

The unreinforced sections at Bothkennar were designed with reference to the work of Giroud & Noiray (1981). The analysis for unreinforced roads presented by Giroud & Noiray is based upon the work of Hammitt (1970) with reference to unreinforced and reinforced unpaved road trials undertaken by Webster & Watkins (1977) and Webster & Alford (1978). New relationships based on this earlier work were proposed by Giroud & Noiray which led to a simple analysis.

Based on Equation 2.6 Giroud & Noiray (1981) suggested that an approximation for standard 80kN axle loading might be:-

$$h = \frac{0.19 \log N_{75}}{\text{CBR}^{0.63}} \quad (2.7)$$

where h is in m.

and  $N_{75}$  is the number of passes to induce a rut depth of 75mm.

It should be noted that in Equation 2.7 the units do not equate. For standard loading it can be seen from the examples shown in Figures 2.3 and 2.4 that Equation 2.7 is a fair approximation to Equation 2.6. However, there is not the large number of empirical trials that one would expect to justify the validity of Equations 2.6 and 2.7. Equation 2.7 has the advantage of being a more simple equation than Equation 2.6 and enables the easy modification for mixed traffic loading by way of the "Fourth Power Law" namely:

$$N_s = \sum N_i \left( \frac{P_i}{P_s} \right)^4 \quad (2.8)$$

where  $N_s$  = number of standard (80kN) axle passes

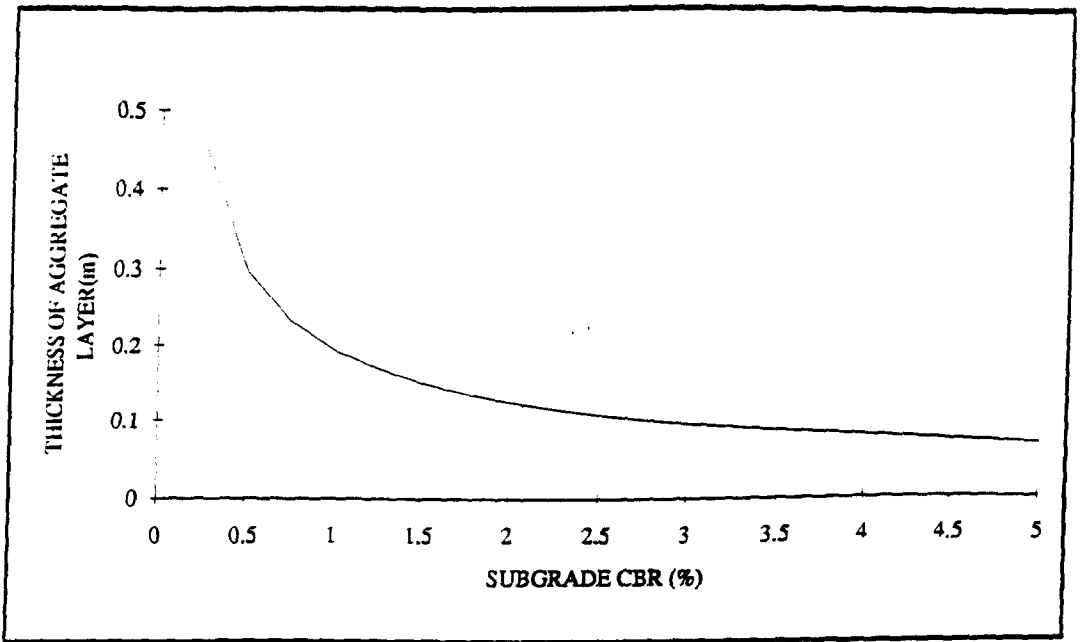


**Figure 2.3 Thickness of Aggregate Required for a 75mm Rut After 10 Passes of an 80kN Axle. After Hammitt (1970) and Giroud and Noiray (1981)**

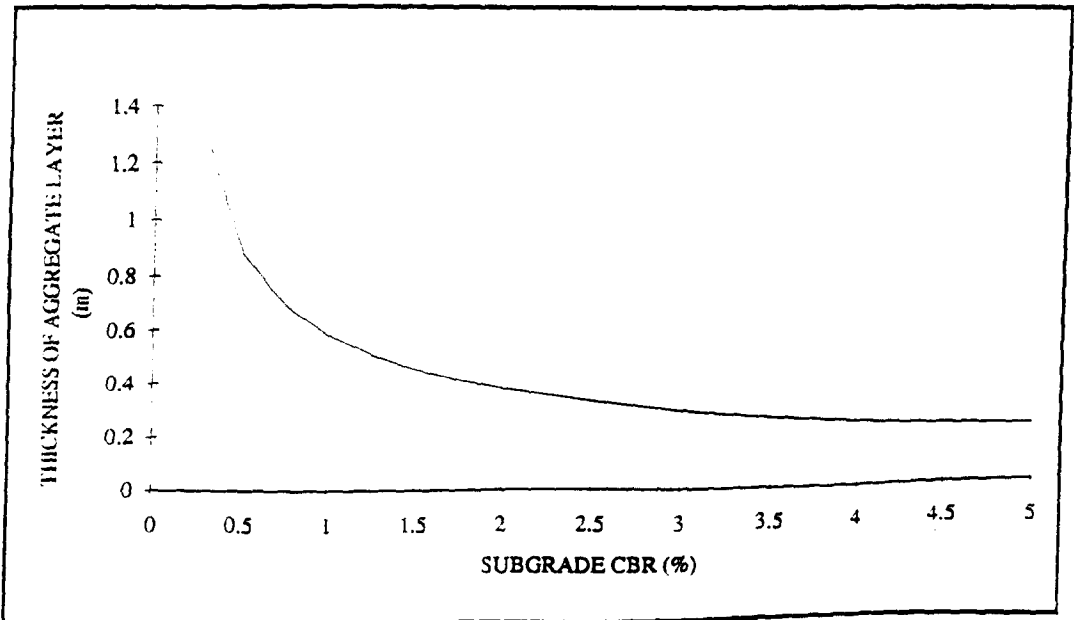


**Figure 2.4 Thickness of Aggregate Required for a 75mm Rut After 1000 Passes of an 80kN Axle. After Hammitt (1970) and Giroud and Noiray (1981)**

$N_i$  = number of actual axle passes

$P_s$  = standard axle load, 80kN

$P_i$  = actual axle load kN.

The use of the Fourth Power Law for unsurfaced pavements is not fully justified by Giroud and Noiray (1981). The Fourth Power Law was developed for surfaced pavements not unsurfaced ones. The applicability of Equation 2.8 is discussed further, in the light of the trials, in Chapter 8.2.2.2.

For rut depths not equal to 75mm the available experimental data on the development of rutting with application of load passes for unreinforced unpaved roads, especially for high rut depths, is sparse. Webster & Watkins (1977) examined six pavement structures to a rut depth of 275mm, only one of which was unreinforced. All of Webster & Alford's (1978) work related to reinforced pavements. However, accepting the contention that rut development is linear with the logarithm of passes of the axle, extrapolation to larger rut depths may be performed with some confidence, in the unreinforced case, because the rate of development of rut depth is constant regardless of the rut depth.

Giroud & Noiray (1981) suggested that, from examination of Webster & Watkins (1977) data, Equation 2.7 could be modified by substituting the following for the number of passes of standard axle to produce a 75mm rut,  $N_{75}$ :

$$\log N_{75} = \log N_r - 2.34 (r - 0.075). \quad (2.9)$$

where  $N_r$  is the number of passes of a standard axle to produce a rut depth  $r$  in mm.

Equation 2.9 thus enables the designer to choose a rut depth not equal to 75mm and the substitution into Equation 2.7 yields the following expression.

$$h = \frac{0.19 (\log N_r - 2.34 (r - 0.075))}{\text{CBR}^{0.63}} \quad (2.10)$$

For any given CBR and  $N_r$ , it can be seen that  $h$  is proportional to  $r$ . Giroud & Noiray's approximation is plainly inadequate at  $r = 0$ , because no matter how large  $h$ , the passage of some axles ( $N_r$ ), will produce some rut. Also it is possible for  $r$  to be negative which is clearly unreasonable. However, as a simple design calculation,

based upon empirical data, Equation 2.10 represents a valuable first estimate of the design thickness of aggregate layer required in an unreinforced road.

### 2.3 REINFORCED PAVEMENT DESIGN

Within this thesis the term reinforced pavements refers to those pavements including geosynthetics at the aggregate/subgrade interface. For low stiffness geosynthetics the term reinforcement can be a little misleading as the geosynthetics are producing little or no reinforcement effects but are principally acting as separators (Figures 1.1 and 1.2 apply).

Generally, the reinforced pavement designs within this section attempt to show the value of including geosynthetics in unpaved roads either by predicting an increase in service life or a reduction in the thickness of the aggregate layer. The methods by which the designs perform this role varies from the empirical to the theoretical.

The design methods chosen here for examination are but a few of those that are widely available. They are the methods used to design the full-scale trials at Bothkennar and generally cover all of the assumed mechanisms controlling reinforced unpaved roads. A new design method was proposed by Sellmeijer (1990) during the course of the trials that was sufficiently different to current thinking to be of value to this thesis and as such is discussed in Chapter 2.4.

#### 2.3.1 Reinforced Pavement Design - The Bidim Approach

The simplest method of empirical design is to examine case histories and choose a design based upon experience. The Comité Français des Geotextiles (1981) produced 88 variations of possible designs, based on traffic type, axle loads, permissible rut depth, subgrade CBR, thickness of granular layer and fill type. On comparison of the specific design requirements with the example which most closely matches these case studies, the required characteristics of the geosynthetic are obtained. This approach is adopted for the design of pavements reinforced with Bidim, the polyester needle-punched geosynthetic used in Sections C & L.

This type of method has many drawbacks in that it is restricted to the field of experience to date, is unable to predict the effects of changing the material properties in the system and is unable, analytically or empirically to demonstrate the advantage

of including a geosynthetic. However, it does give a simple to use, rough-and-ready approach to design and given that the design of haul roads is not an exact science this quick method could be satisfactory.

### **2.3.2 Reinforced Pavement Design - The Polyfelt Approach**

Resl & Werner (1986) noticed that the inclusion of geosynthetics in the soil-geosynthetic-aggregate system improved the bearing capacity. Although they were unable to explain this improvement in any analytical terms, they recognised that the inclusion affected the failure mechanism of the system.

A series of plate bearing tests utilising a specific geosynthetic and comparisons with the control case with no geosynthetic present yielded design charts for the thickness of material required to withstand the application of one load cycle and this forms the basis of the design approach for Polyfelt, the needle-punched polypropylene geosynthetic used in Section O & P: Polyfelt (undated). This thickness is then modified to take account of the many repetitions of load by reference to the Comité Français des Geotextiles (1981).

While this technique demonstrates the value of including geosynthetic, the manner in which it does so must be questioned. The mechanisms of failure in the single plate loading test are likely to be different to those occurring under repeated loading and in-field service conditions. Under normal contact stresses, the surface transient deformations are not altered by the inclusion or otherwise of the geosynthetic (Sellmeijer, 1990) and neither is the stiffness of the pavements (King, 1990).

Because it is believed that separation and filtration are significant factors in the design of unpaved roads, particularly when using "low" stiffness geosynthetics, design methods for these products often carefully check the survivability of the geosynthetic during the construction and trafficking process and the hydraulic properties required by the geosynthetic. It is obvious that the inclusion must remain integral if it is to act as a separator in the pavement and should not have an adverse effect on local pore water pressures that might develop during transient loading. However, if the value of low stiffness geosynthetics in unpaved roads is to be demonstrated, some analytical or empirical method for determining the value of separation to the pavement needs to be developed.

### 2.3.3 Reinforced Pavement Design - The Tensar Approach

The design approach used for Tensar, a high stiffness polypropylene grid used in Section A & N, is based upon the work of Giroud & Noiray (1981). It is one of the most popular methods of analysis used in the UK for high stiffness geosynthetics. The method makes a static analysis of pavements including geosynthetics and compares this with an unreinforced static analysis to deduce a saving in aggregate thickness which can be achieved.

The stress applied to the aggregate surface by the wheel load is assumed to be rectangular with width  $W$  and length  $L$ . This is transferred to the subgrade via a load spreading angle ( $\alpha$ ) leading to a rectangular stress distribution on the surface of the subgrade. In the unreinforced case the assumed maximum stress permissible on the subgrade is governed by the elastic bearing capacity ( $\pi S_u$ ) whereas in the reinforced case the plastic bearing capacity ( $(\pi+2)S_u$ ) is assumed to provide the limit. It is this change in bearing capacity which generates most of the benefit produced by including the geosynthetic, however, some of the benefit is attributed to the "membrane effect". "The membrane effect" proposes that the vertical stress imposed upon the subgrade is reduced as a direct function of the amount of the vertical component of the tensile force in the geosynthetic shown in Figure 2.5 which is generated as the geosynthetic is stretched and pressed downwards - like a membrane.

A saving of aggregate for the reinforced over the unreinforced case is calculated and applied to the thickness normally required for an unreinforced design based on empirical data of performance under trafficking.

#### 2.3.3.1 Calculation

The stress distribution is assumed to be of the form shown in Figure 2.6.

It can be seen that the stress applied at the base of the aggregate layer is given by Equation 2.11.

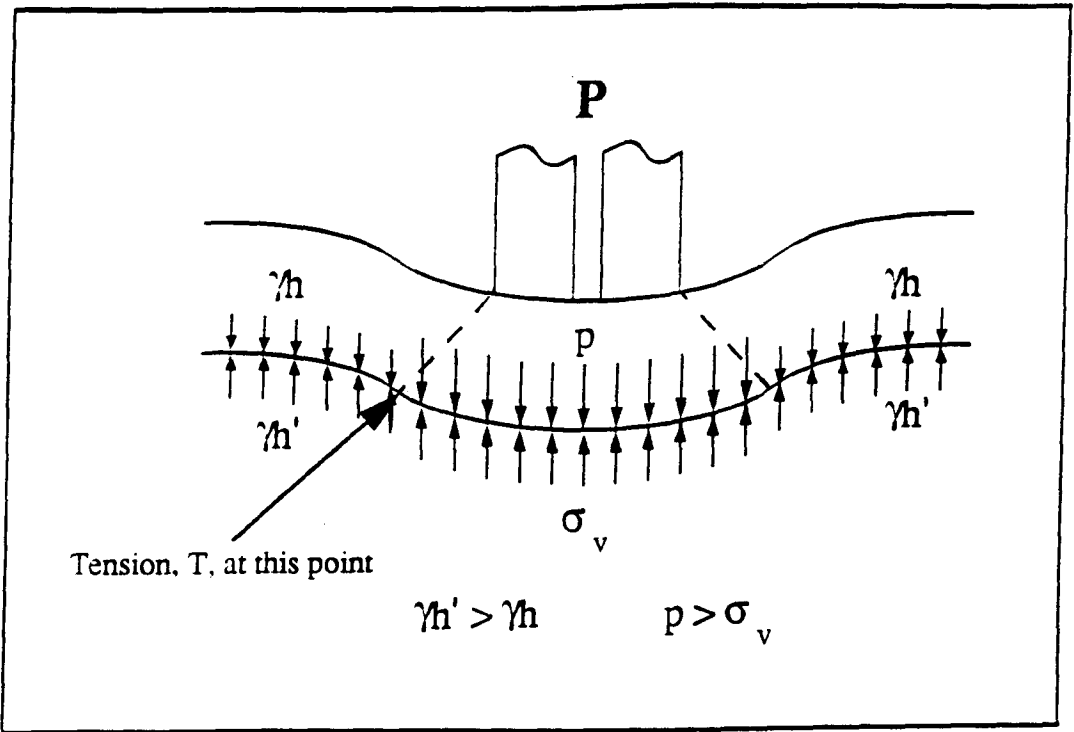


Figure 2.5 The Membrane Effect - After Giroud and Noiray (1981)

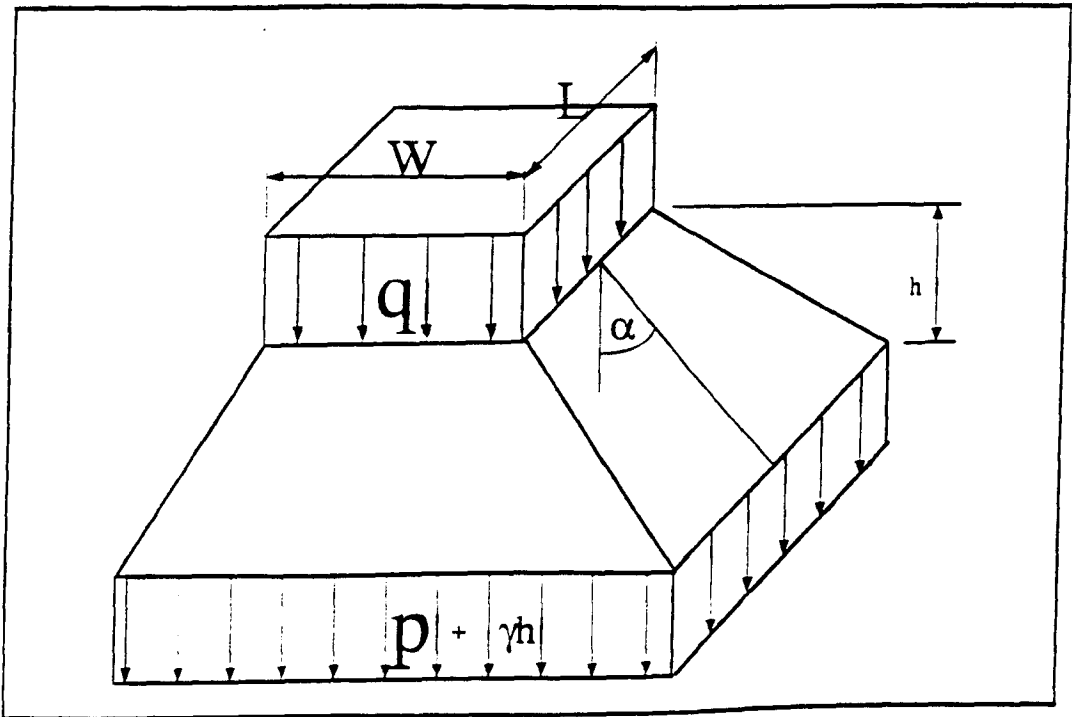


Figure 2.6 Stress Distribution - After Giroud and Noiray (1981)

$$\sigma_v = q \left( \frac{WL}{(W+2h\tan\alpha)(L+2h\tan\alpha)} \right) + \gamma h \quad (2.11)$$

where  $\sigma_v$  = applied vertical stress at the subgrade surface (kPa)

$q$  = applied vertical stress at the aggregate surface (kPa)

$h$  = aggregate layer thickness (m)

$\alpha$  = load spread angle

$\gamma$  = unit weight of aggregate (kN/m<sup>3</sup>)

The thickness of the aggregate layer ( $h$ ) varies in the reinforced and unreinforced cases. Given that the internal angle of friction for the aggregate is  $\phi'$ , a suggested value for  $\alpha$  is given as  $\pi/4 - \frac{\phi'}{2}$  representing the inclination of the shear planes which would occur if the aggregate layer was failed by punching. A characteristic value of  $\alpha$  is taken, such that  $\tan\alpha = 0.6$ , which implies  $\phi'$  is approximately 30°. The load spread angle is deemed not to change from the unreinforced to the reinforced case.

### 2.3.3.2 Unreinforced Static Analysis

If the deflections of the subgrade are to be small then the pressure exerted on it must be limited by the elastic bearing capacity,  $q_c$ , such that:

$$\sigma_v = q_c + \gamma h = \pi S_u + \gamma h$$

where  $\gamma h$  = the adjacent overburden stress

$S_u$  = undrained shear strength of the subgrade (kPa)

and by combining this with Equation 2.11 above

$$\pi S_u = q \left( \frac{WL}{(W+2h\tan\alpha)(L+2h\tan\alpha)} \right) \quad (2.12)$$

Thus a solution to  $h$  can be found.

### 2.3.3.3 Reinforced Static Analysis

In the reinforced case the stress imposed upon the subgrade is permitted to rise to the ultimate, or plastic value of  $(\pi+2)S_u$ . This change in the value of bearing capacity adopted is not properly justified but it will be shown later, in Chapter 2.3.5, that the inclusion of the geosynthetic alters the nature of the stresses applied to the subgrade and thus in the "fully" reinforced case a bearing capacity of  $(\pi+2)S_u$  is a fair assumption. Chapter 2.3.5 also defines "full" reinforcement.

Therefore, in the reinforced case the maximum stress that can be imposed upon the subgrade is  $(\pi+2)S_u+\gamma h$ , and it is this increase in bearing capacity, from  $\pi S_u$  in the unreinforced case, which produces most of the benefit attributed to the geosynthetic.

However, at large rut depths, the membrane effect will start to affect the stress on the surface of the subgrade. Thus the maximum permissible stress at the base of the aggregate layer can exceed the maximum permissible on the surface of the subgrade such that:

$$\sigma_v = p+p_r \quad (2.13)$$

where  $p_r$  = the reduction in vertical subgrade stress attributable to the membrane effect (kPa)

$p$  = vertical stress applied to the surface of the geosynthetic (kPa).

Unlike some analytical design methods where the shape of the membrane is described mathematically (eg Neiuwenhuis, 1977), the membrane is assumed to deform in the shape of a simple parabola. The strain, and therefore stress, induced in the geosynthetic is calculated by utilizing the properties of parabolas. The geosynthetic is assumed to take a concave parabolic shape under the wheel of length  $2a$  and a convex shape between the wheels of length  $2a'$ , as shown in Figure 2.7.

The authors make the assumption that no internal deformation occurs within the aggregate layer. Thus the vertical displacement(s) at the surface is mirrored at the aggregate/subgrade interface as shown in Figure 2.6. They further assume that the subgrade is incompressible and does not change volume during deformation. Hence

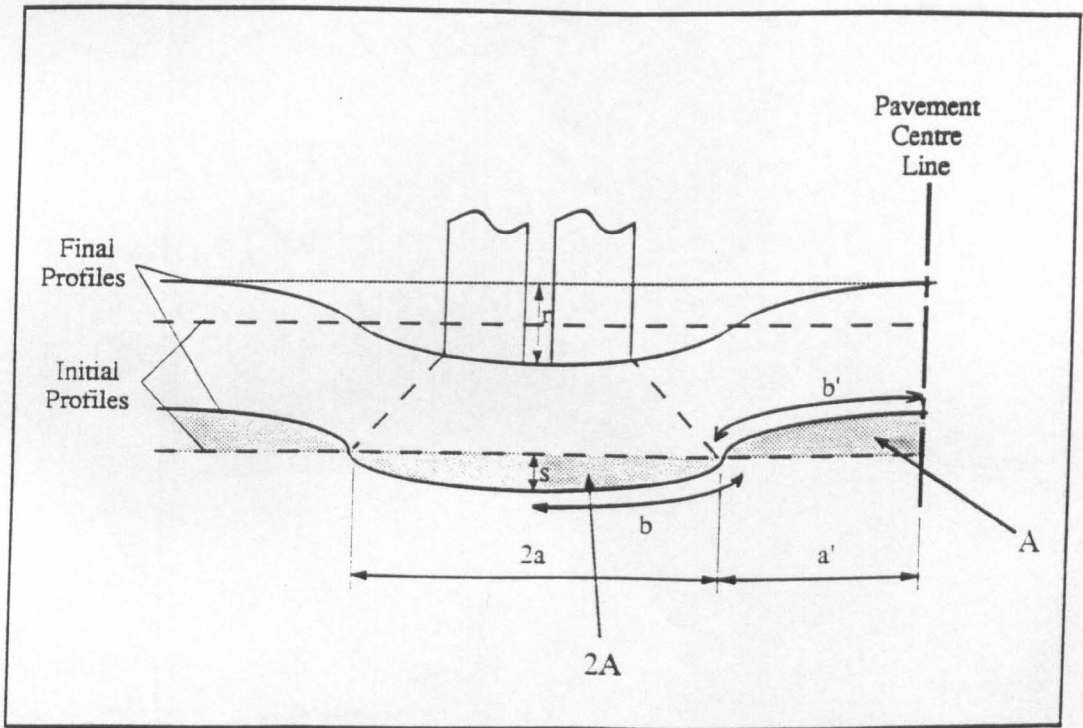


Figure 2.7 Geometry of the Deformed Profile  
After Giroud and Noiray (1981)

the volume of subgrade displaced from under the wheel paths is equal to the volume contributing to the hog between them.

For most (thin) pavements the dimension  $a'$  is greater than  $a$  and as a result of the assumption that the areas displaced from under the wheel equals the log between then the tension under the wheel path is therefore greater than between them. The authors then make the additional assumption that the overburden stresses in the  $a'$  area are insufficient to prevent slipping of the geosynthetic and hence the geosynthetic is in constant tension across the pavement. Thus the geosynthetic strain will be as shown in Equation 2.14.

$$\epsilon = \frac{b+b'}{a+a'} \tag{2.14}$$

where  $a$  = initial geosynthetic length  
 $b$  = final geosynthetic length  
 and the superscript ' = between the wheel loaded area.

The reduction in the pressure on the subgrade can be calculated by examining the angle the geosynthetic makes to the vertical ( $\beta$ ) at the edge of the loaded area.

$$ap_r = T \cos \beta \tag{2.15}$$

where  $T$  is the tension in the geosynthetic (kN/m)

According to the theory of the parabolas:

$$\tan \beta = \frac{a}{4s} \tag{2.16}$$

and as the tension in the geosynthetic is given as:

$$T = E\epsilon \tag{2.17}$$

where  $E$  is the geosynthetic stiffness (kN/m<sup>2</sup>)

$$p_r = \frac{E\varepsilon}{a\sqrt{1 + \left(\frac{a}{2s}\right)^2}} \quad (2.18)$$

Thus the stress permitted at the top of the aggregate layer is controlled by Equation 2.19 by combination of 2.18 and 2.11.

$$(\pi+2)S_u = q \left( \frac{WL}{(W+2htan\alpha)(L+2htan\alpha)} \right) - \frac{E\varepsilon}{a\sqrt{1 + \left(\frac{a}{2s}\right)^2}} \quad (2.19)$$

This leads to a required thickness of aggregate,  $h$ . By comparison to Equation 2.12 a saving of aggregate by including a geosynthetic is calculated and this saving is applied to the design of unreinforced pavements as calculated by reference to the work of Hammitt (1970). It must be highlighted that the thickness of aggregate,  $h$ , is that thickness required to resist the single application of a wheel load. The actual thickness required in any given pavement will be increased to allow for the affects of trafficking.

Chapter 8.6 gives the design calculation on this basis for the Tensar-reinforced pavements constructed at Bothkennar.

### 2.3.4 Reinforced Pavement Design - Typar Approach

The design approach used for Typar - a heat-bonded polypropylene non-woven used in Sections B & M is based on the work of Tonus (undated). It is essentially an empirical design based upon the work of Hammitt (1970). The design method, however, introduces the concept of aggregate restraint. Tonus believes that the geosynthetic provides restraint to the aggregate particles adjacent to it, preventing them from moving away from the loaded area. He considers this confinement to increase the aggregate's modulus and in turn decrease the stress on the subgrade below.

A series of empirically derived curves based on the square root of the axle load are presented, which are similar in form to Figure 2.4. From these an estimate of the required thickness of aggregate for 1000 passes of an axle for any given subgrade CBR can be established.

The design makes allowances for the number of load repetitions if different from 1000 in a similar format to Hammitt (1970) (Equation 2.4). For Tylar the traffic influence factor is set such that

$$f = 0.27\log N + 0.19 \quad (2.20)$$

This is slightly different to Hammitt's (1970) equation to allow for the benefit in service life due to the installation of Tylar.

Tonus (undated) further recognises that the life span of the pavement will depend upon the quality of the aggregate employed. A series of empirically derived "aggregate efficiency" factors are presented which for unbound materials range from 1.0 (Type 1 sub-base) to 0.4 (loose gravel).

In a similar manner to the Polyfelt design approach discussed in Chapter 2.3.2, emphasis is placed upon checking the survival of the geosynthetic through the installation and trafficking processes. However, in the case of Type 1 sub-base placed on all but the weakest of subgrades (<1% CBR) only the lightest grade of Tylar is required.

The expected permanent deformation is not given. At rut depths of a third of the pavement thickness the geosynthetic is thought to be under sufficient tension to be generating some membrane type of reinforcement but this is not quantified within the design method. It is suggested that at this rut depth the ruts are filled with fresh material.

### **2.3.5 Reinforced Pavement Design - The Oxford Approach**

The majority of the improvement in performance predicted by the Giroud & Noiray (1981) design method was caused by the arbitrary shift from a bearing capacity of  $\pi S_u$  in the unreinforced case to  $(2 + \pi)S_u$  in the reinforced. Milligan et al (1989a) noted that when a vertical load is applied to the surface of a granular layer over a finite width, the increase in horizontal compressive forces is partly resisted by earth pressures and partly by shear stresses on the aggregate/subgrade interface. Shear stresses on the surface of the subgrade can reduce the bearing capacity by up to one half of the value that could be obtained for purely vertical loading (see below). If the inclusion of a geosynthetic leads

to the transferring of all of the shear stress, which would otherwise have been carried by the subgrade, to the geosynthetic, then purely vertical forces are transferred to the subgrade below. Thus, the full bearing capacity can be mobilized and this is termed the "fully reinforced" case.

### 2.3.5.1 Bearing Capacity

If the shear stress at the aggregate/subgrade interface is  $\tau$  and the vertical subgrade stress under the wheel load is  $\sigma_v$ , and away from the wheel load  $\gamma h$ , then the solution of the upper and lower bound theorems of plasticity theory gives the exact solution.

$$\frac{\sigma_v - \gamma h}{S_u} = N_{ca} = 1 + \frac{\pi}{2} + \cos^{-1}\psi + \sqrt{1 - \psi^2} \quad (2.21)$$

where  $\psi$  is a non-dimensional parameter  $\frac{\tau}{S_u}$   
and  $N_{ca}$  is the available bearing capacity factor.

It should be noted that when the shear stress applied to the surface of the subgrade,  $\tau$ , equals 0,  $\psi = 0$  and so  $N_{ca} = (2 + \pi)S_u$ ,

and that when  $\tau = S_u$ ,  $\psi = 1$  and so  $N_{ca} = \left(1 + \frac{\pi}{2}\right)S_u$

It can be seen that Giroud & Noiray's (1981) assumption that the bearing capacities of  $\pi S_u$  in the unreinforced case and  $(2 + \pi)S_u$  in the reinforced, bear close similarities to this more rigorous treatment of the subgrade properties.

However a range of possible subgrade shear forces are possible depending upon the geometry and properties of the system and therefore a range of values of  $\psi$ , and thus bearing capacities, are permissible. This is shown in Figure 2.8 as the lines A,B,C,D.

### 2.3.5.2 Stress Distribution Through the Granular Layer

Figure 2.9 shows the stress distribution through the aggregate layer. It should be noted that a load spread angle ( $\alpha$ ) is again utilised which yields a stress imposed upon the subgrade ( $\sigma_v$ ) of:-

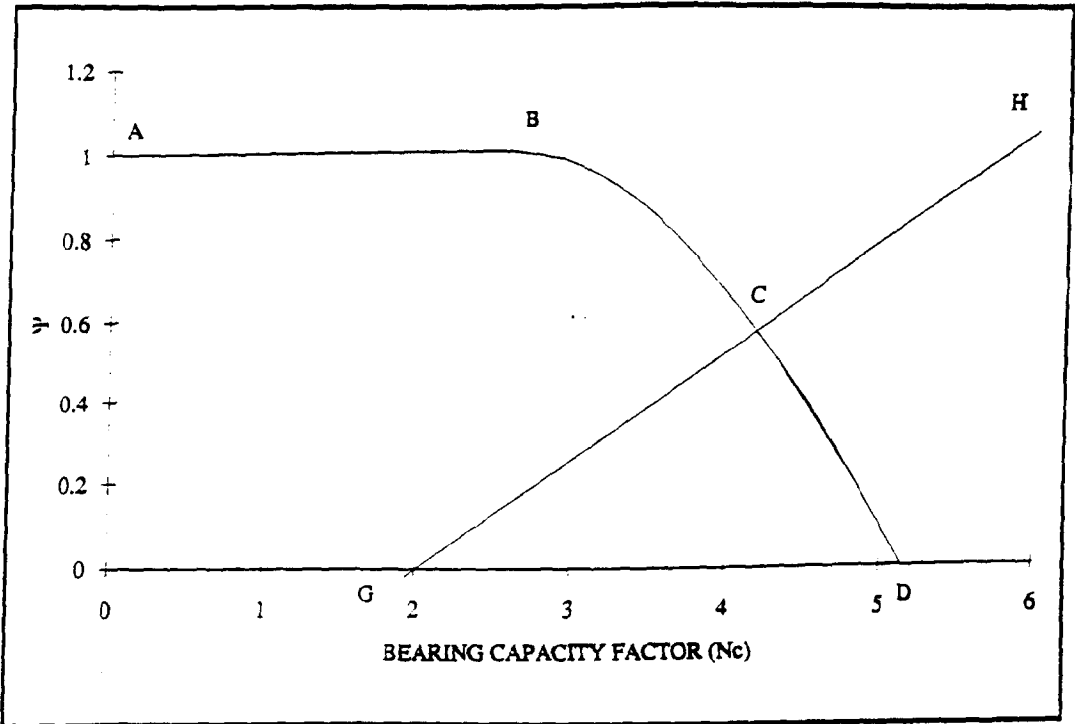


Figure 2.8 Interaction Diagram - After Milligan et al (1989a)

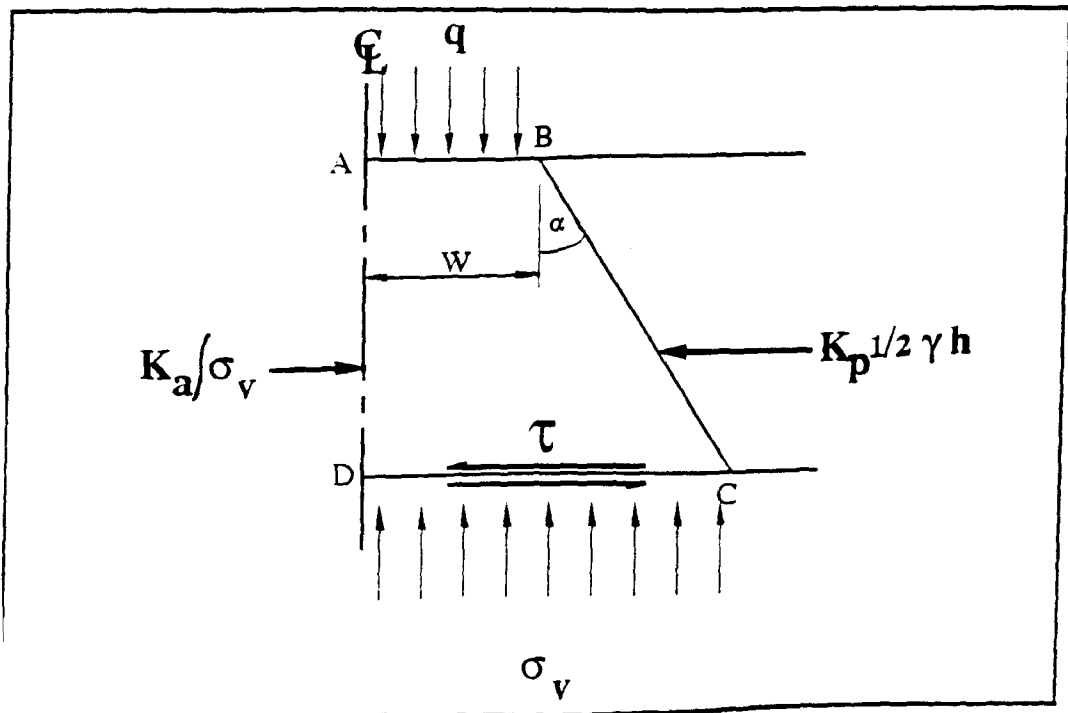


Figure 2.9 Stress Distribution - After Milligan et al (1989a)

$$\sigma_v = q \left( \frac{W}{W + 2h \tan \alpha} \right) + \gamma h \quad (2.22)$$

where  $W$  = footing width

$q$  = contact stress

This is the same as Equation 2.11 except that a plane-strain rather than a three dimensional formulation is used. As can be seen in Figure 2.9 active earth pressures are developed along the centre line as the driving force of the wheel load attempts to move the aggregate out of the wheel path.

If the active earth pressure coefficient,  $K_a$ , is defined such that:

$$K_a = \frac{1 - \sin \phi'}{1 + \sin \phi'}$$

where  $\phi'$  = the angle of the internal friction of the subgrade material

then it can be seen that the force on the surface AD on Figure 2.9 is given by Equation 2.23.

$$K_a \int \sigma_v dh \quad (2.23)$$

By substituting Equation 2.22 into Equation 2.23 it can be seen that:

$$K_a \int_0^h \sigma_v dh = K_a \gamma h^2 + \frac{K_a q W/2}{h \tan \alpha} \ln \left( \frac{W/2 + \tan \alpha}{W/2} \right) \quad (2.24)$$

These active forces are resisted by both the passive resistance and the shear forces at the aggregate/subgrade interface. The passive resistance is a maximum at the base of the aggregate layer and is equal to as  $K_p \gamma h^2$  where the passive earth pressure coefficient  $K_p$ , is defined such that:

$$K_p = \frac{1 + \sin \phi'}{1 - \sin \phi'}$$

So, as the shear stress at the aggregate/subgrade interface is the difference of the active and passive forces:

$$\tau(W/2 + h \tan \alpha) = \frac{1}{2} (K_a - K_p) \gamma h^2 + \frac{K_a q W/2}{\tan \alpha} \ln \left( \frac{W/2 + h \tan \alpha}{W/2} \right) \quad (2.25)$$

By taking the minimum value of active force and the maximum value of passive force. Equation 2.25 provides a means of obtaining the minimum value of  $\tau$  generated. However, passive forces usually require large strains to mobilize maximum values so it would appear likely that the value of the shear stresses will be higher.

Equation 2.25 can be expressed in a non-dimensional form by the substitutions

$$\psi = \frac{\tau}{S_u}$$

$$\text{and } N_c = \frac{q W/2}{S_u (W/2 + h \tan \alpha)}$$

Thus, Equation 2.25 becomes:

$$\psi = \frac{1}{2} (K_a - K_p) \frac{\gamma h^2}{S_u (W/2 + h \tan \alpha)} + N_c \left[ \frac{K_a}{\tan \alpha} \ln \left( \frac{W/2 + h \tan \alpha}{W/2} \right) \right] \quad (2.26)$$

which is the line GCH in Figure 2.8

For the unreinforced case, the appropriate design occurs at the largest available value of  $N_c$ , that is at the intersection point C in Figure 2.8. Having found the mobilized value for  $N_c$  the permissible surface stress,  $q$ , can be calculated as:-

$$q = N_c S_u \left( \frac{W/2 + h \tan \alpha}{W/2} \right) \quad (2.27)$$

In the fully reinforced case the subgrade is subject to pure vertical loading and thus  $N_c$  takes a maximum value of  $2 + \pi$  and  $q$  is determined by Equation 2.27 using  $N_c = 2 + \pi$ .

The tension in the reinforcement should then be calculated as shown in Equation 2.28.

$$T = \tau (W + h \tan \alpha) \quad (2.28)$$

An example of this calculation method is shown in Chapter 8.8 for the sections constructed at Bothkennar.

### **2.3.6 Reinforced Pavement Design - Tensile Reinforcement Approach**

It has been observed by McGown et al (1990) that the inclusion of elements with tensile and bending stiffness at the aggregate/subgrade interface increases the bearing capacity of the system. A series of monotonic loading tests on a system containing clay, Polyfelt TS600, bamboo rods and Leighton Buzzard sand generated a group of results that showed that the increase in bearing capacity, over clay and sand alone, could be as high as 300%.

The tests were performed in a glass-sided tank of width 300mm with bamboo poles of 11mm diameter. The tests included 2, 4 and 8 poles covering 7%, 15% and 29% of the subgrade area respectively. Differing depth ratios were employed and settlement applied at 1mm per minute to a settlement ratio of 0.60.

The bearing capacity improvement from the inclusion of the bamboo rods could be utilized in many of the design methods mentioned but the validity of the concept under repeated loading was a subject for validation in the full-scale trials undertaken at Bothkennar.

## **2.4 REINFORCED PAVEMENT DESIGN - OTHER METHODS (SELLMIEJER 1990)**

During the course of the full-scale trials a new design method was published by Sellmeijer (1990). It is sufficiently different in some respects to those methods mentioned in Chapter 2.3 that a brief critique is offered here. It is a plane strain approach revolving around the calculation of wheel load, by examining the shear modulus of the aggregate layer and by solving the deflection equation. Sellmeijer argues that the stiffness of the aggregate layer far exceeds that of even the stiffest geosynthetics and, therefore, the inclusion does not directly improve the performance. However, there is a recognition that the inclusion improves the bearing capacity of the subgrade, but the failure stresses used are not defined.

Instead, the required properties of the geosynthetic are determined by considering the strain compatibility of the system. Under the vertical stresses imposed by the wheel load horizontal stresses are generated. This stress is at its maximum under the wheel and reduces to a residual value at some point away from the line of application of the vertical load. The change in horizontal stress results from the frictional resistance at the aggregate/geosynthetic interface which generates forces, and hence strains, in the geosynthetic.

The change in horizontal stress also generates horizontal strains in the aggregate layer and, according to Sellmeijer, the most efficient design occurs when the strains in the geosynthetic and aggregate are matched, which yields a well defined stiffness requirement from the calculated stresses and strains in the geosynthetic.

### **2.4.1 Stress Distribution**

#### **2.4.4.1 Vertical Stress**

The assumed vertical stress distribution on an element is shown in Figure 2.10. It can be seen that the aggregate is assumed to undergo shear strain which is resisted by the shear modulus of the aggregate. Furthermore, there is assumed to be a frictional component between the aggregate and the geosynthetic and cohesive and frictional components between the subgrade and the geosynthetic.

The geometrical layout is shown in Figure 2.11. At failure, the length over which the plastic vertical subgrade stress, ( $\sigma_v$ ), acts ( $b$ ) is determined by vertical equilibrium. The concept of a load spread angle is not utilised and indeed, if the subgrade shear stress,  $S_u$ , is high enough, the length  $b$  could be less than the width of the surface loaded area. The contact stress,  $q$ , is assumed, for the purposes of analysis, to act on the top of the geosynthetic over the same length as at the surface.

#### **2.4.1.2 Shear stress**

The shape of the deformed pavement is controlled by the shear modulus of the aggregate and can be found by the solving of Equation 2.29. The derivation of the solution comes from an examination of Figure 2.10 and is shown in Appendix 1.

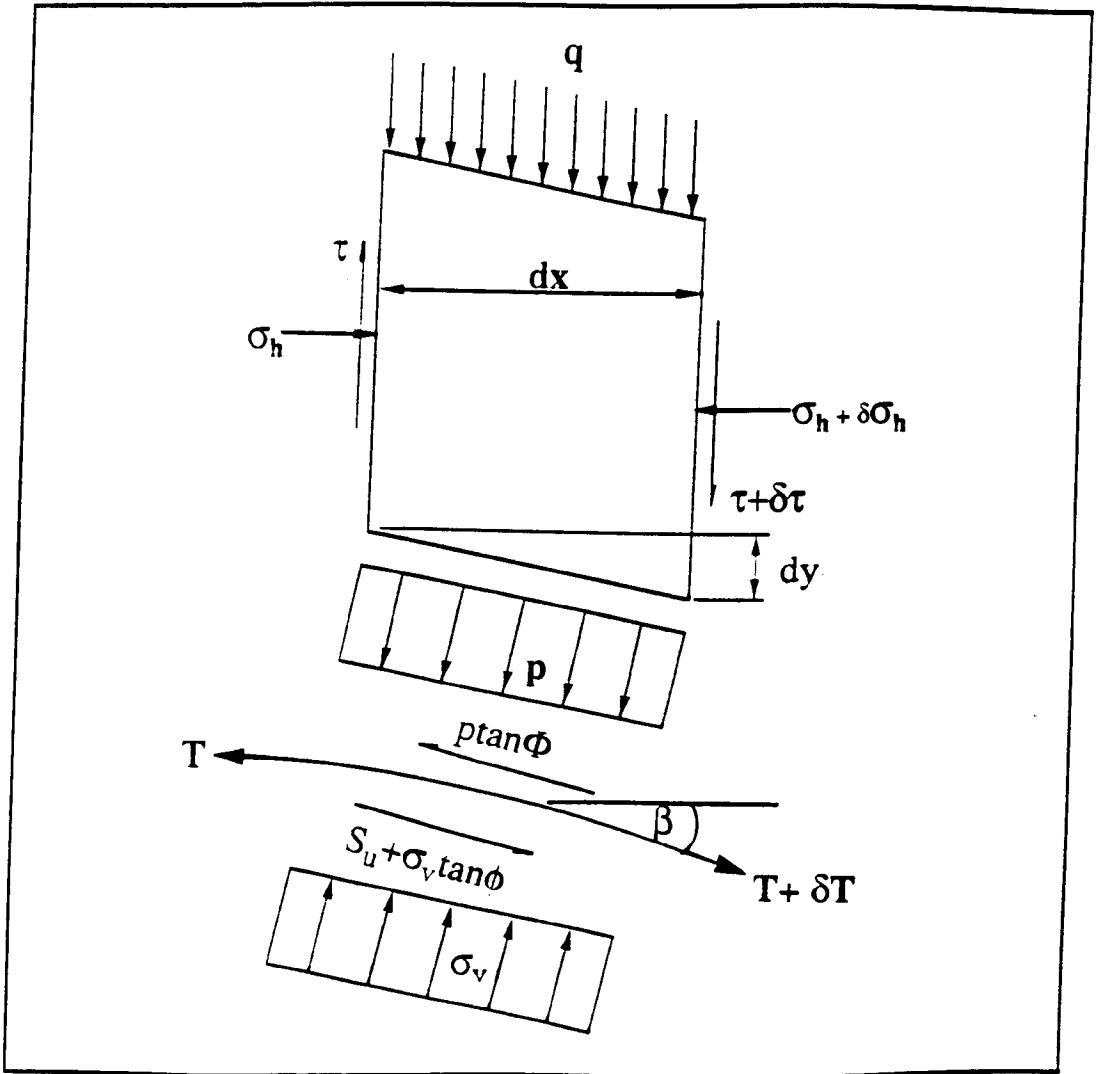


Figure 2.10 Forces Acting upon an Element - After Sellmeijer (1990)

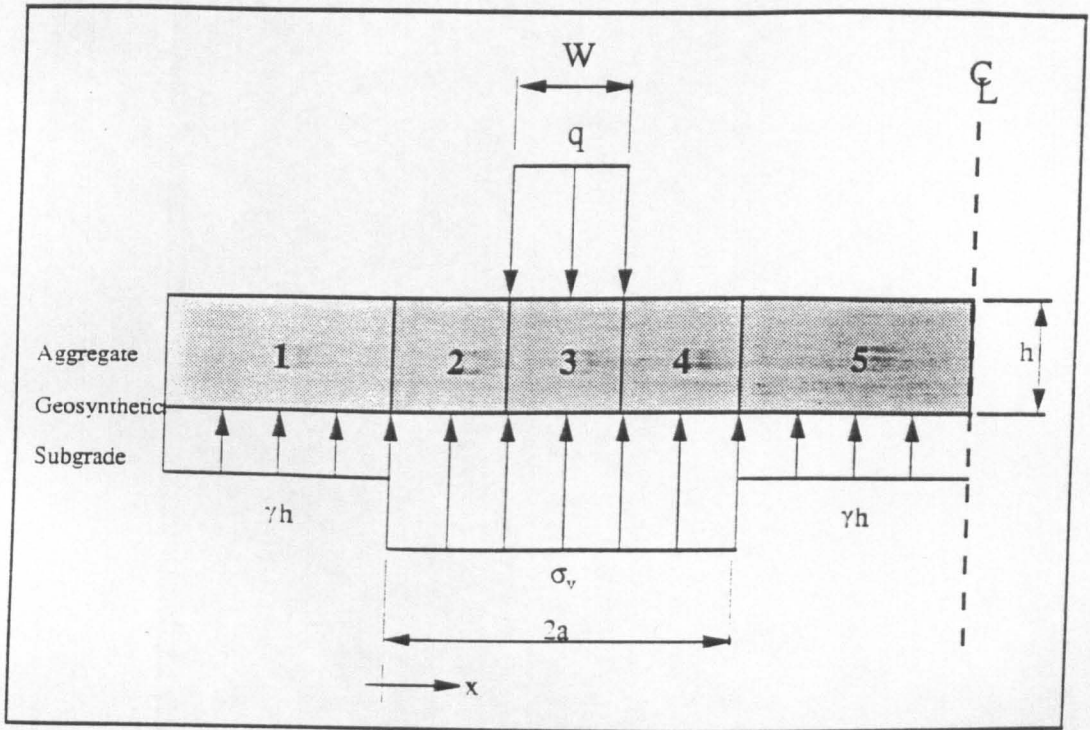


Figure 2.11 Geometrical Layout - After Sellmeijer (1990)

$$Gh \frac{d^2y}{dx^2} = \Delta\sigma_v - q \quad (2.29)$$

where  $G$  is the shear modulus of the aggregate layer (MPa).

It can be seen from Equation 2.29 that the solution will generate a catenary type of curve. It should be noticed that the deformation is controlled by shear modulus of the aggregate,  $G$ , and that no properties of the geosynthetic are considered. However, the inclusion is assumed to give a higher permissible value of subgrade vertical stress,  $\sigma_v$ , as in pavements including geosynthetics. Sellmeijer (1990) argues, a plastic bearing capacity can be developed, although the magnitude of this bearing capacity is not defined.

Equation 2.29 can be integrated twice to obtain the solution for the vertical deformation ( $\Delta w$ ) under the wheel load.

$$\Delta w = (b - W)^2 \frac{q}{8Gh} \frac{\Delta\sigma_v}{q - \Delta\sigma_v} \quad (2.30)$$

#### 2.4.2 Horizontal Stress

In order to prevent passive failure within the aggregate layer, the horizontal stresses generated by the imposition of the wheel load must be examined. The maximum horizontal stress that can occur at the interface of Sections 2 & 3 (as shown in Figure 2.11) will either be determined by the passive resistance of the aggregate at the interface coupled with the frictional resistance of the aggregate along the base of Section 2, or as a result of the stresses induced directly from the wheel load. The maximum stresses at these two interfaces are described by the Mohr's circles shown in Figures 2.12 & 2.13.

From Figure 2.13 the horizontal stress generated by the wheel load can be determined given by Equation 2.31 and an indication of its derivation is shown in Appendix 1.

$$\sigma_{h \max} = (\sec^2\phi' - 1) (\sigma_v + q) - \sec\phi' \sqrt{(\sigma_v + q)^2 \tan^2\phi' - \Delta\sigma_v^2 \left(\frac{b-W}{h}\right)^2} \quad (2.31)$$

where  $\sigma_h$  = the horizontal stress in the aggregate layer (kPa).

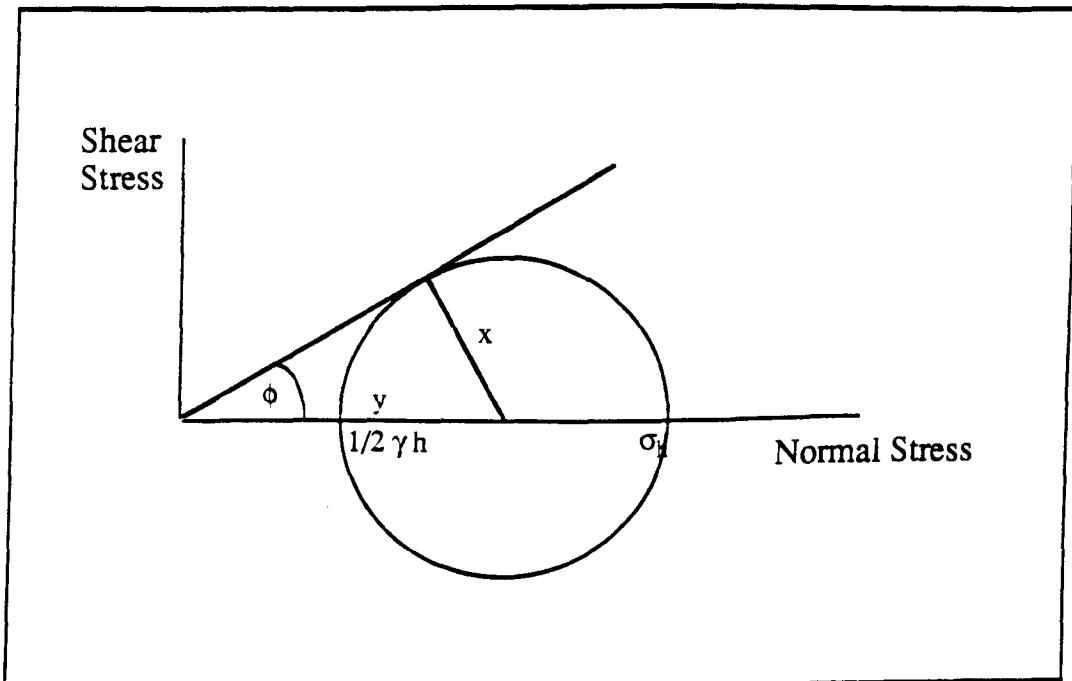


Figure 2.12 Mohr's Circle for Stresses at mid-height in the aggregate at the Junction of Sections 1&2 - After Sellmiejer (1990)

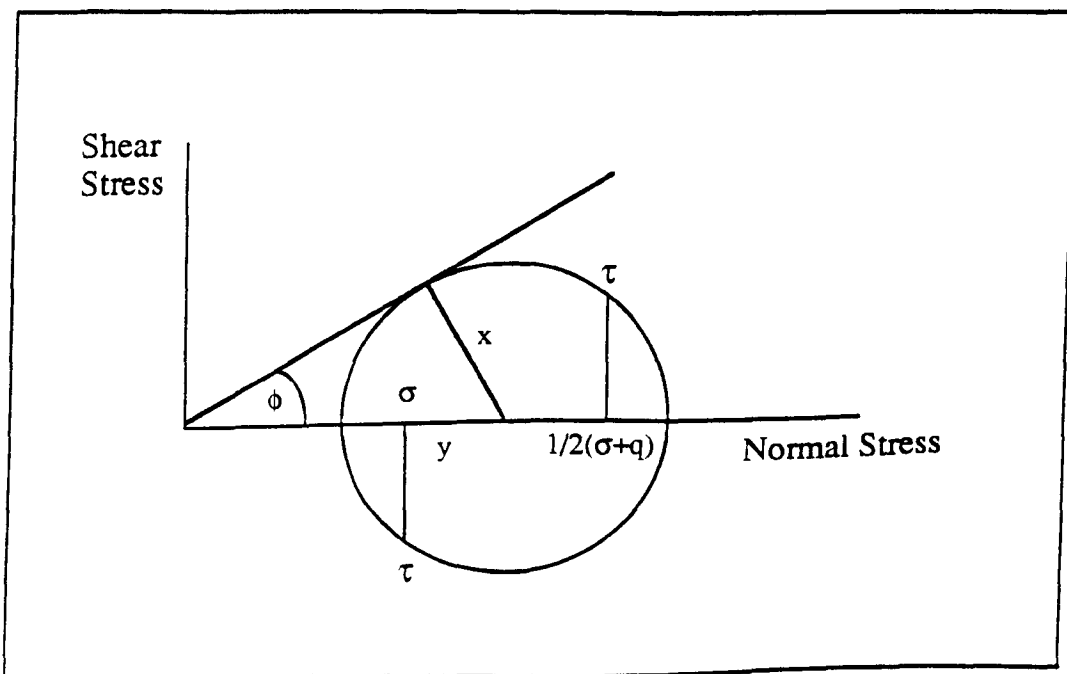


Figure 2.13 Mohr's Circle for Stresses at mid-height in the aggregate at the Junction of Sections 2&3 - After Sellmiejer (1990)

Sellmeijer (1990) argues that if the pavement is not to fail as a result of the aggregate layer then the horizontal stress determined in Equation 2.31 should not cause passive aggregate failure at the junctions of section 1 & 2. Thus the maximum horizontal force is further limited by Equation 2.32 and the design calculations should check that this restraint is not exceeded.

$$\sigma_{h \max} = \frac{1}{2} \frac{(b - W)}{h} \sigma_v \tan \Phi + \frac{1}{2} \gamma h \frac{1 + \sin \phi'}{1 - \sin \phi'} \quad (2.32)$$

where  $\Phi$  = the aggregate/geosynthetic friction angle.

### 2.4.3 Strain Compatibility

Sellmeijer (1990) argues that for an efficient design, the strain induced in the aggregate layer should be matched to the strain induced by tension in the geosynthetic. This leads to specific stiffness requirements for the geosynthetic, too stiff and the resulting design is likely to be inefficient, not stiff enough and the surface deformations will increase. The equations for calculating the strain compatibility of the aggregate and geosynthetic are complex, but an indication of their derivation is given in Appendix 1.

## 2.5 DISCUSSION OF DESIGN METHODS

The purpose of this discussion is to highlight the key elements of unreinforced and reinforced design. Many of the design methods have similar elements and will be discussed in turn. Furthermore, an indication is given as to which of the elements could be validated as a result of full-scale trials and which will have to remain for theoretical debate.

### 2.5.1 Unreinforced Pavement Design

The design of unsurfaced, unreinforced pavements relies on the empirical data of Hammitt (1970) and Webster & Watkins (1977). The data supporting the prediction of conditions which would yield a 0.075m rut are reasonably comprehensive, however, the data to predict rut depths not equal to 0.075m is a little more sparse. There is a

large degree of scatter in Hammitt's (1970) data which concentrates on pavements of relatively short life expectancies (generally less than 300 passes). However, at this time, models predicting the deformations that will occur within the aggregate layer and subgrade are likely to be less accurate than for Hammitt's data base.

There is an implicit assumption in most of the design methods that the reinforced pavement can provide aggregate savings over the unreinforced case and following on from this that a reinforced pavement can be expected to deform in a similar manner to a thicker unreinforced one. This is a reasonable assumption if one assumes that the inclusion itself does not affect the mechanism of the deformation. It is difficult to validate this assumption but in order to use the empirical data of Hammitt (1970) the assumption has to be made. Such existing data as there is does not contradict the assumption.

From the work done by Hammitt (1970) on pavements not including geosynthetics, it is possible to predict the thickness of aggregate such that a given number of passes will generate a 0.075m rut. In any full-scale trial, the axle load and number of passes applied are easy to obtain and the CBR of the subgrade can be accurately determined either by direct measurement or by conversion from subgrade shear strength or stiffness. Thus the validation of the design method as the aggregate layer thickness against the development of permanent deformation with passes should be relatively straight forward.

## **2.5.2 Reinforced Pavement Design**

### **2.5.2.1 Bearing Capacity**

Most of the reinforced pavement methods described above suggest that the inclusion of geosynthetics at the base of the aggregate layer changes the bearing capacity of the system. Many of these assumptions are empirical, based upon experimental observation although some are based on analytical calculation of the layered system. A summary of bearing capacity and improvement factors obtained from both of these methods are shown in Table 2.1.

Author	Unreinforced	Reinforced
Giroud & Noiray (1981)	3.14	5.14
Milligan et al (1989a)	$(1+\pi/2) \min$	$2+\pi$
Sellmeijer (1990)	Elastic (undefined value)	Plastic (undefined value)
McGown et al (1990) for Polyfelt & bamboo	1*	up to 3*
Resl & Werner (1986) for Polyfelt	1*	1.15*
De Groot et al (1986)	3	5
Bender & Barenberg (1978)	3.3	6
Steward et al (1977)	2.8	5

\* Improvement Factors

**Table 2.1 Bearing Capacity & Improvement Factors Used in Design Methods.**

Generally the design methods assume that the bearing capacity is limited to some elastic value in the unreinforced case and by some plastic value in the reinforced case. Milligan et al (1989a) suggest that plastic conditions always apply but that a variety of bearing capacities exist in the unreinforced case depending on the properties and geometry of the system and that in the fully reinforced case the lack of subgrade shear stress allows the full upper bound plastic solution to be applied. This appears to be the most sensible and rigorous treatment of the subgrade's properties. However, the assumption that any geosynthetic is going to have a miraculous effect on the bearing capacity appears flawed. There must be a range of reinforced bearing capacities varying between the unreinforced value and  $(2+\pi)S_u$  dependent upon the stiffness of the geosynthetic or, more particularly, its relative stiffness to the aggregate.

The inclusion of geosynthetics at the base of the aggregate layer does improve the bearing capacity of the system (as can be seen from the experimental and theoretical results summarized in Table 2.1). To repeat these tests in full-scale trials would be of little academic value. However, it should be highlighted that under trafficking, the pavements are generally not subjected to stresses exceeding the elastic condition. Permanent deformation occurs as a result of many applications of stress below this level. The use, therefore, of bearing capacity calculations or observations derived from monotonic loading should be treated with some caution in the repeated loading case seen in full-scale trials.

However, the prediction of permanent deformation resulting from trafficking is difficult to obtain. The monotonic approach may give some indication of the transient

performance of the pavements which, in turn, may or may not be related to the permanent condition.

### 2.5.2.2 3D/Plane Strain Analysis

The type of analysis used within the design methods is either three dimensional or plane strain. Both methods have their advantages and disadvantages as follows:

Three dimensional analysis (Giroud & Noiray (1981), Milligan et al (1989b)). The three dimensional approach more accurately models the transient loading of each wheel loading in that the stresses under the wheel load will be distributed through the pavement in this manner. However, this type of analysis does not model the permanent deformation which occurs as this is essentially plane strain.

Plane strain analysis (Milligan et al (1989a) etc). The plane strain approach more accurately models the permanent deformation of the system. However, as suggested above, three dimensional analysis more accurately reflects the actual stress distribution. Plane strain analysis is often less complex than the three dimensional alternative.

Hence, the type of analytical method is open to criticism which ever is chosen.

### 2.5.2.3 The membrane effect

Design methods which claim to be concerned with the contribution to the system of the membrane such as (Giroud & Noiray (1981) and Tonus (undated)) often make further assumptions about the bearing capacity of the subgrade. The reduction in vertical stress imposed upon the subgrade as a result of the tensioned membrane varies from nothing at low rut depths to little at even quite large deformations for all but the stiffest of geosynthetic (see Chapter 8.6). The amount of deformation that occurs in an unpaved road is subject to a large degree of scatter and it may be that the contribution that any membrane effect might make is significantly lower than this scatter.

Knowing the geosynthetic load/strain behaviour with time, an estimate of the value of the membrane effect could be calculated if the strain profile of the geosynthetic was

measured. So, the membrane effect should be straight forward to validate in full-scale trials.

#### 2.5.2.4 Separation

Although the value of separation is highlighted in many of the design methods (Resl & Werner (1986) and Tonus (undated)) especially those relating to less stiff geosynthetics, no analytical or empirical models exist for predicting the amount of aggregate that is lost to the subgrade in the unreinforced case. It is unfortunate that this is the case because separation is a function that all proprietary geosynthetics perform and is probably the principal mechanism by which less stiff geosynthetics benefit the pavement. It probably also represents a large proportion of the benefit obtained from including geosynthetics whose major role might otherwise be considered to be solely reinforcement. An examination of the subgrade aggregate interface after a series of full-scale trials might give some indication of the value of separation as an aggregate saving mechanism.

#### 2.5.2.5 Aggregate Properties

The role of the aggregate within the soil-geosynthetic-aggregate system is plainly important. The active and passive earth pressures generated within the aggregate are included within both the Milligan et al (1989a) and Sellmeijer (1990) models and the magnitudes of these developed stresses are controlled by the quality of the aggregate. The value of the aggregate quality is also recognised by Tonus (undated). Sellmeijer (1990) further argues that the shear modulus of the aggregate will influence the magnitude of the transient pavement deflection. However, the transient response of unpaved roads is unlikely to be of as much interest as the permanent deformation characteristics. The permanent deformations resulting from repeated loading are unlikely to be directly related to the transient responses and, therefore, calculations of the transient deformations are not as valuable as they might first appear.

The "stiffness" of the aggregate will effect the transient stress distribution to the subgrade (Peutz et al. 1968) and two methods mentioned above indicate that the earth pressure coefficients are also important. Thus, for full-scale trials the aggregate's properties require determination.

#### 2.5.2.6 Strain Compatibility

If it can be shown that no slippage occurs between the elements of the soil-geosynthetic-aggregate system then strain compatibility must exist within the system. Sellmeijer (1990) presents a method of calculating the strains that occur within the system and by equating them leads to a prediction of the stiffness of the geosynthetic required for an efficient design. The term efficient is ill-defined, but can be taken to mean the limiting stiffness of the geosynthetic, beyond which no further improvement in the performance of the pavement is possible.

## CHAPTER THREE

### BOTHKENNAR

#### 3.1 INTRODUCTION

The intention of this Chapter is to introduce the Bothkennar Soft Clay Site and to examine some of the engineering properties of the surface deposits on the site. A general description of the site is followed by a summary of its *raison d'être*.

The chapter includes details of the engineering properties of the crustal deposits at the site determined prior to, during and after the full-scale trials (Chapter 4). This data is compared to other work published during the course of the trials. Seasonal variation in the crustal properties is also presented.

#### 3.2 PURPOSE AND CHOICE OF SITE

A soft clay site was sought by the Science and Engineering Research Council for use as a national research facility. It was envisaged that research on soft clays might include studies involving large scale testing, site investigation and laboratory testing. It was hoped that by carefully documenting all of the work carried out on the site, a series of inter-relating case studies could be built up.

The original specification envisaged a green field site of approximately 5 hectares with a low risk of vandalism, a minimum of 10m of soft clay with a shear strength of less than 40kPa and, that the deposit should be uniform without significant peaty or sandy lenses.

Several general areas were considered for the site, notably the Severn and Forth Estuaries. Other areas were considered but were thought, for geological reasons, unlikely to produce a suitable site. Finally, the site at Bothkennar, on the banks of the Forth Estuary, was chosen as it most closely fulfilled the criteria required of a soft clay research test bed.

### 3.3 GENERAL DESCRIPTION

The site is situated on the south bank of the Forth Estuary immediately east of the Kincardine road bridge. The propensity of the site to flooding has led to it being used for grazing and hay production, at least over recent years. The site is surrounded on all sides by shallow ditches (which largely control the water table) and an artificial bank stands between the site and the Forth Estuary.

The site is used by a local farmer for grazing and hay production which keeps the vegetation in check. Users of the site need to protect low lying instruments and setting out markers from being damaged by, and causing damage to, agricultural machinery and livestock.

Superb office facilities have been provided by SERC at the site. The low-rise complex contains a workshop, shower block, kitchen, instrument workshop and a small conference room/office with fax, telephone and photocopying facilities. Further conference facilities are available from neighbouring Powfowlis Manor Hotel.

A large hardstanding area has been provided at the entrance to the site.

### 3.4 GEOLOGY

The geology of the area surrounding the Bothkennar Soft Clay site consists of a synclinal carboniferous basin centred on Grangemouth (Fig. 3.1.). This is overlain by glacial deposits consisting of stiff boulder clay, followed by post-glacial soft marine clays and loose silts. Relative sea level rose in the post-glacial period when the marine and estuarine clays were deposited on the site. Isostatic uplift of the area was continuing at a diminishing rate during this period, raising the deposits above sea level (Gostelow & Browne, 1986).

The engineering geology was described by Paul et al (1991) and can be summarized as follows:

It is possible to divide the marine sediment at Bothkennar into four categories, bedded, laminated, mottled and weathered. The sediment originated by tidal transport and the sedimentary structures are recorded by the bedded layers which range in thickness from a few millimetres to 10 centimetres. Local, more energetic conditions led to laminated

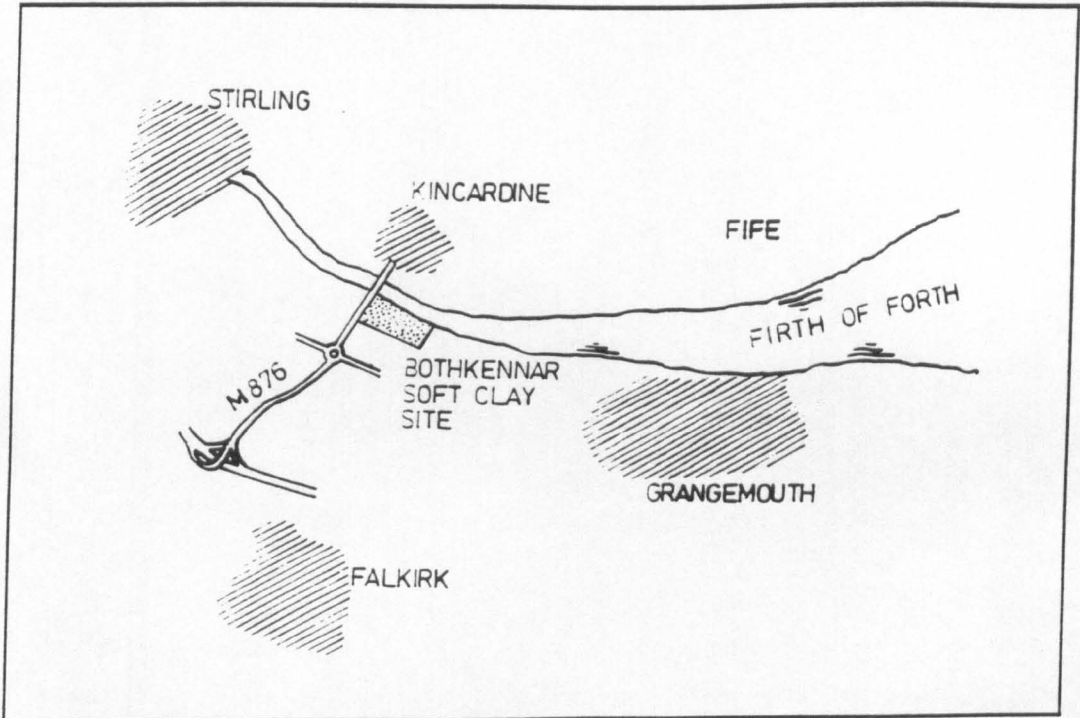


Figure 3.1 Location of the Bothkennar Soft Clay Site

layers while reduced rates of sedimentation allowed burrowing organisms to re-work the deposit, causing the mottled appearance. Weathering and desiccation occurred when the sediment was exposed to the surface elements and is restricted to the top 3m of the site.

The grain size is uniform with depth and the clay minerals are kaolinites and illites. The silt fraction contains quartz, feldspar and ferromagnesium materials. Clay represents between 35 and 45% of the deposit, the rest being mainly silts. The organic content is, on average, 2-3% of dry weight and is thought to be the residue of soft bodied organisms, mostly in the form of oils and fats. It is these residues which are thought to improve the plasticity of the material above that which could be expected from its silt content.

### 3.5 ENGINEERING PROPERTIES OF THE SURFACE DEPOSITS.

In order to determine the engineering properties of the clay at Bothkennar, a series of index and other tests were performed. Some of these were performed in the field such as hand held shear vane tests to determine subgrade shear strength (see Section 3.6.), but a range of samples were recovered for laboratory testing, as detailed below.

The layout of the site is described in Chapter 4 but, briefly, each section of trial pavement was 20m long with an instrumentation reading location at 5m and 15m into each section. Some tests were performed at one location in each section (ie at 20m centres) and others at each reading location (ie at 10m centres).

#### 3.5.1 Samples Recovered from Surface Deposits at Bothkennar

Samples of the subgrade at Bothkennar were recovered at the time of construction from depths of 300mm, 500mm and 600mm below surface level. The moisture content of each sample was determined at the earliest opportunity in order that further moisture loss was minimized. The results of the moisture samples are shown in Appendix 2 and can be seen to vary between those parts of the trials that were constructed at the start of the programme, during high summer of 1989, and the end of the construction phase in the following autumn.

Bulk samples: The bulk samples of subgrade soil were recovered from the side of the trial pavement formation (underside of topsoil) at each reading location. The samples were hand dug from a pit 200 x 300 x 350mm deep and were transported to the laboratory in heavy duty plastic bags sealed by a wire crimp. The samples did not dry out significantly between excavation and subsequent index testing.

38mm diameter triaxial samples: Three 38mm diameter samples were recovered from the formation level (underside of topsoil) at each reading location at the time of construction; one each from the left hand side, centre line and right hand side of the formation. The sample tubes were sealed with wax, capped and stored in a high humidity room until required for quick undrained triaxial testing, as described in Chapter 3.5.2.

U100 samples: U100 samples were recovered at the time of construction by pushing the U100 tubes into the subgrade at formation level with the rear bucket of a JCB3C excavator. The ends were sealed with wax and the tubes were stored in a high humidity room in the laboratory. Some of the samples were extruded to form 38mm diameter triaxial samples if the 38mm diameter samples discussed in the previous paragraph were found to be unsuitable due to collapse on extraction or being too short for testing. Others were used to familiarise the author with the 76mm diameter triaxial apparatus. Finally all of the remaining samples were opened and split to examine the fabric of the material an example of which is shown on Plate 3.1. The description of these split samples were found to be the same as described by Paul et al (1991) and discussed above.

Post trafficking samples: Further U100 samples were recovered in a similar manner to that described above at the end of trafficking from those sections where the geosynthetic was exhumed. These were recovered from formation level in the wheel path and were sealed with wax on site to maintain the in-situ moisture content. They were stored in a high humidity room until they were used for resilient modulus and shear strength testing as described in Chapter 3.5.2.



**Plate 3.1 - A Split U100 Sample Retrieved From Bothkennar**

### 3.5.2 Index Testing

Atterberg limits: Liquid and Plastic Limits were determined for samples taken from the bulk samples described above. The Plasticity Index and Liquid Limit results are shown in Figures 3.2 and 3.3 and the samples are identified by the section letter code plus the reading location from which they were taken (Figure 4.1). This is explained in greater detail in Chapter 4, Section 4.1.

Choice of samples for further analysis: It would have been impractical to perform a wide range of soil tests on the full range of soil samples and therefore, based on the results of the Atterberg Limit tests, a selection of soils was chosen for further study.

From the results presented in Figures 3.2 and 3.3 it appears that four slightly differing soils can be identified.

- a) A group of intermediate plasticity.
- b) A group of clays of high plasticity.
- c) A group of clays on the border of the two.
- d) A1' and A2 which appear to be in a class of their own although similar to the group of intermediate plasticity.

Some of the subsequent testing was extended to include samples A1' and A2 but for some of the tests this soil group was not included, on the grounds of cost or time, and was then presumed to be included in the clays of intermediate plasticity. Because the results on the samples A1 and O2 were so far removed from other results these soils were tested again yielding the results nominated A1' and O2'. Perhaps some sampling error had occurred because the subsequent results fitted the rest of the data more satisfactorily and hence were considered to fit the other groupings.

Subgrade particle size analysis: The method chosen from BS1377 (1975) to undertake particle size analysis was the sedimentation (Pipette) method. This test was performed on four subgrade samples, one from each of the groups a) to d) above, and the results are shown in Figure 3.4.

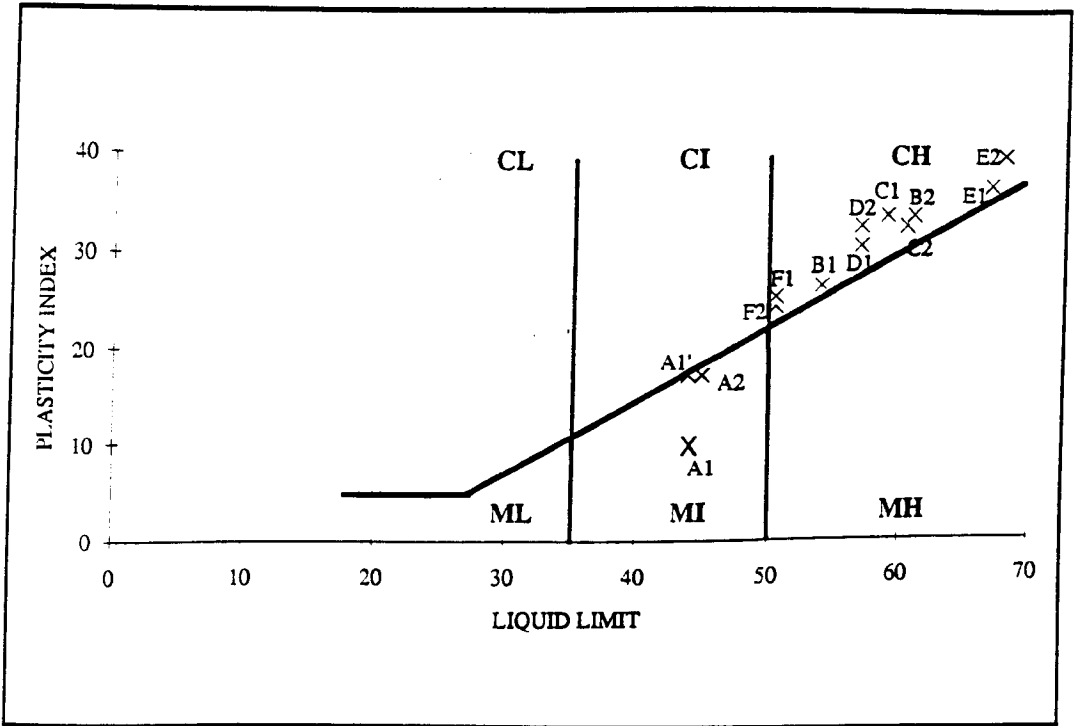


Figure 3.2 Plasticity of Samples from Upper-bound Sections A to E

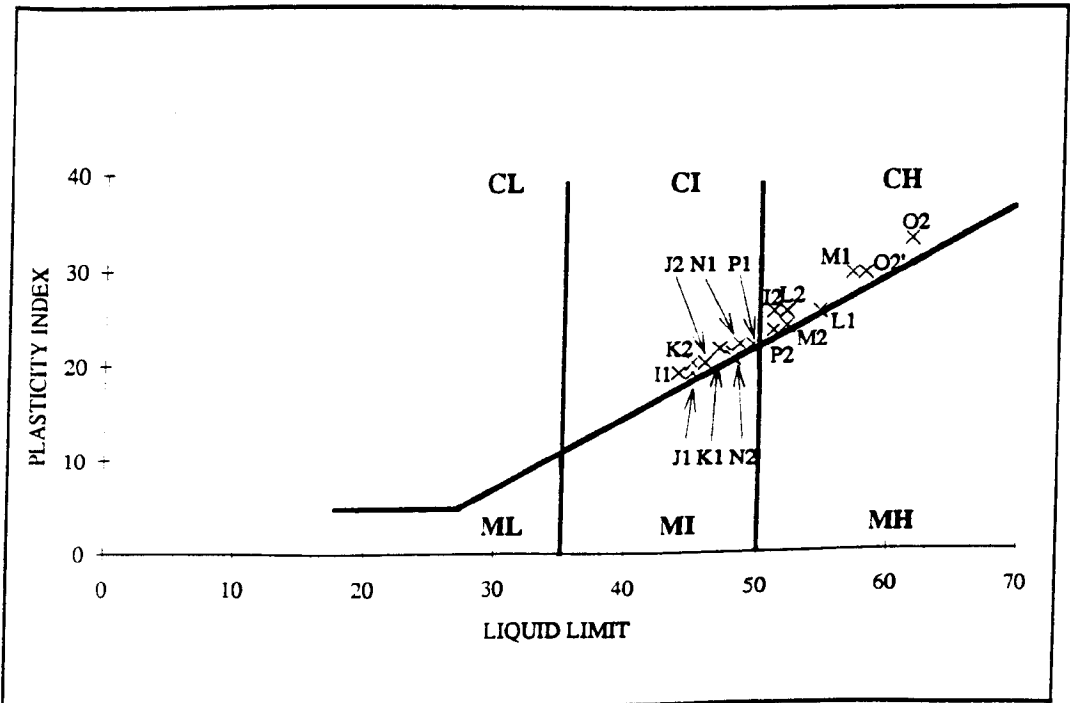


Figure 3.3 Plasticity of Samples from Lower-bound Sections I to P

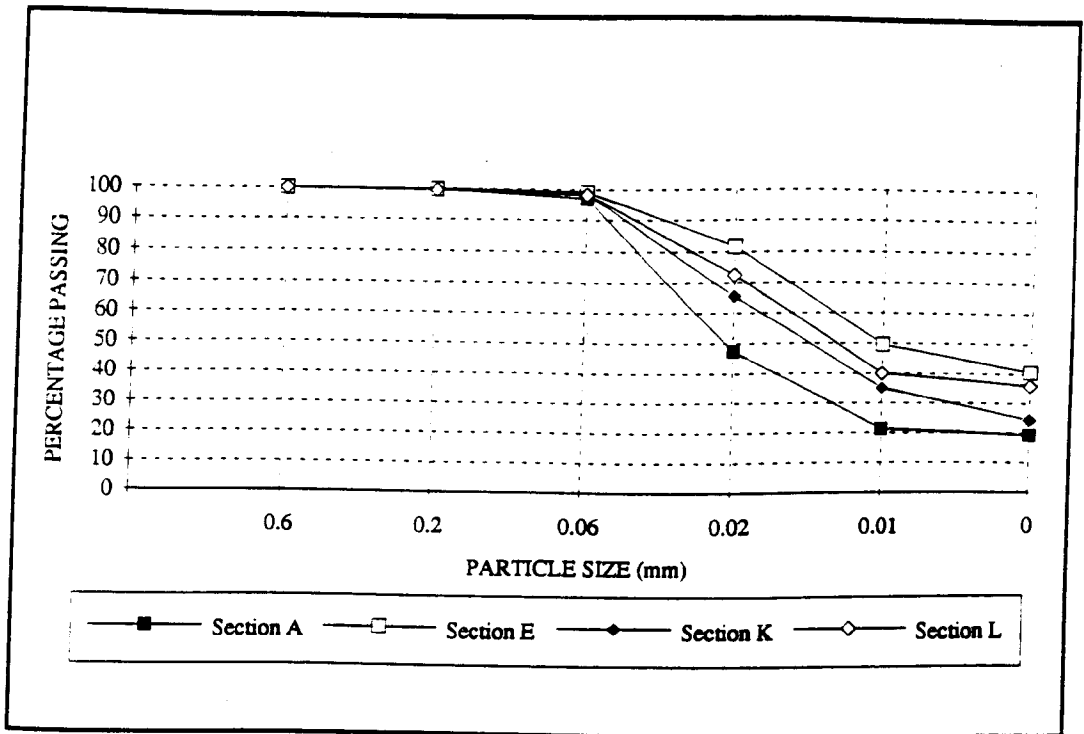


Figure 3.4 Subgrade Particle Size Analysis - After BS 1377 (1975)

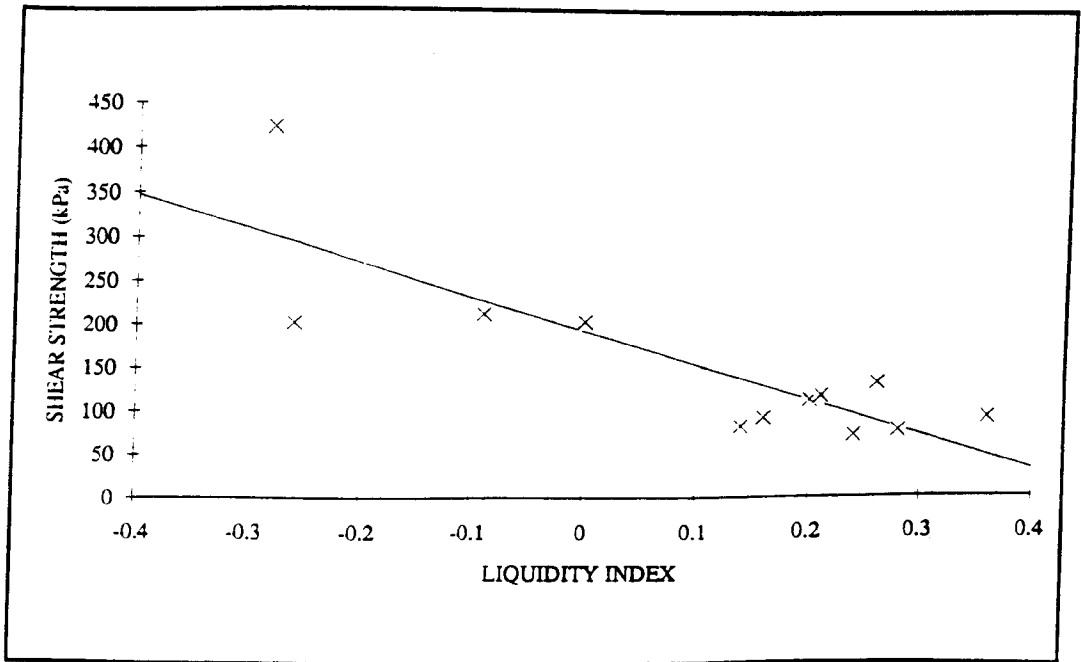


Figure 3.5 Undrained Shear Strength and Liquidity Index  
38 mm Diameter Triaxial Results

Organic content: The organic content of four samples was determined in accordance with BS1377 (1975). The full results are shown in Table 3.1 and as can be seen are in fairly good agreement with those found by Paul et al (1991) who determined that the organic content of the material on the site was between 2 to 3%. As to be expected, the organic content for sections A to K with intermediate plasticity was lower (1.0% to 1.6%) than for sections E to L with higher plasticity (2.3%, 2.0%).

Sample Plasticity	Section Code	Organic Content
A	A1	1.0%
Intermediate	K1	1.6%
Intermediate/High border	E2	2.3%
High	L2	2.0%

**Table 3.1 Organic Contents of the Subgrade**

38mm diameter triaxial results: Standard 38mm diameter quick undrained triaxial tests at confining stresses of 10, 20 and 40kPa were performed on 35 samples. The results were plotted as undrained shear strength against Liquid Index (obtained from the determination of Atterberg Limit on adjacent samples) (Figure 3.5) in the expectation that there should be a relationship between the two and that a first estimate of the on-site shear strength could be accomplished by determination of the moisture content of the subgrade. However, the scatter of the results led to some uncertainty as to the validity of estimated values. Regression analysis of Liquidity Index v undrained shear strength  $S_u$  showed that, for all samples, the coefficient of determination ( $R^2$ ) = 0.57 and that for the average values of each group of samples  $R^2 = 0.73$ . One reason for the scatter could be that the samples were disturbed on excavation and indeed 38mm diameter samples are prone to such disturbance. Thus, it was decided to use a hand held shear vane to determine the on-site shear strength of the subgrade.

Specific gravity of subgrade material: The specific gravity of the subgrade material was determined in accordance with BS1377 (1975). Four samples were tested and yielded a specific gravity of  $2.67 \pm 0.01$ .

### 3.5.3 Other Laboratory Tests

Resilient modulus determination: Four samples, recovered from the wheel path of the post trafficked pavement, were chosen for testing in the 76mm diameter repeated loading triaxial apparatus at the University of Nottingham (Loach 1987). The samples were chosen on the basis of being evenly spaced along the length of the lower-bound sections.

The samples were extruded in the laboratory and carefully pared down to a 76mm diameter. Each sample was then tested using an axial load cycling between 10 and 120kPa and a confining stress cycling between 15 and 66kPa. The frequency of the cyclic load was 1 Hertz and the number of cycles performed was approximately 2,000. The samples were not equipped with on-sample instrumentation and so only the confining stress, axial stress and axial strain were monitored: no measure of radial strain was recorded. Data was captured from the monitoring instruments, using an analog to digital device and a personal computer, in blocks of 25 cycles around 0, 1,000 and 2,000 cycles. Figures 3.6 to 3.9 show the stress strain relationships that the four samples exhibited during testing and a summary is shown in Table 3.2.

SAMPLE LOCATION	MOISTURE CONTENT %	BULK DENSITY kg/m <sup>3</sup>	MEAN INITIAL RESILIENT MODULUS (MPa)
H	32	1933	16.2
J	33	1854	16.3
L	34	2004	11.6
P	33	1912	14.0

**Table 3.2 Resilient Moduli ( $M_r$ ) of Lower-Bound Samples (MPa)**

It should be noted that the resilient modulus of the samples appears not to degrade with the number of cycles and that the incremental plastic axial strain that occurs with each cycle gets progressively smaller as the test continues.

Calibration of the hand held shear vane: Three of the 76mm diameter triaxial samples were subjected to a quick undrained triaxial test at the end of the cyclic testing programme. The results of the quick undrained tests are shown in Table 3.3 which is taken from the plots shown in Appendix 3. The fourth sample was destroyed during a

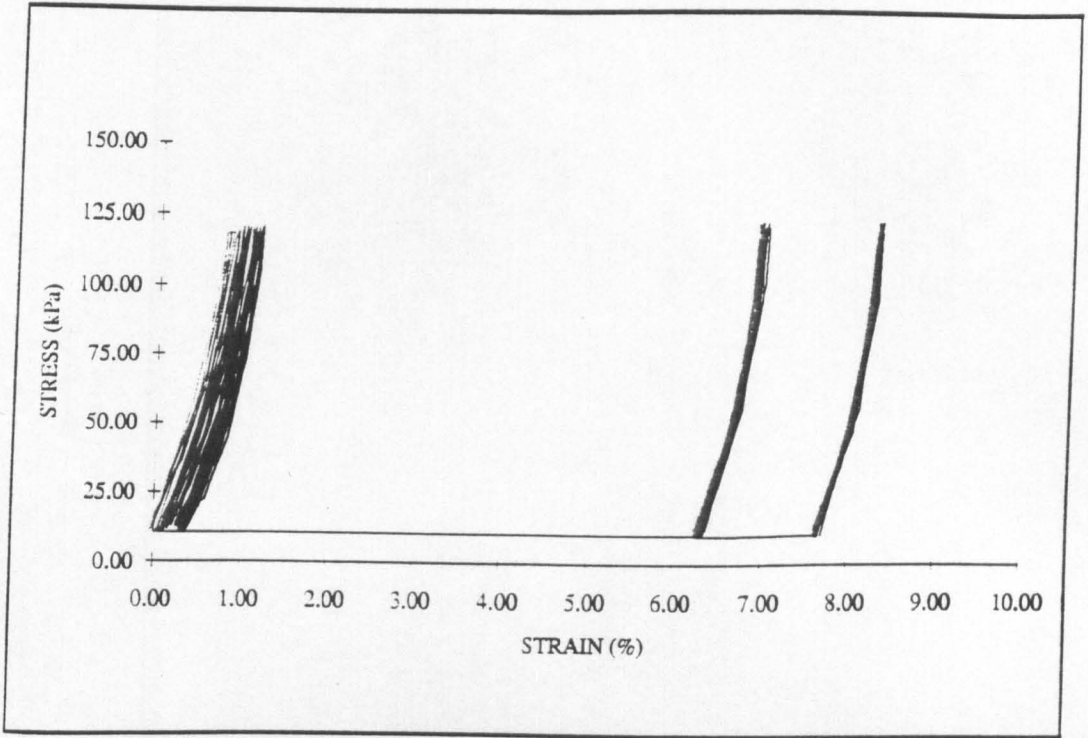


Figure 3.6 Repeated Load Triaxial Test - Section H

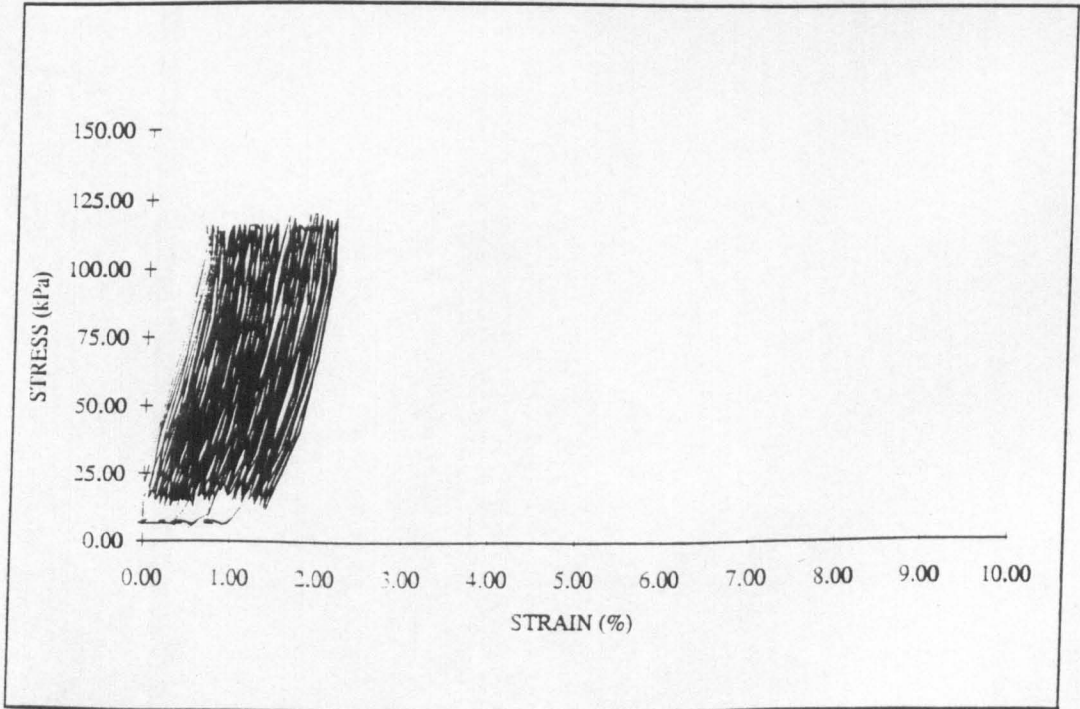


Figure 3.7 Repeated Load Triaxial Test - Section J

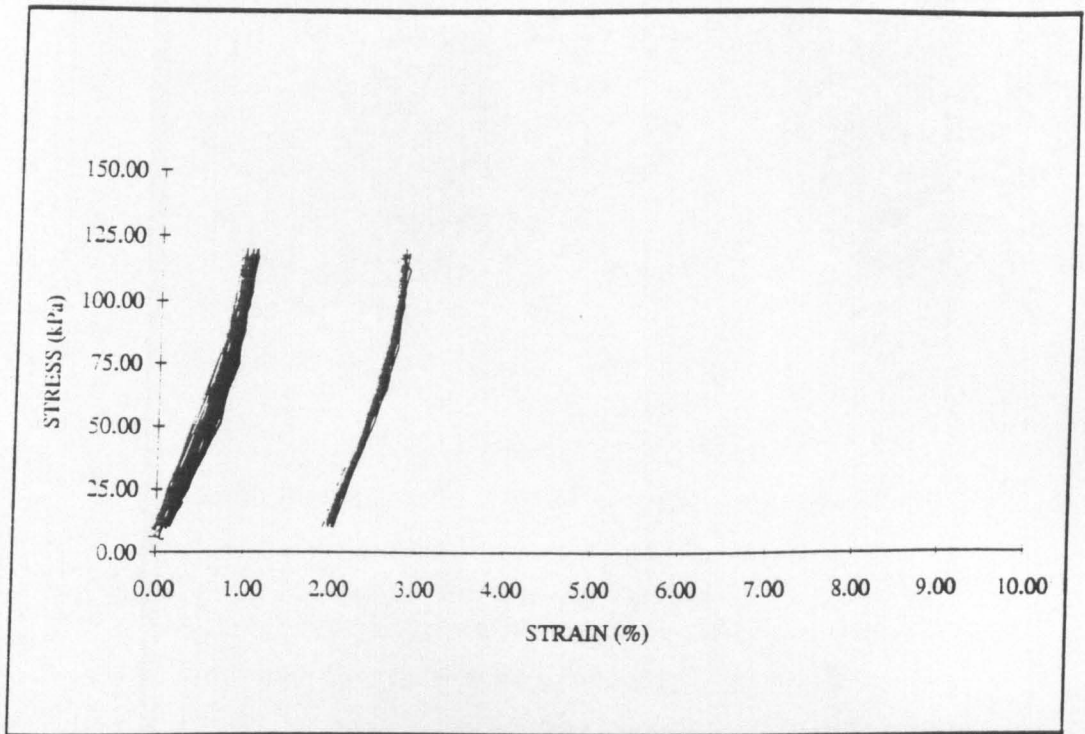


Figure 3.8 Repeated Load Triaxial Test - Section L

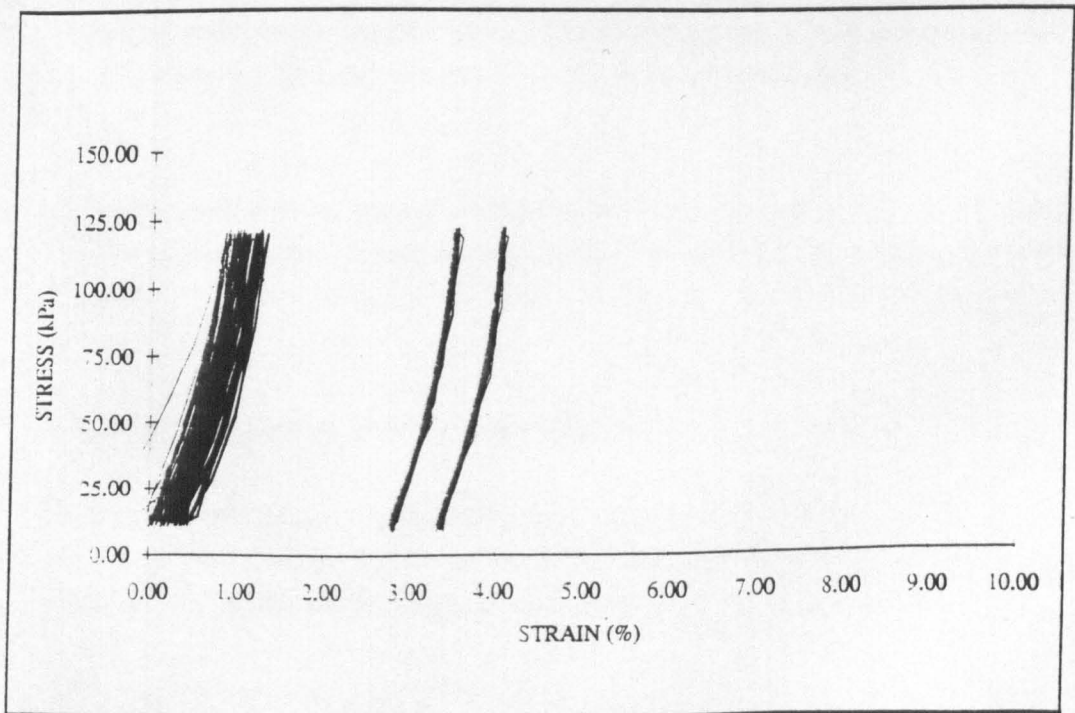


Figure 3.9 Repeated Load Triaxial Test - Section P

surge in the power supply to the triaxial equipment. The results of the quick undrained tests were compared to the mean values obtained from the hand held shear vane taken from around the sample before retrieval. As shown in Table 3.3 the two sets of results were in close agreement. These results, although a little sparse, led to some confidence in the large quantity of shear-vane-determined undrained shear strengths recorded during the course of the trials.

SAMPLE LOCATION	76mm DIAMETER TRIAXIAL (kPa)	HAND-HELD SHEAR VANE (kPa)	LIQUIDITY INDEX
H	81	82	0.35
L	85	77	0.24
P	77	76	0.20

**Table 3.3 Comparison of Quick Undrained Triaxial & Hand-held Shear Vane to Determine Subgrade Shear Strength**

Comparison of the Liquidity Index and shear strength parameters obtained from the 76mm diameter triaxial tests can be compared to those obtained in the 38mm diameter tests discussed earlier. It can be seen from Figure 3.5 that, for the Bothkennar Clay, we might expect that at a liquidity index of 0.30 the shear strength of the material would be around 80kPa. Thus, the two sets of results are in fair agreement.

CBR tests: Bulk samples were recovered for remoulded CBR tests in April 1989 at the in-situ moisture content. These showed that a CBR of 1% existed for the remoulded material.

### 3.5.4 In-Situ Testing During Construction

Shear strength readings were obtained at the time of construction, using a small hand-held shear vane of dimension 19mm by 28mm. Readings were recorded at depths of 30, 200, 300, 400 500 and 800mm at each reading location (see Appendix 2).

Three Clegg Hammer readings of the subgrade were taken at each reading location at the time of construction, as were six cone penetrometer readings. The results of these can be found in Appendix 2.

### 3.6 SEASONAL VARIATION IN CRUSTAL UNDRAINED SHEAR STRENGTHS.

During an initial visit to the site in April 1989 three small trial pits were excavated on the proposed line of the full-scale trials. It was found that the site had approximately 300mm topsoil covering it and that at a depth of 400mm below the surface of the site the undrained shear strength of the material, measured using the hand held shear vane, was around 45kPa. The shear strength profile with depth was not measured on this occasion.

The Summer of 1989 was hot and dry and the Winter of 1989/90 was also comparatively dry. Thus, shear strengths observed in April 1990 when trafficking commenced were higher than those seen in April 1989 when the initial site survey was performed.

The full-scale trials were constructed over two distinct periods, namely Summer and Autumn 1989. The undrained shear strength profiles with depth, as determined using a hand-held shear vane for those two periods are shown in Figures 3.10 and 3.11. It should be noted that the figures are in agreement with the results obtained by Paul et al (1991) as shown in Figure 3.15 in that over the first metre the subgrade undrained shear strength reduces.

The subgrade undrained shear strength was also determined during the trafficking periods of the Spring of 1990 and Spring 1991 and the mid-trafficking period, Autumn 1990, as shown in Figures 3.12, 3.13 and 3.14. It should be noted from Figures 3.10 to 3.14 that the undrained subgrade shear strength remains fairly constant at a depth of 1m at an average of 35kPa. The surface value, however, appears to fluctuate according to the season as shown in Figure 3.16. The surface is at its stiffest during the Summer, softening through the Autumn and at its softest in the Spring.

It was thought in advance of the trials that the Winter weather would produce the softest conditions in the Spring, prior to evaporation and transpiration drying out the site. The figures shown confirm this theory and so trafficking in the Spring appears to give the greatest possibility of soft subgrade conditions.

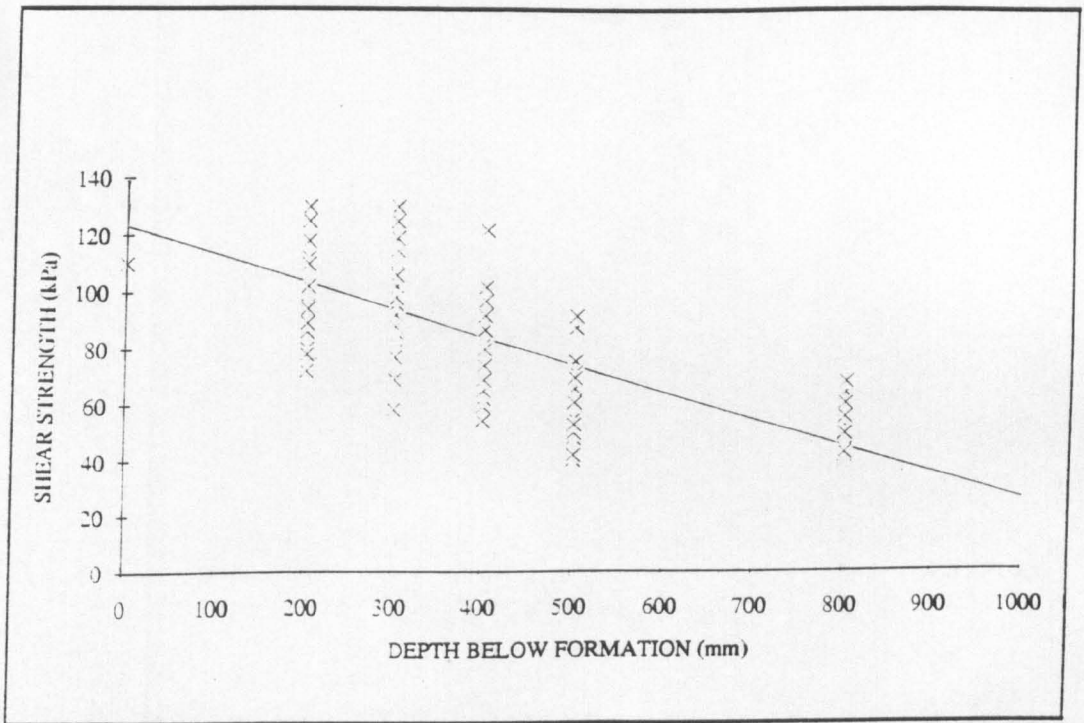


Figure 3.10 Subgrade Shear Strength - Summer 1989

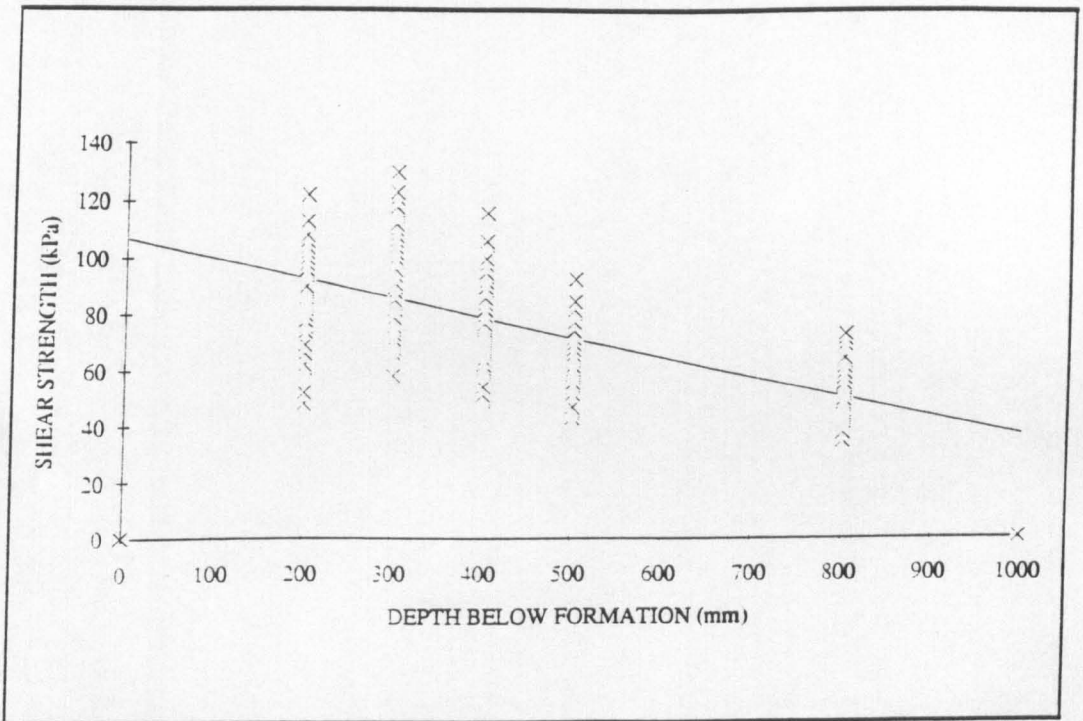


Figure 3.11 Subgrade Shear Strength - Autumn 1989

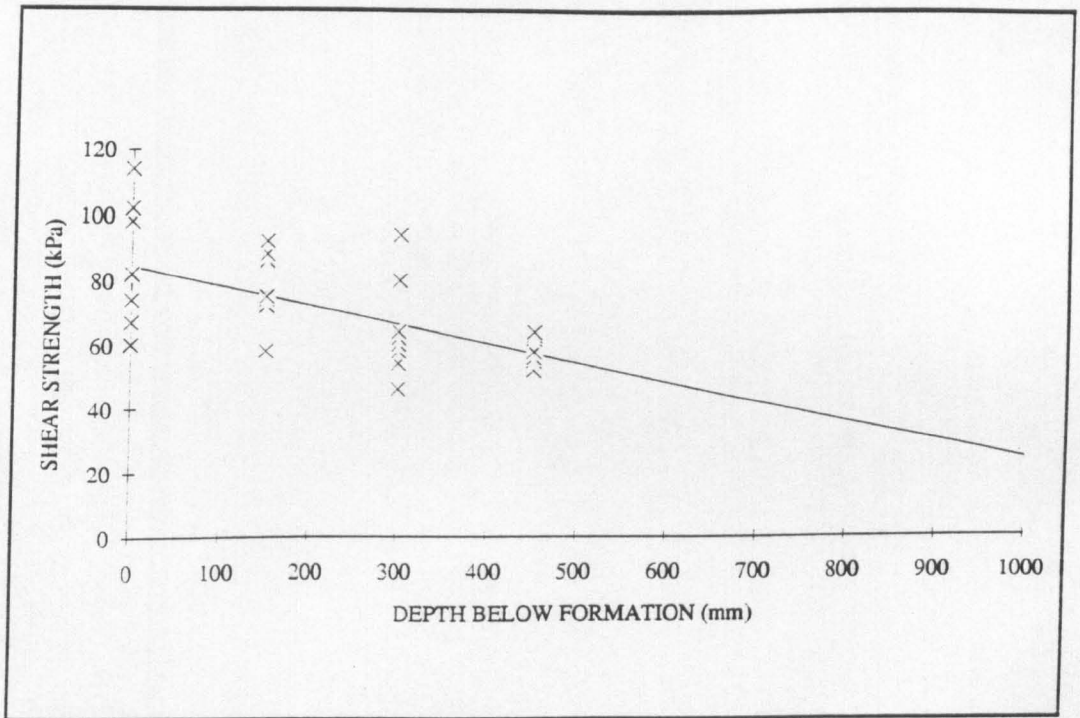


Figure 3.12 Subgrade Shear Strength - Spring 1990

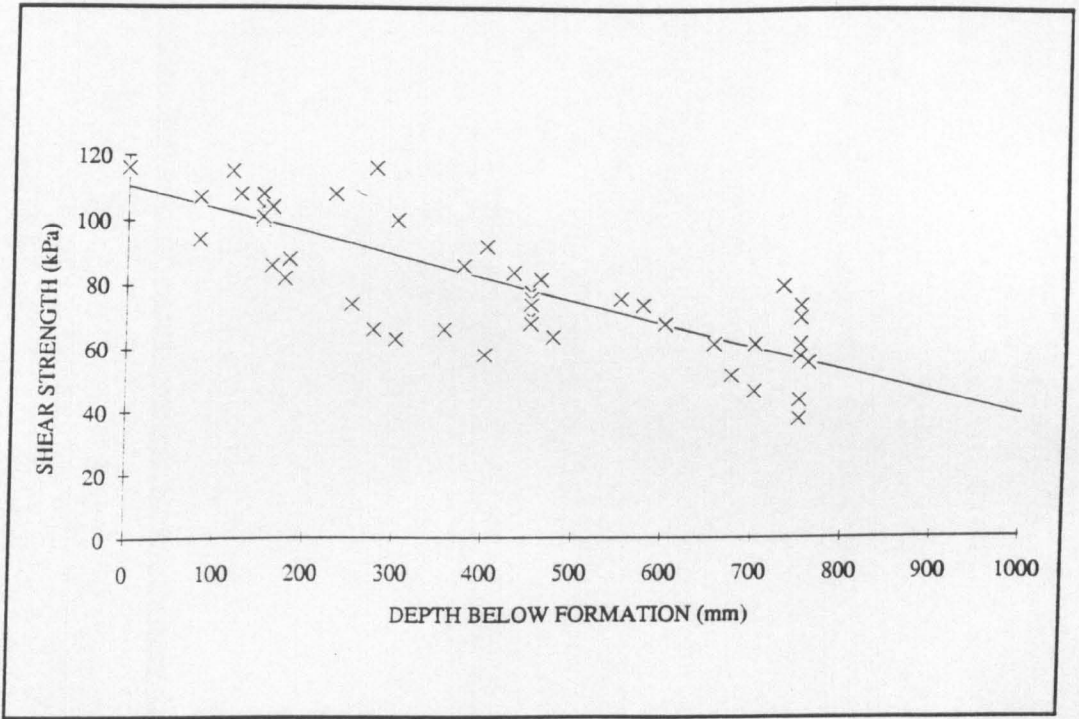


Figure 3.13 Subgrade Shear Strength - Autumn 1990

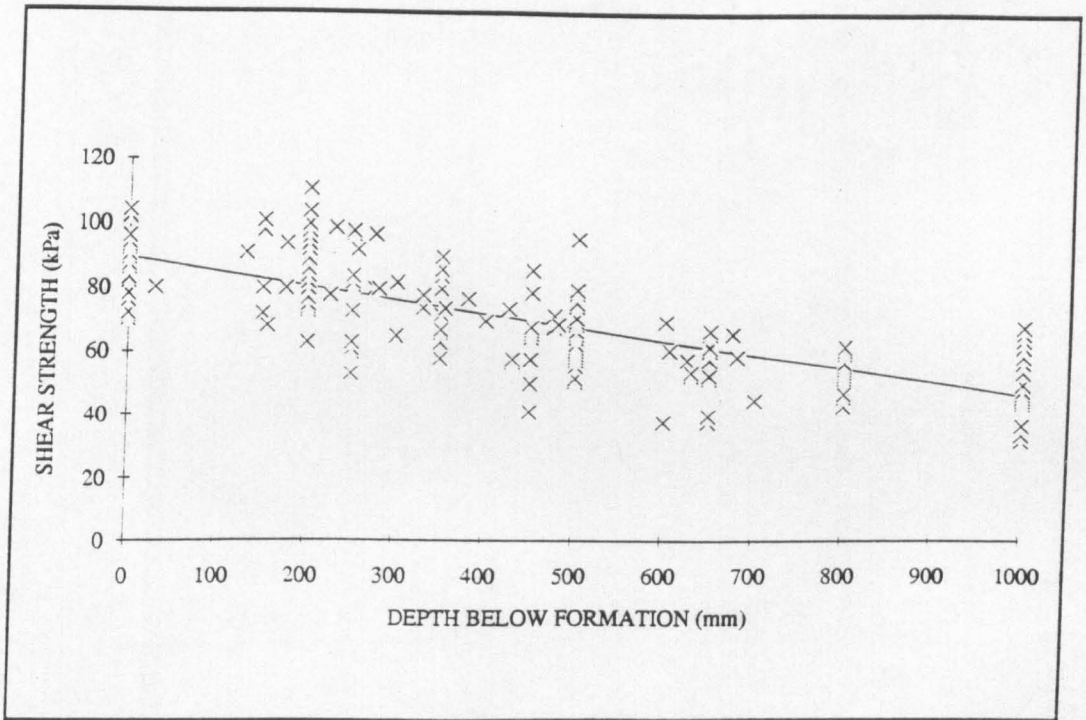


Figure 3.14 Subgrade Shear Strength - Spring 1991

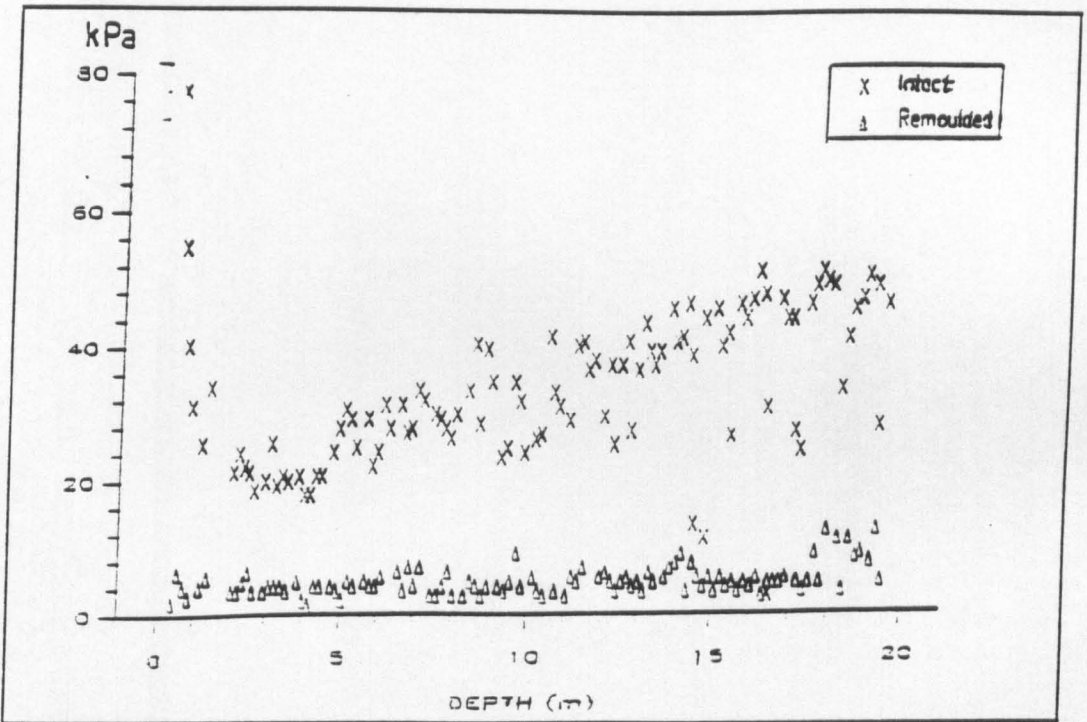
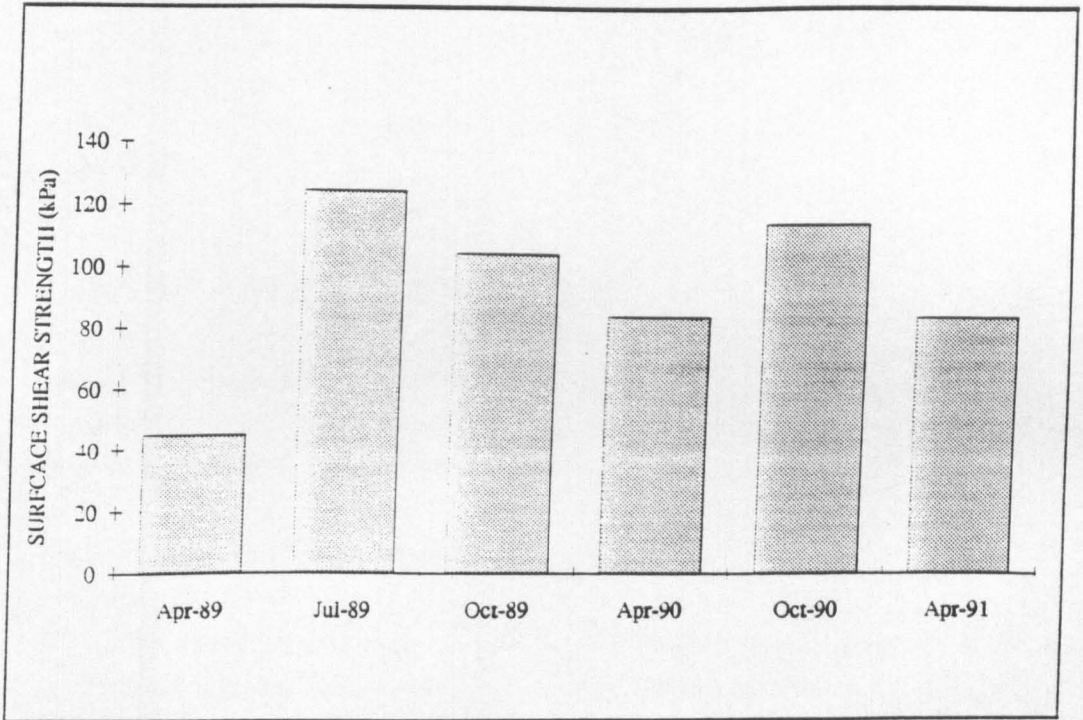


Figure 3.15 Undrained Shear Strength with Depth at Bothkennar  
After Paul et al (1991)



**Figure 3.16 Seasonal Change in Surface Undrained Shear Strength at Bothkennar**

# CHAPTER FOUR

## FULL-SCALE TRIALS

### 4.1 INTRODUCTION

This chapter is concerned with the design and construction of the full-scale trials undertaken at Bothkennar. The construction started on 10 July 1989 and was completed on 8 November 1989. Firstly the chapter discusses the design of the experiment stating the initial parameters assumed and the design methods used to determine aggregate layer thickness. A narrative of the construction of the full-scale trials follows which includes a description of the materials and the loading arrangements.

### 4.2 DESIGN OF THE FULL-SCALE TRIALS

In order to compare and contrast existing design methods, each section was designed to pre-determined performance criteria. This led to differing pavement thicknesses depending upon the design method chosen.

The initial design parameters assumed were as follows:

- 1) The sections would be constructed on a subgrade of shear strength of 45kPa, a value measured from a site survey in April 1989 as described in Chapter 3.6.
- 2) The aggregate would be a crushed rock to the 'Type 1' specification as prescribed by the Department of Transport (1986).
- 3) Two designs for each geosynthetic would be provided. The "lower-bound" design was to be such that the section should withstand the passage of 1,000 80kN axles. The "upper-bound" design was to be for the passage of 10,000 80kN axles.
- 4) Failure was to be defined as an ultimate rut-depth of 150mm, or geosynthetic rupture - whichever occurred first.

- 5) The loading arrangement was to be a two axled "standard" road going lorry with a single rear axle load of 80kN. The vehicle used was as planned and is discussed in further detail in Chapter 4.8.
- 6) The final design constraint was that the geosynthetic was to be placed at the base of the aggregate layer. Some of the design methods, such as Comité Français des Géotextiles (1981) suggest that a geosynthetic within the aggregate layer is necessary in certain circumstances.

The geosynthetics used are described in Chapter 4.4. They cover the common generic ranges of geosynthetic available on the market today. The geosynthetics were mostly donated by their respective manufacturers, however, none produced a woven geosynthetic and so a woven split-film polypropylene geosynthetic was purchased anonymously and will be described in this thesis only by its physical properties.

The instrumentation layout was designed to measure a number of "key" parameters of the soil-geosynthetic-aggregate system as described in Chapter 2.5. Instruments were installed to measure the transient and permanent horizontal strains of the geosynthetic directly under the wheel path in the direction of travel and transversely across the pavement, in order to give some indication of the strain distribution along the inclusion. Transient and permanent vertical strains at the top of the subgrade and at the base of the aggregate layer give an indication of the vertical strain distribution and of the contribution to surface deformations generated at these levels. Transient measurements determine the peak vertical stresses at the base of the aggregate layer and at the top of the subgrade and give some indication of the stress distribution through the aggregate layer. The ratio of stress to strain at each location gives an indication of the insitu stiffness of the aggregate and subgrade layers. The ambient temperature of the geosynthetic was monitored during the trafficking trials and the pore water pressure at the top of the subgrade estimated.

The instrumentation was concentrated in two areas within each section, 5m and 15m from the start, and are referred to as Reading Locations 1 and 2 respectively. The two Reading Locations broadly contain the same instrumentation. This duplication was intended to provide insurance against loss of instruments during construction and trafficking and to generate additional confidence in the results obtained.

The lower-bound sections contain more instruments than the upper-bound ones as they were more likely to show signs of deterioration sooner and, hence, provide more information about the mechanism of the system in a shorter period of time.

The provision and installation of the instrumentation is described in detail in Chapter 5.

### 4.3 LAYOUT OF THE SITE

A total of sixteen sections were constructed (Figure 4.1) together with un-instrumented bends and three un-instrumented, ad hoc, bays. Each section had dimensions of 20m long by 4.5 to 5m wide. This width enabled the geosynthetics to be installed at the manufactured width without longitudinal laps or, reducing the width of the delivered material. However, the bamboo reinforced section (O) was the exception as discussed in chapter 4.5.3. No attempt was made to pre-tension or place end restraints on the geosynthetics. For measurement and instrumentation purposes, (see Chapter 5), "Reading Locations 1 and 2" were set at 5 and 15m, from the start of each section.

The sections were assigned a letter code as shown on Figure 4.1 to enable simple identification. The upper-bound sections are on the Northern side of the circuit and are coded A to G. The lower-bound sections, on the southern side, are sections H to P.

A general view of the haul roads is shown in Plate 4.1.

### 4.4 SUMMARY OF DESIGNS USED

The design of the Tensar sections (A & N), Typar sections (B & M), Bidim sections (C & L) and the Polyfelt section (P) were supplied by the manufacturers of the geosynthetics. The control sections (D, G, H & K) were designed at the University of Nottingham based upon the unreinforced pavement design method suggested by Giroud & Noiray (1981). The woven geosynthetic sections (E & J) were also designed at the University of Nottingham using the reinforced pavement design methods suggested by Giroud & Noiray (1981).

The Oxford sections (F & I) incorporate a geogrid and were designed at Oxford University based upon the method of Milligan et al (1989a). This design method indicates comparative improvement in performance between the reinforced and

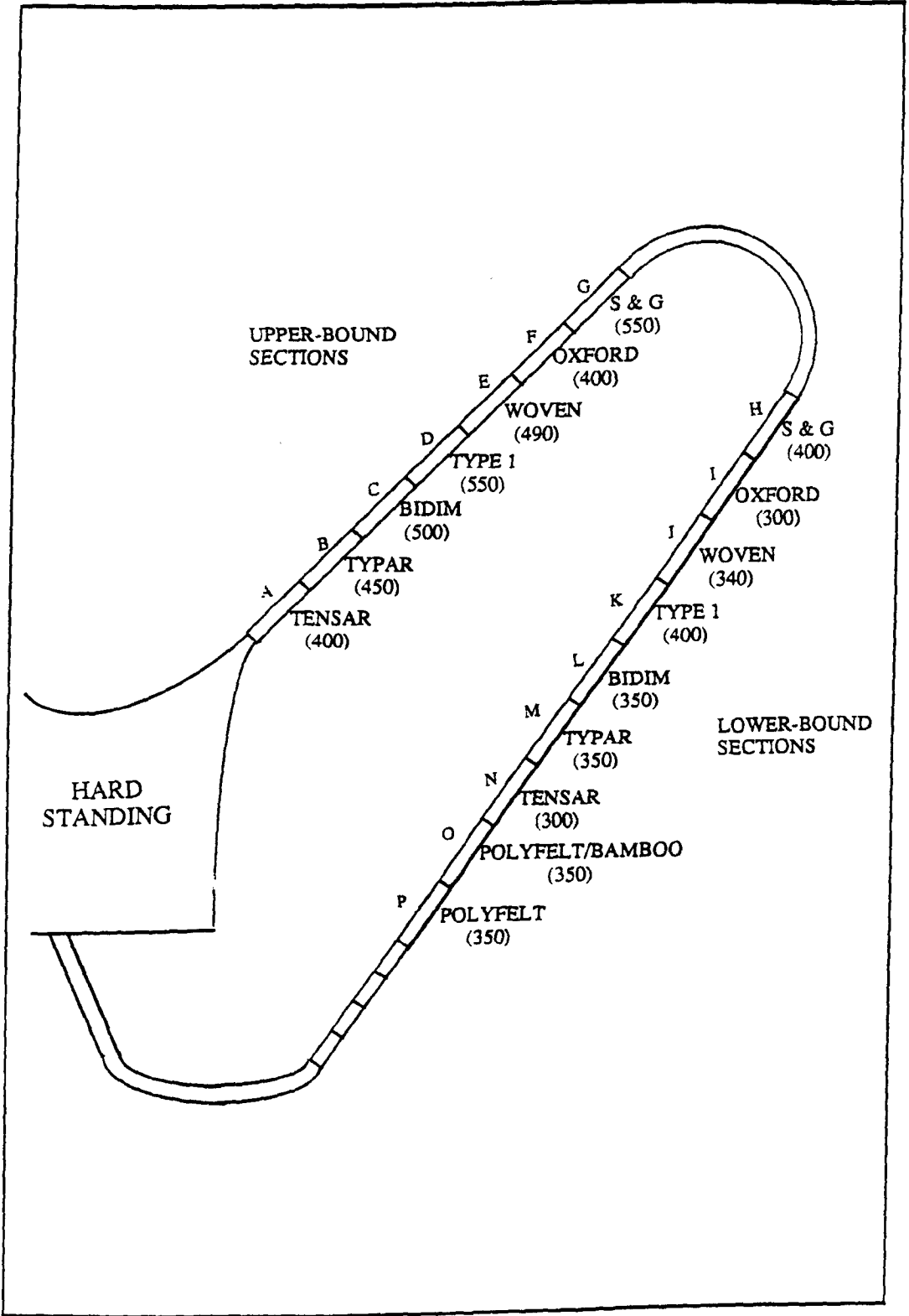


Figure 4.1 Site Layout



Plate 4.1 - General View of the Lower-bound Sections

unreinforced conditions increasing with decreasing aggregate shear strength. Therefore, the team at Oxford University requested that an aggregate of lower internal shear strength be used for their sections. Although this was different to the design parameter 2 set out in Chapter 4.2 it was agreed as validation of the method was important. Also, the Oxford sections incorporate a geogrid similar to that used in Sections A and N and a repetition of that design construction, albeit with a somewhat different aggregate thickness would not be so useful. Accordingly, a sand and gravel was used in Section F & I and for two additional control Sections G & H.

The Polyfelt and Bamboo section (O) (see Plate 4.2) was designed at Strathclyde University based upon the method of McGown et al (1990). The bamboo for the trials was purchased from Tropical Cane Ltd in Glasgow. The poles were 60 - 65mm in diameter and 3.1m long and were placed at 300mm centres. The test pavement was 5m wide and so the poles were overlapped 1.2m at the centre-line.

A summary of the designs is shown in Table 4.1.

SECTION	GEOSYNTHETIC	GENERIC TYPE	AGGREGATE	THICKNESS	DESIGN LIFE	MANUFACTURER
A	Tensar SS2	Grid	Crushed Rock	400	10,000	Netlon
B	Typar 3407	Heat-bonded	Crushed Rock	450	10,000	DuPont
C	Bidim B2	Needle-punched	Crushed Rock	500	10,000	Rhône Poulenc
D	None	-	Crushed Rock	550	10,000	-
E	Woven	Woven	Crushed Rock	490	10,000	-
F	Tensar SS1	Grid	Sand & Gravel	400	10,000	Netlon
G	None	-	Sand & Gravel	550	10,000	-
H	None	-	Sand & Gravel	400	1,000	-
I	Tensar SS1	Grid	Sand & Gravel	300	1,000	Netlon
J	Woven	Woven	Crushed Rock	340	1,000	-
K	None	-	Crushed Rock	400	1,000	-
L	Bidim B2	Needle-punched	Crushed Rock	350	1,000	Rhône Poulenc
M	Typar 3407	Heat-bonded	Crushed Rock	350	1,000	DuPont
N	Tensar SS2	Grid	Crushed Rock	350	1,000	Netlon
O	Polyfelt/Bamboo TS.500	Needle-punched	Crushed Rock	350	1,000	Polyfelt
P	Polyfelt TS.500	Needle-punched	Crushed Rock	350	1,000	Polyfelt

Table 4.1 Summary of Designs

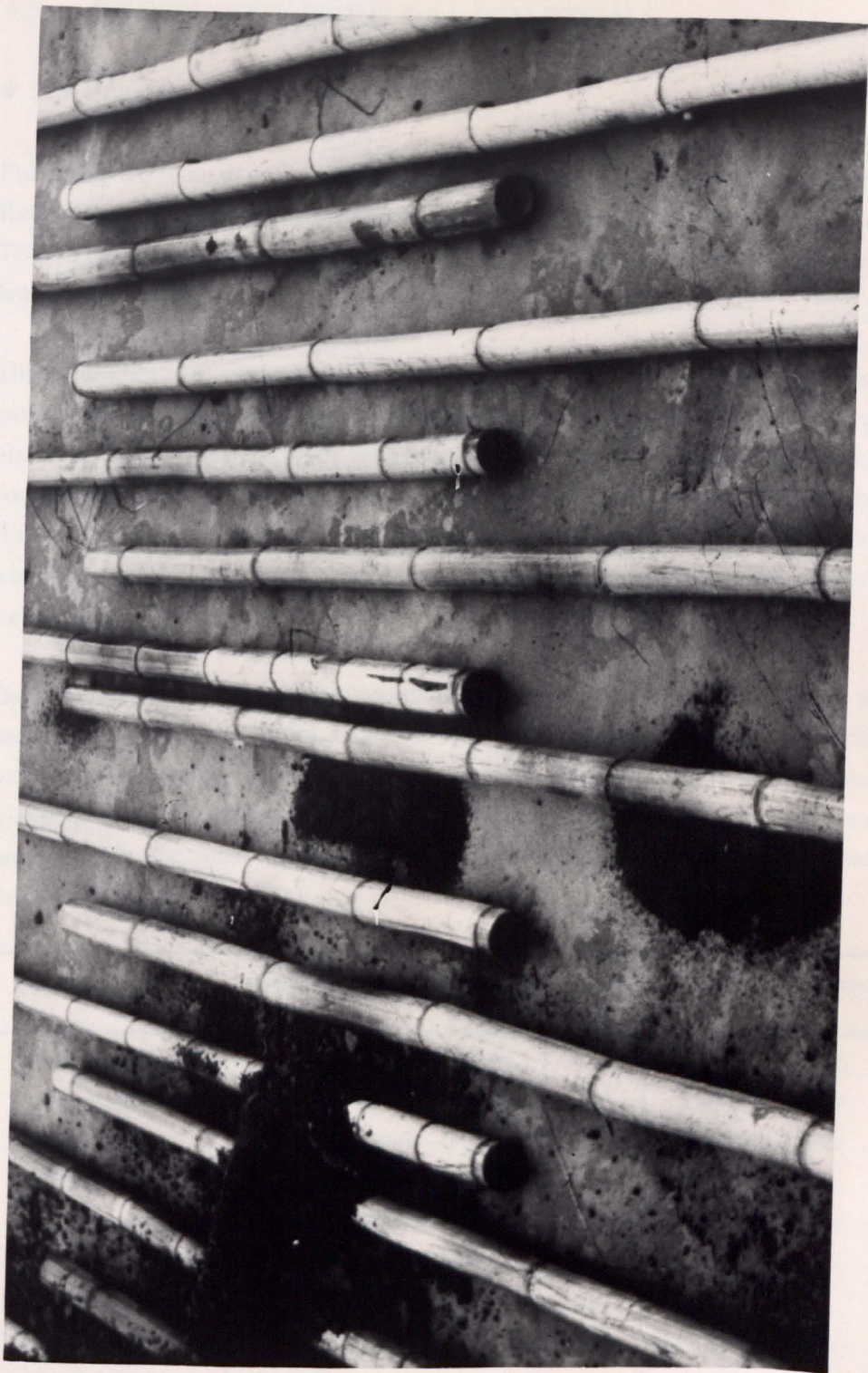


Plate 4.2 - Polyfelt and Bamboo (Section O) General Arrangement

## 4.5 CONSTRUCTION OF THE FULL-SCALE TRIALS

### 4.5.1 Construction Method

Following the issue of tender documents (Little, 1990), Denny Construction of Kilsyth Road, Hags, by Bonnybridge, Scotland was appointed as Contractor for the works. This included site preparation, geosynthetic and aggregate placement, compaction, site fencing and trafficking.

The contractor was originally requested in the specification for the works to use the pavements, as constructed, as a platform from which to work. This was specified because, on the first site visit in April 1989, the ground was so soft that it was considered unlikely that it would be able to withstand the construction traffic. However, the dry summer of 1989 resulted in a firmer crust developing on the site, which enabled the construction traffic to run directly on the surface. Thus, no sections were trafficked during construction.

The dates when each section was constructed are given in Table 4.2. It should be noted that sections constructed during July 1989 were built on much firmer ground conditions than those constructed in October of the same year. However, the subgrade remained relatively firm throughout the whole period and even in October, when the weather remained fair, the shear strength of the soil was as high as 100kPa (as assessed by hand held shear vane).

GEOSYNTHETIC	Section Code	Upper-bound Sections	Section Code	Lower-bound Sections
Tensar SS2	A	11/7/89 - 14/7/89	N	4/10/89 - 5/10/89
Typar 3407	B	17/7/89 - 19/7/89	M	28/9/89 - 29/9/89
Bidim B2	C	19/7/89 - 20/7/89	L	24/9/89 - 27/9/89
Crushed Rock Control	D	21/7/89	K	2/10/89 - 3/10/89
Woven	E	5/9/89 - 6/9/89	J	11/9/89 - 12/9/89
Oxford SS1	F	8/8/89 - 12/9/89	I	12/9/89 - 14/9/89
Sand & Gravel Control	G	11/9/89	H	12/9/89
Polyfelt/Bamboo TS500			O	23/10/89 - 25/10/89
Polyfelt TS500			P	26/10/89 - 28/10/89

Table 4.2 As Built Programme for the Haul Roads at Bothkennar

The amount of exposed formation at any one time was limited to 40m because, firstly, the exposed formation was vulnerable to changes caused by the weather (ie drying out or becoming too wet) and, secondly, because the method provided an efficient use of plant as it represented a day's work for the tracked excavator on site.

The removal of 40 linear metres of topsoil exposed more formation than could be instrumented at any one time. Therefore the formation was covered with heavy duty polythene with the aim of protecting it in the event of rain. However, as it transpired, the major beneficial effect of the covering was to prevent moisture loss from the subgrade. Even so, some drying of the formation did occur in the hot, dry weather experienced at the start of the project. Also, the polythene did not keep out all weathers and at the end of the project the rain did manage to get under the polythene and had a significant effect on the condition of the subgrade. These effects are noticeable from the shear vane tests that were taken at the time. Some of the shear vane readings for the surface of the formation were regularly off the scale of the instrument in July (ie they were greater than 126kPa) and became as low as 60kPa later in the year.

The fill material was placed on the geosynthetics with as much care as could be expected from any contractor. The material was never tipped directly onto the geosynthetics, but placed using the back-actor of the machine. In this manner the construction damage should have been kept to the minimum likely under normal construction processes.

The fill material was compacted in accordance with the Specification for Highway Works (Dept of Transport 1986). The compaction plant was a 1000kg/m twin drum vibratory roller and the layers were put down in thicknesses not greater than 150mm.

#### **4.5.2 Miscellaneous Observations on the Construction**

An uncapped borehole from a previous site investigation was discovered in the lower-bound grid section (Section N). The borehole was located 5.5m past the start of the section on the centre-line of the pavement. Because of its central location it was not possible to relocate the section, and anyway it was thought that it would have little effect on the performance of the section. However, as a precautionary measure, the first reading location was moved from 5m to 3m into the section. The depth of the hole

was in excess of 4m. It was capped using a timber board at a depth of approximately 500mm beneath the formation level and back-filled with suitable material prior to placing the geogrid.

The contractor had to undertake some remedial work on 12 September 1989 when he inadvertently buried the heavy duty polythene that was covering the sand and gravel control section (G) as described in Chapter 4.5.1. In the removal of the material, geosynthetic in the Oxford upper-bound section (F) was damaged at 17.4m from its start. The damage was so severe that it was decided to remove the remains of the damaged section and replace it with new geosynthetic. This was done using a lap length of 1m from 16.4m to 17.4m from the section's start point.

The Polyfelt/Bamboo section, designed by the team at Strathclyde University (McGown et al (1990)), contained 3.1m long x 60/65mm diameter bamboo placed directly on top of the geosynthetic, with 350mm of crushed rock aggregate. No attempt was made to restrict the movement of the bamboo in relation to the geosynthetic by stitching or enclosing it in geosynthetic "envelopes". The bamboo itself was not instrumented so the section was instrumented in the same manner as the other lower-bound sections. The bamboo came from a supplier in Glasgow, Tropical Cane Limited, but its strain and country of origin is uncertain. This section is 5m wide, as opposed to the other sections which are 4.5m, in order to obtain the required overlap of the bamboo on the centre-line. The bamboo was laid at 300mm centres transversely to the direction of the traffic flow, with a lap length of 1.2m.

During installation of the instrumentation (see Chapter 5) an accident caused damage to the upper-bound grid section (A). The result of this damage was an "L"-shaped tear that was 7 nodes long in the direction of trafficking and 13 nodes wide. The event was photographed and recorded but the section was not reconstructed. The accident was used to examine, at least qualitatively, the effects of severe construction damage on the life of expectancy at that location. The damage occurred at one of the two reading locations on the un-instrumented half of the pavement. There is no evidence that instrument readings were affected. This part of the section was monitored closely but no premature rutting attributable to the construction damage was noted. The vertical inspection tubes (described in Chapter 5) were moved to a different location from the damage.

During October 1989 the Oxford and the Woven fabric lower-bound sections (I,J) were subject to flooding with water standing on the aggregate surface. In order to remove the surface water from the aggregate layer of the affected sections a rubble drain was installed along the side of all sections from the sand and gravel lower-bound control to the Bidim lower-bound sections inclusive (Sections H to L). The invert of the drain was at formation level and the outfall was piped in a sealed trench to the test field's boundary ditch.

The test sections themselves were fenced off with wooden posts and plain wire. This precautionary measure was undertaken to prevent people from using the haul road as an access route to other parts of the site. While use of the upper-bound sections for this purpose was never ruled out, the existence of the fencing and the gated ends enabled some control to be exercised over access.

#### 4.6 AGGREGATE PROPERTIES

Two types of aggregate were used in the construction of the haul road and these were both obtained locally. The most used material, known locally as 'Whinstone', was obtained from the nearby Wimpey Asphalt quarry. It was crushed rock of igneous origin, probably a diorite, and met the requirement of Crushed Rock as specified by the Department of Transport (1986). A sand and gravel mixture was also obtained locally but had to be separately blended. The specification for the sand and gravel mixture was obtained from the Sand & Gravel Association Limited (undated). The use of sand and gravel as a sub-base material in this part of Scotland appears to be limited, hence the mixture was more expensive than the crushed rock material.

##### 4.6.1 Sampling

Aggregate samples were not taken on a section by section basis, but were taken on a chronological basis. The aggregate could not be placed on each section individually without substantially effecting the contractor's work pattern. Aggregate was therefore placed on several adjoining sections simultaneously and thus it was more sensible to take aggregate samples on a time basis. Six crushed rock samples were taken during the construction of the twelve crushed rock sections, and two samples of the sand and gravel mixture were taken. The date when each sample was taken and the broad location which it represents is shown in Table 4.3 and was recovered from one lorry-

load of material before it was placed and was taken from more than one location around the aggregate pile to avoid sampling errors.

## 4.6.2 Index Testing

### 4.6.2.1 Aggregate Particle Size Analysis

The samples were riffled and sieved in accordance with BS 812 (1975). Particle size distributions are shown in Figures 4.2 to 4.5. As can be seen from the plots the sand and gravel mixture falls within the specified envelope very satisfactorily, being almost in the centre of the two allowable limits. This should have been expected because the material was blended to the project's specific requirements.

The gradings of the crushed rock material generally fell within the envelope specified. However, samples 1 and 2 fell marginally outside the permitted envelope at a few sieve sizes. This material was placed on the Polyfelt and Bidim lower-bound sections (O/P & L) and on the second lift of the Tensar lower-bound section (Section N). It was felt that the material was not significantly out of specification. As will be seen from the Nuclear Density Meter results in Table 4.4 and 4.5, the out of specification grading did not affect the final compacted densities.

Sample No	Date retrieved	Section	Aggregate Type
1	25/10/89	O/P	Crushed Rock
2	26/09/89	L	Crushed Rock
3	12/07/89	A	Crushed Rock
4	20/07/89	C/D	Crushed Rock
5	12/09/89	J	Crushed Rock
6	29/09/89	M	Crushed Rock
7	11/09/89	F/G	Sand & Gravel
8	14/09/89	H/I	Sand & Gravel

**Table 4.3 Aggregate Sample Locations**

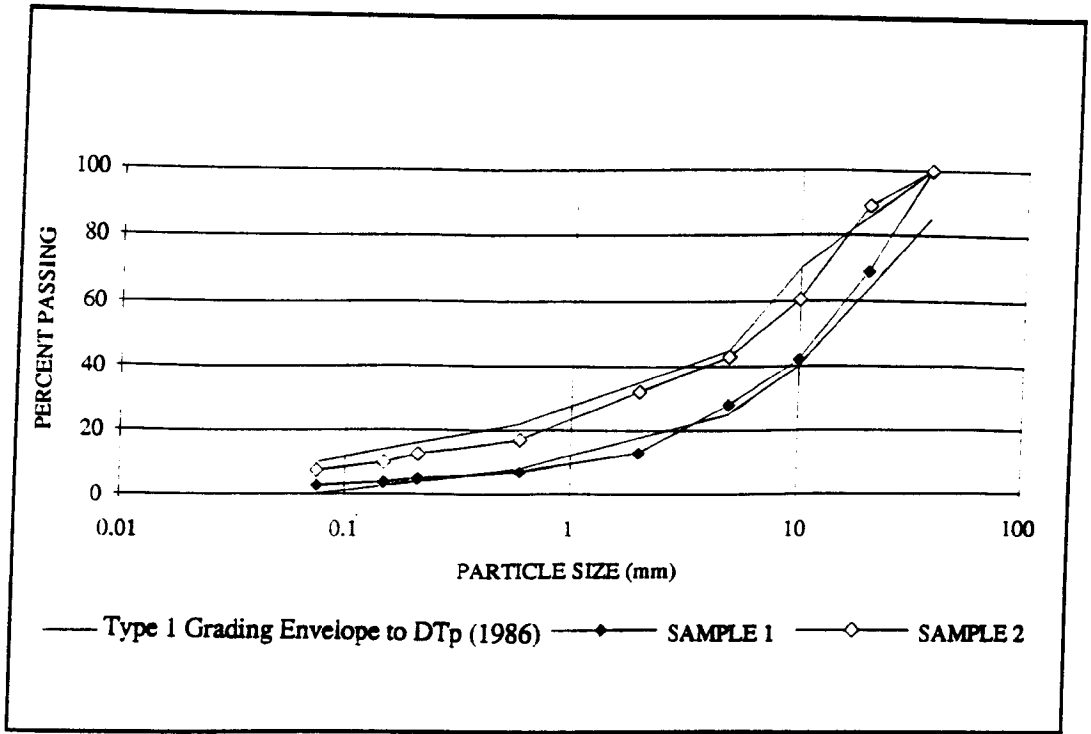


Figure 4.2 Aggregate Particle Size Analysis After BS 812 (1975)

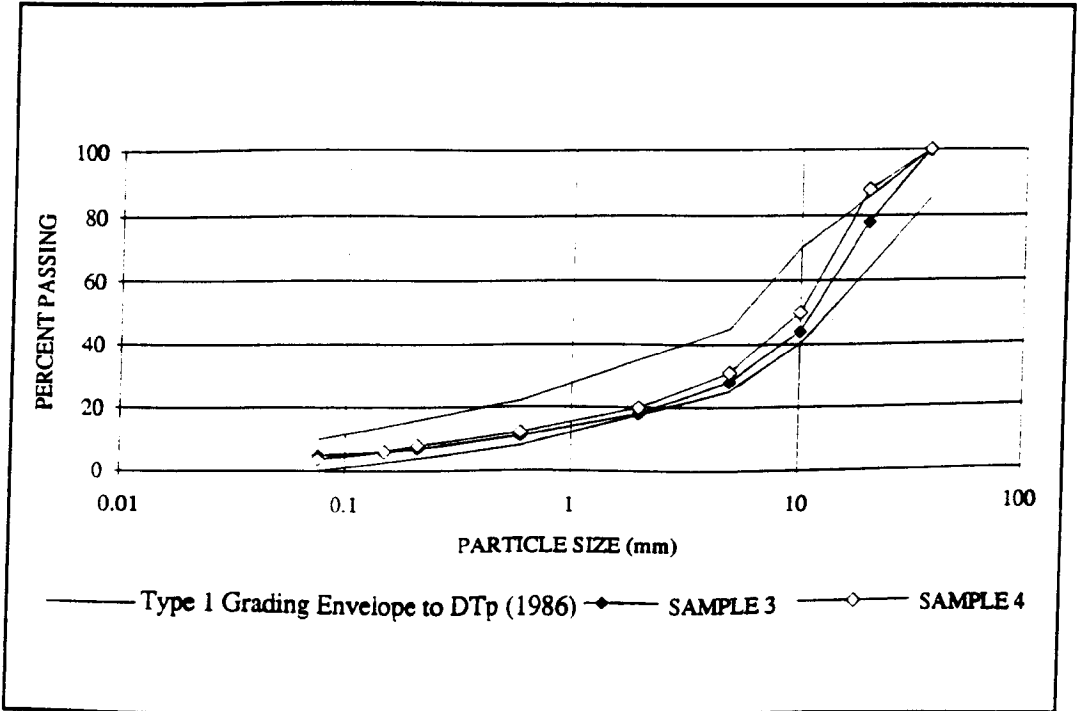


Figure 4.3 Aggregate Particle Size Analysis After BS 812 (1975)

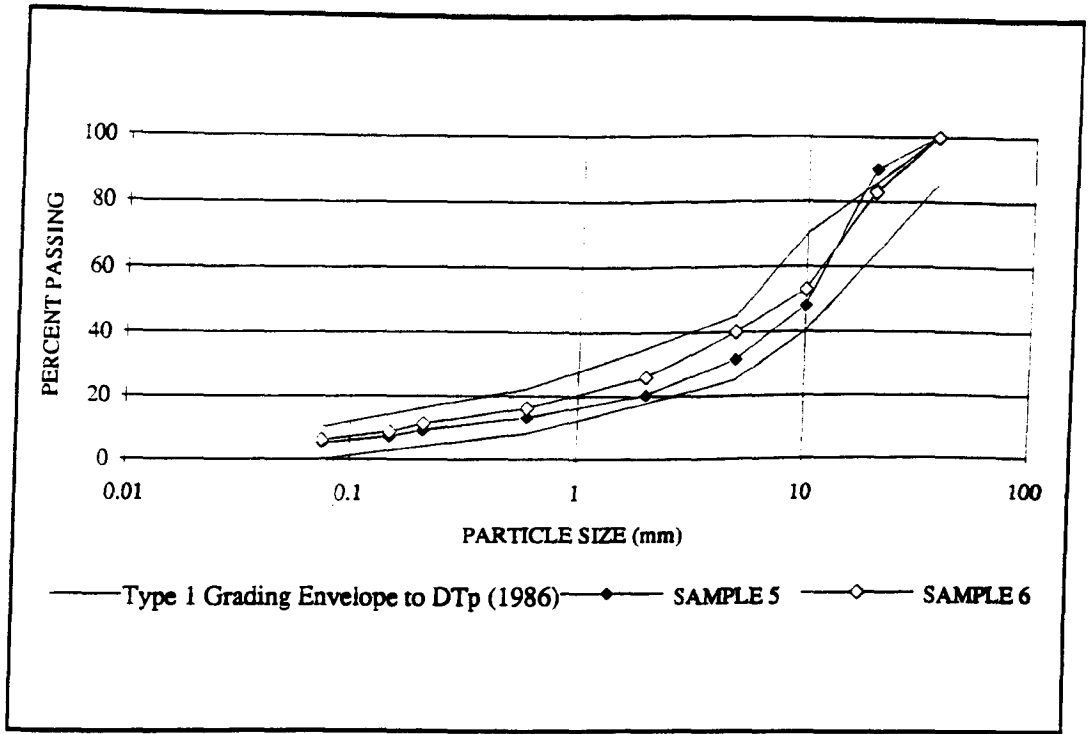


Figure 4.4 Aggregate Particle Size Analysis After BS 812 (1975)

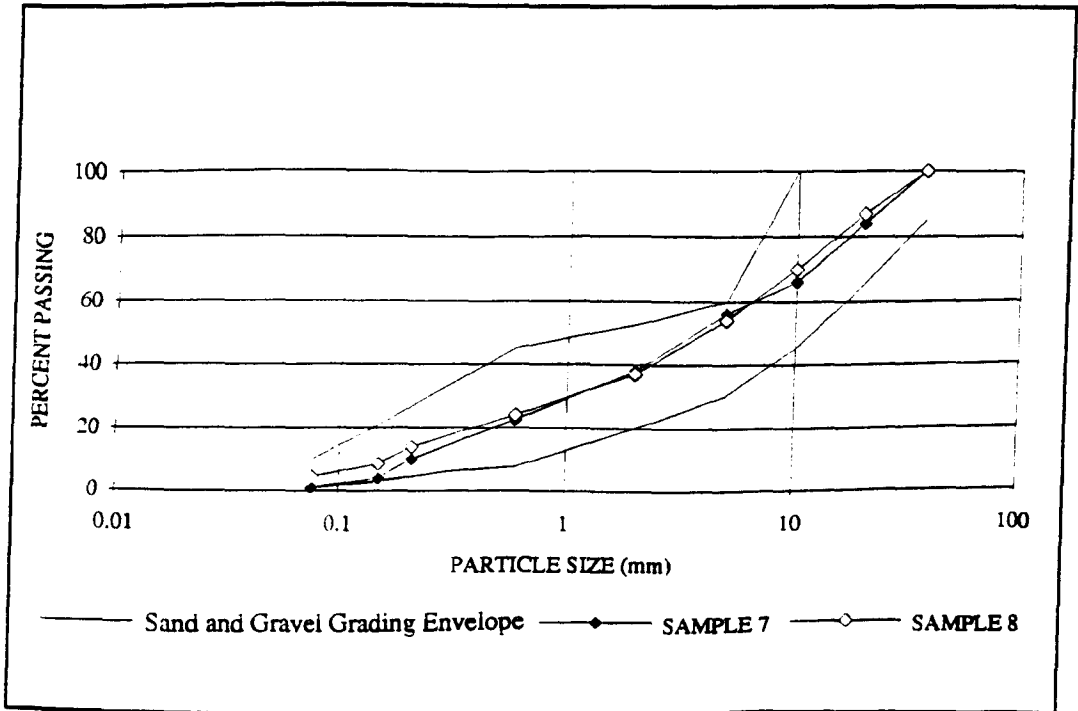


Figure 4.5 Aggregate Particle Size Analysis After BS 812 (1975)

#### 4.6.2.2 Specific Gravity

The specific gravity of the aggregates was determined according to BS 1377 (1975). The specific gravity of the crushed rock was found to be 2.85 and that of the sand and gravel was 2.74.

#### 4.6.3 In Situ Density Measurements

The density of the aggregate was determined in the instrumented wheel path of each section, prior to trafficking in March 1990, using a Campbell Pacific Nuclear Density Meter. It was operated in the direct transmission mode and the moisture content, bulk density and dry density of the top 200mm, 150mm, 100mm and 50mm of the aggregate layer were determined in two directions. The process was repeated at three locations on each section: at Reading Locations 1 and 2 and at the mid-point of each section. The mean results at each location are shown in Table 4.4.

Section	Distance into Section (m)	Measured Bulk Density (kg/m <sup>3</sup> )	Measured Dry Density (kg/m <sup>3</sup> )	Measured m/c (%)
A	5	2247	2118	5.9
	10	2122	2002	5.9
	15	2225	2115	5.2
B	5	2176	2077	4.7
	10	2179	2072	5.1
	15	2175	2064	5.1
C	5	2286	2168	5.3
	10	2293	2172	5.5
	15	2378	2234	6.3
D	5	2337	2208	5.8
	10	2331	2190	6.3
	15	2322	2178	6.5
E	5	2313	2167	6.6
	10	2350	2210	6.3
	15	2292	2160	6.0
F	5	2300	2145	7.1
	10	2255	2091	8.0
	15	2285	2127	7.3
H	5	2298	2135	7.5
	10	2196	2047	7.2
	15	2208	2056	7.3
I	5	2312	2153	7.3
	10	2263	2104	7.4
	15	2263	2102	7.6
J	5	1958	1877	4.2
	10	2320	2171	6.7
	15	2304	2173	5.9
K	5	2292	2162	5.9
	10	2237	2105	6.2
	15	2270	2130	6.4
L	5	2292	2159	6.0
	10	2363	2212	6.7
	15	2321	2192	5.8
M	5	2329	2195	6.0
	10	2398	2263	5.9
	15	2186	2059	6.1
N	5	2344	2204	6.3
	10	2404	2261	6.2
	15	2327	2186	6.4
O	5	2237	2124	5.2
	10	2358	2212	6.5
	15	2356	2237	5.2
P	5	2230	2102	6.0
	10	2310	2179	5.9
	15	2367	2229	6.1

**Table 4.4 Nuclear Density Meter Results for the Aggregate Layer**

At Reading Location I, a distance of 5m into Section J a noticeably low density was recorded. The aggregate at this point exhibited a high degree of segregation and the low density may help to explain the subsequent poor performance of the haul road at this location, as described in Chapter 6.

The statistical analysis of the nuclear density meter results is shown in Table 4.5.

Aggregate type	Bulk Density (kg/m <sup>3</sup> )		Dry Density (kg/m <sup>3</sup> )		Moisture Content (%)	
	mean	Standard deviation	mean	Standard deviation	mean	Standard deviation
Crushed Rock	2284	87	2154	75	5.9	0.5
Sand & Gravel	2264	38	2109	34	7.4	0.3

**Table 4.5 Statistical Analysis of Results from the Nuclear Density Meter**

The measured variation in bulk density, dry density and moisture content was small.

The nuclear density meter was calibrated by taking a nuclear density reading and performing a sand replacement test at the same location. Four sand replacement tests were performed in accordance with BS 1377 (1975) and the results are shown in Table 4.6. The results show a tendency for the sand replacement test dry densities to be slightly higher than those obtained from the nuclear density meter. Also the moisture contents determined by the nuclear density meter were slightly higher than those obtained in the replacement test. However, this latter difference may either be explained by a small amount of moisture loss between Bothkennar and Nottingham despite the fact that the aggregate was stored in sealed polythene bags or by the moisture content determination by the nuclear density meter being slightly out of adjustment. The meter measures bulk density and calculates dry density from moisture content determination. As can be seen in Table 4.5 the bulk densities determinations are in better agreement than the dry densities.

Test Location	Nuclear Density Meter			Sand Replacement Test		
	Bulk Density kg/m <sup>3</sup>	Dry Density kg/m <sup>3</sup>	Moisture Content (%)	Bulk Density kg/m <sup>3</sup>	Dry Density kg/m <sup>3</sup>	Moisture Content (%)
Crushed Rock upper-bound	2279	2156	5.7	2271	2194	3.5
Crushed Rock lower-bound	2311	2150	7.5	2390	2232	7.1
Sand & Gravel upper-bound	2178	2011	8.3	2278	2153	5.8
Sand & Gravel lower-bound	2178	1971	10.5	2349	2187	7.4

**Table 4.6 Nuclear Density Meter Calibration using the Sand Replacement Test**

The value of calibrating nuclear density meters by comparison with the sand replacement test must be questioned. The latter is subject to great operator variability which may exceed the range of error of the nuclear density meter. The absolute values of the density of the aggregate at Bothkennar may not be as determined by the nuclear density meter, however, it is not sensible to make a correction on the basis of so few sand replacement tests, especially as the difference between determinations resulting from the two methods was small. The benefit of the nuclear density meter is the large number of non-destructive tests it is possible to perform in a short space of time. The absolute values of the densities may not be as shown in Table 4.3 but they do give a good guide to the consistency of the layer.

#### 4.6.4 Falling Weight Deflectometer (FWD) Testing

A Falling Weight Deflectometer (FWD) (Plate 4.3) was used to assess the stiffness of the pavement layers prior to trafficking. On each section five tests were carried out in the instrumented wheel path, three on the centre line and, three in the un-instrumented wheel path. The mean results are shown in Table 4.7.

The FWD applies a measured stress to the surface of the aggregate by utilising a weight falling onto a platen. Seven remote geophones monitor the resulting deflection of the surface and the 'deflection bowl' generated is recorded. The shape of the bowl is a function of the stiffness of the various layers within the pavement structure and the results are back-analysed in an iterative manner until a theoretical bowl, generated by a computer program using estimated stiffnesses of the layers, matches that measured in the field.

There are several computer programs that can be used to back-analyse FWD deflection bowls. The one used in this study is PADAL: (PAvement Deflection AnaLysis) (Tam 1987), which is a self-iterating program. PADAL seeks to predict the observed deformations by progressively better estimates of the stiffness of the layers. The results obtained from PADAL in this study are not completely satisfactory. There was often a poor match between the calculated and measured deflections at some geophones. As this error, which was up to 25%, was often at the remotest geophone it does not imply that the final calculated stiffnesses, especially of the upper layers, are in error to the same degree. However, the program is principally designed to analyse



Plate 4.3 - Falling Weight Defectometer

pavement structures with bound layers and the high deflections, obtained from the Bothkennar pavements, are not typical. The nature of aggregate surfaces, being uneven, also causes problems as the geophones may not lie properly on the surface. This causes a distortion of the results, particularly at the remotest geophone's position, where the readings are smallest. There is a granular materials version of PADAL called PADALGR. However, the program requires the input of estimated layer stiffnesses from the operator for each iteration and is consequently time consuming to perform. Given that there were 165 FWD results to be analysed, PADALGR was not a useful option.

The PADAL program assumes that the stiffness of the subgrade increases with depth. However, at Bothkennar there is a stiffer crust on the surface of the site (as shown in Figure 3.15) and therefore an artificial layer, 0.7m thick, was created in the input of the program in an attempt to model this effect. Table 4.7 shows that the stiffness of this crust is back-calculated to be little different from that of the lower subgrade - and sometimes less. This seems unreasonable and thus the computed stiffnesses need to be cautiously regarded.

Section	Aggregate Layer Stiffness (MPa)	Crust Stiffness (MPa)	Subgrade Stiffness (MPa)
A	81	31	38
B	103	64	32
C	134	40	25
D	203	40	56
E	129	38	38
F	100	31	32
H	84	22	34
I	98	17	16
J	76	17	17
K	83	16	31
L	97	14	24
M	87	22	28
N	100	27	28
O	70	20	39
P	63	15	38

**Table 4.7 Mean Wheel Path Stiffnesses Calculated from FWD Data using PADAL (after Tam 1987)**

As can be seen from Table 4.7 the aggregate layer appears to be stiffer for the thicker pavements. This may be the result of the final aggregate layer being compacted upon a firmer base than its thinner counterpart, leading to better compaction and a higher stiffness. It should be noted that the sand and gravel aggregate appears to be of the same stiffness as the crushed rock. Comparison of pavements of the same design thickness but including different aggregates (A & F, H & K, I & N) show similar results.

Overall, the calculated elastic stiffness of the aggregate layer varied between 63 and 203MPa. This is a reasonable result as a typical value of 100MPa is often assigned to Type 1 granular or sub-base material. The subgrade stiffness both of the crust and at 0.7m depth were on average 20 to 40MPa, perhaps as expected for a material having a shear strength of 85kPa. Furthermore, the stiffness measured is of the same magnitude as the 76mm  $\phi$  triaxial test results discussed in Chapter 3.5.3.

#### **4.6.5 The ODIN Device (Boyce et al (1989))**

The ODIN Device (Boyce et al (1989)) is essentially a large drop hammer which has the ability to vary the contact stresses by the use of plates of differing sizes and using different drop heights (see Plate 4.4). It is being developed by Geotechnics Ltd and Loughborough University and calculates the stiffness of the pavement by double integration of the deceleration (to get vertical displacement) and by measuring contact stress. The device was used to determine the apparent modulus on impact of a selection of sections. The mean results from ODIN are shown in Table 4.8 and the range of values obtained from each section is shown in Figure 4.6.

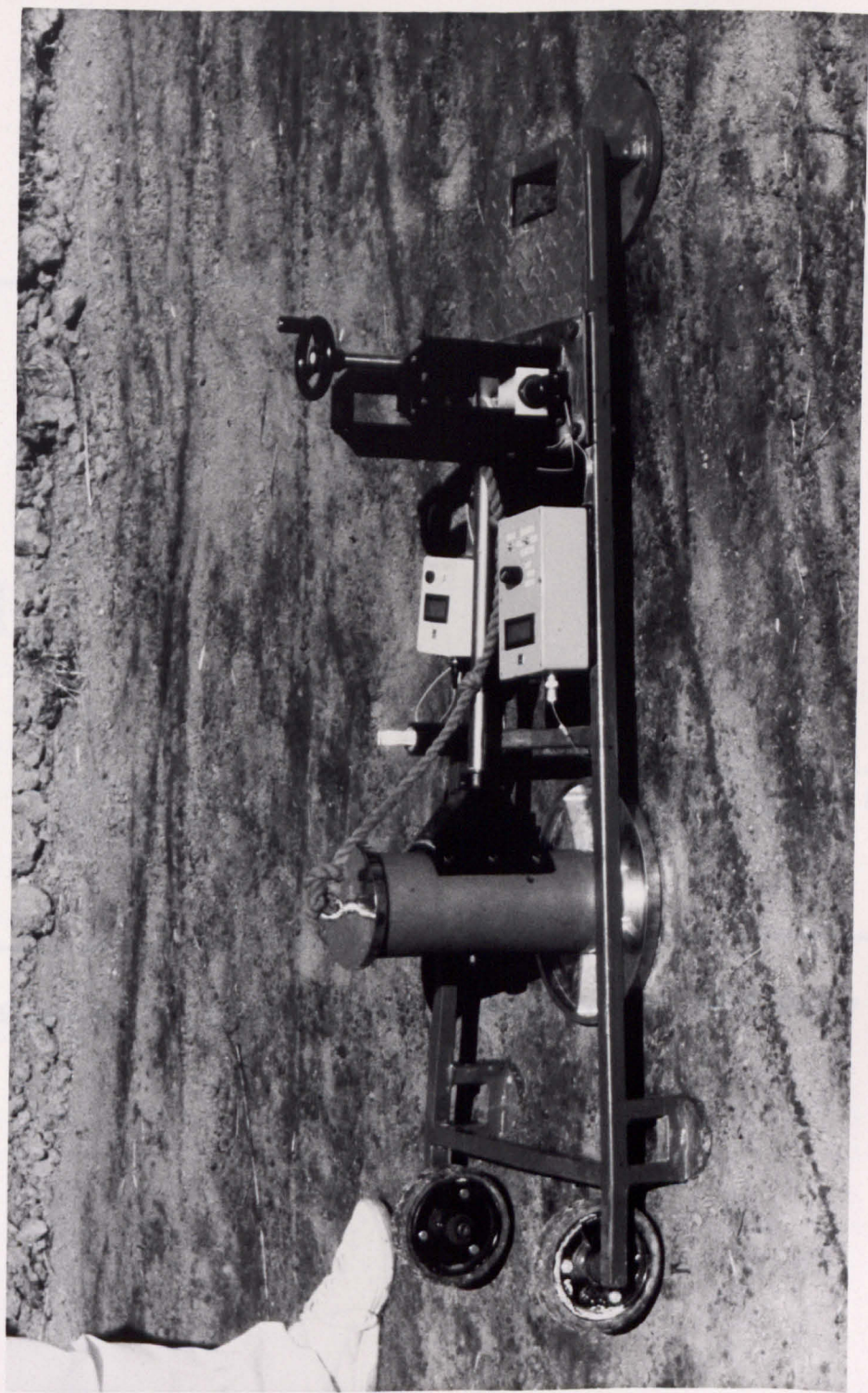


Plate 4.4 - The ODIN Device

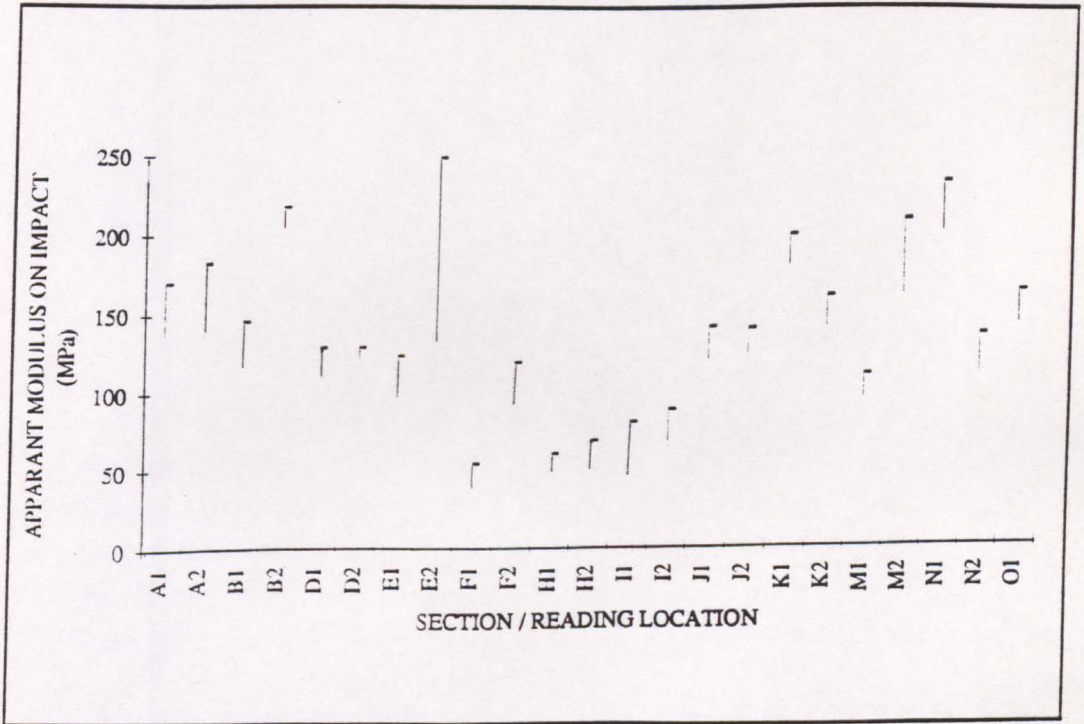


Figure 4.6 The Range of Results Obtained with the ODIN Device

Section	Apparent Modulus on Impact (MPa)
A	160
B	160
D	120
E	150
F	75
H	60
I	70
J	130
K	170
M	140
N	170
O	150

**Table 4.8 Apparent Modulus on Impact as Determined by ODIN**

The ODIN device gives a different comparative value of the stiffnesses of the sand and gravel, and crushed rock. In disagreement with the FWD, ODIN implies that the sand and gravel is less than half as stiff as crushed rock. ODIN and the FWD work in a similar manner and the difference may thus be a result of the analysis of the results obtained from each device. The stiffness of the aggregate layers as determined by the ODIN Device, however, varies between 60 and 250MPa which, in general, is very similar to those values obtained by the FWD.

#### **4.6.6 280mm Diameter Triaxial Testing**

Both aggregates were tested using the 280mm diameter triaxial apparatus developed at the University of Nottingham by Cheung and Dawson (1990) as shown in Plate 4.5. Each sample was 560mm long and was contained within a loose fitting PVC membrane. The confining stress to the sample was supplied by a vacuum line, which lowered the air pressure within the sample, and the axial stress was applied using a hand jack.

Samples of the aggregates, retrieved from Bothkennar, were prepared in a suitably sized mould. The moisture contents of the aggregates had been previously adjusted to the values obtained from the mean site values as shown in Table 4.4. The aggregates

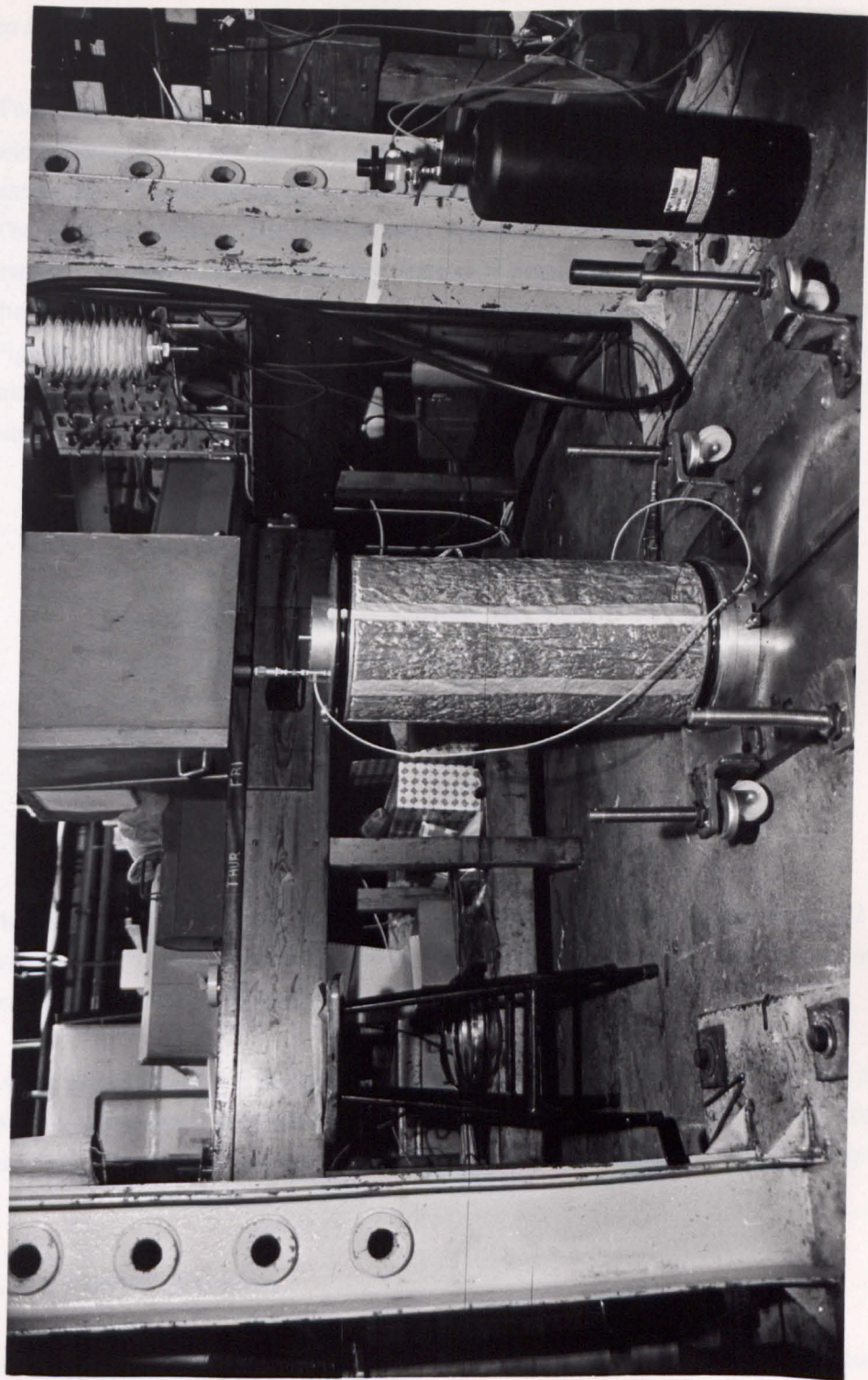


Plate 4.5 - 280mm Diameter Triaxial Apparatus - After Cheng and Dawson (1992)

were compacted in the mould using a vibratory hammer in eight layers each of 70mm, to a density equal to the mean bulk density values shown in Table 4.4.

Two confining stresses of approximately 15kPa and 50kPa were applied to each sample and a deviator stress of approximately 100kPa was applied in a cyclic manner using the hand jack. 25 load/unload cycles were performed for each confining stress and sample. The resilient modulus was determined for each test, as was the Poisson's ratio of the material. Finally a multi-stage quick undrained triaxial test was performed to determine the angle of internal friction for each aggregate, the results of which are shown in Figures 4.7 and 4.8. The results are summarized in Table 4.9. The test on the sand and gravel did not give a conclusive value of angle of internal friction test but, on the basis of Figure 4.7, 51° seems likely to be conservative.

	Crushed Rock		Sand & Gravel	
Confining stress (kPa)	20	45	11	50
Poissons ratio	0.33		0.40	
Resilient modulus (MPa)	360	450	325	600
Angle of Internal Friction	54°		51°	

**Table 4.9 Triaxial Testing of Aggregates - Summary of Results**

#### 4.7. GEOSYNTHETIC PROPERTIES

The six geosynthetics used in these trials namely the Bidim, Typar, Tensar (2 No), Woven and Polyfelt materials are described in this section. The basic properties are described in Tables 4.10 to 4.14.

As the properties of the geosynthetics were likely to change during the course of the trial a range of index tests were performed on the geosynthetics at various stages during the trials. The index tests were carried out on recovered samples as described below.

##### 4.7.1 Control Samples

It was necessary to identify index values of the materials delivered to site so that the geosynthetics could be properly defined. Samples were cut from all of the geosynthetics delivered to site and stored in a windowless container on site. The

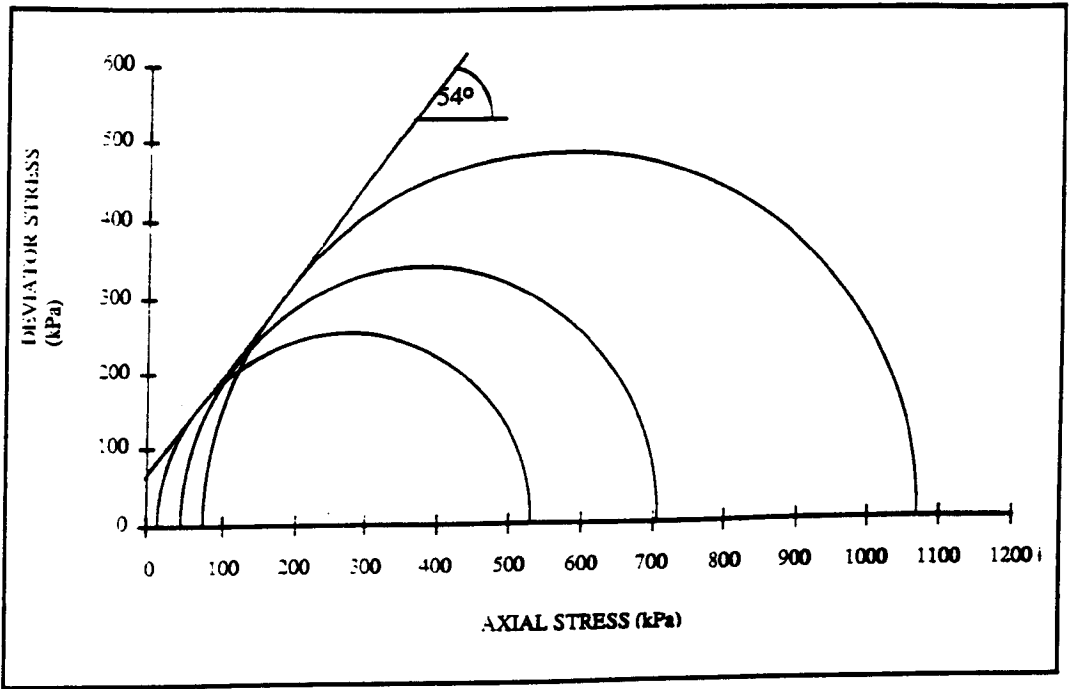


**Figure 4.7 Multi-Stage 280mm Diameter Triaxial Test  
- Crushed Rock Sample**

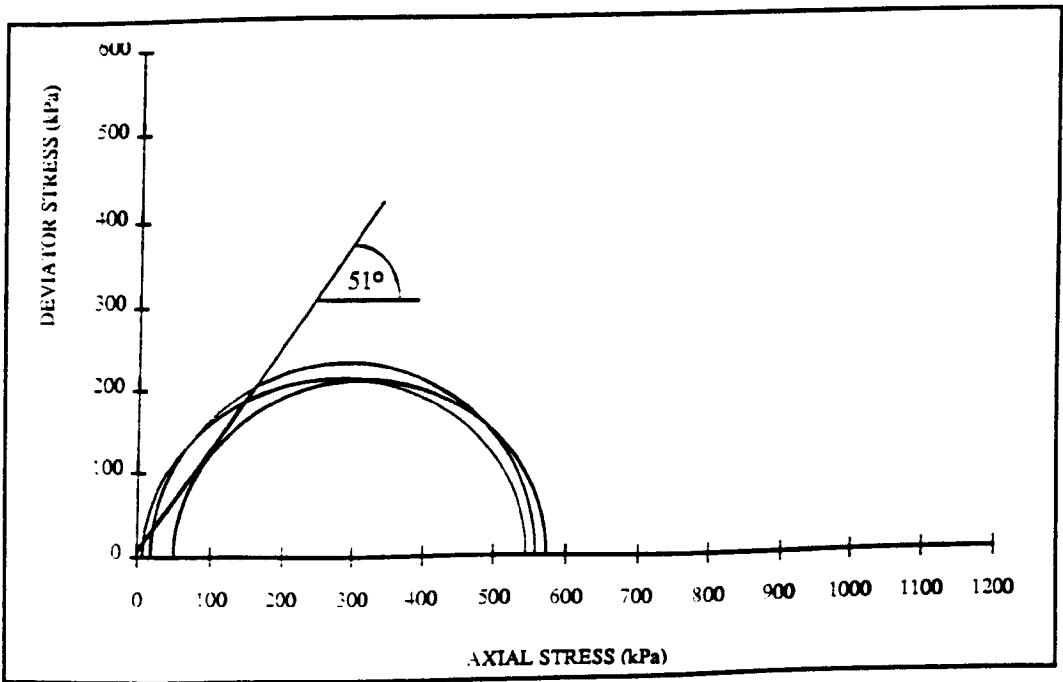


**Figure 4.8 Multi-Stage 280mm Diameter Triaxial Test  
- Sand and Gravel Sample**

container, when closed, was virtually light free. The first and last 5m of each roll of geosynthetic was not included in the trials as a precaution against any end effects arising from the production or transport of the materials. Control samples were not cut from the geogrids because after discarding the ends of the roll, there was none spare. The geosynthetics remained on site until January 1991 when samples were taken to examine the effects of the construction processes on the properties of the materials. Post construction and site stored samples were transferred to Strathclyde University, where they were stored in a dark room until required for testing.

#### **4.7.2 Simulated Compaction Damage Samples**

When a road containing a geotextile is constructed the geotextile is damaged as aggregate is placed and stone compacted onto it. To ascertain the degree of damage a compaction damage trial was made at Bothkennar independently of the haul road construction. Earlier tests performed at the TRRL by Watts & Brady (1990) were considered to be too severe as the geosynthetics were installed on a subgrade represented by a steel plate. Thus, the compaction damage trials at Bothkennar tried to more accurately model the subgrade and hence the effects on the geosynthetics. A steel plate, of approximate dimensions 2.6 x 1.3m, was covered in 150mm of re-moulded subgrade material which was compacted with a 1000kg/m vibratory roller. The geosynthetics were placed on top of the re-moulded subgrade material and attached to one end of the steel plate using a bar and clamps. Crushed rock material was then laid on top of the geosynthetics in layers of 150mm and compacted with 16 passes of a 1000kg/m vibratory roller. 300mm of aggregate was compacted over each geosynthetic and then the whole sample was lifted, by the steel plate, from one end (as shown in Plate 4.6). The aggregate then fell off the sample, or was easily removable causing minimal further damage to the geosynthetic. The samples were then stored in dark conditions with constant temperature and humidity at Strathclyde University until required for testing.

#### **4.7.3 Traffic Damaged Samples**

At the end of the trafficking of the haul road, samples of each type of geosynthetic were recovered. A full roll width of each material, by 3 or 4m along the length of the pavement, was recovered across each lower-bound pavement (except the Tensar SS1



Plate 4.6 - Retrieval of a "Compaction Damaged" Geosynthetic Sample



Plate 4.7 - Recovery of a Post-Trafficking Geosynthetic Sample

which was recovered from the upper-bound section). The aggregate was excavated by machine until 70 to 100mm of material remained above the geosynthetics. The remaining amount was excavated by hand. Care was taken to minimise damage to the geosynthetics during exhumation from either the excavating tools or undue stresses on the materials. Any areas where the operators believed damage was attributable to the exhumation process, were marked with paint and were excluded from testing. The samples were transferred to Strathclyde University for testing. An excavated section (J) is shown in Plate 4.7.

#### **4.7.4 Index Testing**

A full range of standard index tests were performed on the geosynthetics at Bothkennar and the results are given in Tables 4.9 - 4.14. These index tests were carried out by a research assistant working under the direction of Professor A McGown at Strathclyde University. They principally included tensile strength (BS 6906 part 1 (1987)), Mass per unit area, the CBR plunger tests (BS 6906 part 4 (1989)) and the cone drop test (BS 7906 part 6 (1990)). It is interesting to note that the properties of the geosynthetics alter as the damage state of the sample changes.

GEOSYNTHETIC	CONDITION	LOAD AT 5% STRAIN (kN)	MAX LOAD (kN)	MAX STRAIN (%)
BIDIM M/D	CONTROL	0.74	8.86	54.38
	COMPACTION DAMAGED	1.28	4.21	35.40
	TRAFFIC DAMAGED	0.67	4.12	10.04
BIDIM X-M/D	CONTROL	0.32	7.38	61.20
	COMPACTION DAMAGED	1.29	5.29	41.50
	TRAFFIC DAMAGED	0.85	5.43	32.25
WOVEN M/D	CONTROL	8.86	54.75	16.08
	COMPACTION DAMAGED	9.02	33.77	11.33
	TRAFFIC DAMAGED	12.66	42.14	8.44
WOVEN X-M/D	CONTROL	32.20	48.35	7.89
	COMPACTION DAMAGED	32.10	49.24	8.04
	TRAFFIC DAMAGED	13.80	18.90	10.44
TYPAR M/D	CONTROL	3.53	6.79	35.40
	COMPACTION DAMAGED	3.34	5.65	21.75
	TRAFFIC DAMAGED	3.22	5.65	23.41
TYPAR X-M/D	CONTROL	3.44	7.86	40.65
	COMPACTION DAMAGED	3.31	6.72	27.10
	TRAFFIC DAMAGED	3.33	4.60	13.25
POLYFELT M/D	CONTROL	0.70	9.02	75.15
	COMPACTION DAMAGED	1.48	8.39	58.85
	TRAFFIC DAMAGED	5.58	7.15	7.36
POLYFELT X-M/D	CONTROL	1.94	9.80	36.6
	COMPACTION DAMAGED	2.74	8.33	25.63
	TRAFFIC DAMAGED	2.97	7.57	22.34
TENSAR SS1 M/D	CONTROL	9.63	12.64	8.942
	COMPACTION DAMAGED	10.26	14.64	17.76
	TRAFFIC DAMAGED	---	21.17	5.12
TENSAR SS1 X-M/D	CONTROL	16.90	32.77	9.66
	COMPACTION DAMAGED	14.23	19.73	10.36
	TRAFFIC DAMAGED	---	11.07	3.51
TENSAR SS2 M/D	COMPACTION DAMAGED	20.11	28.62	7.68
	TRAFFIC DAMAGED	22.10	28.45	8.59
TENSAR SS2 X-M/D	COMPACTION DAMAGED	13.84	19.69	16.27
	TRAFFIC DAMAGED	12.11	15.74	8.13

Table 4.10

Geosynthetic Wide Width Tensile Strengths (after BS6906 part 1 1987)

M/D = Tension Machine Direction (ie along the roll)

X - M/D = Test Across Machine Direction (ie across the roll width)

\* Some Samples Failed at less than 5% Strain. Therefore no Valid Result is Available

The stress/strain response of geosynthetics is probably the most commonly required information for design methods. The findings of Watts and Brady (1990), that compaction damaged geosynthetics become stiffer, weaker and more brittle, has generally been confirmed by the testing programme. It has also been found that this change of property continues further with trafficking. The observation that the ultimate strain is much reduced in the post trafficking samples explains why geosynthetic rupture can occur at relatively low rut depths (which indicates geosynthetic strains far below the failure value of index tests on factory samples).

GEOSYNTHETIC	CONDITION	MASS UNIT AREA(g/m <sup>2</sup> )
BIDIM	CONTROL	144.34
	COMPACTION DAMAGED	462.51
	TRAFFIC DAMAGED	721.67
WOVEN	CONTROL	265.24
	COMPACTION DAMAGED	490.62
	TRAFFIC DAMAGED	456.67
TYPAR	CONTROL	133.76
	COMPACTION DAMAGED	380.96
	TRAFFIC DAMAGED	346.67
POLYFELT	CONTROL	142.43
	COMPACTION DAMAGED	374.46
	TRAFFIC DAMAGED	862.50

**Table 4.11 Geosynthetic Mass per Unit Area (g/m<sup>2</sup>)**

As can be seen from Table 4.11 the geosynthetics all increase in mass per unit area from the control to the compaction damaged cases as the latter samples are contaminated with fines from both the aggregate and the subgrade. The needle-punched materials, the Bidim and the Polyfelt, increased further in mass per unit area during trafficking as fines were worked into the material.

		APPLIED SURFACE PRESSURE		
GEOSYNTHETIC	CONDITION	2KPa	20KPa	200KPa
BIDIM	CONTROL	1.36	1.04	0.54
	COMPACTION DAMAGED	2.33	1.86	0.94
	TRAFFIC DAMAGED	3.78	3.44	1.98
WOVEN	CONTROL	0.87	0.80	0.67
	COMPACTION DAMAGED	1.21	1.03	0.86
	TRAFFIC DAMAGED	1.19	1.10	0.81
TYPAR	CONTROL	0.44	0.41	0.35
	COMPACTION DAMAGED	1.13	0.96	0.67
	TRAFFIC DAMAGED	2.16	1.89	1.35
POLYFELT	CONTROL	1.20	0.93	0.60
	COMPACTION DAMAGED	1.58	1.30	0.87
	TRAFFIC DAMAGED	0.95	0.78	0.53

Table 4.12 Geosynthetic Thickness (mm)

The thickness of the geosynthetics was higher in service than for the control samples. The pattern through control to compaction to trafficked samples appear erratic. The Bidim and Typar samples getting progressively thicker, presumably as containments are contained within the geosynthetic but the pattern with the woven and Polyfelt samples is a little less certain.

GEOTEXTILE	CONDITION	FORCE (KN)	DISPLACEMENT (mm)
BIDIM	CONTROL	1.70	61.8
	COMPACTION DAMAGED	1.31	47.9
	TRAFFIC DAMAGED	1.21	47.3
WOVEN	CONTROL	6.43	36.6
	COMPACTION DAMAGED	5.11	33.6
	TRAFFIC DAMAGED	4.51	37.3
TYPAR	CONTROL	1.35	48.0
	COMPACTION DAMAGED	1.17	44.4
	TRAFFIC DAMAGED	1.12	41.6
POLYFELT	CONTROL	1.63	49.2
	COMPACTION DAMAGED	1.43	43.3
	TRAFFIC DAMAGED	1.59	45.7

Table 4.13 Geosynthetic CBR Plunger Test (after BS6906 part 4, 1989)

GEOTEXTILE	CONDITION	CONE PENETRATION (mm)	ROD DEFLECTION (mm)	GEOTEXTILE DEFLECTION (mm)
BIDIM	CONTROL	33.7	55.4	21.7
	COMPACTION DAMAGED	34.0	51.3	17.3
	TRAFFIC DAMAGED	35.8	57.9	22.1
WOVEN	CONTROL	9.5	29.2	19.7
	COMPACTION DAMAGED	12.2	24.0	11.8
	TRAFFIC DAMAGED	9.8	28.5	18.7
TYPAR	CONTROL	33.1	43.0	9.9
	COMPACTION DAMAGED	36.2	46.1	9.9
	TRAFFIC DAMAGED	37.1	48.4	11.3
POLYFELT	CONTROL	33.8	49.4	15.6
	COMPACTION DAMAGED	34.4	46.5	12.1
	TRAFFIC DAMAGED	34.5	48.8	14.3

**Table 4.14 Geosynthetic Cone Drop Tests (after BS6906 part 6, 1990).**

There is clearly a wealth of data here that, in itself, would warrant further study. However, for the purposes of this thesis the results obtained from the geosynthetic index testing are of value in explaining the observed in-service performance of these materials. Thus, the results have only been lightly discussed above as the causes of the observed changes in the physical properties is, mostly, beyond the scope of this study. The appropriate physical values are used in subsequent chapters when in-service properties for the sections constructed at Bothkennar are of interest.

#### **4.7.5 Interface Friction Angles**

The friction angles developed at the interfaces in unpaved roads were examined by the author using Nottinghamshire County Council's 300mm shear box the base of which is shown in Plate 4.8. The method used was broadly that suggested in BS6906 Part 8 (1991) with the geosynthetic (where applicable) clamped to one end. However, two variations were made to the British Standard Method. Firstly, the full crushed rock grading was used as opposed to the fraction passing 10mm. Secondly, the British Standard suggests that the lower half of the shear box is filled with a rigid substrate but in these tests a model pavement was constructed using the subgrade, geosynthetic and aggregate materials from site. The clay samples were at a moisture content such that the re-moulded shear strength was approximately 85kPa and the aggregate was compacted to a bulk density of 2280kg/m<sup>3</sup> (These values were chosen to model the site conditions



Plate 4.8 - 300mm Shear Box Sample Showing Failure Within the Clay

as shown in Figure 3.14 and Table 4.6.). The geosynthetic was placed at the junction of the two halves of the shear box.

A series of tests were performed where the aggregate was sheared over different geosynthetics. Graphical results are shown in Appendix 3 and summarized in Table 4.15. As can be seen from Table 4.15 the angles of friction determined by the tests, are very close to the angle of internal friction of the aggregate as determined in the 280mm diameter triaxial apparatus (54° (Table 4.9)).

Good or better interlock probably occurs between the geogrids and aggregates as for the aggregate alone, this means that the angle of peak shearing resistance is determined solely by the aggregate. After completing the tests shown in Table 4.15 it was felt that the mechanism controlling the peak angle of shearing resistance was not a function of the geosynthetics, but, rather, of the angle of internal friction of the aggregate. Thus, the remaining geosynthetics were not tested.

Geosynthetic	Normal stress (kPa)	Peak angle of shear resistance	Aggregate
Needle-punched	100	51°	Crushed Rock
Heat-bonded	100	54°	Crushed Rock
	50	64°	Crushed Rock
	10	56°	Crushed Rock

**Table 4.15 Aggregate/Geosynthetic Friction Angles**

A few tests were performed where the subgrade material was sheared over the geosynthetic. It was found that the shear plane occurred within the clay itself, and not along the interface (see Plate 4.8). Thus, it was assumed that the subgrade/geosynthetic shear resistance is controlled by the shear strength of the soil and not the friction angle between the soil and the aggregate.

#### 4.8 THE VEHICLE AND LOADING ARRANGEMENT

Seasonal monitoring of the subgrade as described in Chapter 3.6, suggested that the crustal shear strength was a minimum in late Spring. Therefore, the original intention was to traffic the haul roads in the spring of 1990 to their design life span of 1,000 passes of an 80kN axle.

The lorry used to apply the loading was a road-going vehicle with a single rear axle and twin tyres as shown in Plate 4.9. The dimensions of the wheel base and axle width are shown in Figures 4.5 and 4.6 respectively. The lorry was loaded, for the first 1000 passes, by means of two, 2 Tonne, steel blocks. The axles were individually weighed on a public weigh-bridge and the loads were found to be:-

Front - 8130kg  $\pm$  10kg  
Rear - 3140kg  $\pm$  10kg

The lorry was weighed at the start and end of the trials to ensure that the load remained constant throughout. The rear axle weight was 24kg below the 8154kg specified (80kN). An analysis of the stresses in the pavement was undertaken using a multi-layered linear elastic analysis (Peutz et al (1968)). It showed that the spacing was such that the front axle exerted a negligible influence on the vertical stresses on the subgrade at the aggregate layer interface beneath the rear axle. Similarly at the subgrade/aggregate layer interface directly under one of the wheels, implied that tandem axled vehicles imposed no higher vertical stresses than a single axle and therefore, one assumes, would be no more damaging than the sum of the standard axles applied.

At the time of trafficking the crust on the site was much firmer than planned. Hence, after 1,000 passes of the 80kN axle, little damage was noticeable and complete failure had not occurred in any section. Therefore, it was decided to subject the pavements to at least a further 1,000 passes of a 126kN axle, in the Spring of 1991, in order to generate significant deformations and/or failure in most of the sections.

The vehicle used for the trafficking trials in 1991 was the same road-going lorry used in the 1990 phase of loading. Added Kentledge was provided by concrete blocks placed over the rear axle. An initial 15 passes of an 80kN axle were applied in order to re-compact any looseness of the aggregate surface that might have resulted from frost heave or other movement over the intervening year. A further 100 passes were then applied to the pavement in order that a comparison between the damage done by a 80kN and higher axle loads could be made. For the 115 passes of the axle at approximately 80kN, the axle weights were:-

Front - 5620  $\pm$  10kg  
Rear - 8790  $\pm$  10kg

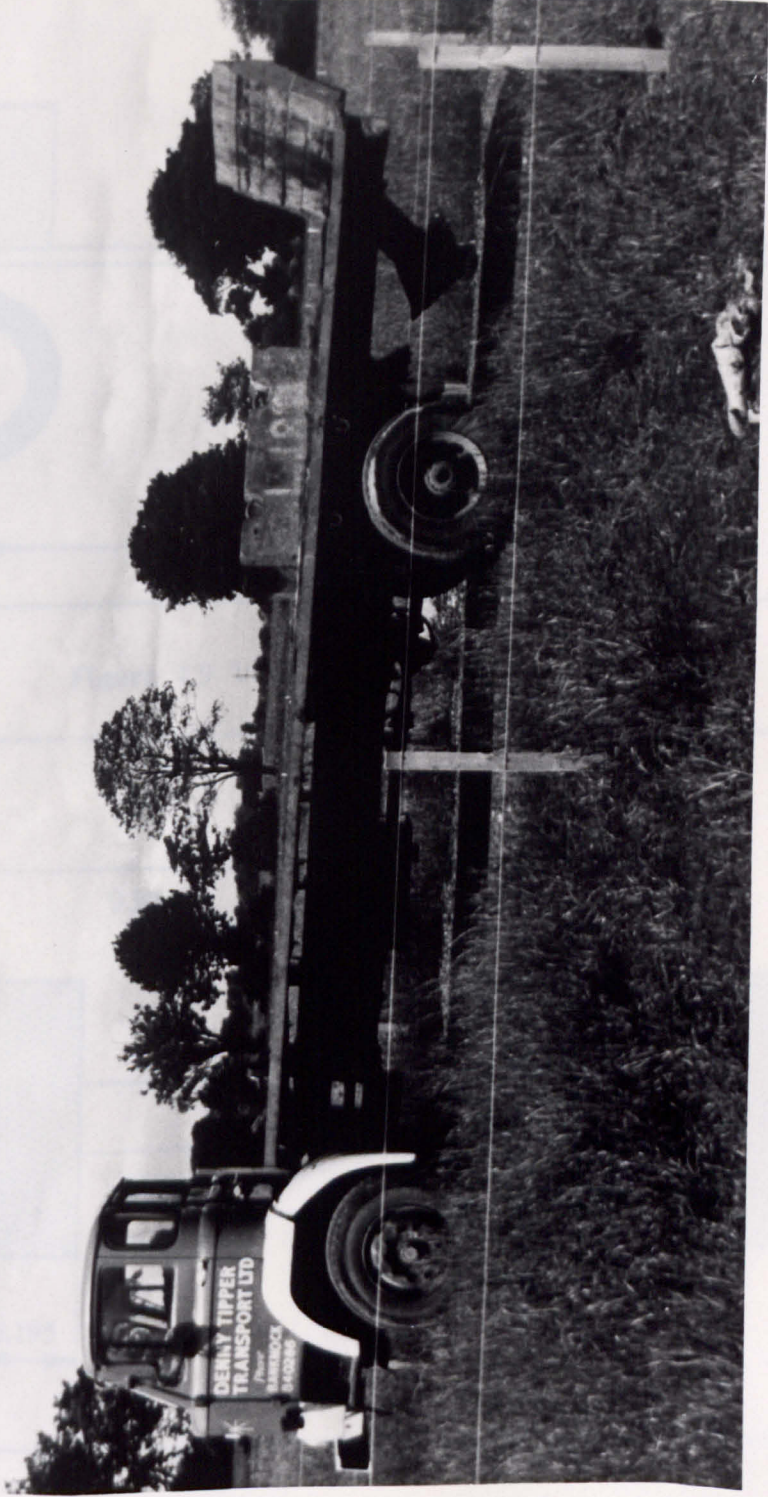


Plate 4.9 - The Trafficking Vehicle



The vehicle was then loaded to the maximum value that the operator judged to be safe and re-weighed. The axle loadings were:-

Front - 5100 ± 10kg  
Rear - 12880 ± 10kg

giving a rear axle load of approximately 126kN.

The two rear wheels were weighed individually and were found to be:-

Nearside - 6700 ± 10kg  
Offside - 6180 ± 10kg

The haul road was loaded by a further 1000 passes at this axle load. Because of direction of trafficking the nearside wheel traversed the outer un-instrumented wheel path of the loop of the trial road.

The lorry proceeded at 3 m/s (6mph) for the first 50 passes in order to permit the pavements to "settle" after construction. After 50 passes the lorry speed was increased to about 10 m/s (20mph) to enable a reasonable number of passes to be applied each day. It was observed that the speed of loading did not affect the rate of rut development in the Sandleheath trials (CIRIA (1986)). The speed was reduced to 3 m/s when the transient response of the instrumentation was measured.

In a final attempt to increase the rate of deformation in the pavements, the lorry's tyre pressures were increased from 70psi to 90psi (490 to 630kPa) after 250 passes of the 126kN axle load as higher tyre pressures should lead to a higher contact stress and hence to higher vertical stresses within the pavement. However, no noticeable increase in the vertical stresses at the base of the aggregate layer or at the top of the subgrade was recorded on the instrumentation.

# CHAPTER FIVE

## INSTRUMENTATION

### 5.1 INTRODUCTION

A total of 430 instruments were used in the full-scale trials, some were electronically controlled and others manually operated. Instrumentation included strain coils to measure horizontal and vertical and permanent strains, pressure cells to measure transient vertical stress, thermocouples, standpipes and horizontal extensometers to measure subgrade transverse strain. This chapter is concerned with the provision, manufacture, installation and mode of operation of each type of instruments. The objectives of the instrumentation will be highlighted and some of the limitations of the instruments will be commented upon.

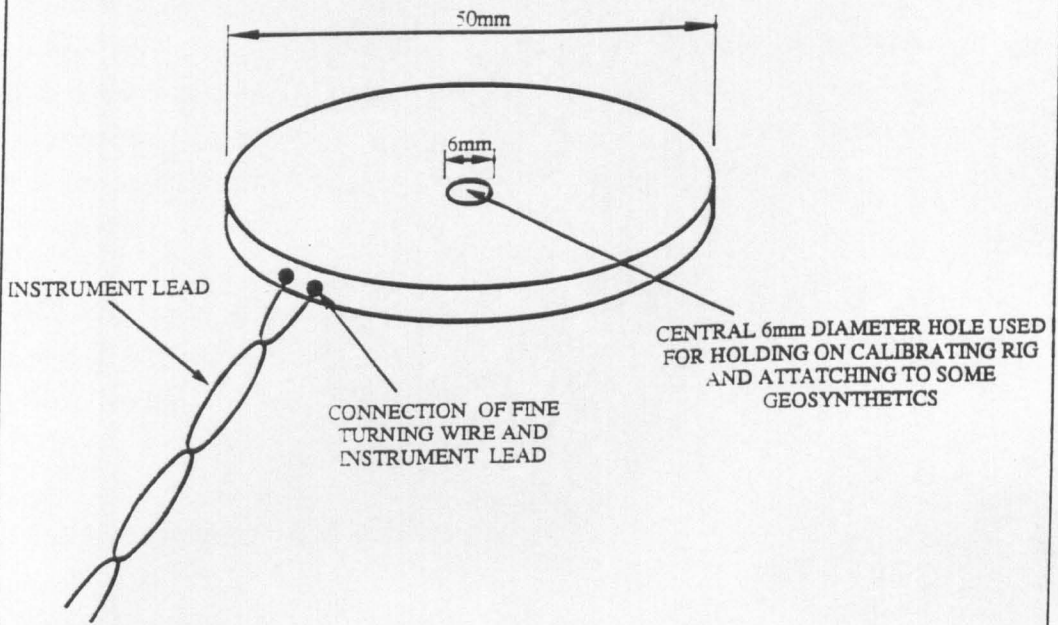
### 5.2 STRAIN MEASUREMENT

#### 5.2.1 Instruments used to measure strain

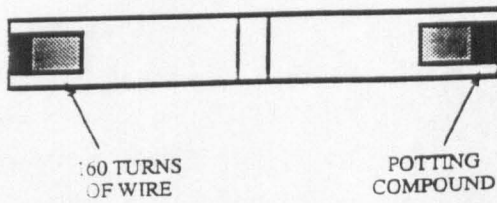
Strains within the system were measured using strain coils. Strain coils are electrical inductance devices which operate in pairs. Each coil consists of a circular former with a rebate around its circumference, as shown in Figure 5.1. Fine gauge wire is wound around the former terminating with a more substantial wire, or lead, to an operating unit. The instrument was then sealed around its circumference with potting compound and dipped in shellac. The strain coils used in the full scale trials were 50mm diameter and contained 160 turns of wire.

The coils are used in pairs a transmitting coil and a receiving one. A high frequency alternating current is passed through the transmitting coil causing a rapid expansion and collapse of electromagnetic flux in the vicinity of the coil. The expanding and contracting flux generates a current in the receiving coil of the same frequency. The induced voltage in the receiving coil is a unique function of its proximity to the transmitting coil.

Two types of readout system are currently available for use with strain coils. The "Bison" system manufactured by Bison Instruments Inc. and the "Emu" system



GENERAL ARRANGEMENT



CROSS SECTION

Figure 5.1 Strain Coils

developed at the University of Nottingham (Dawson (in press)). Both systems give a readout for the coil pair spacing based upon their proximity. The Bison system expresses this as a value, "Amplitude", and the Emu system expresses the returned signal as a voltage.

Both the Bison and Emu systems can also be used to measure "transient" strain coil pair movements, as opposed to the "static" proximity measurement described above. The transient measurement derives from the voltage shift generated by the relative movement of the strain coil pair. This voltage shift is amplified within each system and its magnitude is dependent upon both the initial coil spacing and the size of the relative movement.

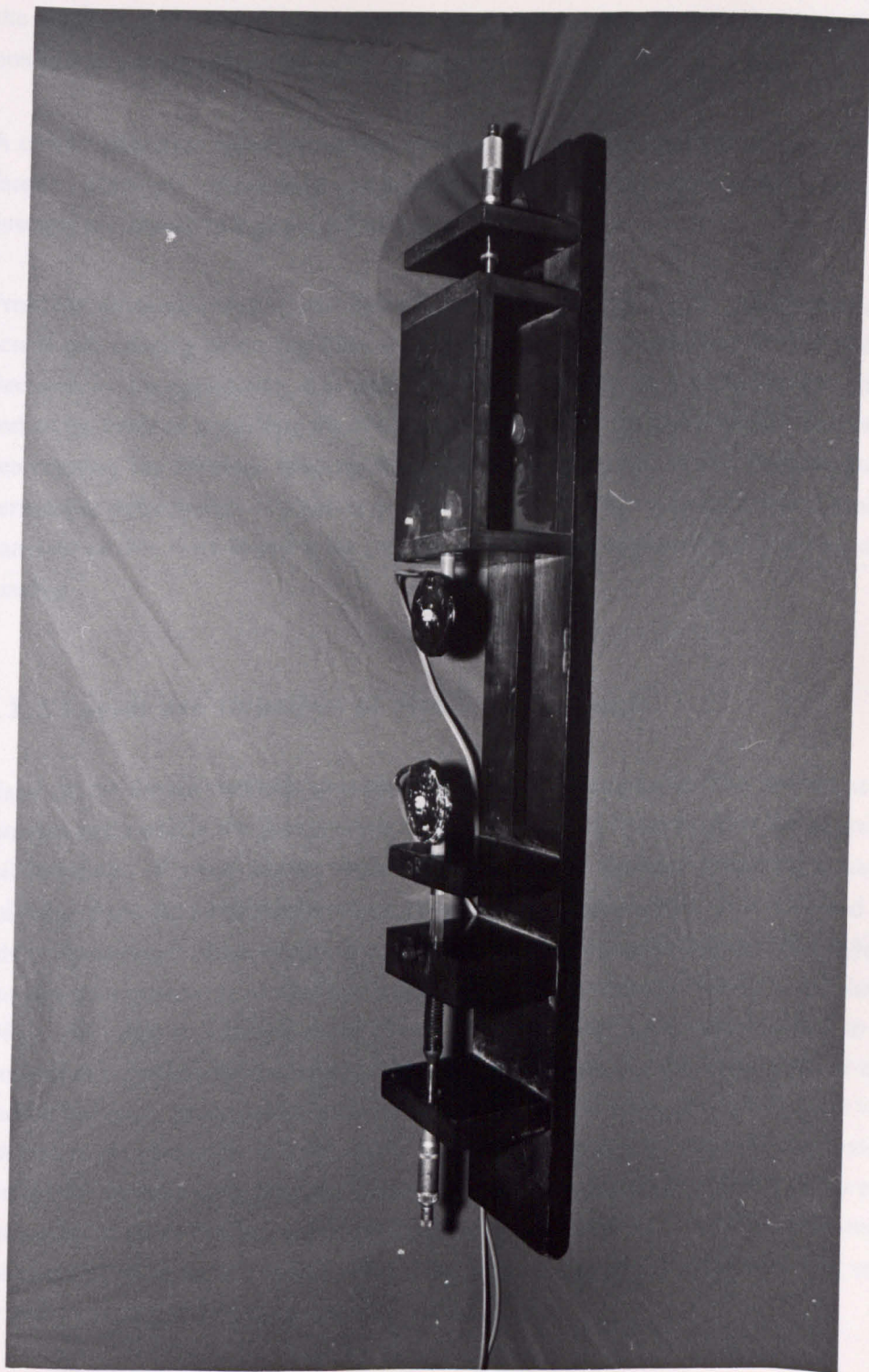
Strain coils may be sensibly operated in either a co-planar or co-axial orientation. The co-axial orientation generates a stronger signal in the receiving coil than when in the co-planar mode.

### **5.2.2 Manufacture and Calibration**

Strain coil formers were fabricated by a local firm in Nottingham using "Carp" grade "Tuffnol", and the coil winding and attaching of cables was undertaken by another local company. Before the coils were installed on site, silicone rubber was used to seal around the coil and the lead in order to exclude water and to increase the strength of the coil-lead joint.

The coils were calibrated out of soil using the Bison equipment for transient and static conditions in the calibrating rig shown in Plate 5.1. The spacing of the coils was measured using a digital vernier and "transient" movements were applied with a micrometer. Full calibration of strain coils consists of readings over the whole range of spacings as the relationship between amplitude or voltage and spacing is not linear. However, full calibrations were not necessary because Dawson (in press) has shown that, for any family of coils, the amplitude/spacing relationship for any individual coil pair can be predicted from three known amplitude/spacing co-ordinates. Furthermore, Dawson found that the out of balance voltage relating to the "transient" movement of the coils is a function of the gradient of the amplitude/spacing curve at the spacing of interest. Thus complete calibrations were generated using 3 amplitude/spacing co-ordinates and 2 out of balance voltage/strain measurements.

Plate 5.1 - Strain Coil Calibration Rig



The strain coils were calibrated using the Bison system as, at the time, the Emu system was still under development. During the full-scale trials the strain coils were read using the Emu system. As the Emu system was cheaper than the Bison system it was possible to use six Emu units which speeded up the data collection process.

A cross-calibration between the two systems was performed using coils of the same family. Example calibrations and the cross calibration between the Bison and Emu systems are shown in Figures 5.2 to 5.5.

From the cross calibrations, and the calibration curves from Bison, a prediction of the actual coil spacing given any Emu output can be made to within an accuracy of 1%. Because, in this application, it is strains, or coil movement, that is of principle interest and as the error in predicting the coil spacing is constant for any coil pair, the error in determining the absolute spacing leads to very small errors in the measurement of permanent deformation (change in spacing). Similarly the cross-calibration errors in transient strains were found to be small as the transient response is a function of the spacing.

### **5.2.3 Layout and Objectives of Strain Measurement**

Many of the design methods described in Chapter 2 emphasize the importance of tensions generated in the geosynthetic inclusion resulting from strain at the aggregate soil interface. If these strains could be measured the tensions generated could be estimated from the stress/strain relationships of the geosynthetics. It is assumed that either the maximum strain occurs directly under the wheel path (Milligan et al 1989a) or that the geosynthetic is in constant strain across the pavement (Giroud and Noiray 1981). In order to validate these concepts a strain coil pair was attached to the geosynthetic directly below, and in a transverse direction to, the wheel path at each reading location. In the lower-bound pavements a further three strain coils pairs were attached to the geosynthetic transversely across the pavement at each reading location. The offsets of these coils from the centre-line of the pavement were different for each reading location as can be seen from Figure 5.6 and Table 5.1. As the geosynthetic was expected to strain in a tensile manner the gauge length of the strain coils was set to the lower spacing of their range (approximately 75mm).

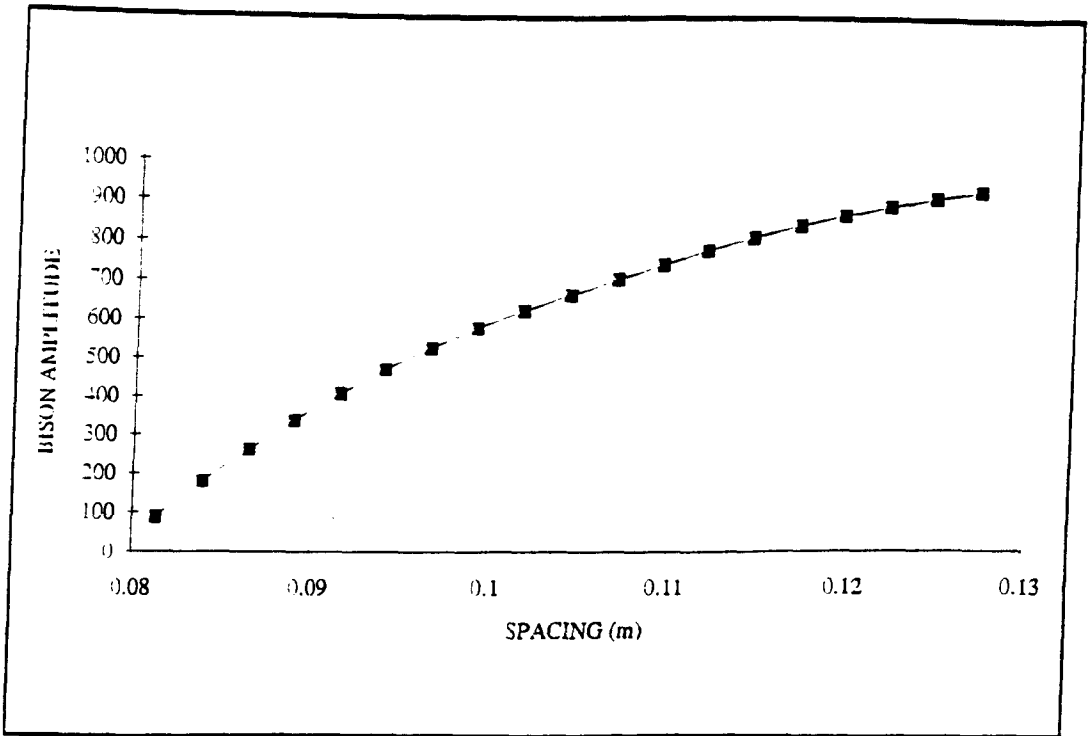


Figure 5.2 Typical Coaxial Strain Coil Calibration

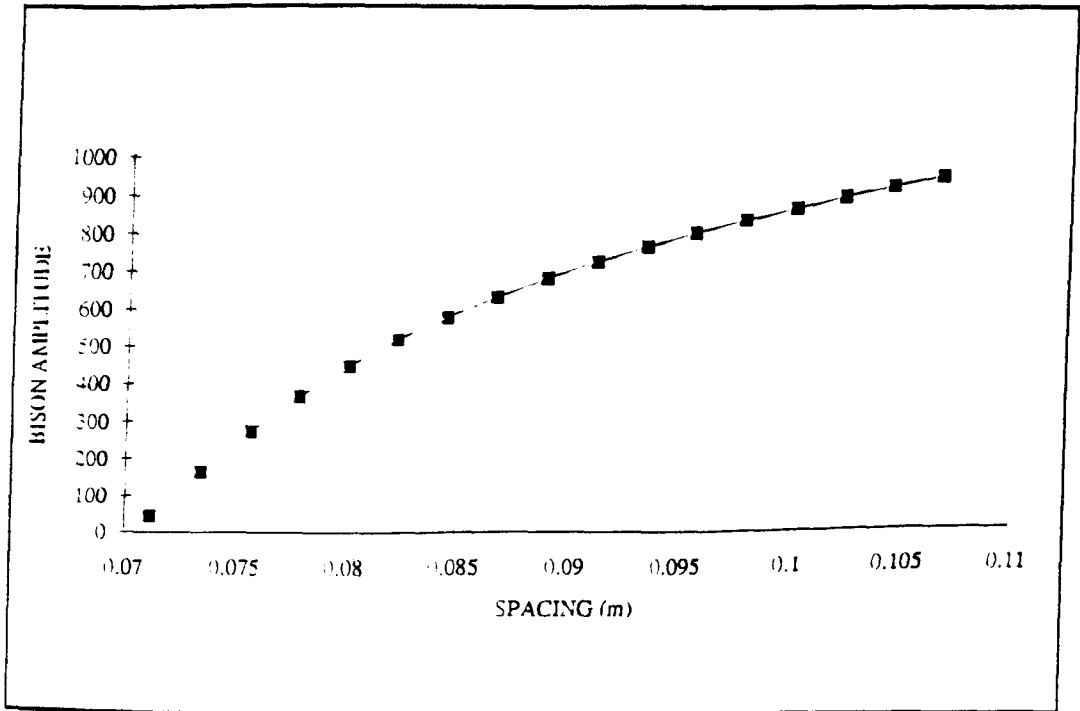


Figure 5.3 Typical Coplanar Strain Coil Calibration

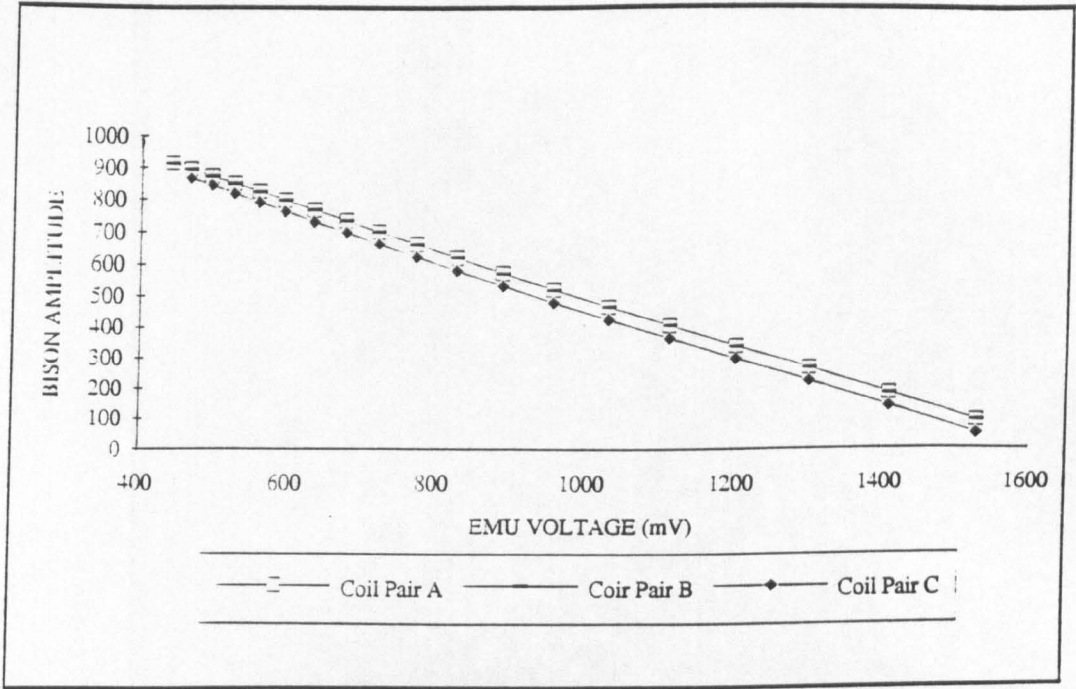


Figure 5.4 Bison/Emu Static Cross Calibration  
 $\text{Emu Reading} \times 0.737 + 1237 = \text{Bison Reading}$

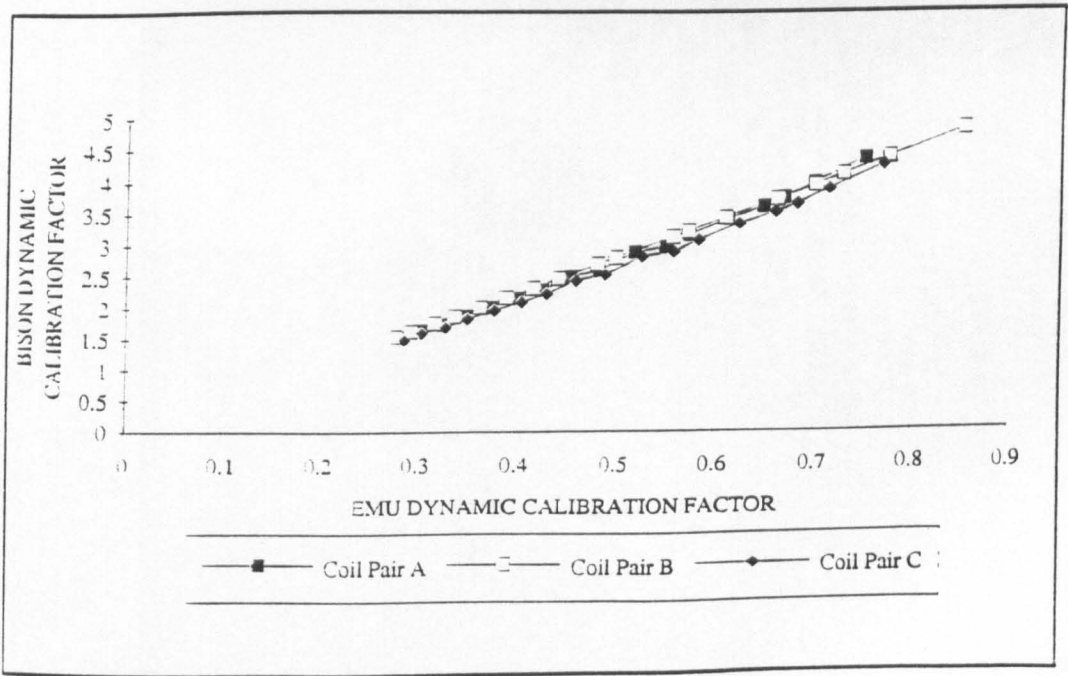
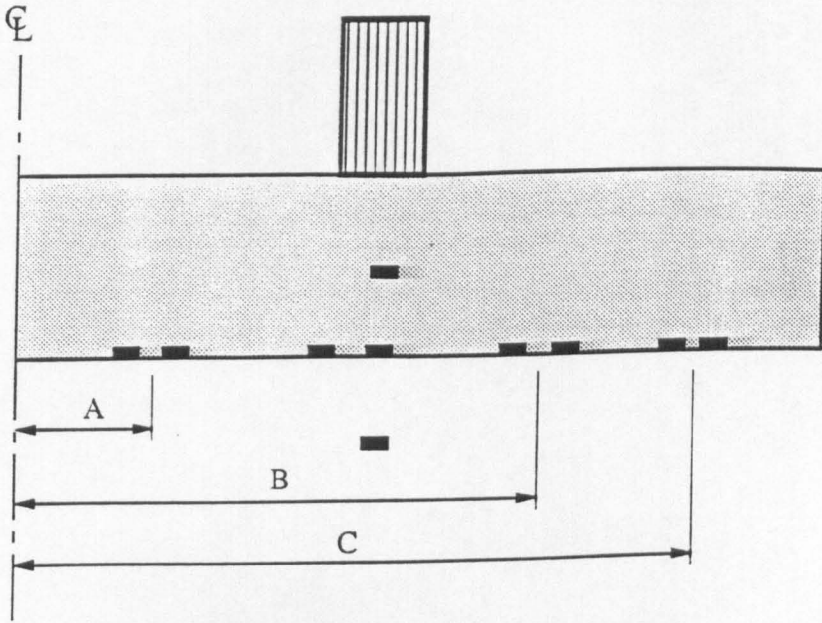


Figure 5.5 Bison/Emu Dynamic Cross Calibration  
 $\text{Emu Reading} / 0.17 = \text{Bison Reading}$



DIMENSIONS A,B AND C  
 AS PER TABLE 5.1

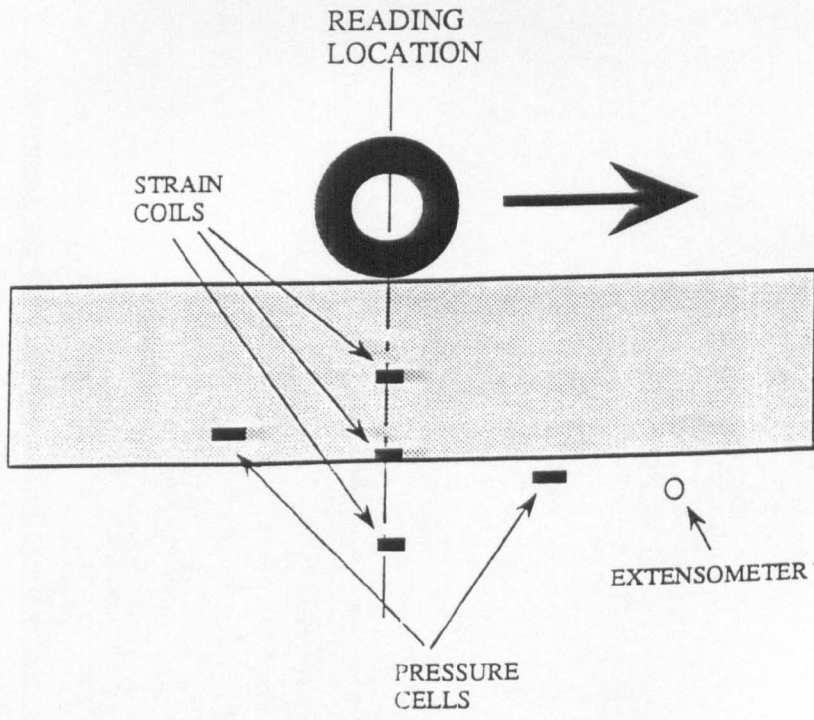


Figure 5.6 Strain Coil Layout

Transverse Coil Pair	Reading Location 1	Reading Location 2
A	0.35m	0.65m
B	1.50m	1.40m
C	2.00m	1.75m

**Table 5.1 Location of Remote Geosynthetic Strain Coils**

It was considered preferable that the strain coils did not embed themselves either in the aggregate or the subgrade, which could cause resistance to any slip that might naturally occur at the geosynthetic interfaces. In an attempt to minimize any inaccuracies that this effect might generate, a patch of the same geosynthetic was placed between the strain coil and the subgrade, and a little sand was used to produce a smooth profile as shown in Figure 5.7.

The coils were attached to the non-woven heat-bonded geosynthetics (Sections B & M) by melting a 6mm diameter hole through the fabric with a soldering iron. The coil was then attached to the fabric by the use of a 0BA nylon nut and bolt which fitted tightly into the 6mm diameter hole in the centre of the strain coil. The coils were attached to the woven (Sections D & J) and non-woven needle-punched geosynthetics (Sections B, L, O & P) in a similar manner to the heat-bonded non-woven except that the fibres of the material were eased apart and the 0BA bolt was pushed through. Strain coils were attached to the grid (Section A, F, I & N) using small plastic clamps and four nylon 4BA screws on each corner of a node. It was thought to be unnecessary to create a "patch" between the grid and the subgrade, because it was assumed that the interlock between the geosynthetic and the aggregate would prevent any occurrence of slip between the elements of the system.

The section constructed in conjunction with Strathclyde University (Section O) (McGown et al (1990)) using Polyfelt and bamboo consisted of 3.3m long, 65mm diameter poles placed at 150mm centres transversely to the direction of the traffic flow, immediately on top of the geosynthetic. It was not feasible to instrument the bamboo itself and so the geosynthetic was instrumented in exactly the same manner as the other lower-bound sections.

A small quantity of finer material, that part of the aggregate passing a 1.18mm sieve, was placed on the geosynthetic above the strain coils to protect them from damage during compaction of the aggregate layer. Some aggregate was then placed carefully over the strain coils prior to the section being filled. This helped to prevent the coils

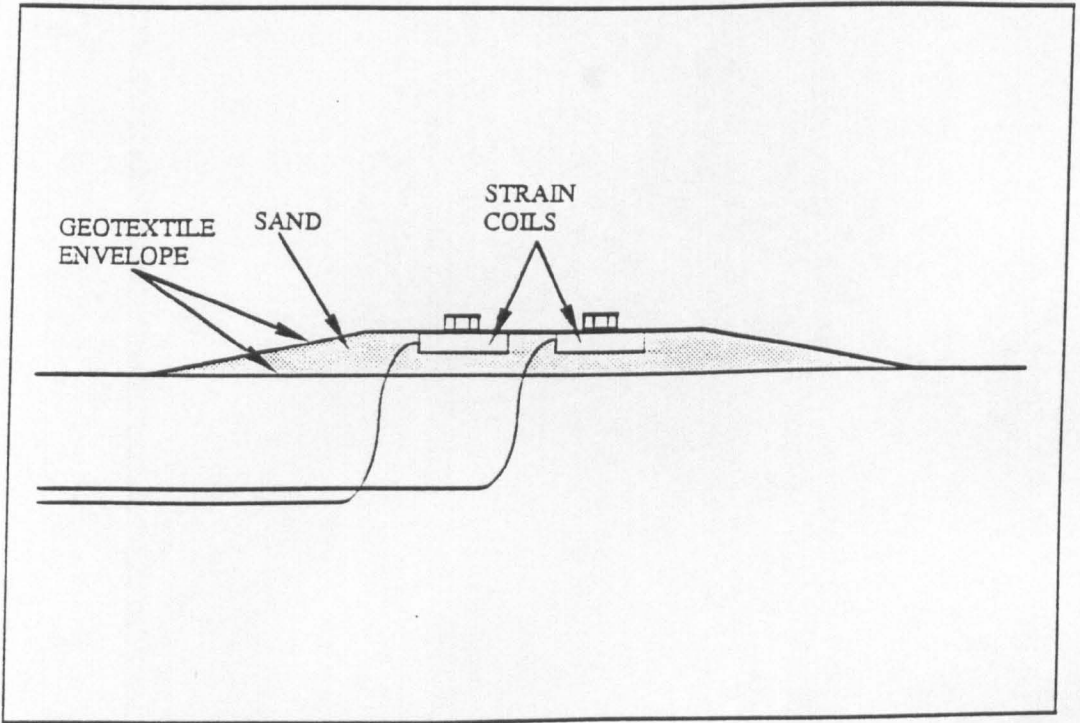


Figure 5.7 Strain Coil Attachment to Geotextiles

moving away from their position during construction and minimized damage to the coils.

It was expected that some internal aggregate strain would occur under repeated wheel loading which would make a contribution to the total surface deformation. In order to quantify this, a strain coil pair was installed under the wheel path at each reading location in a vertical, co-axial orientation, with an initial gauge length of 100mm, at the base of the aggregate layer and with the lower coil being attached to the geosynthetic. The upper coil was surrounded with finer material (passing 1.18mm) sieved from the aggregate. Bedding of the instrument on fines using a bulls eye bubble level enabled the coil to be installed horizontally which is important for this type of instrument as the calibration is sensitive to tilt in the coils. The fines also prevented the coils from becoming damaged during the compaction or trafficking processes.

Permanent strain in the subgrade material would make the remaining contribution to surface deformations. To measure a full strain profile with depth was impractical but a strain coil pair was installed in a vertical, co-axial orientation at the top of the subgrade directly beneath the wheel path at each reading location. The gauge length was set to approximately 100mm by burying the lower coil in the subgrade, and backfilling above it with hand compacted subgrade material. Combined with the aggregate strain coil above, the vertical strain distribution across the geosynthetic could thus be examined.

## 5.3 STRESS MEASUREMENT

### 5.3.1 Instruments Used to Measure Stress

Stresses within the system were measured using earth pressure cells. These consist of a titanium steel body and an integral diaphragm on which are mounted 4 electrical strain gauges (Plate 5.2). These are wired in a balanced Wheatstone bridge configuration which goes out of balance when the diaphragm is deflected due to an applied stress. This out-of-balance voltage is proportional to the stress applied.

There is uncertainty in the operation of the pressure cells as the inclusion of the pressure cell alters the stress field in the medium. The amount by which the cell over or under reads is defined as the cell registration. The cell registration was defined by Brown (1977) as a function of the aspect ratio of the cell and the flexibility factor,  $F$ .

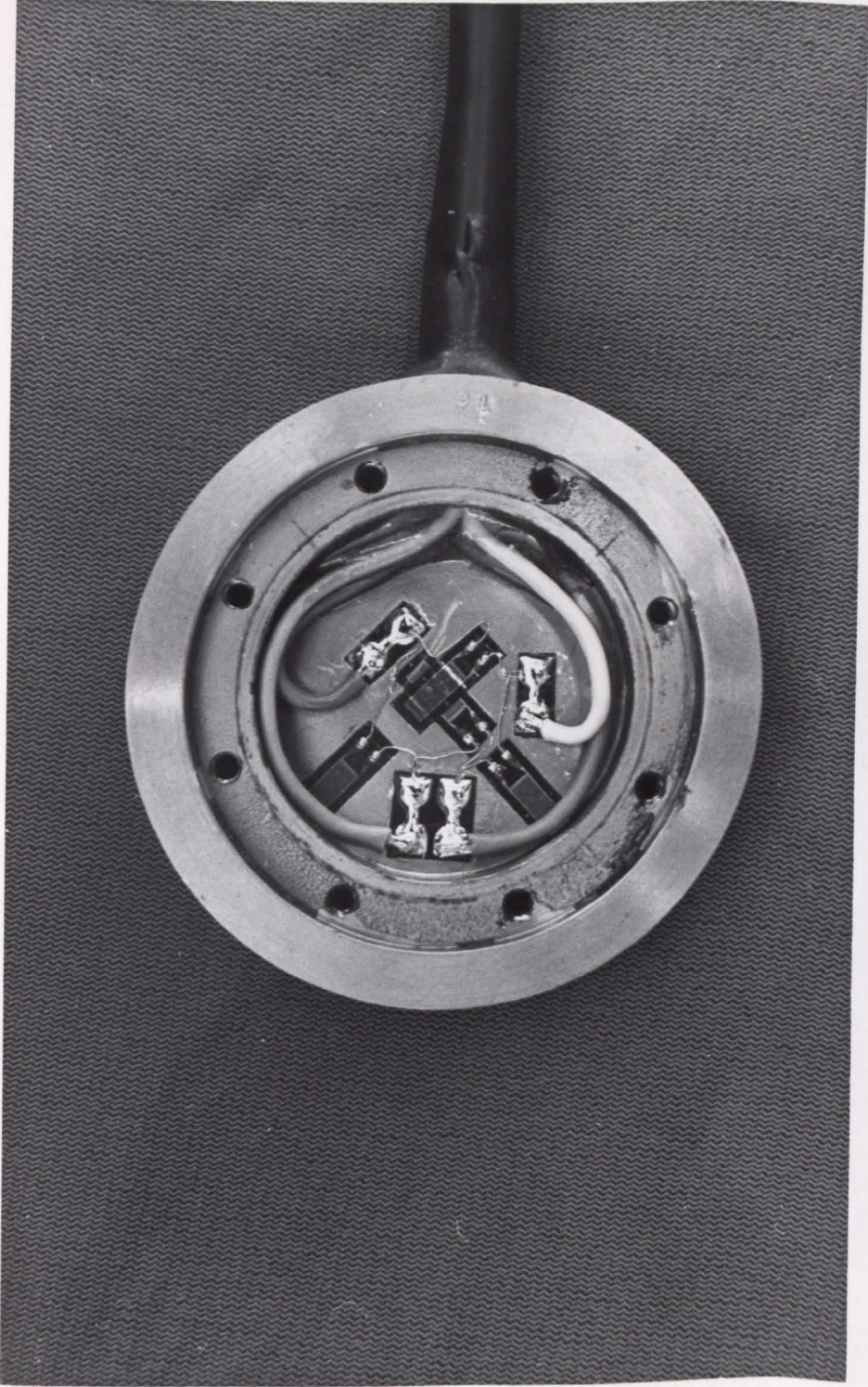
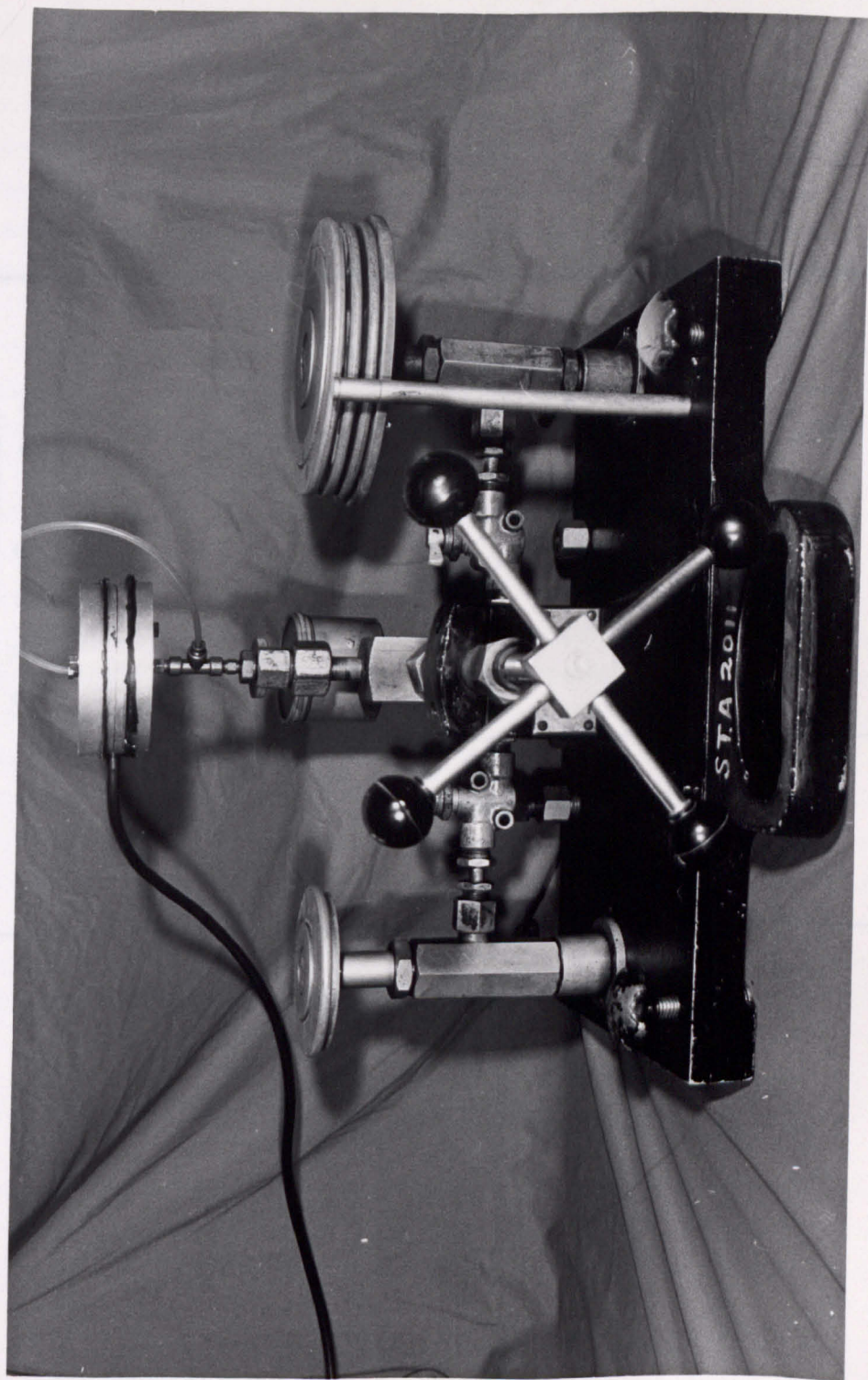


Plate 5.2 - Inside a Nottingham University Pressure Cell

Plate 5.3 - Pressure Cell Calibration Rig



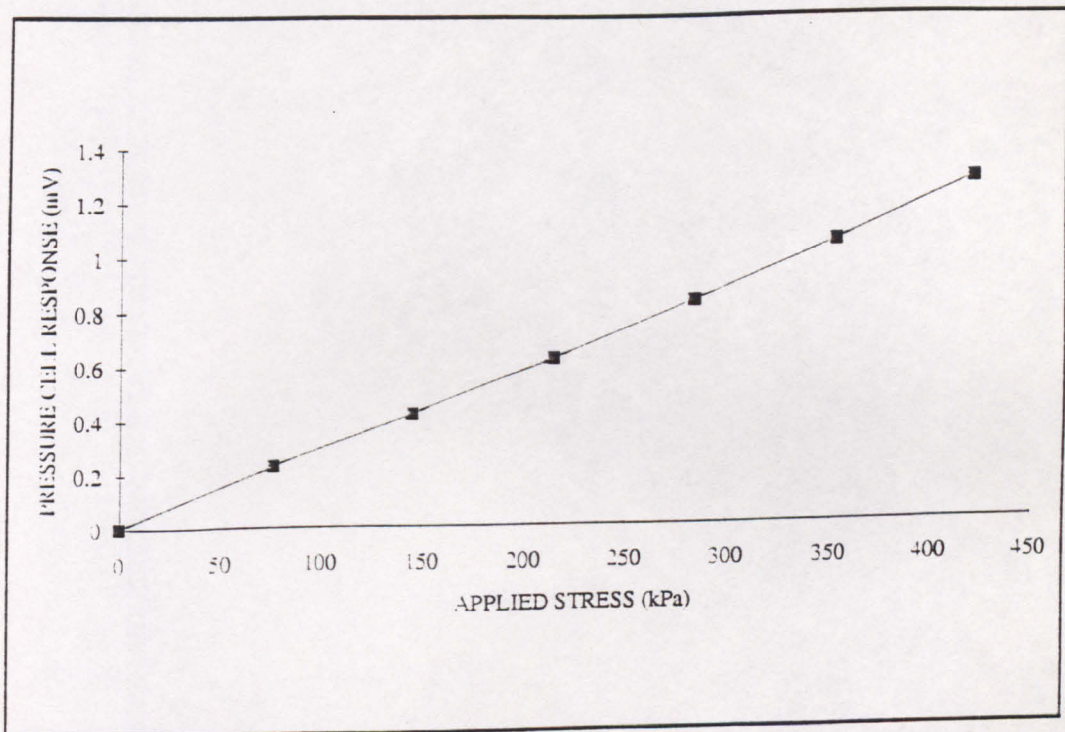


Figure 5.8 Typical Pressure Cell Calibration

**PAGE  
MISSING  
IN  
ORIGINAL**

500mm past each of the reading locations. The pressure cells were installed horizontally with the diaphragm 50mm above the geosynthetic. They were bedded on finer material, passing 1.18mm, sieved from the aggregate. Unfortunately, some variation in the cell registration does occur either as a result of point loads being applied to the diaphragm or by arching of the stress field over the diaphragm. Fines were placed on top of the pressure cell diaphragms to protect them from damage and to improve the reading accuracy of the instruments by reducing the possible effects mentioned above. Each instrument and fines were installed within a thin walled plastic bag to ensure that the fines remained in place during construction and trafficking.

Design methods based on the membrane effect (eg Giroud and Noiray 1981) assume that the stress imposed upon the subgrade is less than that applied to the surface of the geosynthetic. In order to validate this, two pressure cells were installed in the subgrade of each section at a chainage 500mm in advance of each of the two reading locations in order that the results could be compared to the aggregate pressure cells described above.

The subgrade pressure cells were installed in advance of the reading location because previous trials (Brunton and Ackroyd (1990)) have shown that as vehicles approach an instrumented cross section, the subgrade pressure cell generates a rise in the out-of-balance reading, which can be used to prompt the data acquisition system to start recording. The cells were buried horizontally with the top of the diaphragm 20mm below the surface of the formation. This protected the instrument from being damaged by angular pieces of aggregate pressed onto the casing and thus aided reading accuracy.

In conjunction with the strain coils it was hoped that a measure of aggregate and subgrade stiffness could be obtained.

#### 5.4 PORE WATER PRESSURE MEASUREMENT

The pore water pressure within the subgrade is not contained within any of the design methods discussed in Chapter 2. However, it would appear that the pore water pressure is a fundamental property of the subgrade material and as such should be recorded if possible.

Two high air entry Bishop-type piezometers were installed, one under the wheel path and one on the centre-line, both at the second reading location. These were buried with

the centre of the ceramic portion of the piezometer at a depth of approximately 200mm from the surface of the formation. This depth enabled all the fittings close to the instrument to be comfortably buried. All the piezometers were soaked in water overnight before being placed in the ground in order to saturate the ceramic portion prior to installation.

Normally, piezometers are permanently connected, via an arrangement of taps, to a pressure transducer. This is done to exclude air from the system and, hence, ensure an intimate connection between the pressure of water in the piezometer tip and that measured at the transducer. However, the size of the site was such that it was not possible to permanently connect all of the piezometers to a read-out unit. Instead a portable system was used which contained a supply of de-aired water and a measuring unit. This could be coupled to each piezometer in turn via a tap which was permanently attached to each instrument.

In order to monitor ground water levels, standpipes were installed next to Sections A, F, H and P. Four pipes were driven vertically into the ground near to the side of the pavements to depths of 0.5, 1, 1.5 and 2m below ground level. Each pipe was equipped with a sacrificial conical tip which was pushed clear of the end of the pipe after installation. The water level in the pipes was left to reach equilibrium for three months before trafficking in the Spring of 1991. The level of the standing water was then monitored by passing a sonde, which responded to the water level, down the pipe. This appeared to be a quick, easy and reliable method of determining the ground level and the results are shown in Chapter 6.

The piezometers were less successful however. It was found that on each occasion that the measuring unit was connected to the piezometers, a small amount of air entered the system thus destroying the suctions that the unit was attempting to measure. In order for the suctions to develop again the unit was left attached overnight. However, it was still not possible to obtain stable readings and so, unfortunately, subgrade suctions had to be estimated from the ground water levels.

## 5.5 MEASUREMENT OF GEOSYNTHETIC PROFILE

The shape of the deformed geosynthetic is important to design methods which are based on the membrane effect (eg Giroud and Noiray (1981)) as the shape controls the theoretical strains generated. Thus, in an attempt to monitor the geosynthetic profile an

extremely economic technique was tried in which a set of six vertical inspection tubes were placed in equal distances transversely over the uninstrumented half of the pavement from the centre line to the edge of the geosynthetic at each reading location. These tubes were heavy duty "vaccuflex" and gave direct access to the geosynthetic below. Direct profiles of the geosynthetic were thus obtained during the course of the trial by levelling the top of a 1m long bar lowered into the tube and placed on the geosynthetic.

The top of the tubes were plugged in an attempt to prevent them being filled with stones. However, the plugs often became dislodged and the tubes filled with stones carried by the lorry's tyres, or the plugs would be pushed into the tube by loose stones and would then be impossible to remove. The deformations at the interface were small and uncertainty in the quantity of materials that may be in the tubes led to a low degree of confidence in the readings obtained.

On final excavation, it was found that the subgrade material had been forced up some of the tubes causing a small mound in the subgrade as shown in Plate 5.4. Thus the results of the geosynthetic profile obtained from these tubes will not be included in this thesis as there would appear to be too many problems in obtaining reliable results from this method.

## 5.6 MEASUREMENT OF GEOSYNTHETIC TEMPERATURE

As geosynthetics are manufactured from polymers, generally polypropylene or polyester, their properties are temperature dependent. Thermocouples were used to measure the temperature. Robust thermocouple wire was purchased from a propriety manufacturer and thermocouple junctions were welded at the University.

Thermocouples were not included in all sections as the temperature of the geosynthetics was unlikely to vary significantly between one section and the next. The upper-bound sections contained three thermocouples in total and the lower-bound contained four.

The thermocouples were monitored throughout the two trafficked periods using a propriety reading unit. All of the welded tips survived the construction and trafficking processes and gave sensible readings of the temperature of the geosynthetics. Generally it was found that during the trafficking period, the temperature of the geosynthetic was between 11 and 15°C.

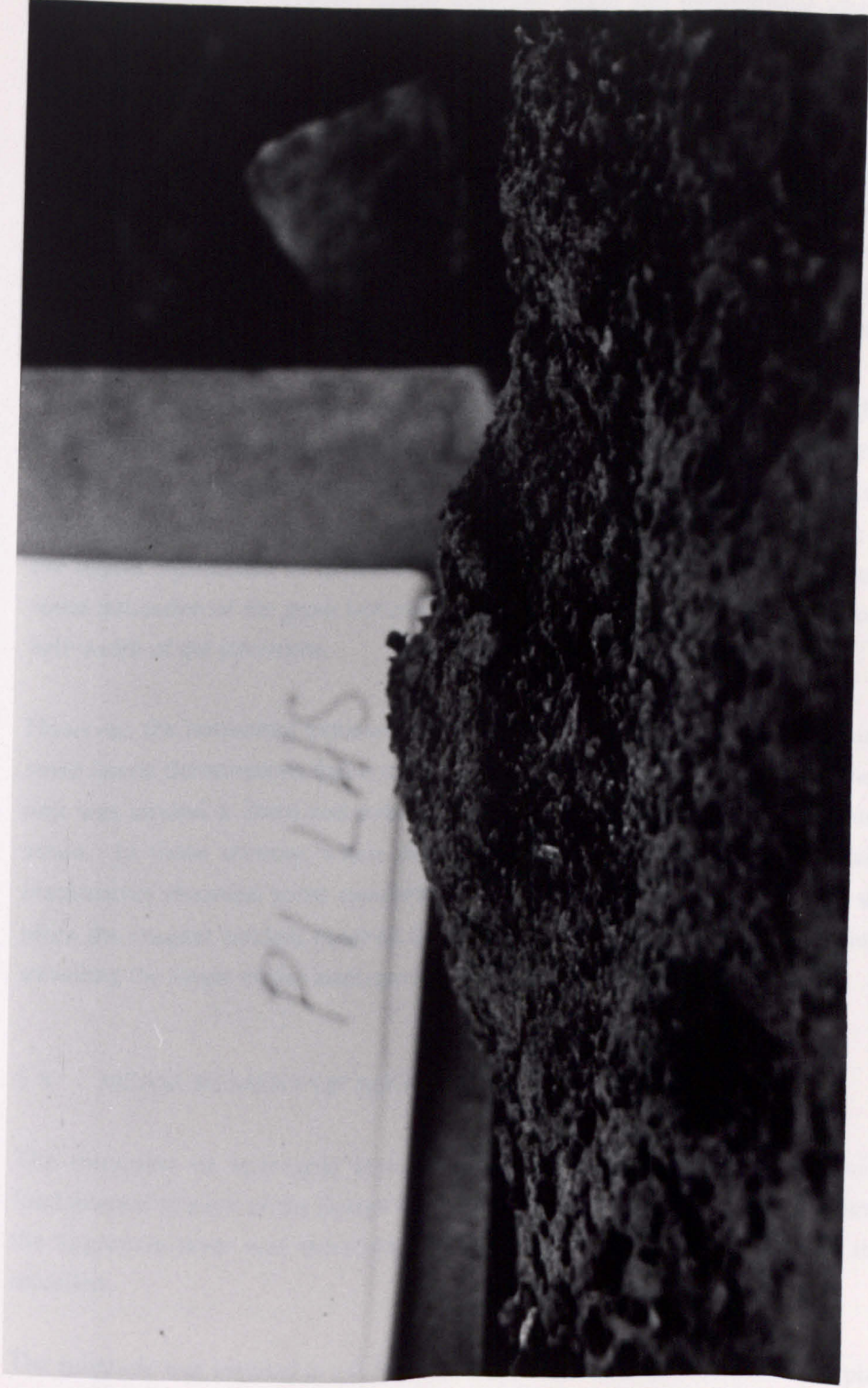


Plate 5.4 - Damage to Polyfelt Section (P) Caused by the Vertical Inspection Tubes

## 5.7 MEASUREMENT OF LATERAL SUBGRADE STRAIN

If the relationship between lateral subgrade strain and geosynthetic strain could be determined it might give some indication of the mechanisms involved in the deformation of the system. The geosynthetic strain can be monitored by the strain coil array described earlier. In order to examine lateral subgrade deformations a horizontal extensometer was installed 3m past the first reading location in each section. Each extensometer consisted of a 20mm diameter plastic tube and six extensometer plates as shown in Figure 5.9. The holders for the magnets for the horizontal extensometer were manufactured by the University Engineering Faculty Workshop and the magnets were bought from a company in West Midlands. The units were then fabricated on site.

A sonde containing a reed switch was passed down the extensometer tube and the magnets on the extensometer plates caused the switch to close completing an electrical circuit. The six extensometer plates, carrying the magnets, were spaced so that the first magnet was located on the centre-line of the pavement, the last on one edge, and the others equidistant in between. It was hoped that the extensometers would give some indication of the gross horizontal strains occurring in the subgrade across the full half-width of the pavement.

However, the horizontal extensometers were not sensitive enough for monitoring the small lateral deformations that occurred in most sections. The resolution of the read-out unit was around  $\pm 2\text{mm}$  and over a gauge length of 400mm this represents  $\pm 0.5\%$  strain. In those sections where the deformations were large, close to failure, the instruments recorded some movement, however, these movements were small and often the magnet holders pinched the extensometer tube preventing the sonde from travelling the length of the instrument.

## 5.8 MEASUREMENT OF AGGREGATE THICKNESS

The thickness of aggregate layer required to resist the deformation criteria is fundamental to each of the design methods described in Chapter 2. The thickness of the aggregate layer was therefore carefully controlled and the achieved thickness recorded.

The subgrade was levelled in a 0.5m grid before aggregate and geosynthetic placement so that it could be compared to the level of the furnished aggregate surface. The level

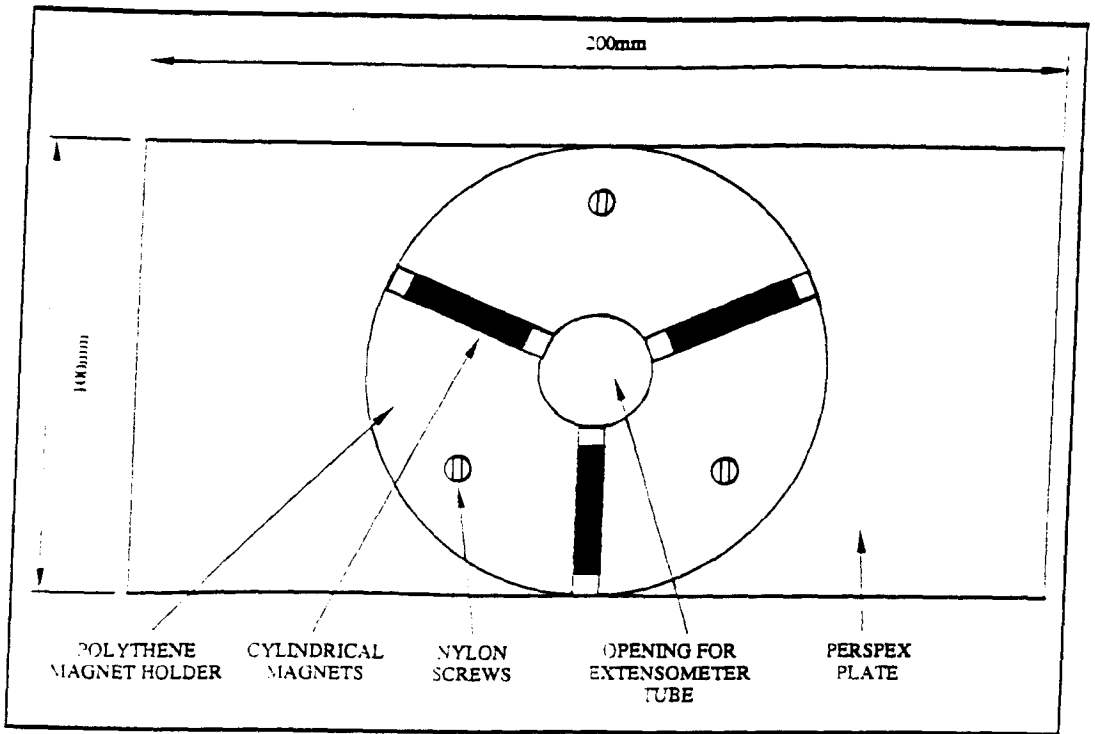


Figure 5.9 Magnetic Extensometer Plate

information was also used to determine the finished level of the aggregate layer. A "base formation level" was calculated on the basis that 85 percent of the formation level readings fell below it. The required thickness of aggregate was added, by the contractor, using a laser level which was set so that the foresight reduced level was the base formation level plus the required thickness. Thus, it was hoped that 85 percent of the section would be covered by the appropriate design thickness of aggregate or more.

The final aggregate surface was levelled in a 0.5m grid after compaction but before any trafficked commenced and the results were compared to the results obtained from the levelling of the subgrade. The exact thickness of material at each location on the 0.5m grid was then calculated and is summarized in Table 5.2

Section	Instrumented Wheel Path Thickness (mm)		Pavement Thickness (mm)		Design Thickness (mm)
	Mean	Standard Deviation	Mean	Standard Deviation	
A	430	16.5	430	18.0	400
B	495	33.4	493	32.3	450
C	527	23.6	526	26.9	500
D	580	33.5	580	33.7	550
E	536	23.4	541	28.5	490
F	436	16.8	428	20.8	400
H	428	12.7	431	21.3	400
I	350	29.3	342	28.1	300
J	262	13.9	265	12.6	340
K	394	29.4	397	25.1	400
L	354	23.4	352	26.0	350
M	372	16.3	372	17.2	350
N	332	30.9	340	28.4	300
O	366	22.9	366	21.4	350
P	360	18.8	368	20.8	350

**Table 5.2 Aggregate Thickness**

It should be noted that the thickness of Section J, the lower-bound woven section, is notably thinner than the design requirement. This was due to a calculation error in the determination of the base formation level and only came to light at the end of the trial period. The thinness of the pavement reduces the expected life of the pavement but

does not invalidate the section. Indeed, given the insitu ground conditions during trafficking the constructed thickness was probably more suitable. It should be noted that the average thickness of Section K was very close to the design value; the other sections were constructed with the mean thickness some 20-40mm thicker than the design.

## 5.9 DATA COLLECTION ARRANGEMENTS

All of the signal cables from the electrical instrumentation were terminated in an instrumentation pit by the side of each section. The strain coils and pressure cell cables were fitted with plug sockets to enable a sound and speedy connection to the instrumentation during data collection procedures.

The pressure cell signals were amplified using strain gauge amplifiers before they were recorded, through an analogue to digital converter, to a personal computer. A gain of 4,000 was used which gave an approximate calibration of 1.4V per 100 kPa for these pressure cells.

The static strain coil spacing voltage was recorded manually and the amplified dynamic output was recorded in the same manner as for the pressure cells. The voltage generated by the dynamic output of the Emu device as a result of transient strain depends on the magnitude of the strain, the spacing of the coils, the amplification to the device and the individual coil pair. Therefore, no simple approximate calibration existed for these instruments.

The analogue to digital device was capable of recording twenty channels at the same time, although the maximum that was actually recorded at any one time was eight. The data was recorded at 5 millisecond intervals which ensured that the sampling rate was much higher than the duration of the recorded event. The full-scale range of the analogue to digital machine was set to  $\pm 5V$ . This scale was divided into  $\pm 32,000$  bytes and so the resolution of the output was below 1mV.

Due to restrictions on the number of read-out and recording devices available, it was possible to read only one instrument reading location in any one pass. Since there were un-instrumented areas between the upper-bound and lower-bound sections, where the lorry could wait whilst the data collection location was changed, it was possible to record the transient effects of the pass of the lorry for one upper-bound and one-lower-

bound reading location per circuit. As Sections G and H had no instrumentation, it was possible to read all of the six upper-bound instrumentation reading locations within twelve passes, and the eight lower-bound sections in sixteen passes. Thus, in each complete circuit the data from each upper-bound reading location and its corresponding lower-bound partner were recorded.

## 5.10 FREQUENCY OF MEASUREMENTS

In planning the test programme for the Spring of 1990, it was assumed that damage to pavement structures was a function of the logarithm of the number of passes. Therefore, it was decided to monitor the pavements most frequently at the start of the trial. Readings of permanent deformation were taken after 0, 1, 3, 11, 50, 100, 250, 500 and 1000 passes. As described above the reading of transient stress and strain took 16 passes to collect due to the limited number of monitoring units available and therefore transient values were taken as groups around 8, 50, 100, 250, 500 and 1000 passes.

A more pragmatic approach to the in-situ measurements was taken in 1991. For sections which preformed well, the rate of sampling was reduced, until failure started to occur, when the sampling rate rose sharply. Generally, a full set of readings (static and transient) occurred at or around pass numbers :-

- 1000 (start of 1991 season)
- 1015 (to account for re-compaction due to frost effects etc)
- 1115 (end of 80kN applications)
- 1220
- 1365
- 1615 (lower bound cases only)
- 2115 (end of trafficking)

## 5.11 INSTRUMENT PERFORMANCE

### 5.11.1 General

Some of the instrumentation intended to monitor the pavement performance had been installed ten months before the trafficking commenced. During this time a certain

amount of deterioration was expected. Table 5.3 shows the status of the instrumentation in the Spring of 1990. The effect of long-term exposure to moisture was to render some of the instruments useless, some required remedial work and some were unaffected. The survival rate for the strain coil pairs was encouraging with approximately 80% functioning satisfactorily, considerably more than it was thought would survive the construction process and long term moisture effects.

The pressure cells proved to be slightly less robust with a survival rate to the Spring of 1990 of approximately 60%. Even fewer were operating in the Spring of 1991. Of those that survived most required some form of remedial work to function correctly. This normally entailed addition of high stability resistors, externally to the strain gauge Wheatstone Bridge, in order to re-balance the cell. The addition of resistors over 5000 Ohms was considered not to affect the calibration of the cells. Those which required balancing resistors of less than 5000 Ohms were considered to be unusable. This was partly due to concern that the initial calibration would no longer be valid and partly due to the fact that pressure cells requiring the addition of low value resistors were unlikely to prove stable over time.

At the end of the trial several pressure cells that were not functioning correctly were retrieved for examination. It was found that, despite the efforts taken to protect the cells from the effects of moisture, some corrosion had occurred on the fine wires inside the cell. It is possible that the moisture was able to enter the cell through the cable wall. P.V.C., which was used to sheath the cable, is not water proof and over long periods of time a small quantity of water will pass through the casing and into the wire. This moisture may travel down the wire, by capillary action, into the cell where fine wires are easily corroded.

Section	Pressure Cell Aggregate	Pressure Cell Subgrade	Wheel Path Geosynthetic Coil Pair	Wheel Path Aggregate Coil Pair	Wheel Path Subgrade Coil Pair	Coil Pair A	Coil Pair B	Coil Pair C
A1	X	X	✓	✓	✓	N/A	N/A	N/A
A2	X	X	✓	X	✓	N/A	N/A	N/A
B1	X	X	X	✓	X	N/A	N/A	N/A
B2	X	✓	X	✓	✓	N/A	N/A	N/A
C1	X	X	✓	✓	✓	N/A	N/A	N/A
C2	X	✓	X	✓	✓	N/A	N/A	N/A
D1	✓	X	X	✓	✓	N/A	N/A	N/A
D2	✓	✓	X	✓	✓	N/A	N/A	N/A
E1	✓	✓	✓	✓	✓	N/A	N/A	N/A
E2	✓	✓	✓	X	✓	N/A	N/A	N/A
F1	✓	X	✓	✓	✓	X	✓	✓
F2	✓	✓	✓	✓	✓	X	✓	✓
I1	I	I	✓	✓	✓	X	✓	X
I2	✓	I	✓	✓	✓	✓	✓	X
J1	✓	✓	✓	✓	✓	✓	✓	X
J2	✓	I	X	X	✓	✓	X	✓
K1	✓	X	✓	✓	✓	N/A	N/A	N/A
K2	✓	X	✓	✓	✓	N/A	N/A	N/A
L1	✓	✓	✓	✓	✓	✓	✓	✓
L2	✓	✓	X	X	X	✓	✓	✓
M1	✓	✓	✓	✓	✓	✓	✓	✓
M2	✓	X	X	X	X	✓	✓	
N1	✓	X	✓	✓	X	✓	✓	✓
N2	✓	X	✓	✓	✓	✓	✓	✓
O1	✓	X	✓	✓	✓	✓	✓	✓
O2	✓	I	✓	✓	✓	✓	✓	✓
P1	✓	✓	✓	✓	✓	✓	✓	✓
P2	✓	✓	✓	✓	✓	✓	✓	✓

KEY: ✓ = Working    X = Not working    I = Intermittent    N/A = Not Applicable

see Table 5.1 for the location of coil pairs A, B and C.

Table 5.3 Status of the Strain Coils and Pressure Cells, Spring 1990

### 5.11.2 Strain Coils

An example of a result obtained from the transient response of a strain coil is shown in Figure 5.10. The strain, obtained from the calibration, has been added. The signal to noise ratio in this example is fairly high, that is that the peaks caused by the passage of the vehicle are clearly distinguishable from the random variation in received voltage of the strain coil. However, the measured transient response is a function of the size of the strain involved, the initial proximity of the strain coils and the amplification applied to the measured signal by the monitoring unit. Therefore, for strain coils where the strains were small, or the initial spacing of the strain coils was large, the results have been lost due to noise in the system. It is unfortunate that strain coils are, by their very nature, good aerials and hence pick up a large range of noise signals. This noise was particularly problematic for those strain coils that were attached to the geosynthetics in a position remote from the wheel path. Thus, the quality of the useful signal generated by the strain coil pairs attached to the geosynthetic deteriorated from the pair beneath the wheel load to the most remote coil pair.

### 5.11.3 Pressure Cells

An example of a result obtained from a pressure cell is shown in Figure 5.11 with stresses, obtained from the calibration, added. As can be seen the signal to noise ratio is high and a clear plot is produced. The balance of the Wheatstone Bridge within the pressure cell wanders slightly over time and therefore there can be no measure of permanent, or locked in, vertical stresses.

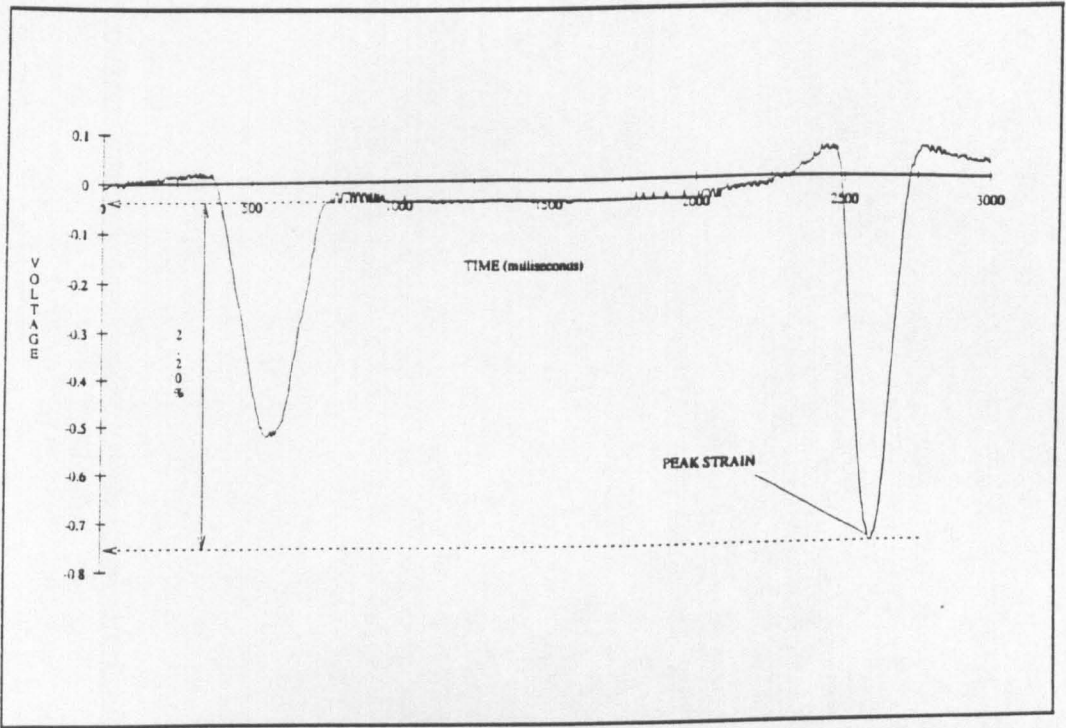


Figure 5.10 Example of the Dynamic Output from the Emu Device

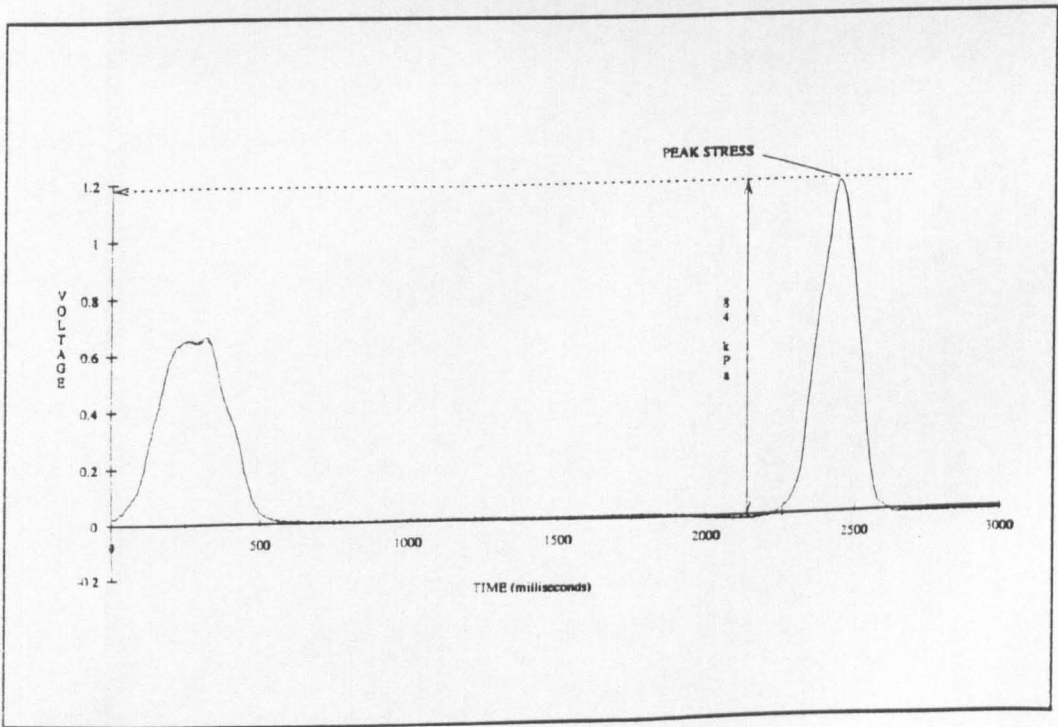


Figure 5.11 Example of the Amplified Output from a Pressure Cell

## CHAPTER SIX

### RESULTS

#### 6.1 INTRODUCTION

This chapter presents some of the results arising from the full-scale trials at Bothkennar. The volume of data obtained was large and therefore, where possible, is summarized. Data is presented to compare the predicted and actual performance of the designs covered and to contrast design methods. All the data obtained is available in spread sheet format on computer disc (Little (1992)).

In relation to the critical parameters in the design methods discussed in Chapter 2 and those that could be measured in the full-scale trials, as discussed in Chapter 5, the following measurements appear to be of most value.

Rut depth development with passes, as the serviceability criteria for design, is important for all the design methods. This relationship was relatively straight forward to obtain for all sections except the sand and gravel upper-bound control (Section G) where it proved difficult to provide consistent channelised trafficking.

Stress and strain distributions are important in order to comprehend the mechanisms involved within the system. They enable the design methods to be viewed critically in the light of the observed and predicted measurements. However, results were obtained with electrical instrumentation and losses did occur, thus some of these results are incomplete.

Other results, such as the final pavement thickness and the position of the water table, are presented which may not be useful in examining the design methods directly, but which either give indications of the mechanisms involved within the system or help to characterise the materials involved in the trials.

No results are presented for Section G, the sand and gravel upper-bound control. The section did not contain any instruments and was intended to only provide rut depth data. However, the proximity of the section to the end of the upper-bound pavement length led to non channelisation of the loading as it turned at different times to negotiate the bend at the top of the circuit. Thus, the results obtained from this section were not

comparable to the other sections and they have, therefore, been removed from the analysis.

## 6.2 SURFACE RESPONSE UNDER TRAFFICKING

### 6.2.1 General Performance

The development of rut depths resulting from the passage of 2,115 passes of the combined axle loadings are shown in Figures 6.1 to 6.15 and will be discussed further in Chapter 6.2.3. However, in summary, two sections, namely the Oxford and Woven lower-bound sections I and J, rutted to a depth in excess of 150mm. One section, namely the Polyfelt and Bamboo - Section O, suffered from geosynthetic rupture over a short length although the overall rut depth for the section was within the failure criteria. None of the remaining sections failed although the rut depths varied from 18mm to 49mm.

Thus, generally, the pavement sections performed well compared to the original design proposals of a 150mm rut after 1000 passes of an 80kN axle. However, this was to be expected given that the shear strength of the subgrade increased markedly between design and trafficking.

On those sections that performed well, the passage of 2115 axles of differing load magnitudes produced little damage. Examination of the trend of rut development implies that failure for some sections was not imminent. However, it was found that the failure tended to be brittle in nature in that the rate of rut depth development increased dramatically upon geosynthetic rupture. Visual inspection of a section close to failure indicated that a large rise in the surface transient deflections occurred. This was coupled with transverse surface cracks appearing in the wheel path which were probably a result of the same mechanisms discussed in 6.2.2.

In the majority of cases the ruts were reasonably uniform along the length of each section. Notable exceptions were Section J, and to a lesser extent Sections O and P, where larger, local rut depths occurred leading to localised failure. The rut depths for each section were measured in the offside (RHS) wheel path. Not surprisingly, given the discrepancy in the wheel loading in the 1991 trials, the nearside (LHS) wheel path suffered greater damage in some sections.

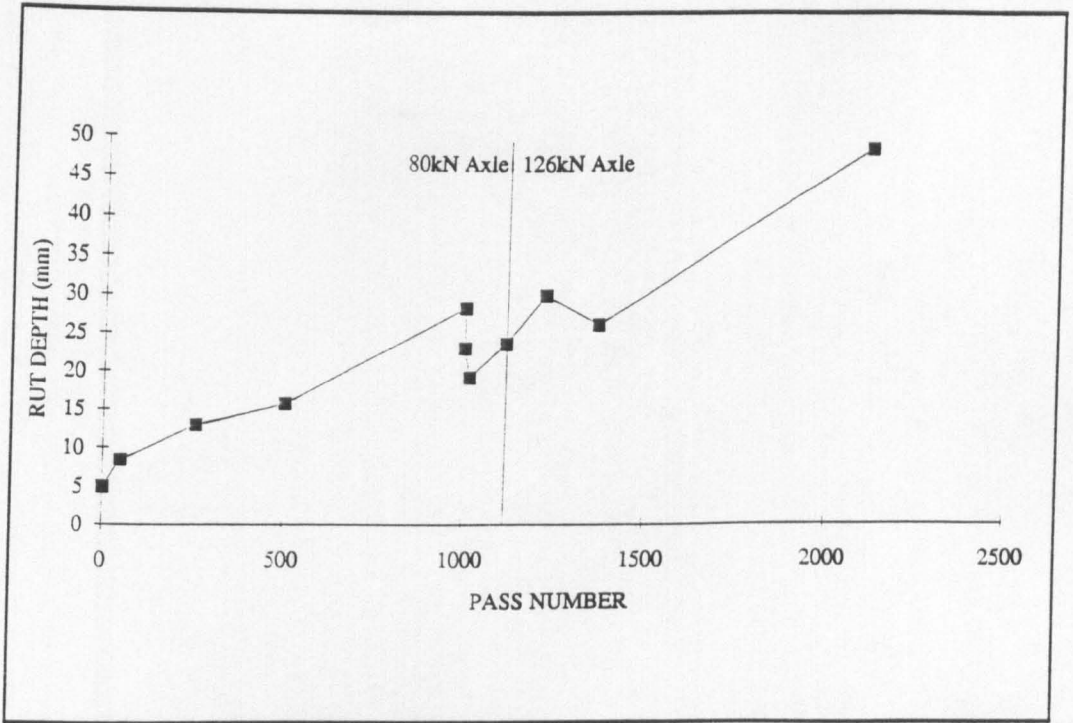


Figure 6.1 Rut Depth Development - Section A

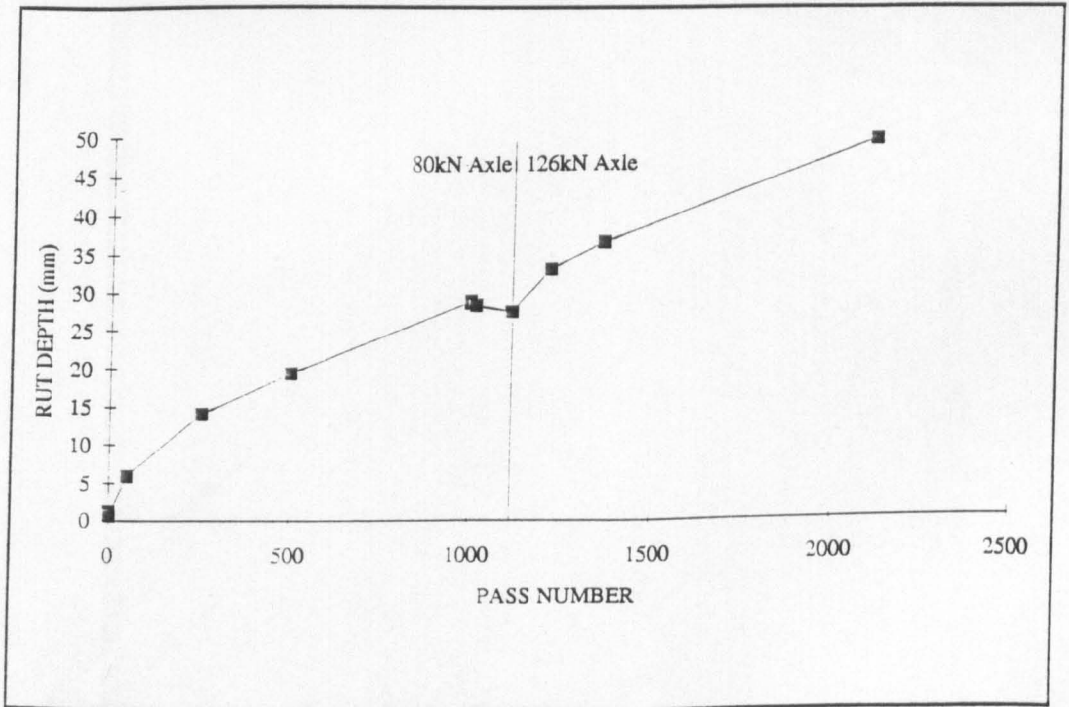


Figure 6.2 Rut Depth Development - Section B

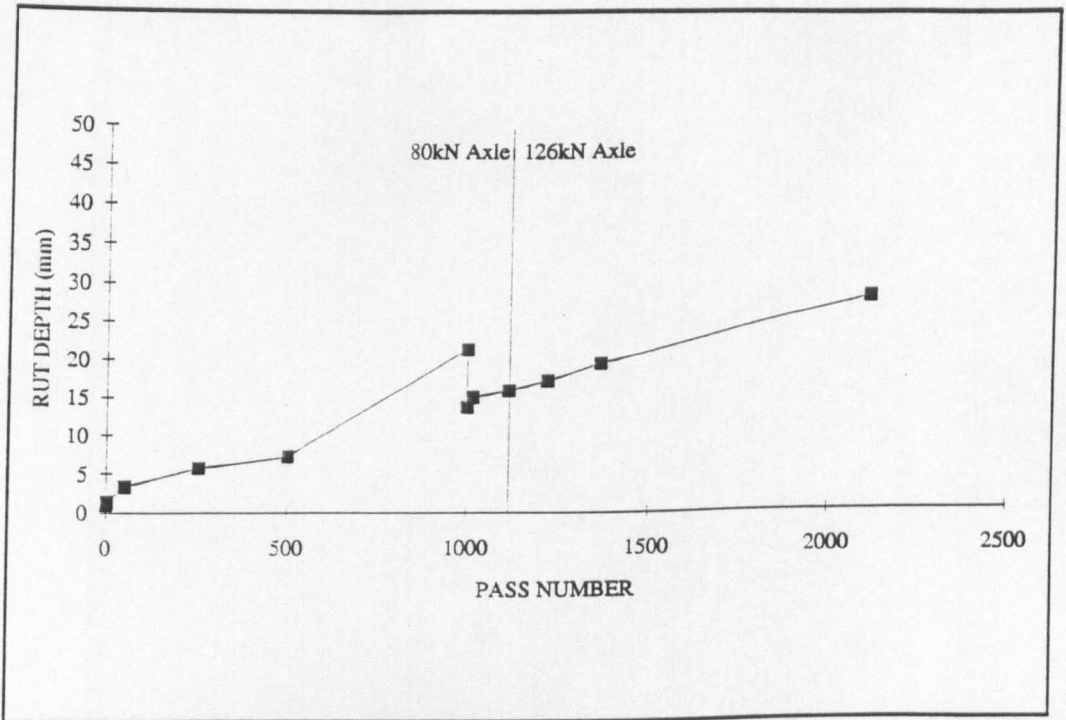


Figure 6.3 Rut Depth Development - Section C

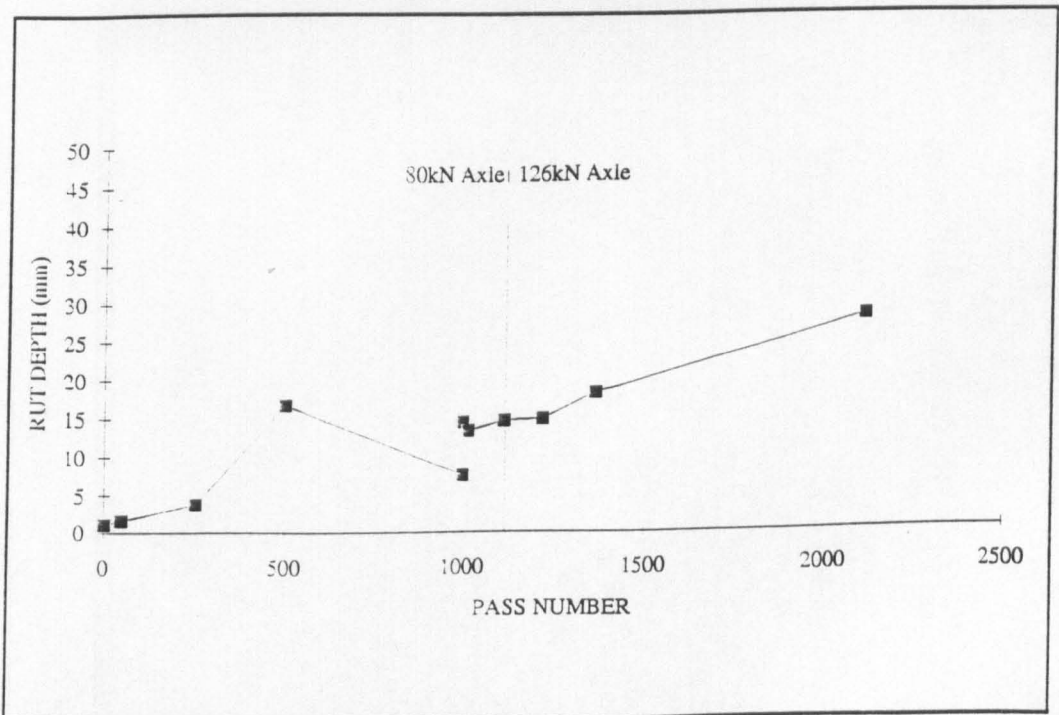


Figure 6.4 Rut Depth Development - Section D

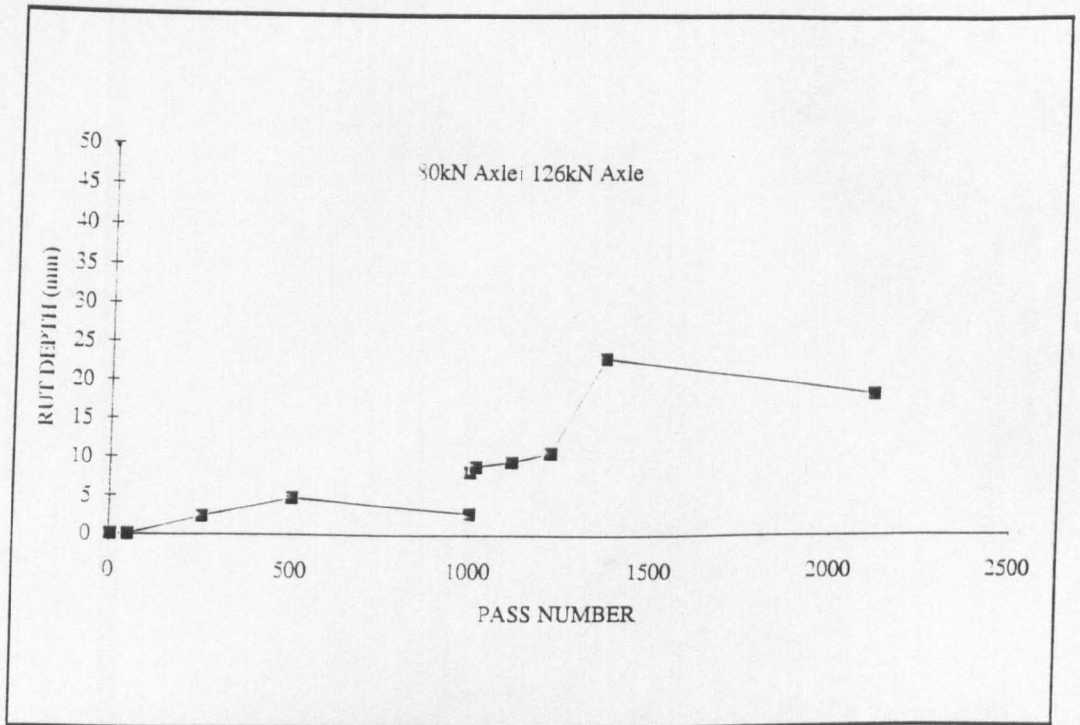


Figure 6.5 Rut Depth Development - Section E

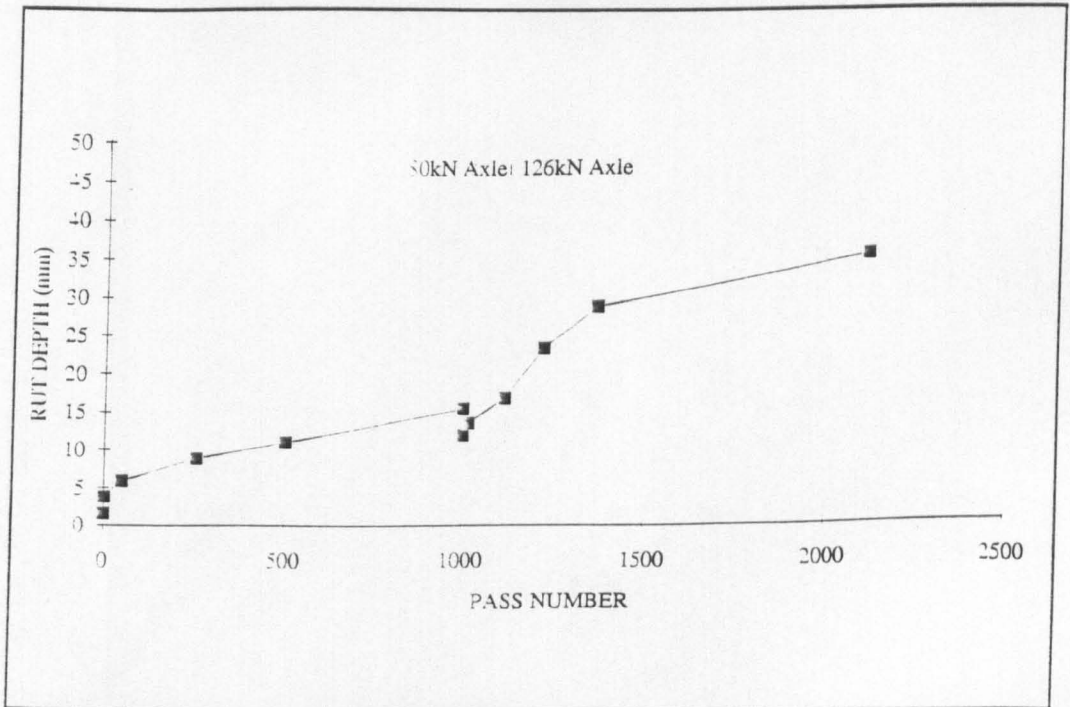


Figure 6.6 Rut Depth Development - Section F

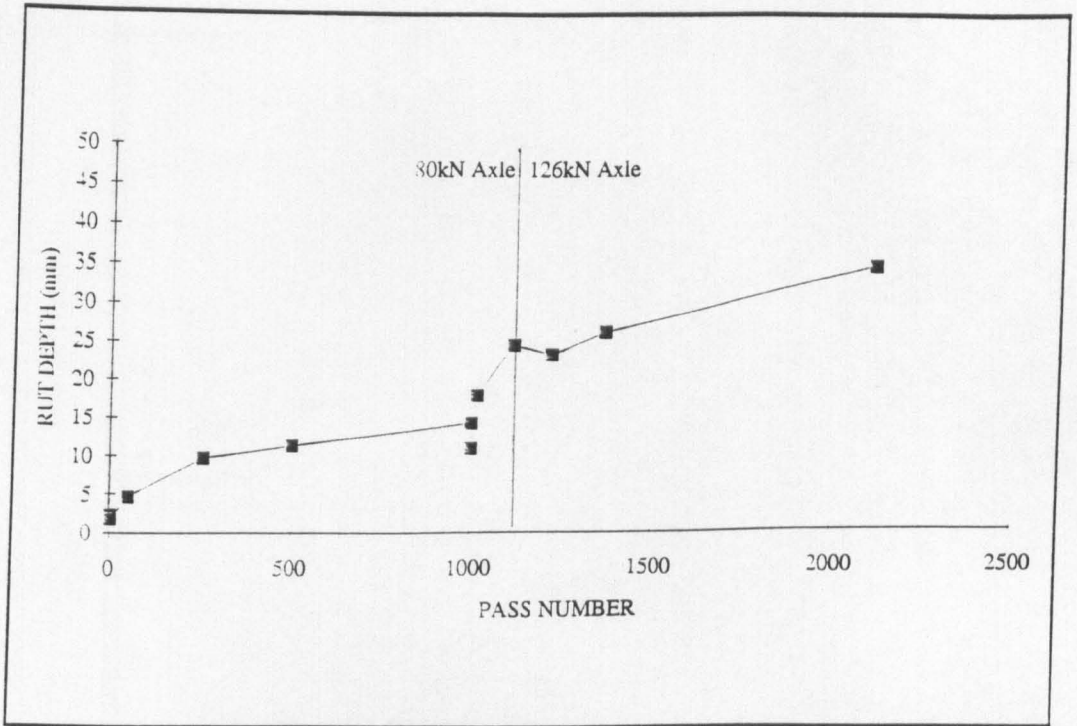


Figure 6.7 Rut Depth Development - Section H

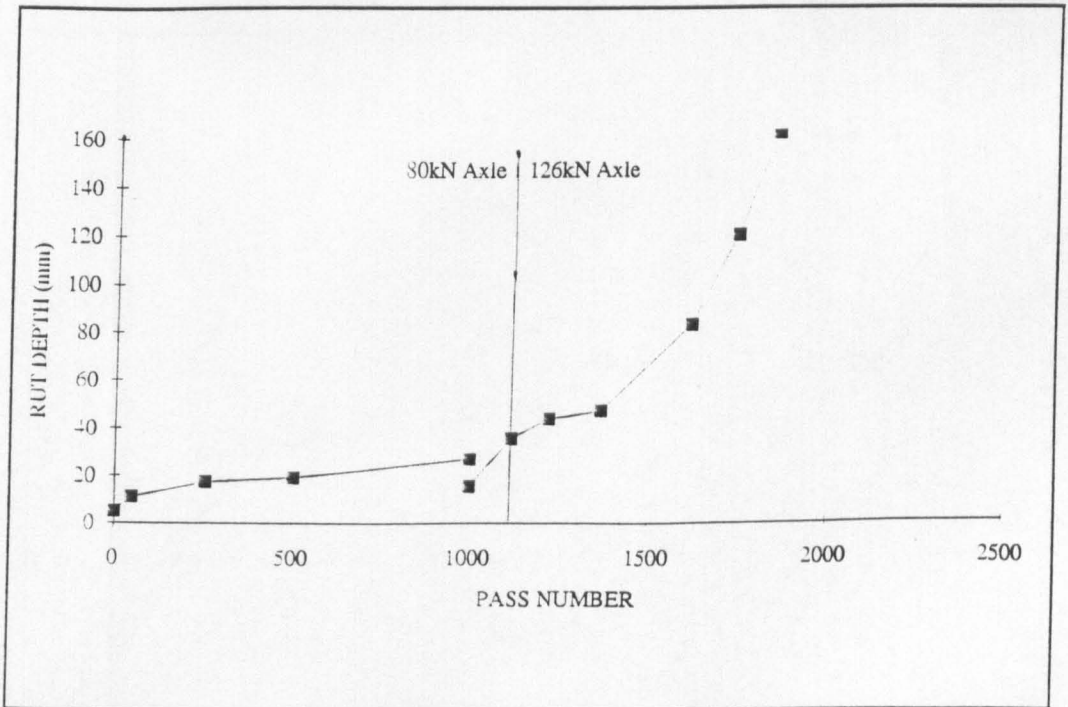


Figure 6.8 Rut Depth Development - Section I

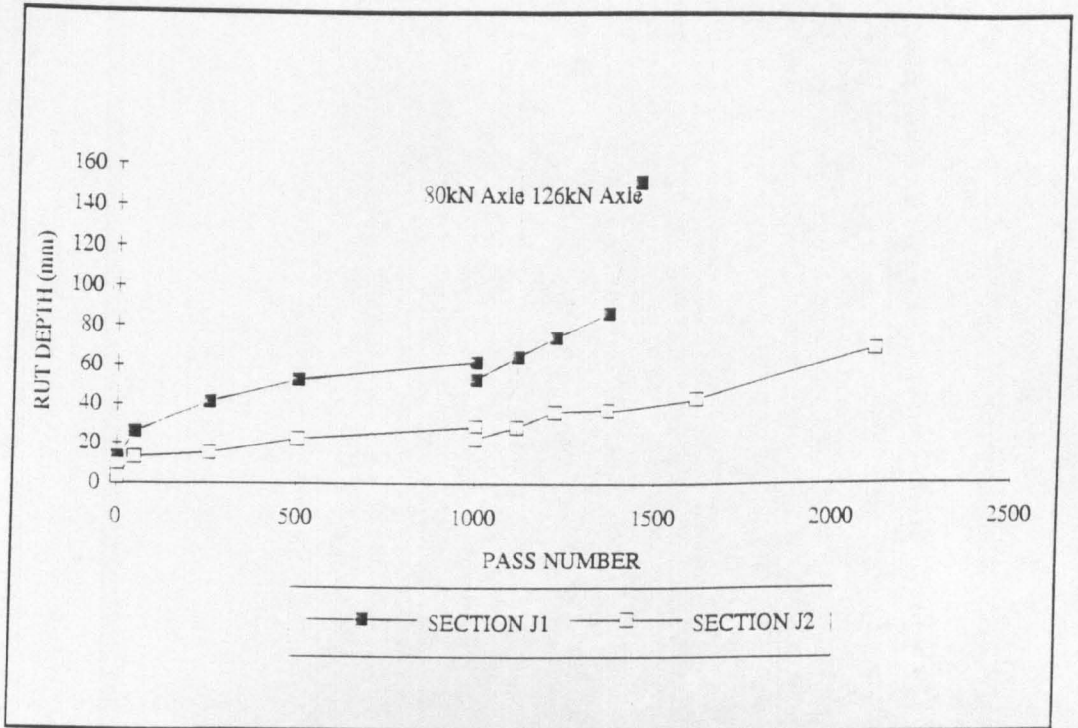


Figure 6.9 Rut Depth Development - Section J

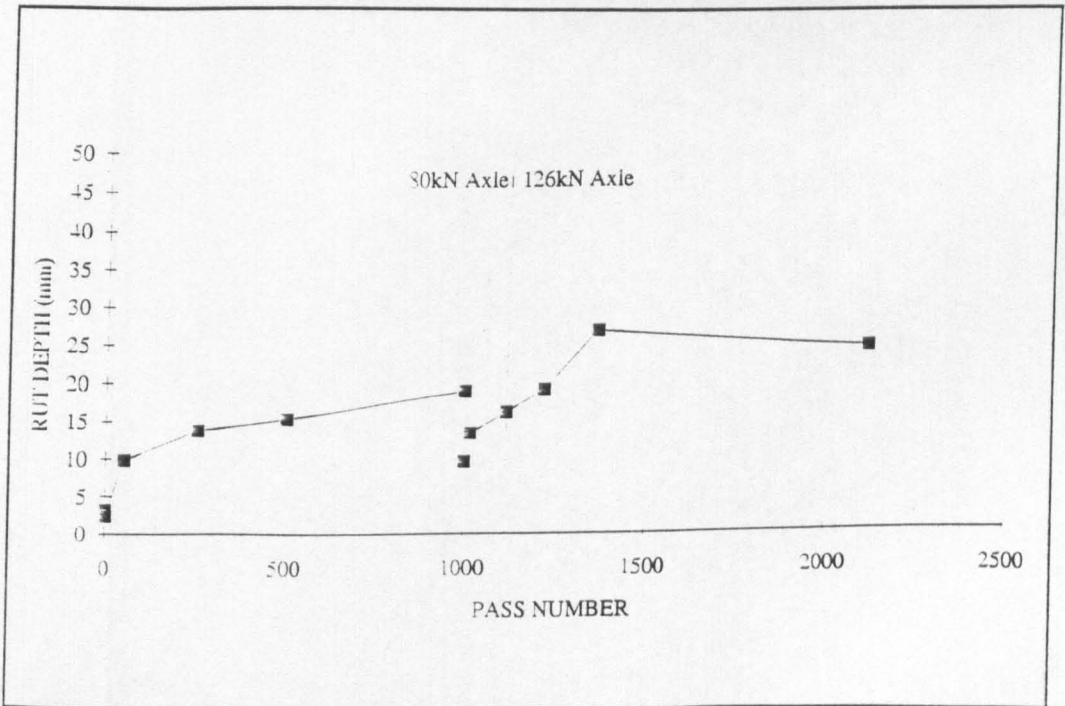


Figure 6.10 Rut Depth Development - Section K

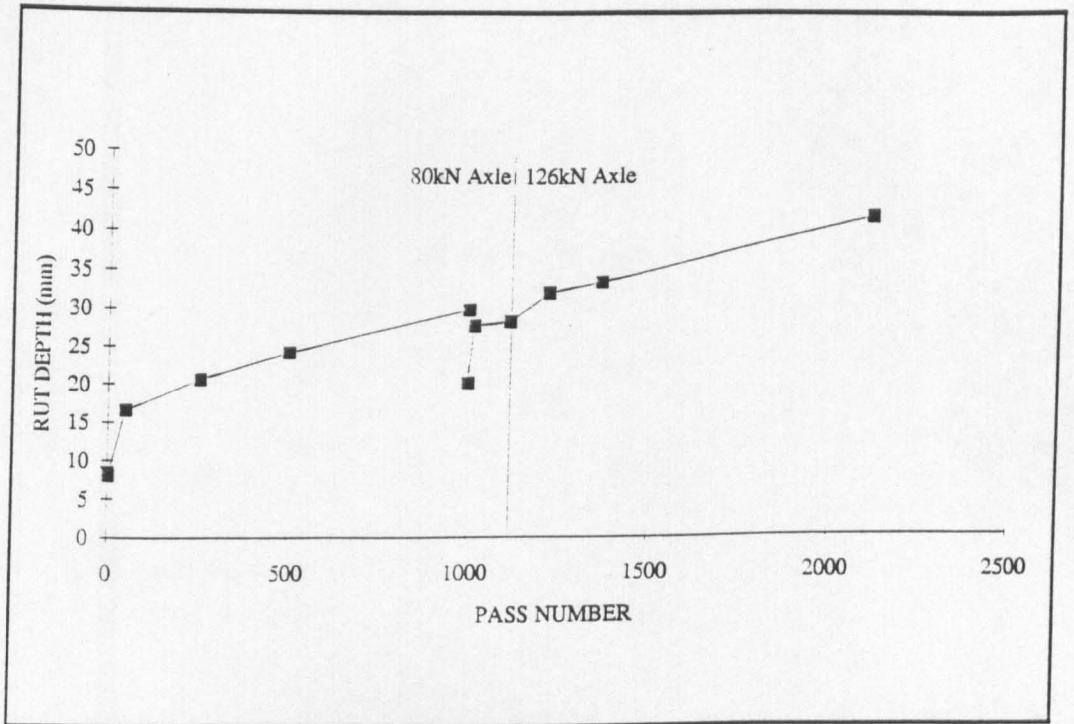


Figure 6.11 Rut Depth Development - Section L

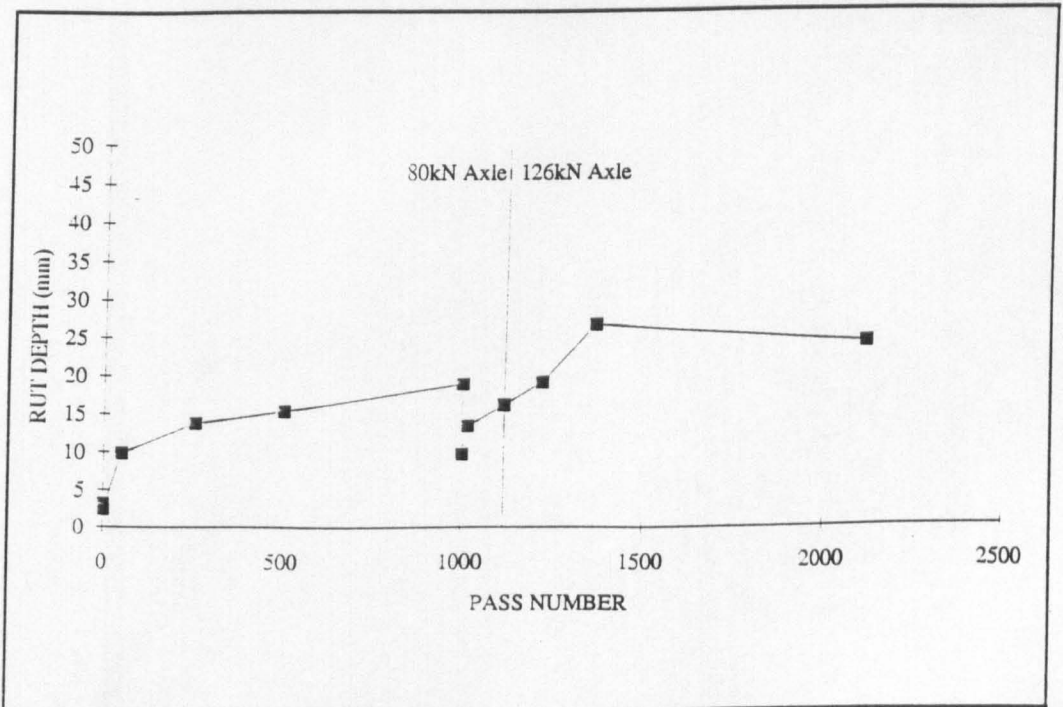


Figure 6.12 Rut Depth Development - Section M

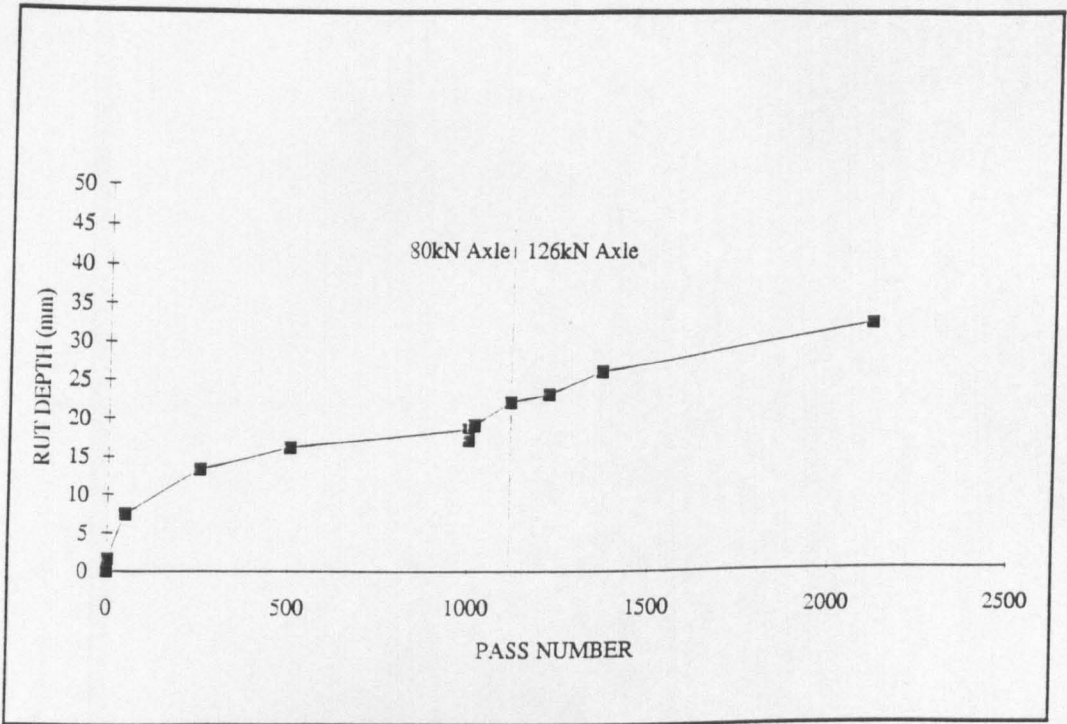


Figure 6.13 Rut Depth Development - Section N

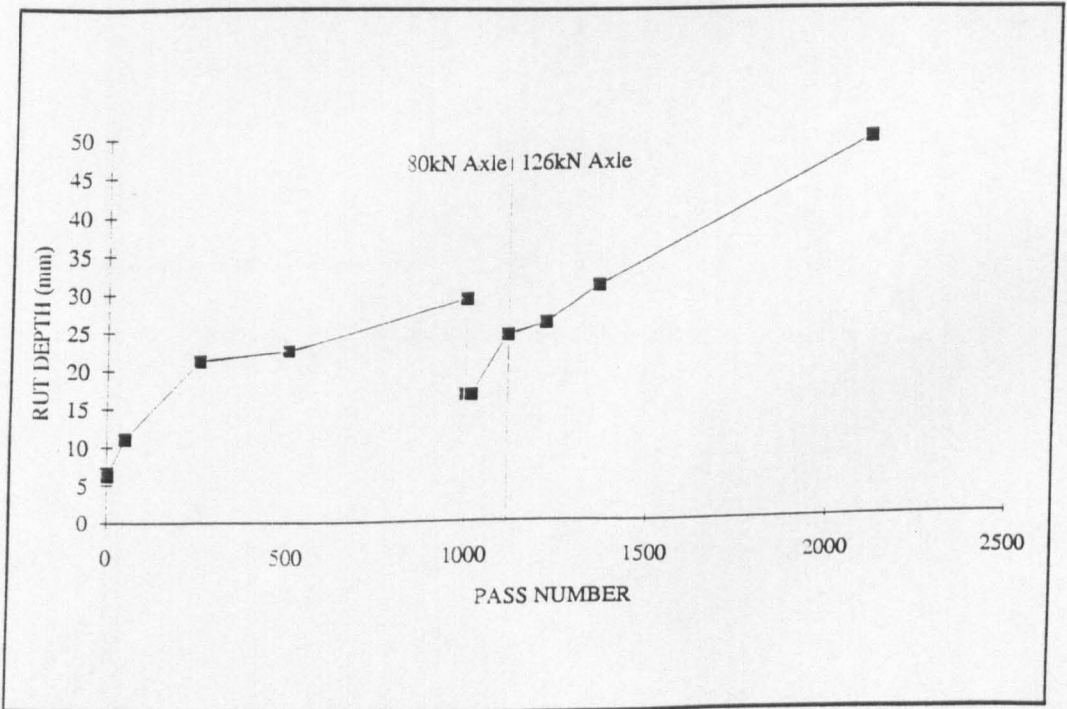


Figure 6.14 Rut Depth Development - Section O

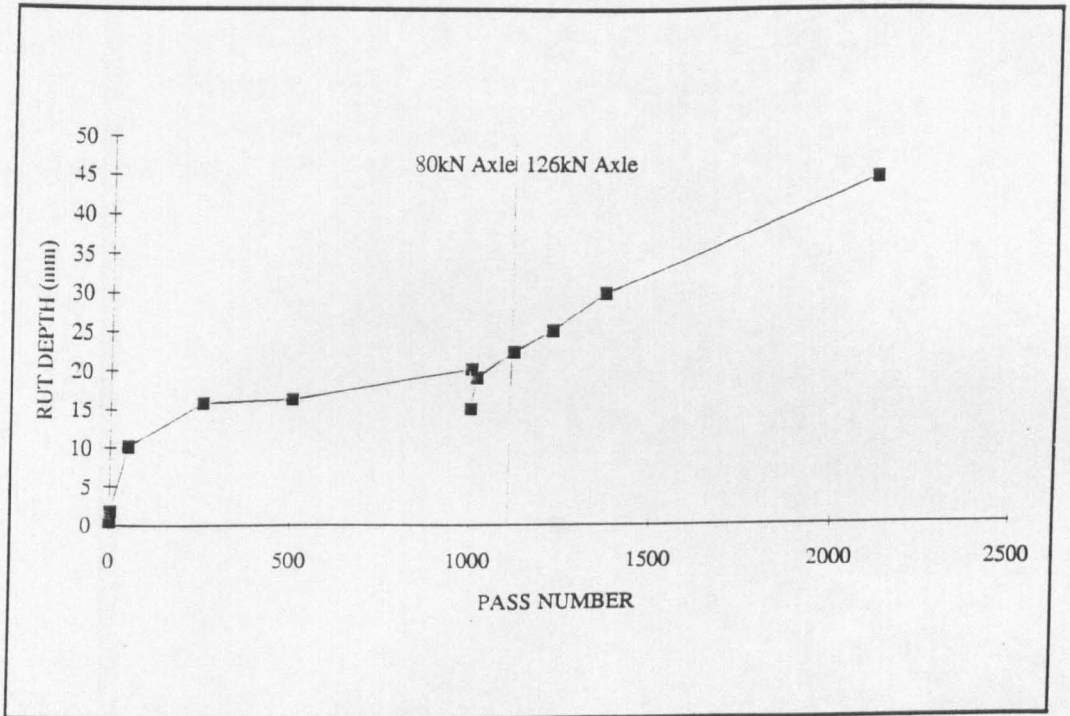


Figure 6.15 Rut Depth Development - Section P

### **6.2.2 Observations on Surface Movements Prior to Significant Rutting**

The progression of rutting with traffic was slow although it was possible to see the lorry's path after a few passes. A small amount of aggregate compaction occurred in the first few passes even though the surface of the aggregate was rolled with a dead 1000kg/m roller prior to the onset of the trials.

It was possible to see significant transient deflections of the pavement surface as the wheel of the lorry passed over. These deflections were more pronounced on the lower-bound sections. The flexing of the pavement structure to this extent probably caused cracking which appeared in the surface of the aggregate layer. These cracks were similar in appearance to fatigue cracks normally associated with asphaltic pavements. It is possible that these were tension cracks generated by the large convex deflections of the pavement surface under the wheel load. Suctions within the aggregate layer may have permitted them to stay open for a short while, during which time small particles may have been displaced into the cracks preventing closure when the suctions dissipated. This effect may have reduced the amount of compaction that could have occurred within the aggregate layer.

### **6.2.3 Rut Depth Development**

The rut depth was measured at six places on each section, three at each reading location, periodically during the first 1000 passes. These readings were supplemented by an additional three readings at the central part of each section, for passes 1000 to 2115.

The development of rut depths with passes are shown in Figures 6.1 to 6.15 and summarised in Table 6.1. It should be noted from Figures 6.8 and 6.9 that large rut depths developed in Sections I and J. Also, it should be noted that in Section J, Reading Location J1 performed very differently to Reading Location J2. This is discussed in further detail in Chapter 6.2.4.

In most sections the first two measurements of rut depth, taken at passes 1 and 3, exhibit a high rate of rut depth development per pass. This high deformation in the first few passes is mirrored by the high axial deformations recorded in the first few cycles of repeated triaxial testing of aggregates (Thom (1988)). Figure 6.16 shows the general



**Plate 6.1 - Cracks in the Trafficked Pavement**

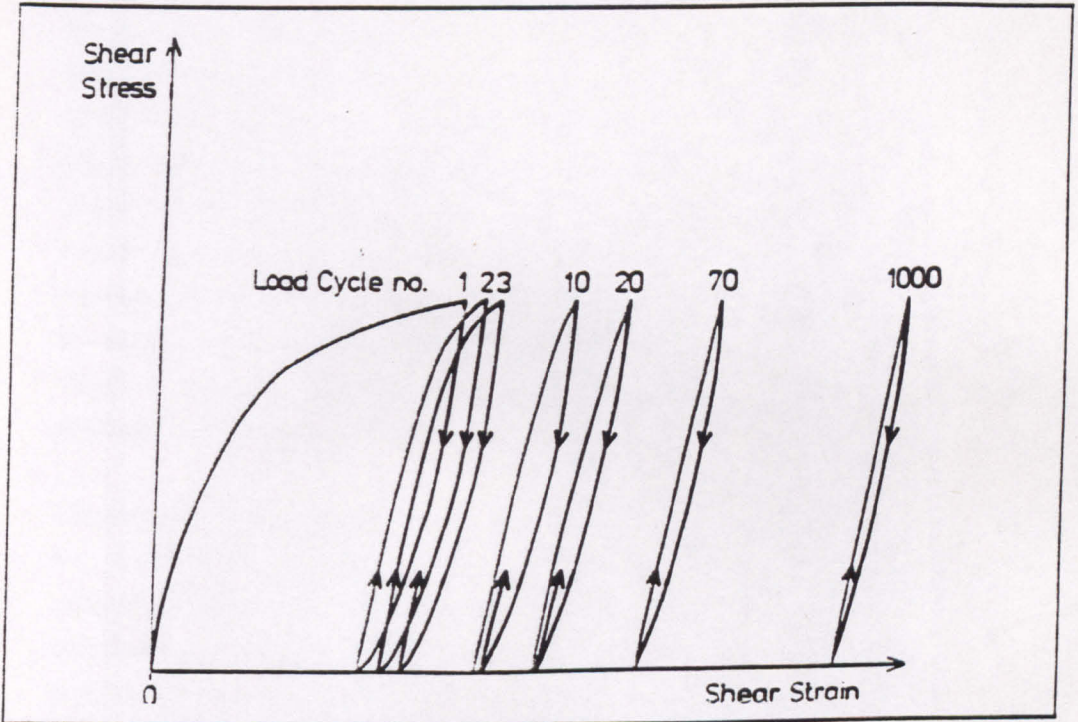


Figure 6.16 Shear Stress and Shear Strain  
for Granular Materials in a Triaxial Test - After Thom (1988)

relationship between shear stress and strain for a granular material subjected to repeated triaxial loading. It may be seen that the graph shows an initial monotonic loading curve followed by a series of load/unload curves which lead to progressively smaller incremental plastic strains. Under the first pass of the axle load the stress-strain response may be expected to move up the monotonic loading line, large strains being generated. Subsequent loadings will then yield smaller values of strain - as can be seen from the figure.

Given that this initial rutting may not be regarded as being indicative of the general pavement performance and that this early rut development is probably an aggregate, rather than pavement, related phenomenon, it is unlikely to be useful in indicating the geosynthetic performance. Therefore, it would appear wise to examine more closely the development of rutting with passes. As the development of ruts in the first few passes has, in some cases, contributed significantly to the overall rut depth, the data was analysed both in terms of the total rut depth for each pavement, and the rate of accumulation of rutting per pass for each axle loading excluding the high initial values. By using the rut development rate, measured in mm per pass, as the comparative measure between pavements, “start-up” errors caused by local variations in the aggregate layer are eliminated.

The rate of rut development with passes, has been calculated and is shown in Table 6.1. It can be seen that the increases in rut depth per pass, excluding Sections I and J1 was, on average, 32% higher for passes 1115 to 2115 (the 126kN axle load range) compared to passes 50 to 1000 (the 80kN axle load range). However, this increase was not noted in all the sections, namely the Typar sections (B & M), the Bidim sections (C & L), the lower bound control section (K) and the lower-bound Tensor geogrid section (N).

#### **6.2.4 Localised Phenomena**

On some of the lower bound sections, localised rutting started to develop at the instrument reading locations. Section J, Reading Location 1, was noticeably poor from near the onset of the trials, as had been expected from the low density of the aggregate at this location as determined by the Nuclear Density Meter (as shown in Table 4.3) and the thickness of the pavement (as shown in Table 5.2). However, other sections showed minor, localised rutting at the reading locations where the instrumentation had

Section	Final total rut depth (mm)	"Start-up" rut depth (mm)	Rut development (mm per pass) passes 50-1000	Rut development (mm per pass) passes 1115-2115
A	48	5	0.021	0.024
B	49	1	0.024	0.022
C	28	1	0.019	0.012
D	28	1	0.006	0.013
E	18	0	0.003	0.009
F	35	4	0.010	0.018
H	34	2	0.010	0.016
I	162 <sup>+</sup>	5	0.016	0.172
J1	150*	11	0.034	0.258
J2	68	3	0.016	0.040
K	24	2	0.009	0.008
L	41	8	0.014	0.013
M	24	2	0.009	0.008
N	32	2	0.012	0.010
O	49	6	0.019	0.025
P	45	2	0.010	0.022

+ failure at 1850 passes

\* failure at 1448 passes

**Table 6.1 Rut Depth Development**

been installed after the construction of the pavement sections, an example of which is Section P, Reading Location 1 which as can be seen from Figure 6.31 showed a large vertical depression in the surface of the aggregate layer around 0.75m past the theoretical location of the aggregate layer pressure cell. This effect was probably caused by the excavation of the aggregate layer during the installation of aggregate pressure cells and strain coils, which disturbed the homogeneity of the layer. This experience highlights one of the difficulties when using instruments, namely that the inclusion itself can alter the structure of the material and, therefore, the properties being measured. In this case, the localised rutting is caused either as a result of aggregate segregation, resulting from the excavation process, or because the excavation disrupted the locked-in lateral stresses that are thought to exist in this type of material, or by poor compaction of the material replaced in the excavated hole. All three causes may have played a part.

It was decided not to undertake any remedial work on the areas of localised rutting in question. The ruts were small and never exceeded 100mm in depth. The fact that these were the areas where the instrumentation had been installed made them important to the trial. It was, therefore, considered better to permit the rut to develop and relate the surface deformations to the internal aggregate strains measured from the instrumentation, rather than to patch the holes with an unknown quantity of material and to lose that correlation.

A localised failure was apparent in the 'Oxford' lower-bound section (Section I) almost from the on-set of the trials. This was on the un-instrumented wheel path near to the junction with Section J. The surface rut at this location rapidly exceeded the design value of 150mm and the geogrid ruptured. The failure caused large amounts of heave to occur on either side of the rut. As the rut developed the heave was so significant that the subgrade was shaved by the front axle of the lorry on every pass, as can be seen in Plate 6.2.

At the end of the trafficking period in 1990 the area in question was excavated to investigate the cause of such localised failure. The subgrade was extensively tested with a hand held shear vane and the results from the wheel path yielded a typical value of about 40kPa. Because the subgrade material at Bothkennar is sensitive and that during failure some re-moulding of the subgrade occurs, the measured shear strength of the subgrade after failure, at 40kPa, might be expected (as shown in Figure 3.15). This remoulding of the subgrade makes it difficult to determine whether a soft-spot existed in the subgrade prior to trafficking or not.

It is possible that the geogrid was damaged at this location on installation, however, no record of such damage had been noted in the contemporary records and the site staff have no recollection of any event which may have caused such damage. The installation of the drain next to the 'Oxford' section may have affected the performance. The drain, installed in an attempt to remove excessive free water standing on the surface of the section, had its invert at formation level. If there had been a low spot in the formation at this point, then water could have entered the formation from the drain. However, the next section, Section J, should also have suffered as the level of the formation there was lower than that of Section I.



Plate 6.2 - Trafficking of the Localised Pavement Failure Within Section I

The geosynthetic in this section was a light-weight geogrid. Index testing on samples recovered after trafficking indicated that the ultimate strain was on average only 3.5% as shown in Table 4.9. If the subgrade rut depth equals the surface rut depth and the deformed geosynthetic profile is parabolic, then it can be shown that 3.5% geosynthetic strain is equivalent to a surface rut depth of 124 mm. Although failure occurred before a 124 mm rut depth was obtained, the 3.5% ultimate strain is an average figure and so at this location geogrid rupture could have occurred at lower strains and, therefore, lower surface rut depths.

The rupture of the geosynthetic was examined carefully and traced back to the edge of the rupture. The grid failed along a line of nodes, with the bars of the grid splitting in half lengthways. Failure was on a line parallel to the direction of trafficking. The area of geogrid next to the point of propagation was plainly in compression as the surface of the geogrid was buckled along an axis perpendicular to the line of trafficking as shown in Plate 6.3.

Before further loading was undertaken, the Oxford section was repaired. The aggregate was removed, the subgrade depression was levelled and, where necessary, refilled with material won from a nearby borrow pit. The subgrade was compacted using a 1000kg/m vibrating roller, a patch of a different geosynthetic was used to replace the damaged geogrid and the aggregate layer was re-installed with an appropriate quantity of aggregate. On further trafficking this part of the section started to show signs of distress but, given the nature of the re-moulded subgrade, this was expected. The rut that developed was filled at an early stage, and the pavement remained traffickable, with occasional repair work, until the end of the trials.

Excavation of Sections I & J at the end of the trials showed that the geosynthetic had ruptured. It would be sensible to assume that rupture occurred when the slope of the rut depth/passes curve increased (Figures 6.8 and 6.9). This happened shortly after the higher axle load was applied. Because in the post-failure pavement a different type of deformation behaviour occurs, the rutting data obtained in the range from 1000 to 2115 passes for these two sections must be treated with caution.

### **6.2.5 Vertical Displacement**

The development of the vertical displacements along each section after 1000 and 2115 passes are shown in Figures 6.17 to 6.31 and was measured by recording the level of



Plate 6.3 - Failure of the Geogrid -Tensor SS1 Section I

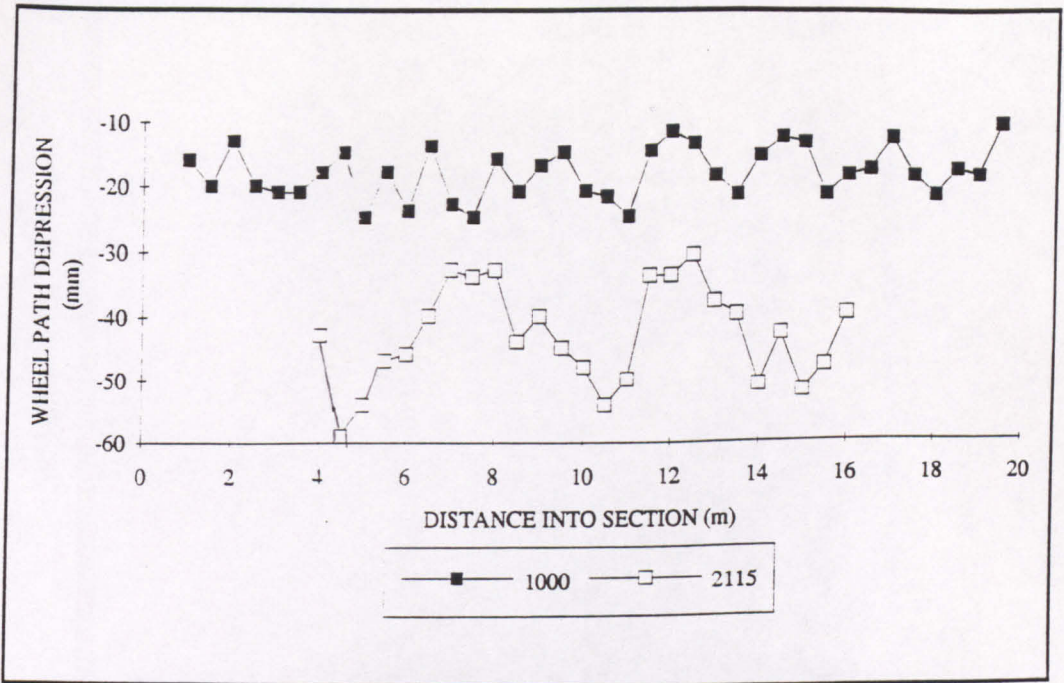


Figure 6.17 Vertical Depression of the Aggregate Surface after 1000 and 2115 Passes - Section A

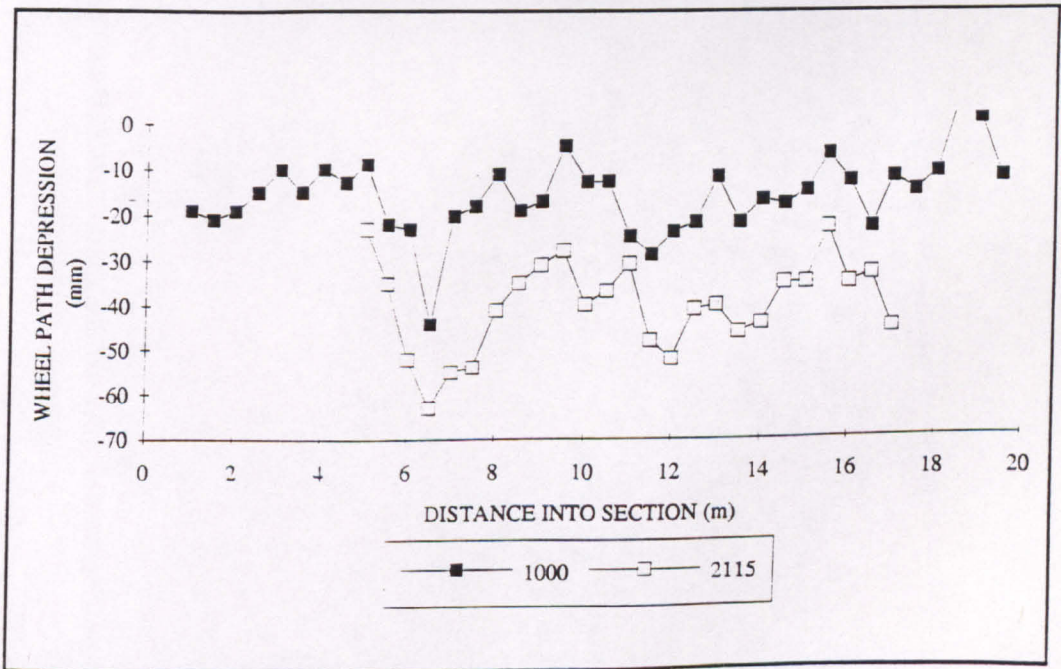


Figure 6.18 Vertical Depression of the Aggregate Surface after 1000 and 2115 Passes - Section B

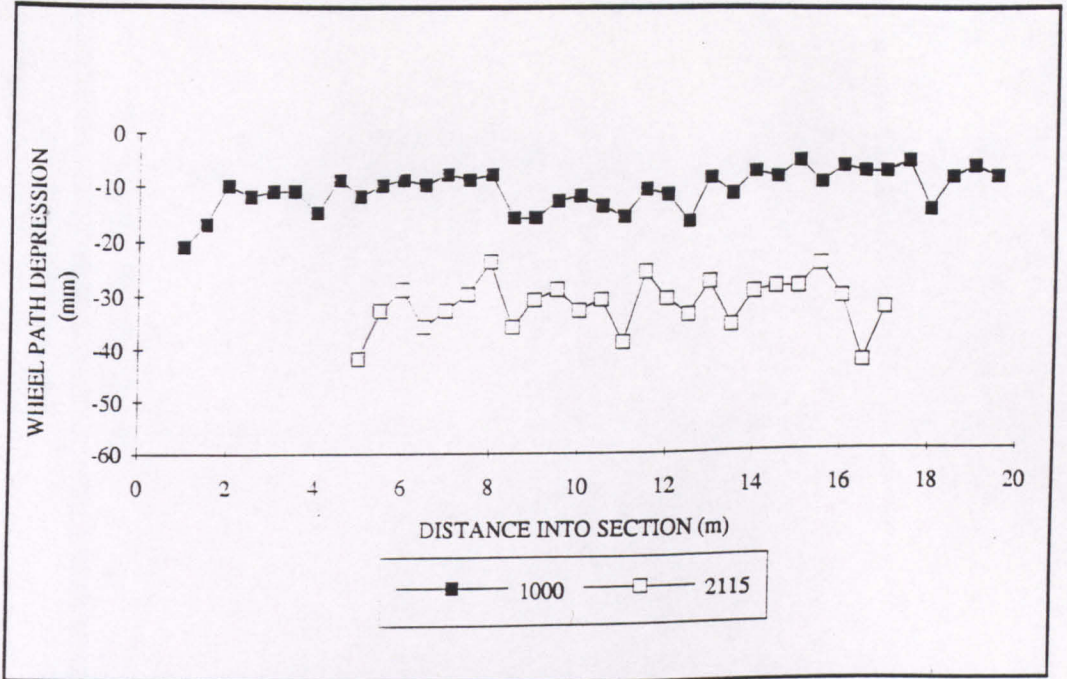


Figure 6.19 Vertical Depression of the Aggregate Surface after 1000 and 2115 Passes - Section C

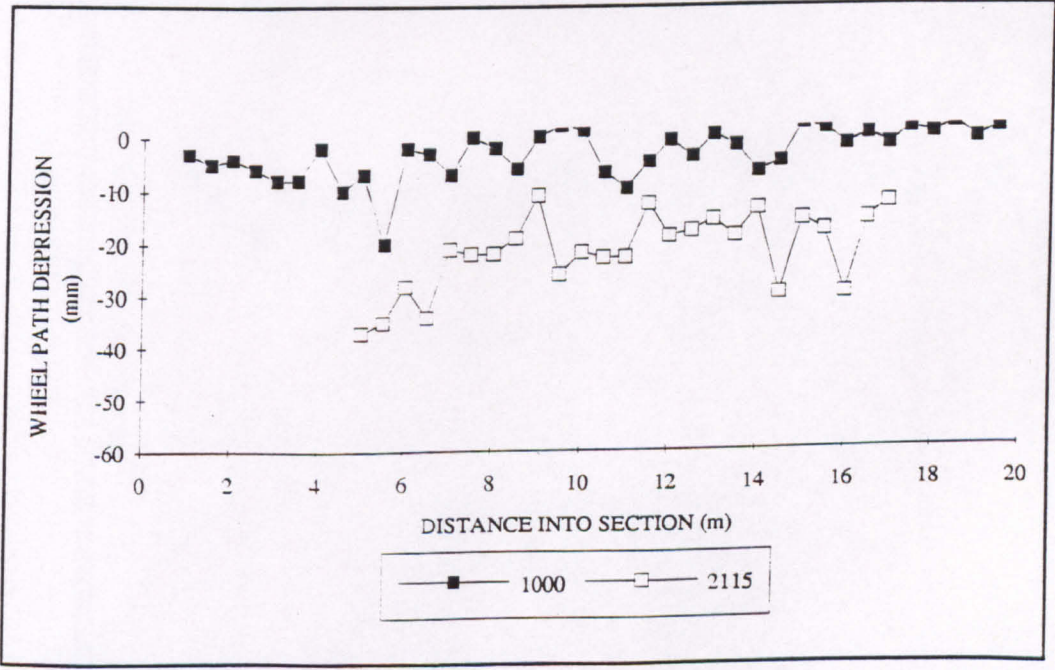


Figure 6.20 Vertical Depression of the Aggregate Surface after 1000 and 2115 Passes - Section D

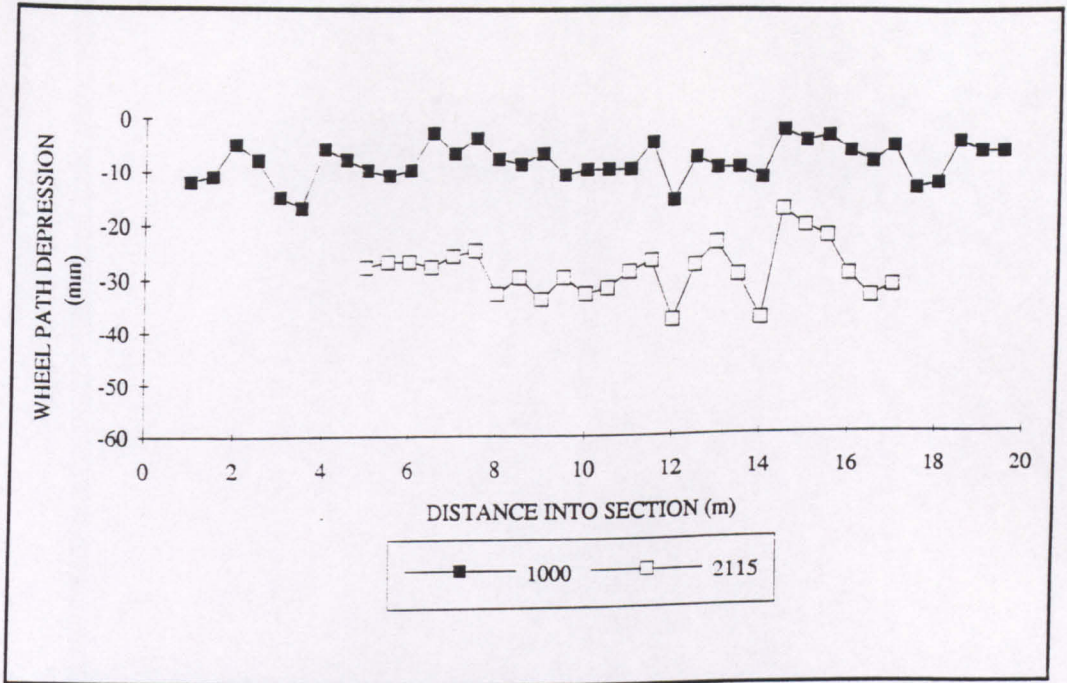


Figure 6.21 Vertical Depression of the Aggregate Surface after 1000 and 2115 Passes - Section E

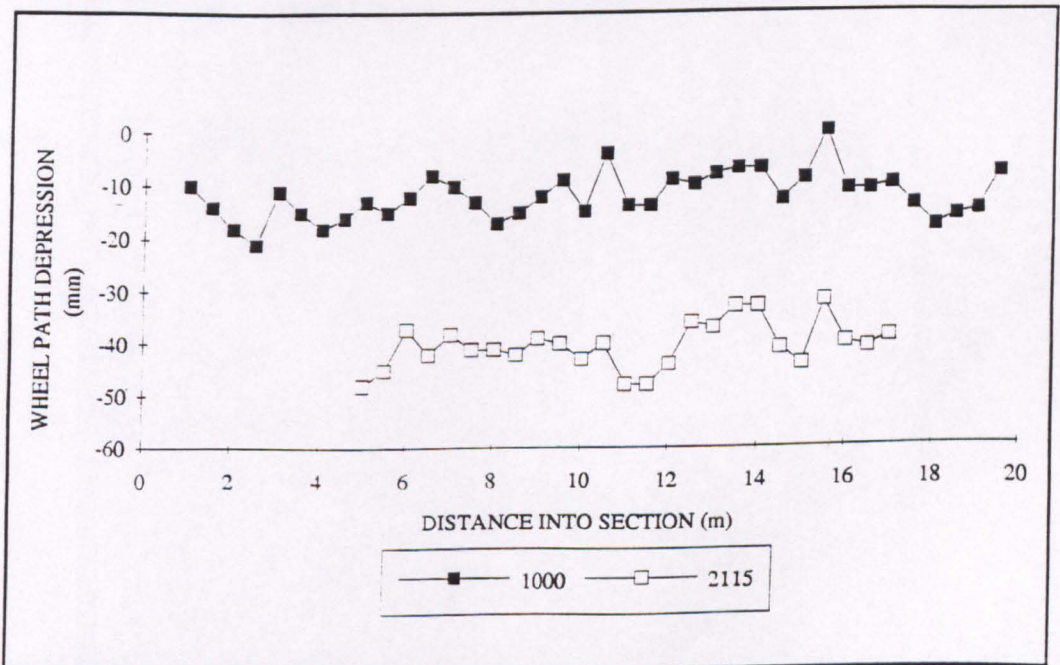


Figure 6.22 Vertical Depression of the Aggregate Surface after 1000 and 2115 Passes - Section F

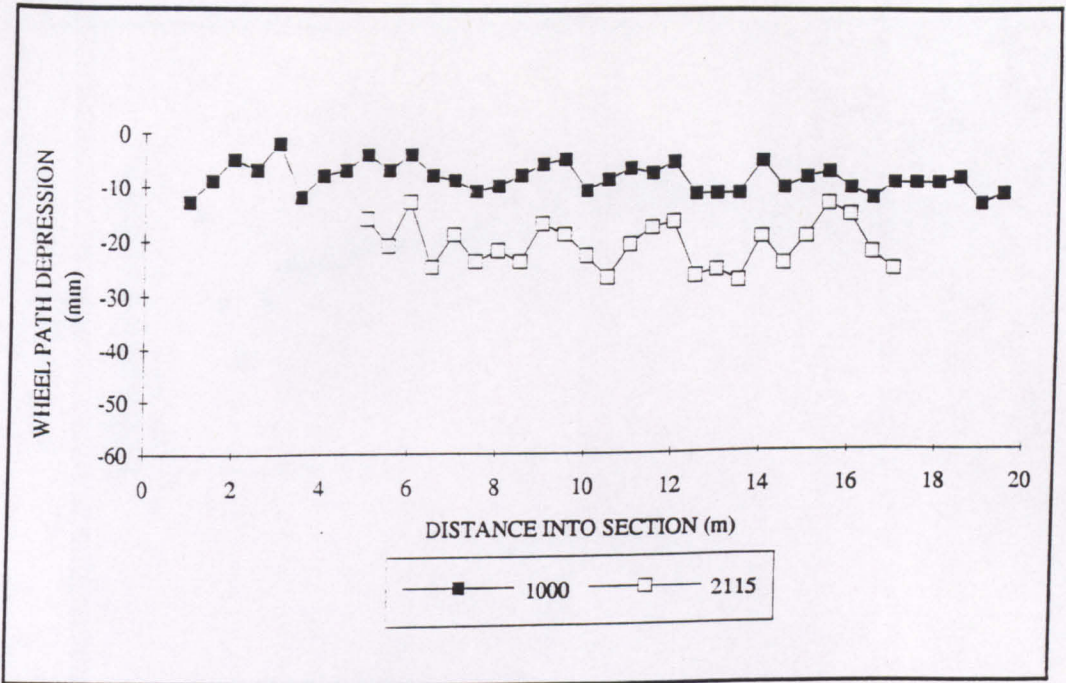


Figure 6.23 Vertical Depression of the Aggregate Surface after 1000 and 2115 Passes - Section H

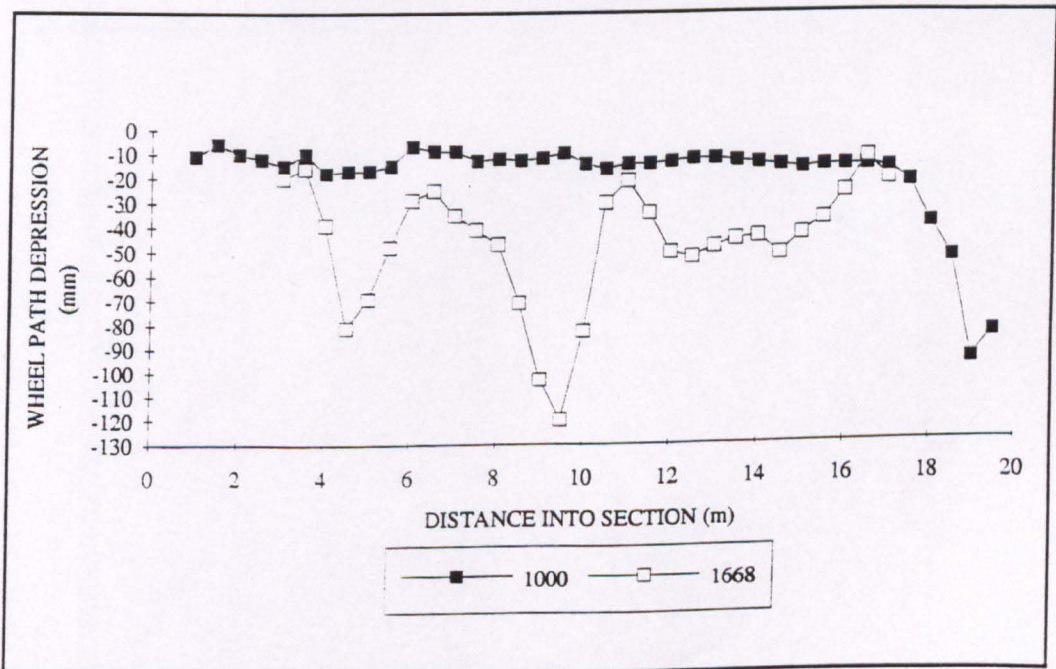


Figure 6.24 Vertical Depression of the Aggregate Surface after 1000 and 2115 Passes - Section I

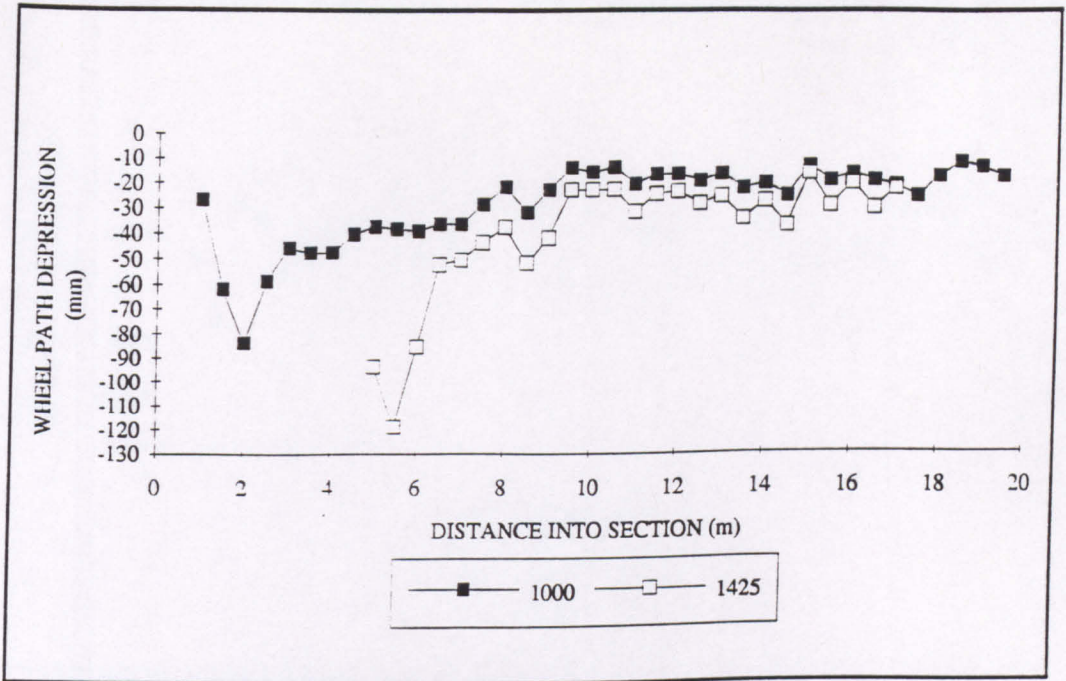


Figure 6.25 Vertical Depression of the Aggregate Surface after 1000 and 2115 Passes - Section J

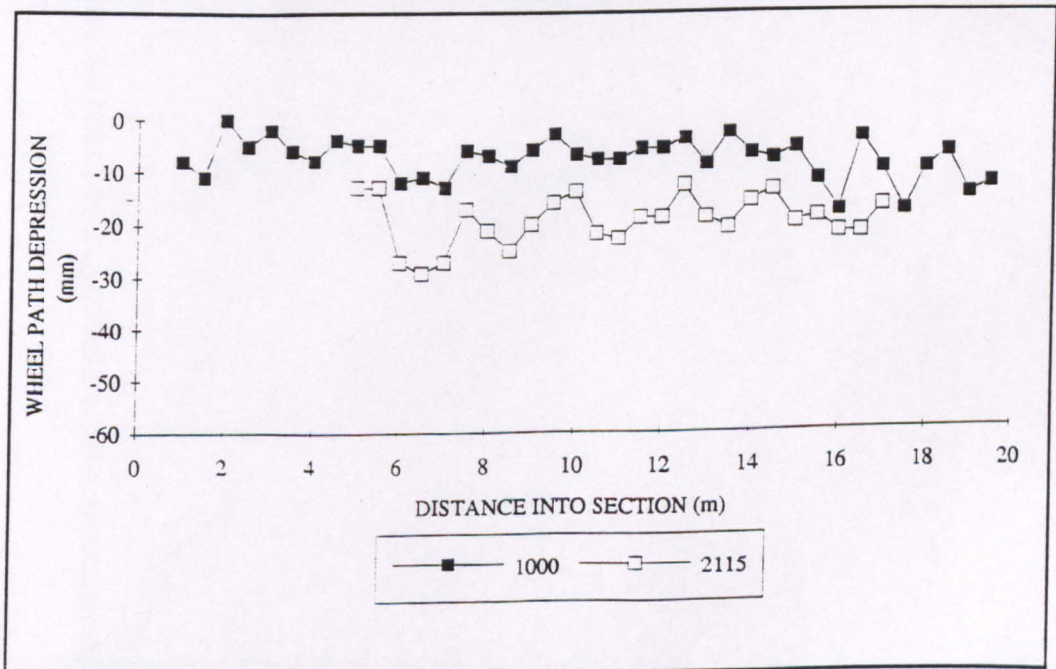


Figure 6.26 Vertical Depression of the Aggregate Surface after 1000 and 2115 Passes - Section K

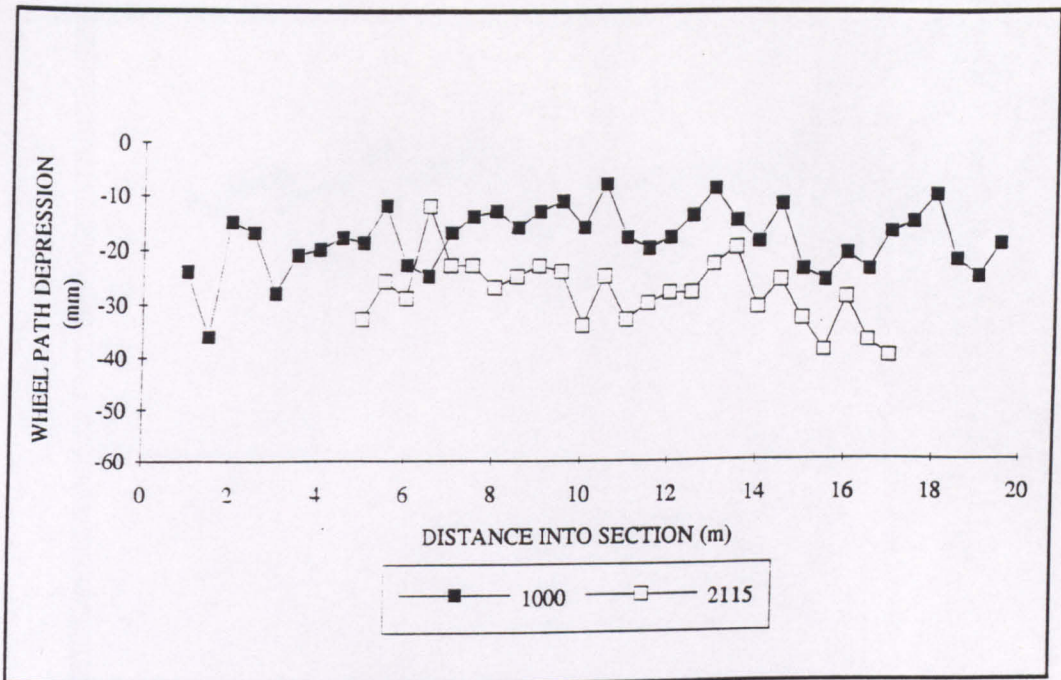


Figure 6.27 Vertical Depression of the Aggregate Surface after 1000 and 2115 Passes - Section L

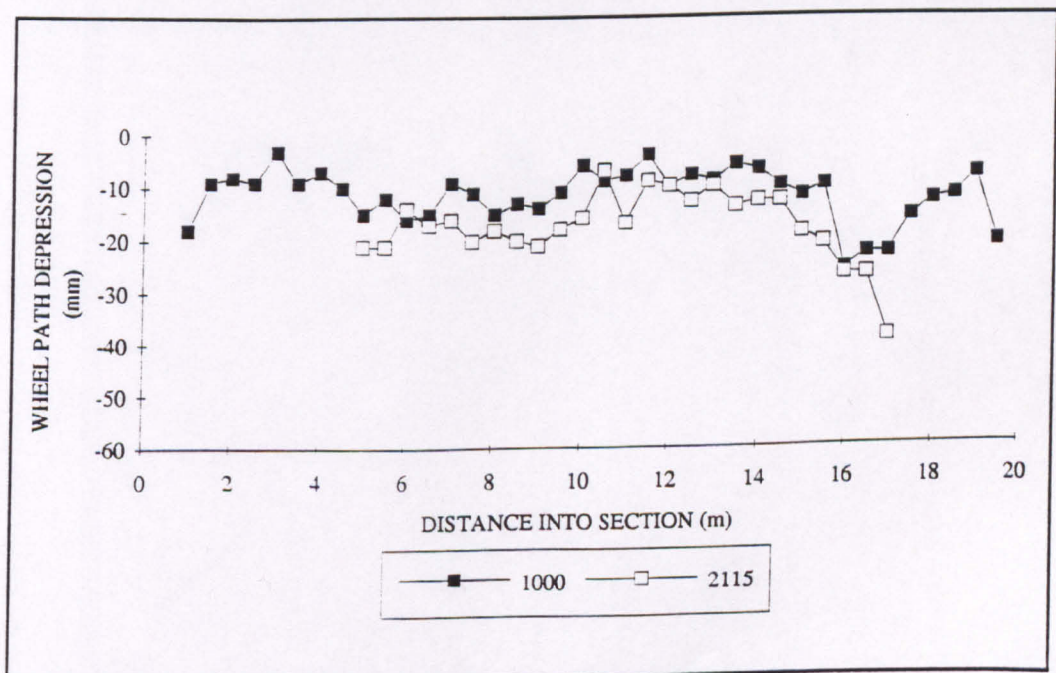


Figure 6.28 Vertical Depression of the Aggregate Surface after 1000 and 2115 Passes - Section M

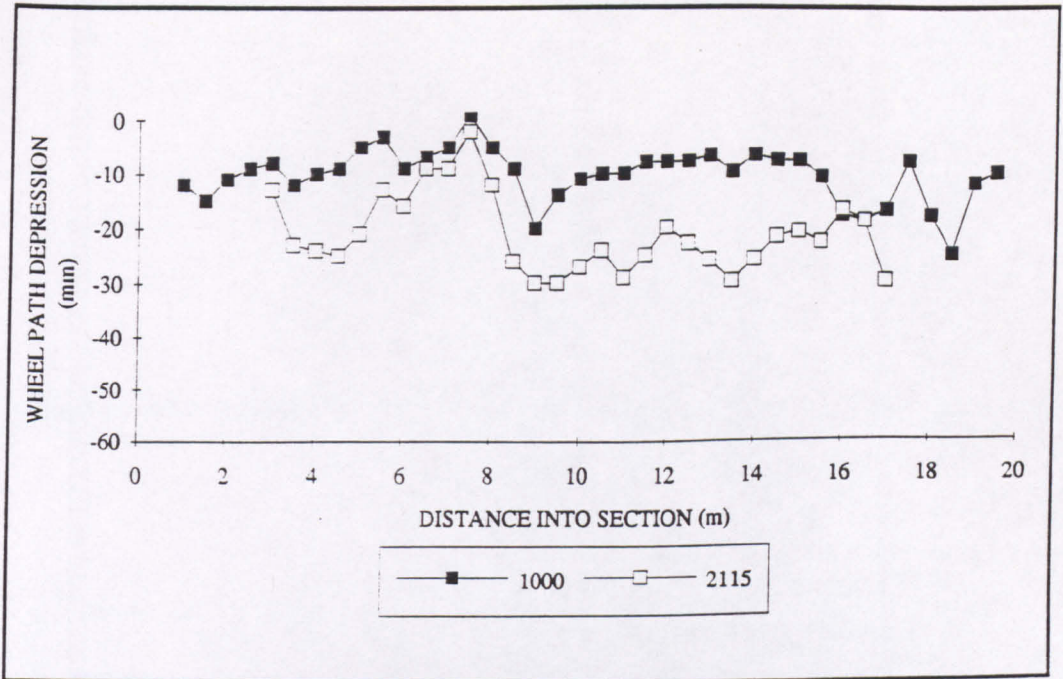


Figure 6.29 Vertical Depression of the Aggregate Surface after 1000 and 2115 Passes - Section N

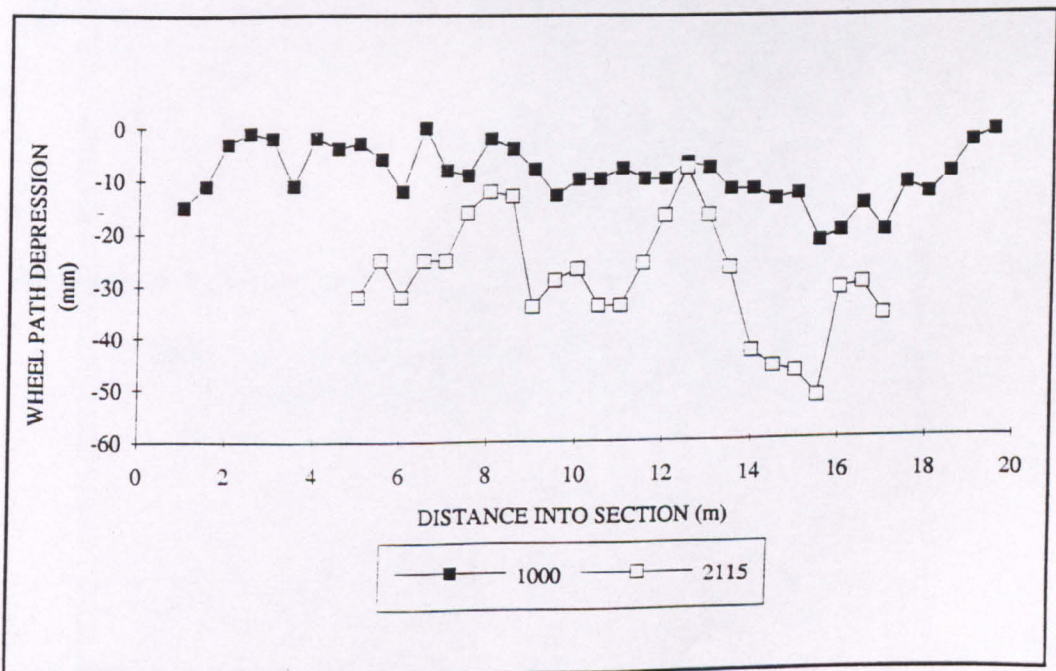


Figure 6.30 Vertical Depression of the Aggregate Surface after 1000 and 2115 Passes - Section O

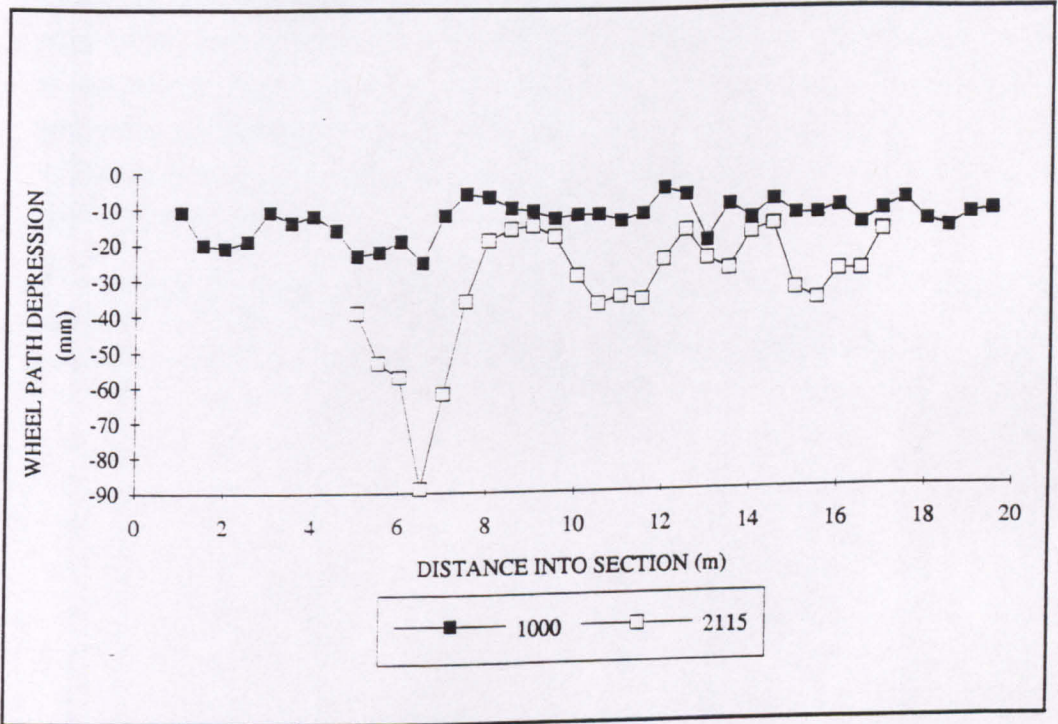


Figure 6.31 Vertical Depression of the Aggregate Surface after 1000 and 2115 Passes - Section P

the aggregate surface in the wheel path during the course of the trials and by calculating the movement away from the initial value.

It can be seen that in many sections the development of vertical displacement is not constant along the length of the section. It would appear a fair assumption that the vertical deformation is related to the rut depth, especially within any given section. The values of the rut depths shown in Table 6.1 may be dependent on whether the location of the measurements is at a low or a high point along the longitudinal profile. Therefore, for each section, the nine individual final measures of rut depth (three at each of the two reading locations and three at the centre) and the final vertical depression at those points was compared. The rut depth was then corrected in proportion to the difference between the mean value of vertical displacement along the whole section and the vertical depression at the selected points. These results are shown in Table 6.2.

Section	Reading Location Rut Depth (mm)	Reading Location Vertical Displacement (mm)	Rut Depth/ Vertical Displacement	Vertical Displacement Mean Value (mm)	Estimated mean rut depth (mm)
A	48	50	0.96	43.2	41.5
B	49	40	1.23	40.1	49.1
C	28	33	0.85	32.0	27.2
D	28	26	1.08	21.8	23.5
E	18	28	0.64	29.0	18.6
F	35	39	0.90	40.5	36.3
H	34	19	1.79	21.2	37.9
I	failed	failed	-		
J	failed	failed	-		
K	24	22	1.09	19.5	21.3
L	41	28	1.46	28.0	41.0
M	24	21	1.14	17.6	20.1
N	32	17	1.88	21.2	39.9
O	49	32	1.53	28.7	43.9
P	45	49	0.92	32.7	30.0

**Table 6.2 Estimate of the Mean Section Rut Depth After 2115 Passes**

### 6.3 TRANSIENT STRESS DISTRIBUTION

Transient vertical stresses were measured using strain-gauged diaphragm pressure cells as discussed in Chapter 5 and, as seen from Figure 5.11, the generated signal was relatively free of noise. Mean aggregate layer and subgrade vertical stresses are shown in Table 6.3. By consideration of vertical equilibrium it is clear that, except possibly at large rut depths, the vertical stresses measured at the base of the aggregate layer and at the top of the subgrade are largely unaffected by the inclusion of a geosynthetic. The scatter in the data in Table 6.3 is largely caused by the inherent variation due to differences in installation and to the variation in thickness of the aggregate layer, both due to design and construction. The mean value of a number of pressure cells, installed in the same environment, would generate a reliable value. However, the degree of redundancy required is so high that, for this project, the costs of manufacture and the time required for installation were prohibitive. Thus, individual measurements of absolute stress should be treated with caution, whereas percentage changes in stress readings are likely to be more reliable.

Section	PASSES 0-1000		PASSES 1115-2115		PERCENTAGE INCREASE	
	Aggregate stress (kPa)	Subgrade stress (kPa)	Aggregate stress (kPa)	Subgrade stress (kPa)	Aggregate	Subgrade
A	-	-	139	82	-	-
B	52	-	-	-	-	-
C	-	110	-	173	-	57
D	52	55	80	76	54	38
E	81	76	94	90	16	18
F	73	69	82	-	12	-
I	169	117	127	134	-25	14
J	185	126	160	139	-14	-13
K	75	-	176	122	134	-
L	46	80	35	74	-24	-7
M	62	63	81	77	31	22
N	64	98	116	124	81	27
O	82	117	131	-	60	-
P	111	83	-	-	-	-

**Table 6.3 Mean Aggregate and Subgrade Vertical Stresses**

A multi-layer, linear elastic analysis of the stress distribution throughout the pavement structure using the BISTRO program (Peutz et al (1968)) for a typical lower-bound section at Bothkennar was performed. It included a standard axle load, an aggregate stiffness of 100MPa and a subgrade stiffness of 30MPa (as determined on site by FWD testing), and a contact stress of 500kPa. The program predicted that the vertical stresses 50mm above the base of the aggregate layer and 20mm below the surface of the subgrade would be 69.4kPa and 56.2kPa respectively. These stresses are of a similar magnitude to the mean values observed at Bothkennar under the 80kN axle load shown above in Table 6.3.

During the trials in the Spring of 1991 the tyre pressure on the lorry, and therefore presumably the pavement contact stress, was raised from 500kPa to 650kPa. However, it can be demonstrated using a linear elastic layered analysis that, at depth, the vertical stress is dependent on the magnitude of the load rather than the contact stress. An examination of the measured vertical transient stresses, before and after this increase, imply that these changes in contact stress did not increase the vertical stresses at the base of the pavements. However, insufficient data from these trials exist for a full examination of the effects of contact stress on pavement stresses. Therefore, it is assumed in the analysis of the results that the stresses are purely dependent on the load magnitude.

It was noted that the increase in the vertical stresses, as measured at the base of the aggregate layer and the top of the subgrade, generated by the passage of the 126kN axle load, as opposed to the 80kN axle load, were less than might have been expected. The 58% increase in load led, on average, to a 32% increase in vertical stress at the base of the aggregate layer and a 20% increase in the vertical stress at the top of the subgrade.

It can be seen that not all sections demonstrated an increase in applied vertical stress within the pavement structure for increasing load. Sections J (lower-bound woven), L (lower-bound Bidim) and the aggregate layer of the sand and gravel with lightweight geogrid (Section I). These observations do not correlate to rut depth performance (see Table 6.1) although may correlate to the observed strains as shown in Chapter 6.4.

By knowing the time lag between the pulses of the pressure cells, generated by the two axles of the lorry, and knowing the distance between the axles, it is possible to calculate the speed of the lorry and therefore convert the time before and after the peak readings

into longitudinal distance of the rear axle from the cell. The longitudinal stress distribution can be calculated from such an analysis and is shown in Figure 6.32.

The vertical stress distribution within the pavement structure may be different in the longitudinal and transverse directions, especially in the sections with geosynthetics which have notably different properties in each direction and in those sections which have rutted. However, Figure 6.32 was generated from Section P early in the trials, before significant rut depths had developed, and therefore the longitudinal stress distribution shown is probably also a fair indication of the transverse stress distribution.

It should be noted from Figure 6.33 that the subgrade transient stress does not appear to decay with increasing rut depth. The example shown is taken from Section I (the sand and gravel with geogrid section) where, with large rut depths and a stiff geogrid, one might have expected to see such a reduction if the membrane effect was the prominent mechanism within the pavement.

#### 6.4 TRANSIENT STRAINS

The mean transient strains observed in the wheel path at the base of the aggregate layer, the geosynthetic and the top of the subgrade are shown in Table 6.4. In a similar manner to the the vertical stresses, it is observed that the transient strains did not increase linearly with the increase in axle load. The 58% increase in load has led, on average, to a 22% increase in transient vertical aggregate strain, a 43% increase in transient vertical subgrade strain and a 31% increase in transient transverse geosynthetic strain.

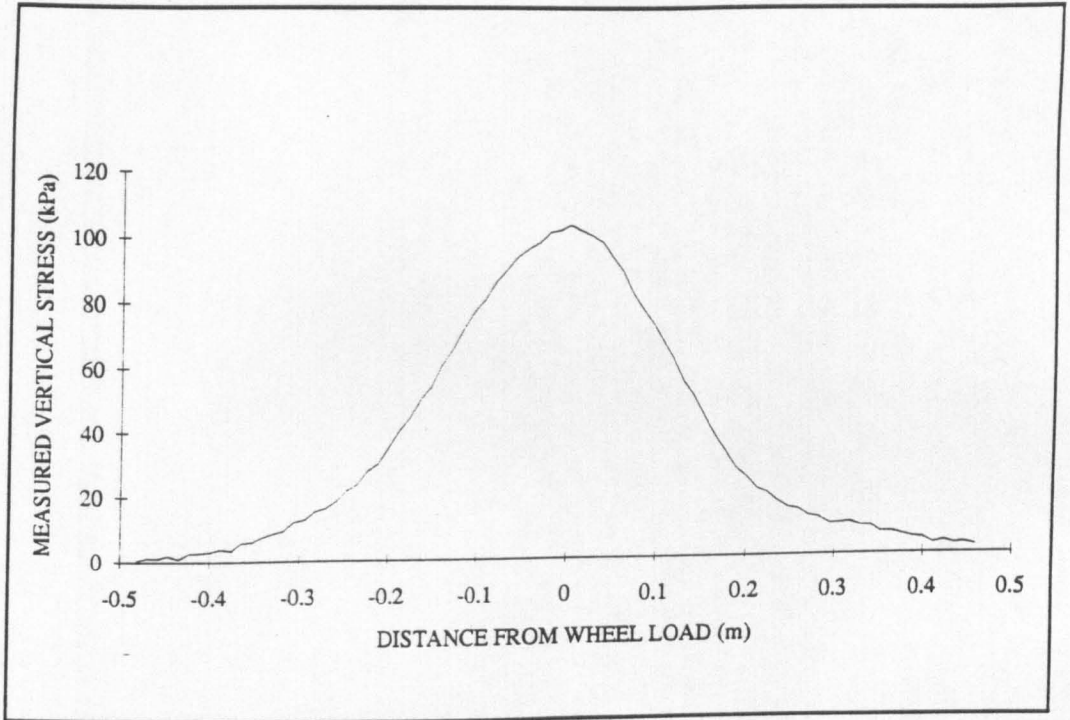


**Figure 6.32 A Typical Longitudinal Stress Distribution at the Base of the Aggregate Layer (Section P, Pass 5)**

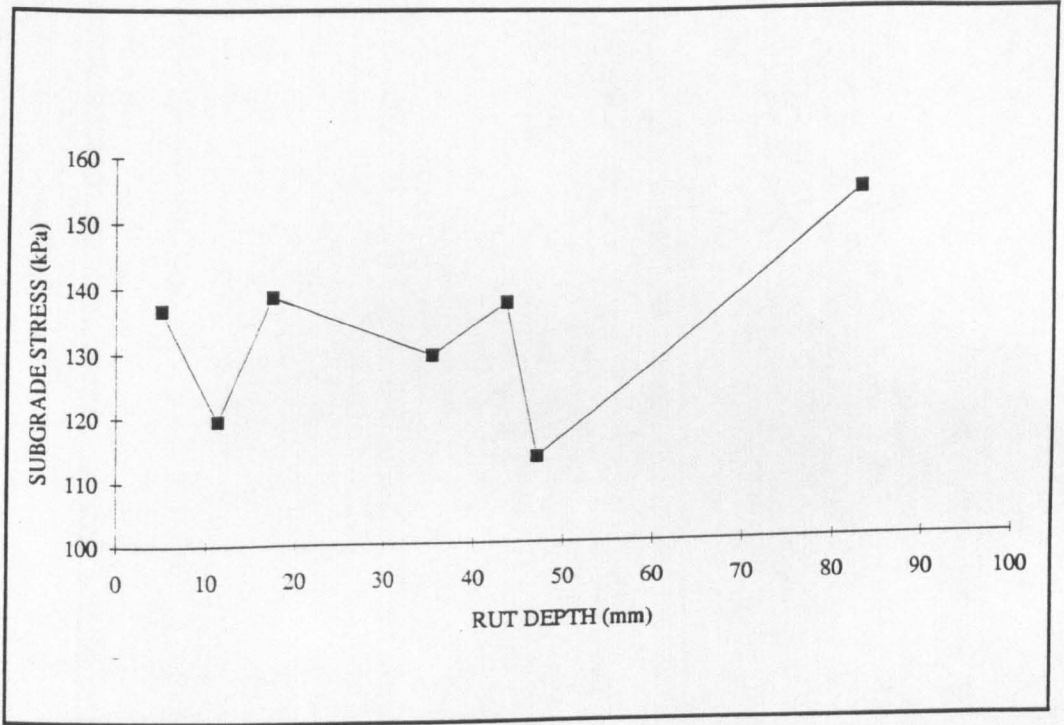


Figure 6.33 Rut Depth and Subgrade Transient Stress - Section I

Section	PASSES 0 - 1000			PASSES 1115 - 2115		
	Wheel-path Vertical Aggregate Strain ( $\mu\epsilon$ )	Wheel-path Vertical Subgrade Strain ( $\mu\epsilon$ )	Wheel-path Transverse Geosynthetic Strain ( $\mu\epsilon$ )	Wheel-path Vertical Aggregate Strain ( $\mu\epsilon$ )	Wheel-path Vertical Subgrade Strain ( $\mu\epsilon$ )	Wheel-path Transverse Geosynthetic Strain ( $\mu\epsilon$ )
UPPER BOUND						
A	3100	7500	-1800	4300	10000	-3000
B	2500	6200	-	3100	7000	-
C	2400	4400	-2000	2800	5100	-2300
D	2000	2800	-	2900	3800	-800*
E	1600	4000	-1100	1800	6000	-1700
F	2800	6700	-2400	3100	8800	-3700
LOWER BOUND						
I	4200	12600	-	7600	36300	-9500
J	12300	29800	-5500	10200	35700	-4600
K	4600	10600	-3300*	4900	13400	-3300*
L	3900	12200	-2900	3600	16600	-3100
M	2600	8900	-2900	500	10300	-3300
N	6700	12700	-3500	12200	18100	-6500
O	3700	14800	-4700	5200	21200	-4800
P	5600	14600	-3700	10600	21800	-5700

\* Control section, the value shown is the horizontal subgrade surface strain.

**Table 6.4 Transient Strains**

The additional wheel load in passes 1115 to 2115 induced smaller strains in the aggregate layer of the lower bound sections J, L & M (Woven, Bidim and Tyvar respectively). There is some correlation between this observation and that for stress shown in Table 6.3. However, this does not appear to relate to pavement performance, namely rut depth.

Multi-layer elastic analysis (Peutz et al (1968)) implies that, for a typical lower-bound section, (350mm thick and stiffness values taken from soil testing results) transient elastic strains of  $900\mu\epsilon$  could be expected at the base of the aggregate layer and  $1300\mu\epsilon$  at the top of the subgrade. For this type of analysis, these strains are calculated to increase in both aggregate and subgrade layers by 56% for a 58% increase in load. The non-linear model FENLAP (Almeida et al (1991)) suggests that transient elastic strains of  $800\mu\epsilon$  could be expected at the base of the aggregate layer and  $1000\mu\epsilon$  at the top of the subgrade. The increase in these strains caused by the increase in loading are

calculated to be of the order of 22% at the base of the aggregate layer and 33% at the top of the subgrade. The measured transient strains of the aggregate layer/subgrade interface were higher than those predicted by either analysis, the reasons for which are unknown.

It was found during the analysis that strains on the geosynthetic outside the loaded area (as defined by the widely held concept of a load spread angle), exhibited small transient strains. Indeed, for many sections, the strain induced in the geosynthetic, away from the wheel path, was below the noise threshold of the strain coils. Figure 6.34 shows how the transient geosynthetic strains dissipate with distance from the wheel path. It is interesting to note that the transient transverse strains tend to become compressive at a distance from the load.

## 6.5 PERMANENT STRAINS

The application of 2115 passes generated permanent deformations in the aggregate layer geosynthetic and subgrade. The permanent strains, directly under the wheel path, at the base of the aggregate layer, the top of the subgrade and the geosynthetic are shown in Table 6.5 and, where possible or sensible, the results are the mean of the two reading locations.

Geosynthetic strain coils, remote from the wheel path, showed little or no permanent strain as shown in Figure 6.35. This is hardly surprising given that they exhibited little or no transient strain. It should be noted that although the transient strains were higher at the top of the subgrade than at the base of the aggregate layer, the permanent deformations are generally more pronounced in the aggregate layer.

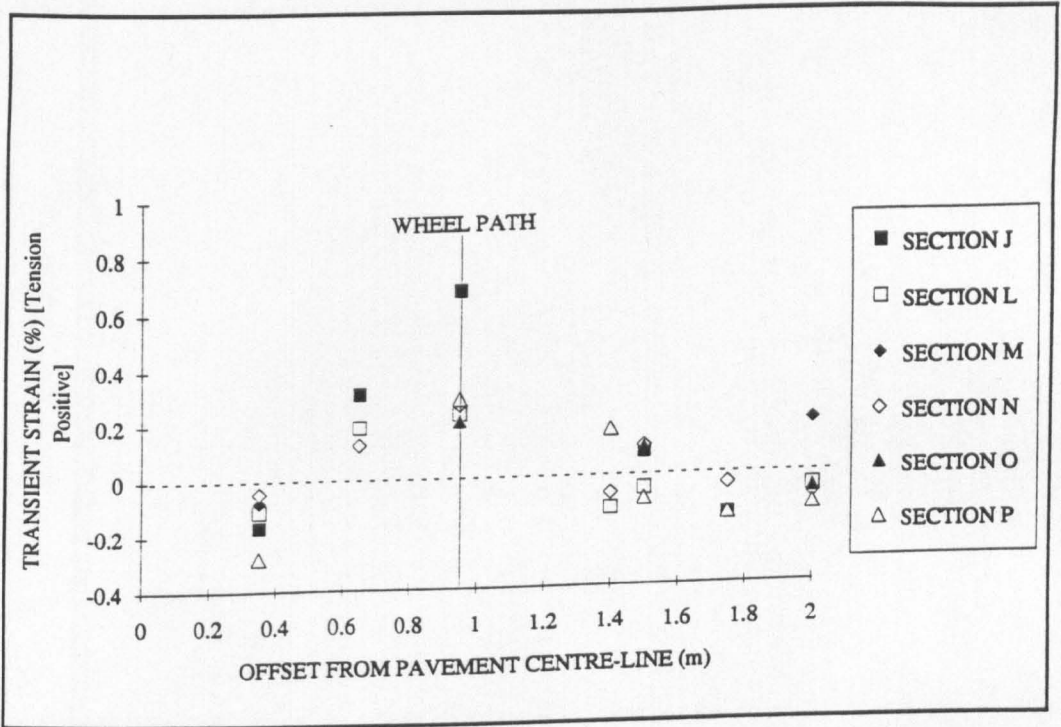
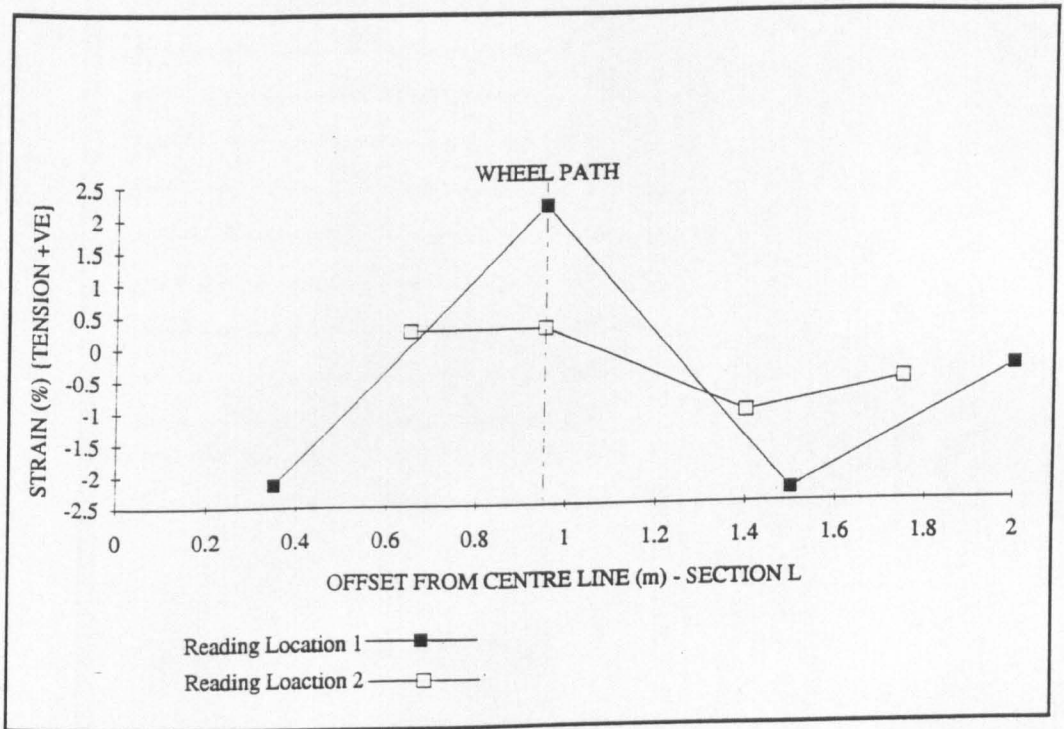


Figure 6.34 Transient Geosynthetic Strain Away from the Wheel Path



**Figure 6.35 Permanent Geosynthetic Strain Away from the Wheel Path for a Typical Section at Bothkennar - Section L**

Section	Vertical Aggregate Permanent Strain ( $\mu\epsilon$ )	Vertical Subgrade Permanent Strain ( $\mu\epsilon$ )	Wheel path Geosynthetic Permanent Strain ( $\mu\epsilon$ )
A	18800	7600	-11800
B	19700	11800	-
C	15800	2900	-2500
D	16400	-2300	-
E	8800	4400	0
F	30800	18900	-
I	48000	21900	-
J1	97300	44000	-7400
J2	-	12700	-
K	14800	5100	-700*
L	24400	9000	-4600
M	5200	6800	0
N	8500	15600	-4300
O	24600	25700	-2500
P	21800	19100	-10700

\* Control section, the value shown is the transverse subgrade surface strain (compression positive)

**Table 6.5 Mean Accumulated Permanent Wheel Path Strain After 2115 Passes**

## 6.6 EXCAVATED CROSS SECTIONS

Recovery of the geosynthetics for analysis at the University of Strathclyde enabled an examination of the post trafficking cross-section profiles which are presented as Figures 6.35 - 6.43. An overall measurement of aggregate layer strain in the wheel path was determined from the initial and final thicknesses. It should be noted that two years elapsed between the measurements of thickness and the method of measurement, with a level and staff, is not conducive to a high degree of accuracy. This probably explains the observation that no strain had occurred within the aggregate layer of Section M, whilst the aggregate strain coil reading in Table 6.5 shows a compressive permanent strain. Generally, it is interesting to note that the strains measured by the strain coils at the base of the aggregate layer are significantly lower than the overall aggregate strain. As could have been predicted, the majority of the strain must therefore occur near to the surface of the pavement, where the stresses imposed by the wheel load are greatest.

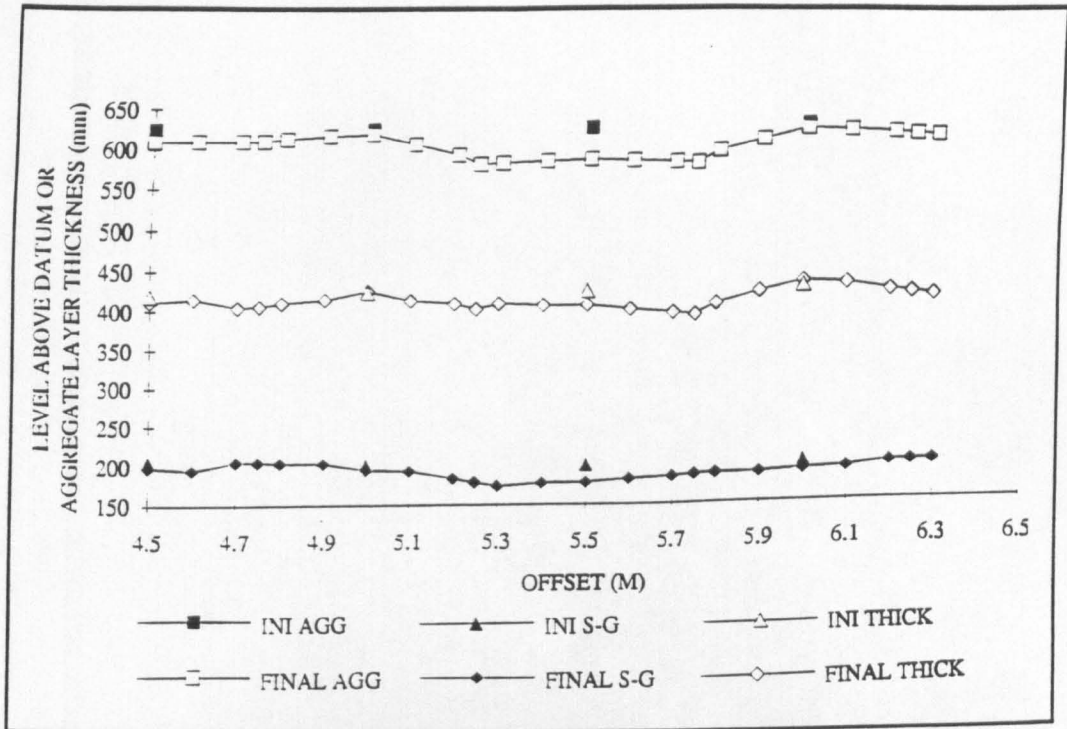


Figure 6.36 Post-Trafficking Transverse Cross-Section - Section F

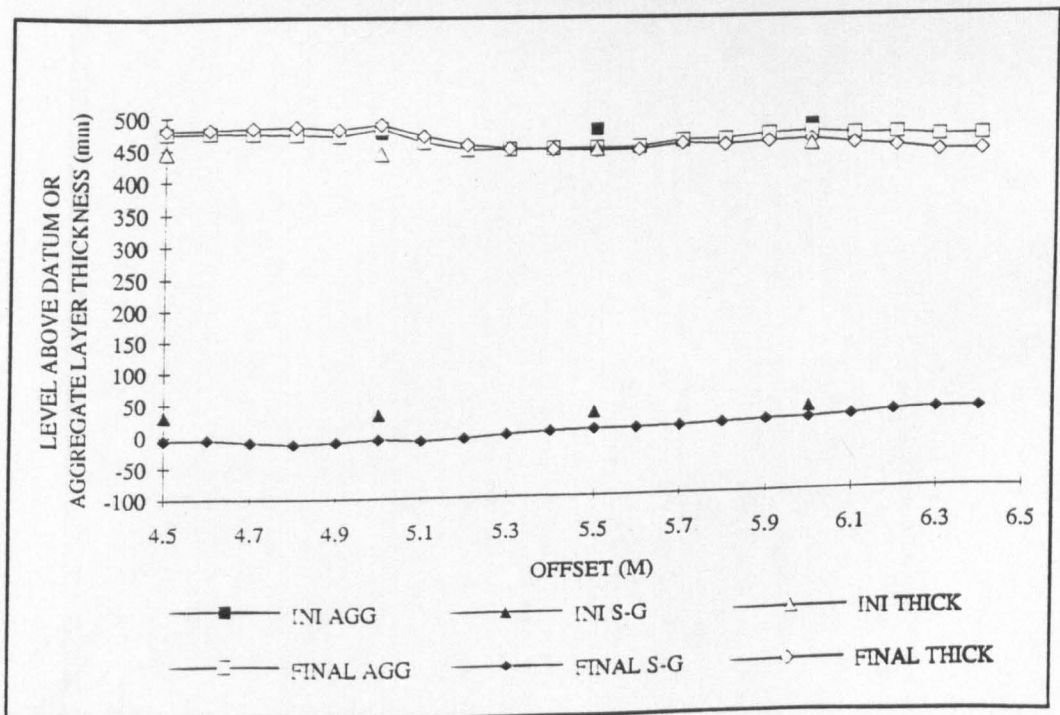


Figure 6.37 Post-Trafficking Transverse Cross-Section - Section H

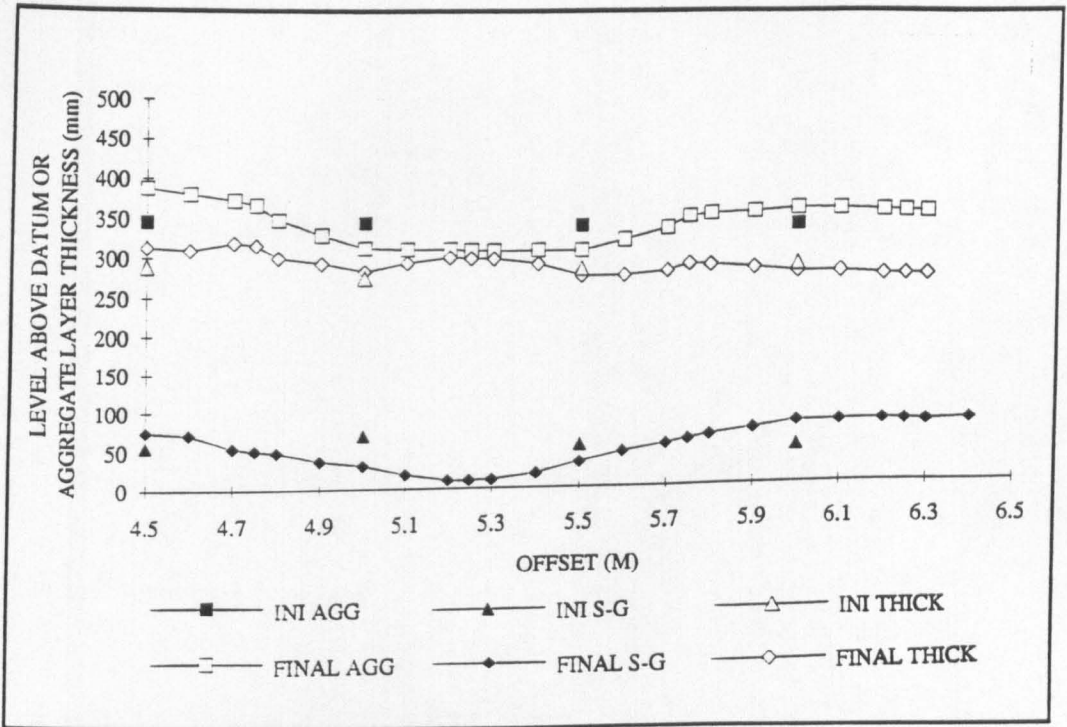


Figure 6.38 Post-Trafficking Transverse Cross-Section - Section J

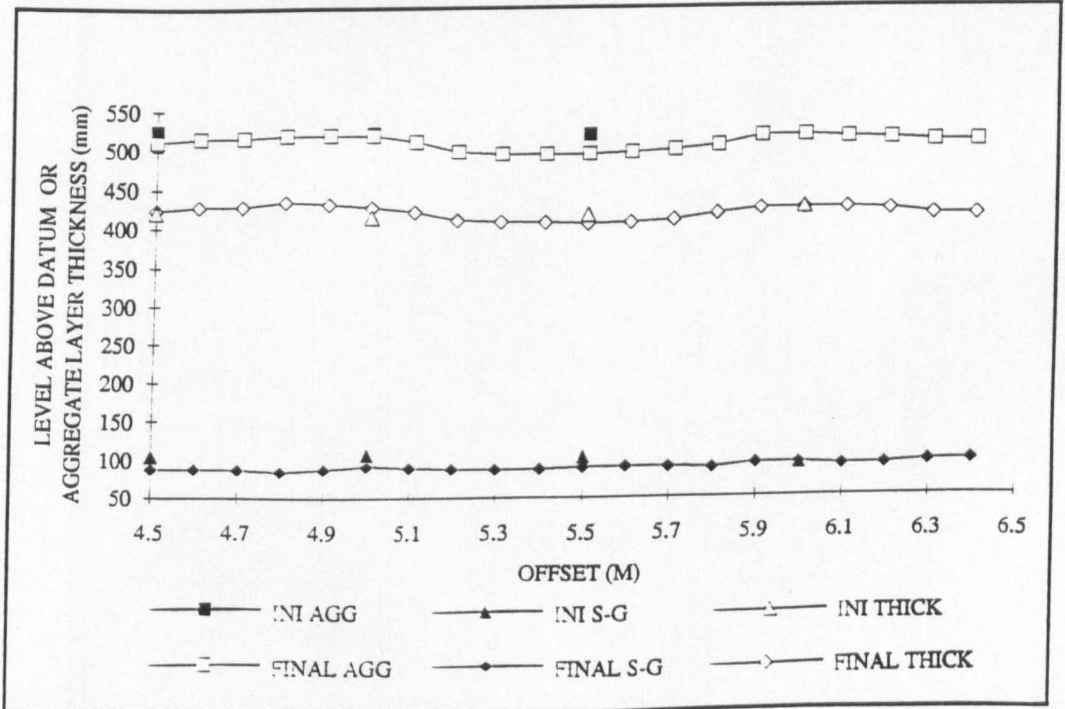


Figure 6.39 Post-Trafficking Transverse Cross-Section - Section K

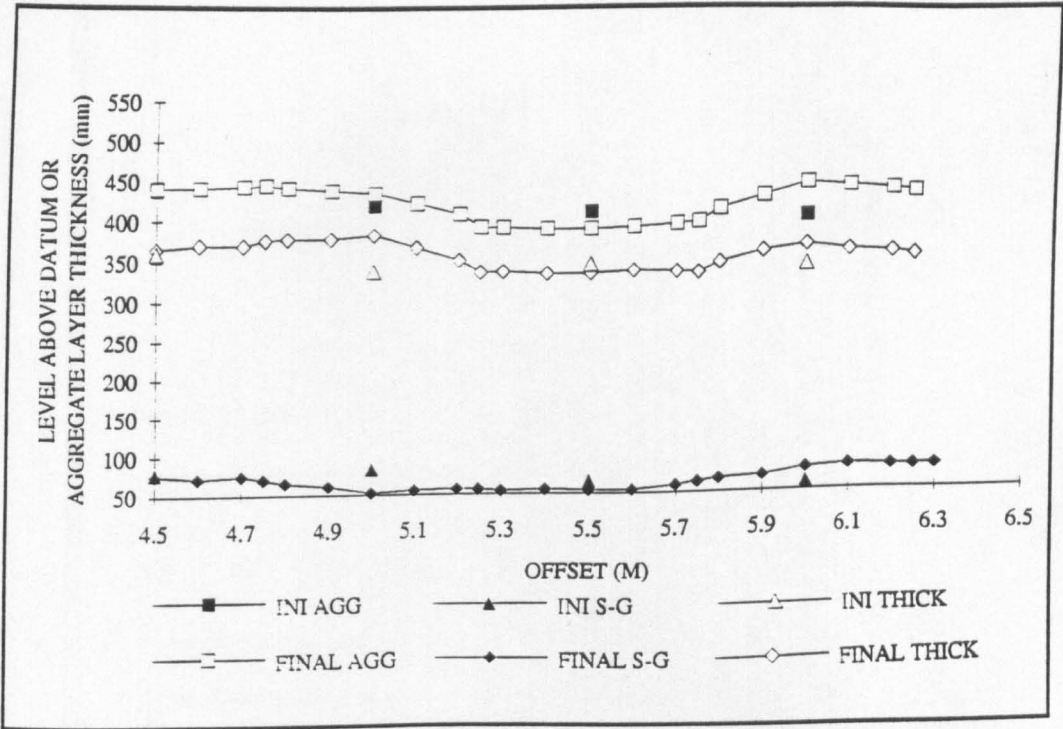


Figure 6.40 Post-Trafficking Transverse Cross-Section - Section L

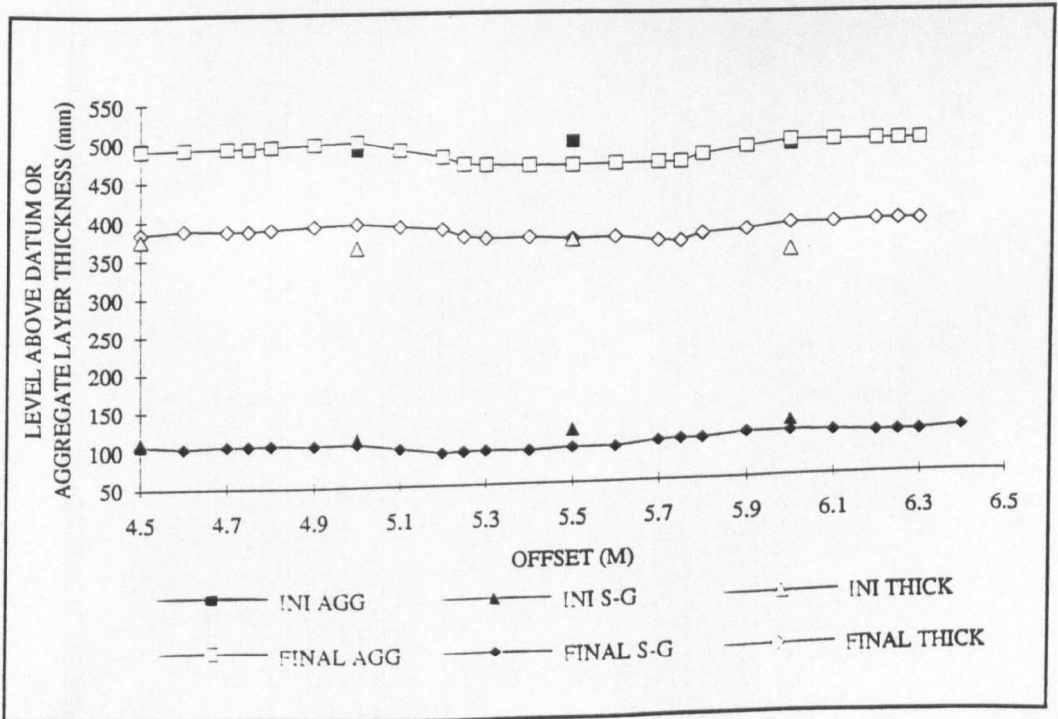


Figure 6.41 Post-Trafficking Transverse Cross-Section - Section M

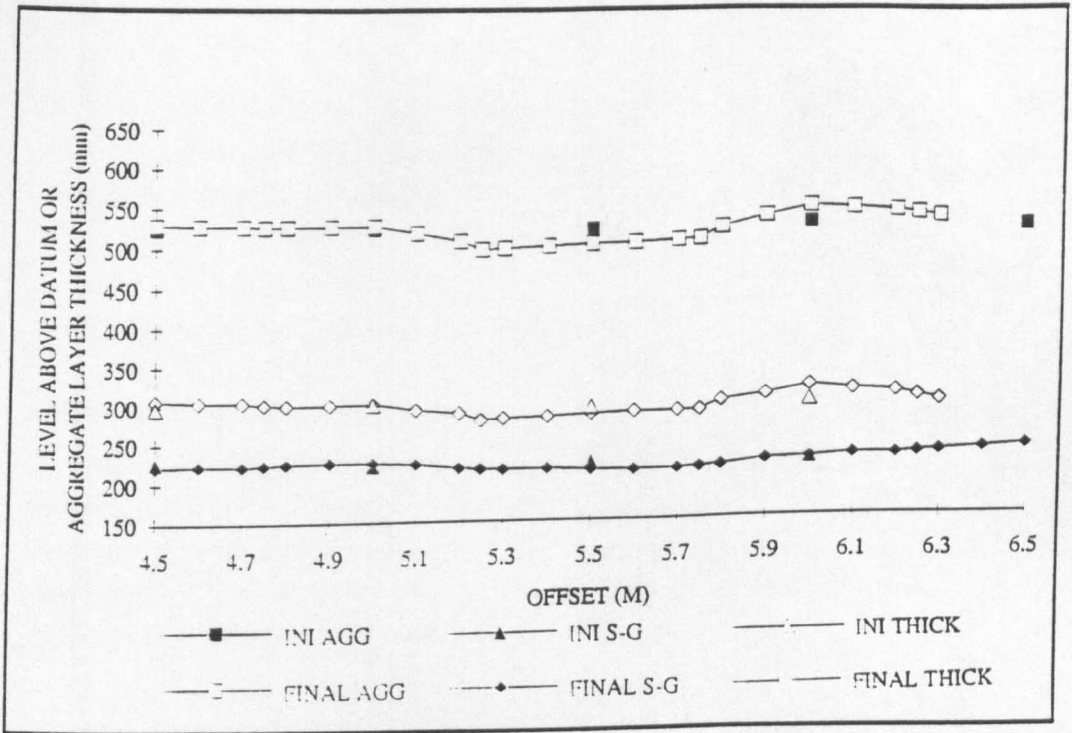


Figure 6.42 Post-Trafficking Transverse Cross-Section - Section N

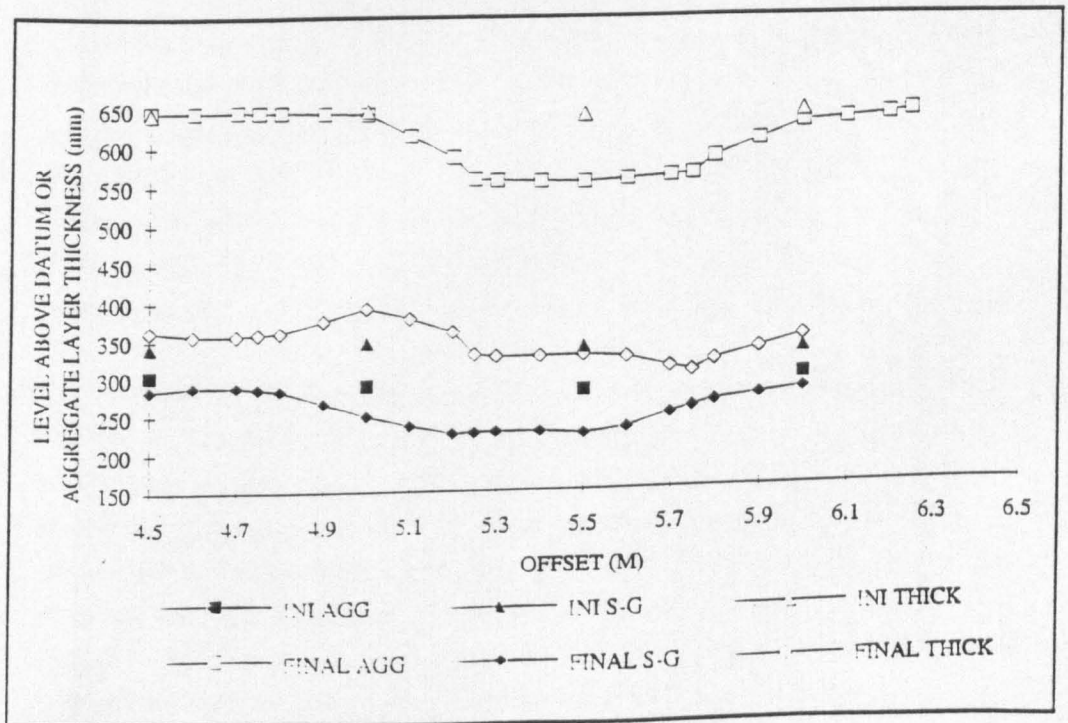


Figure 6.43 Post-Trafficking Transverse Cross-Section - Section P

Examination of the eight excavated sections at Bothkennar indicate that deformation within the aggregate layer makes up between 0% and 33% to the total surface rut depth, with a mean of 21%, the remainder being the result of subgrade deformation.

#### **6.6.1 Loss of Aggregate to the Subgrade**

It was noted, during the excavation of the post trafficked pavements, that in the control section, K, the aggregate particles were mixed with the subgrade. The aggregate was embedded within the subgrade to a depth of approximately 25mm. This was not the case on any of the other sections that were excavated and demonstrates that all of the geosynthetics used acted as separators, all "saving" 25mm of aggregate that would otherwise be pushed into the subgrade.

### **6.7 SUBGRADE SHEAR STRENGTH**

The subgrade shear strength was tested at intervals during the course of the trials, using a hand held shear vane, and the shear strength of the subgrade was found to remain constant throughout the period of trafficking. The mean surface shear strength of the subgrade was calculated during the two trafficking periods and it was found to be around 85kPa on both occasions. There is an inherent variability in the results obtained from such an instrument due to both the operator and the fact that the vane tests a small local sample. Thus, the results shown in Figures 3.10 to 3.14 from the vane show a high degree of scatter, but mean values are probably reasonably accurate.

The shear strength profile with depth shows a strength reducing markedly with depth. The crust of firmer material on the site is caused by evaporation and transpiration, which in turn causes pore-water suctions which leads to the soil being slightly over-consolidated and gives a drier, stiffer material. The shape of the profile obtained from the shear vane matches closely the one reported by Paul et al (1991) which shows a shear strength of 80kPa near to the surface decreasing to 20kPa at a depth of 2m (see Figure 3.15). However, this inversion of the shear strength profile makes numerical analysis difficult because most programs assume a linear increase in strength with depth.

After trafficking the subgrade was exposed in many of the sections either to recover post-trafficking geosynthetic samples or defective pressure cells. These excavations presented an opportunity to determine the shear strength of the surface of the formation using the hand held shear vane. Three determinations of shear strength were made of each exposed formation and the results are shown in Table 3.3. Only surface values were recorded as it was expected that the shear strength at depth was unlikely to change significantly from the values as shown in Figure 3.14. By reducing the number of data points that are considered, the mean value of the shear strength for each section can not be determined with the same degree of confidence that can be done for the site as a whole. It might be argued from the results presented in Table 6.6 that the thicker sections (A to F) have a higher mean surface shear strength and, if that is indeed the case, it might be attributable to the slightly larger overburden stresses causing a small amount of subgrade consolidation.

Section	Mean Surface Shear Strength (kPa)
A	105
B	90
C	90
E	96
F	75
H	81
I	77
J	98
K	90
L	74
M	82
N	82
O	82
P	77

**Table 6.6 Formation Level Shear Strength**

## 6.8 WATER TABLE

The Water table on the site was determined by using the standpipes which were installed in January 1991. Generally it was found that the water table level was between 0.2 and 0.7m below the formation level of the pavements, as shown in Table 6.7. Because the site was next to the tidal Firth of Forth, it was thought that the water table might be affected by the nearby tidal movement. It was found, by monitoring the water table level over a 12 hour period, that the water table on the site was stable.

Depth below site surface (m)				
Section	15 April '91	24 April '91	30 April '91	7 May '91
A	0.70	0.80	0.83	0.84
F	0.02	0.07	0.29	0.71
H	0.49	0.70	0.64	0.62
P	0.99	0.73	0.75	0.75

**Table 6.7 Water Table Level in m Below Formation Level.**

As can be seen from Table 6.7, the ground water level fell steadily during the course of the second phase of trafficking. It had been raining heavily prior to the trials commencing and water was standing on the surface near to Section F, which is in a slight hollow. This surface water probably raised the ground water levels near to Section F at the start of the trials and during the course of the trials these came to equilibrium with the rest of the site as the surface water filtered into the site. During the course of the trials the weather was mainly dry and over-cast, which explains the gradual fall in the ground water levels.

## CHAPTER SEVEN

### REVIEW AND COMPARISON OF RESULTS

#### 7.1 INTRODUCTION

This chapter examines some of the results given in Chapter 6 and, where possible, compares the results obtained from the different sections. Variation in aggregate layer thickness and type of geosynthetic create difficulties for direct comparison. However, certain key parameters are compared to highlight the difference in the performance of sections.

Due to the high number of sections, comparisons are made, for simplicity, between those sections containing "high stiffness" geosynthetics (Sections A,E,F,I,J & N), those containing "medium/low stiffness" geosynthetics (Sections B,C,L,M,O & P) and the control sections (Sections D,G,H,K). These definitions are somewhat subjective but "high stiffness" is taken to comprise the grid and woven products and "medium/low stiffness" is taken to comprise the non-woven products.

As can be seen from Table 4.10, for the control samples, the wide width tensile tests to BS 6906, part 1 (1987) showed that, at 5% strain, the load carried by the high stiffness geosynthetics in the cross-machine direction was in excess of 15kN/m and for the medium/low stiffness ones was less than 4kN/m.

#### 7.2 TRANSIENT STRESS

##### 7.2.1 Comparison of Stress Readings

As explained in Chapter 6.4 the inherent variation in each earth pressure cell's measurement of stress leads to difficulty in the determination of absolute values. Therefore, comparison of the mean vertical stresses at the base of the aggregate layer between sections is rather inconclusive. However, from the results shown in Table 6.3 it can be seen that for high stiffness geosynthetics the vertical stresses at the base of the aggregate layer vary from 64 (Section N) to 185kPa (Section J) in the lower-bound pavements. Similarly, for the medium/low stiffness geosynthetics the values range from 46 (Section L) to 111kPa (Section P) and for the control (Section K) 75kPa.

Therefore there was considerable overlap in the range of vertical stresses for the high, medium/low stiffness geosynthetics and indeed, the control sections. Similarly for the upper-bound (52 to 81kPa) and lower-bound sections (46 to 185kPa). However, considering the range of stresses, one deduction could be that the higher stiffness geosynthetics lead to higher vertical stresses at the base of the aggregate layer. Initially such a deduction seems rather surprising, but it could be due more to the difference in aggregate layer thickness than geosynthetic type as the stiffer geosynthetics generally had lower design thicknesses.

### 7.2.2 Stress Distribution

It is a widely held concept that the vertical stress distribution, in this case at the base of the aggregate layer, can be determined using a load spread angle. This, in turn, gives a rectangular, stepped vertical stress distribution at any given depth which is convenient for analysis. However, it is known that the concept of the load spread angle is an approximation, and that the true vertical stress distribution is more bell shaped. Many of the analytical methods only consider the case of plane strain, limiting themselves to a consideration of stress and strain within a transverse section of the pavement. Even those which are axisymmetric do not consider the manner in which the rut depth or the geosynthetic properties may alter the stress distribution in the pavement structure.

Stress distribution across the pavement was not measured in the trials, but the longitudinal stress distribution is likely to be a better approximation of it than the concept of a load spreading angle. The longitudinal vertical stresses at the base of the aggregate layer may be obtained from a study of the changes in the measured vertical stress as the vehicle load approached the instrument position, as was shown in Figure 6.32 and discussed in Chapter 6.4.

Although analysis of the system may be possible using these measured stress distribution profiles, Finite Element calculations by Brocklehurst (in press) suggests that the errors, generated as a result of using a load spread angle approximation, are small.

Figure 7.1 shows the normalised stress distribution for typical high and medium/low stiffness geosynthetic reinforced pavements and for a control section (Sections I, P and K respectively).

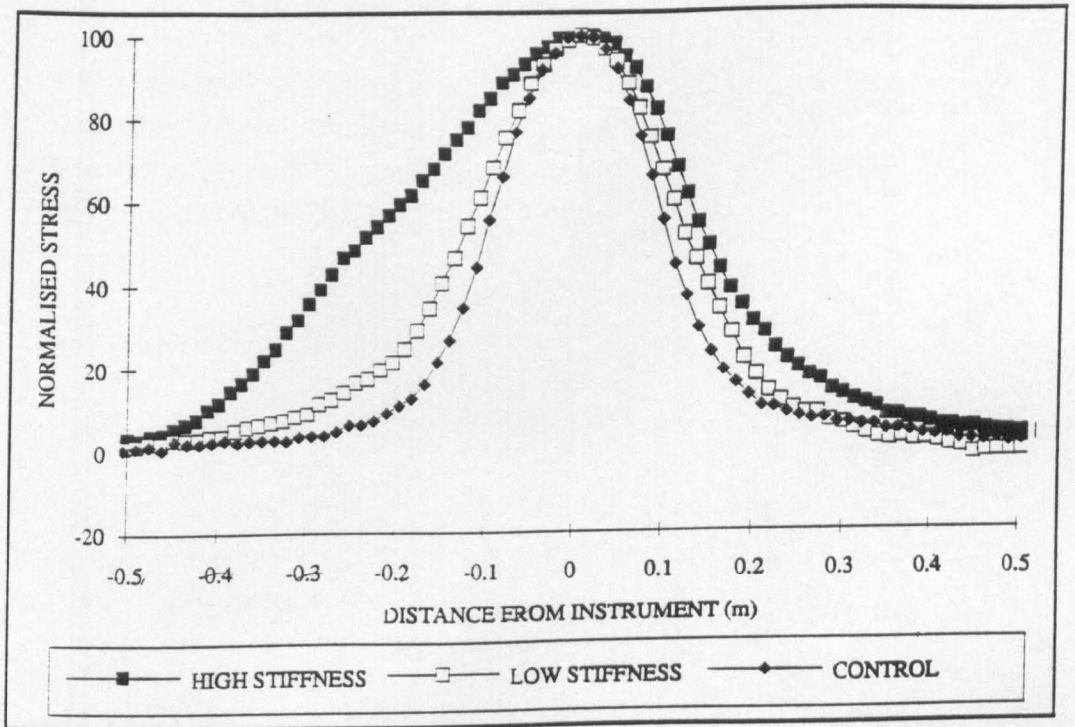


Figure 7.1 Normalised Stress Distribution at the Base of the Aggregate Layer - Sections I, P, and K

The stress has been normalised with respect to peak stress readings and the distance from the load to the instrument calculated as discussed in Chapter 6.4. It can be seen from Figure 7.1 that the stress distribution becomes wider as the pavements change from unreinforced through to stiffly reinforced. Furthermore, it should be noted that the thickness of the pavements used in this example are not constant but are 300mm, 350mm and 400mm thick on Section I, P and K respectively. Giroud and Noiray (1981) suggest that the field of influence of the load increases with depth in accordance with a load spread angle. Therefore, the relative thickness of the pavements will be reducing the observed effect.

The stress distribution figures shown imply that the peak stresses observed for the stiffer geosynthetics should be less than for the less stiff ones. However, this was not observed to be the case as was shown in Chapter 7.2.1. The distribution in Figure 7.1 thus makes the observed results more difficult to explain.

### 7.3 TRANSIENT STRAINS

#### 7.3.1 Comparison of Transient Strain Readings

The mean transient strains observed during the trials are given in Table 6.4. In this sub-section the transient strain responses of the lower-bound sections to the passage of the 80kN axle (passes 1-1000) are discussed.

The mean vertical transient strains, measured at the base of the aggregate layer can be compared between sections as follows: the high stiffness geosynthetics exhibited strains ranging from 4200 $\mu\epsilon$  (Section I) to 12300 $\mu\epsilon$  (Section J) but as Section J behaved unusually, due to aggregate segregation and a thinner pavement, the maximum value could be taken as 6700 $\mu\epsilon$  (Section N). The medium/low stiffness geosynthetics had transient strains ranging from 2600 $\mu\epsilon$  (Section M) to 5600 $\mu\epsilon$  (Section P) - less than that for the higher stiffness fabrics. The control (Section K) gives strain values which fall within the range of the medium/low stiffness geosynthetics.

The mean transient vertical subgrade wheel path strains, as measured at the top of the subgrade layer, may be summarised as follows: the high stiffness geosynthetics had subgrade strains of between 12600 $\mu\epsilon$  (Section I) and 29800 $\mu\epsilon$  (Section J). These strains are notably higher than those found in the medium/low stiffness geosynthetics

[8900 $\mu\epsilon$  (Section M) to 148000 $\mu\epsilon$  (Section O)]. The control (Section K) again has strain values which fell in the ranges of those measured beneath the medium/low stiffness geosynthetics.

The average, transient, transverse geosynthetic wheel path strains were in the range 3500 $\mu\epsilon$  (Section N) to 5500 $\mu\epsilon$  (Section J) for the high stiffness geosynthetics. The medium/low stiffness geosynthetics produced results varying from 2900 $\mu\epsilon$  (Section L) to 3700 $\mu\epsilon$  (Section P) - again these were less than those from the high stiffness group. In the control section (K) no geosynthetic exists, but the transverse strain at the surface of the subgrade was measured at 3300 $\mu\epsilon$  which was, again, in the range of values obtained from low/medium geosynthetic stiffness group. This observation implies that Sellmeijer (1990) is correct in his assertion that the transient behaviour of the pavement is controlled by the aggregate and subgrade stiffnesses and not by the geosynthetic stiffness.

Generally, therefore, it would appear that the transient strains within the entire system are higher for the high stiffness geosynthetic group than for the medium/low stiffness geosynthetic and control groups. Furthermore, the higher strains are associated with pavement sections in which larger vertical transient stresses were also recorded. This is initially rather surprising but, as suggested in Chapter 7.2.1, variation in pavement thickness might be the cause. Commonly, the high stiffness geosynthetic pavements are thinner than their medium/low stiffness geosynthetic counter parts. This may explain some of the difference but it should be pointed out that the design thickness of the lower-bound woven section (J) is 340mm compared to all of the lower-bound non-wovens which had design thicknesses of 350mm. This thickness would appear insufficient to explain the differences observed in the transient strains observed.

Instrument variability is another possibility to explain the observed results. There is a large scatter of data in the results obtained. However, the large number of results obtained and the repetition of the observation on all instrument comparisons tends to discount this explanation.

### 7.3.2 Transverse Geosynthetic Strain Profile

Figure 7.2 shows the mean transverse geosynthetic strain profile for the high stiffness geosynthetics and for the medium/low stiffness ones. The strain distribution has been normalised with respect to the peak transient strain in the wheel path.

The observed transient strains in the geosynthetic decay rapidly from peak values under the wheel path, as shown in Figure 7.2. Outside the loaded area of the geosynthetic, as calculated assuming that the aggregate performs load spreading with an angle  $\tan\alpha = 0.6$ , the strains induced in the inclusion by the wheel load are small, tending to zero, or even becoming slightly compressive. This leads to the conclusion that the geosynthetic has no transient function outside this area, and so, for transient loading, is not in need of anchorage. Furthermore, at positions remote from the wheel path these observations suggest that, in the transient case, the aggregate is pushing the geosynthetic away from the loaded area. This observation has some parallels with the monotonic explanation of strain predicted by Milligan et al (1989a) and Brocklehurst (in press).

As can be seen from Figure 7.2 the shape of the strain distribution is approximately the same for both cases, with the point of zero strain occurring around 0.5m away from the centre of the load.

## 7.4 PERMANENT DEFORMATION

### 7.4.1 Early Rut Formation

The aggregate surface of all the sections was given a final roll with the roller before the start of trafficking in order to ensure that there was no looseness of the surface of the aggregate which might affect the results. After a few passes it was possible to see the path that the lorry had taken, as can be seen in Plate 7.1, and it was initially thought that a small amount of surface compaction had occurred. However, on analysis, it became apparent that all sections had undergone varying and sometimes large amounts of deformation between the first and third pass. It is considered that this "start-up" rut was due solely to movements within the aggregate and that the variation in the start-up ruts was caused by small differences in the aggregate layer. This initial deformation would thus be unrelated to the performance of either the pavement in general or of the geosynthetic in particular.

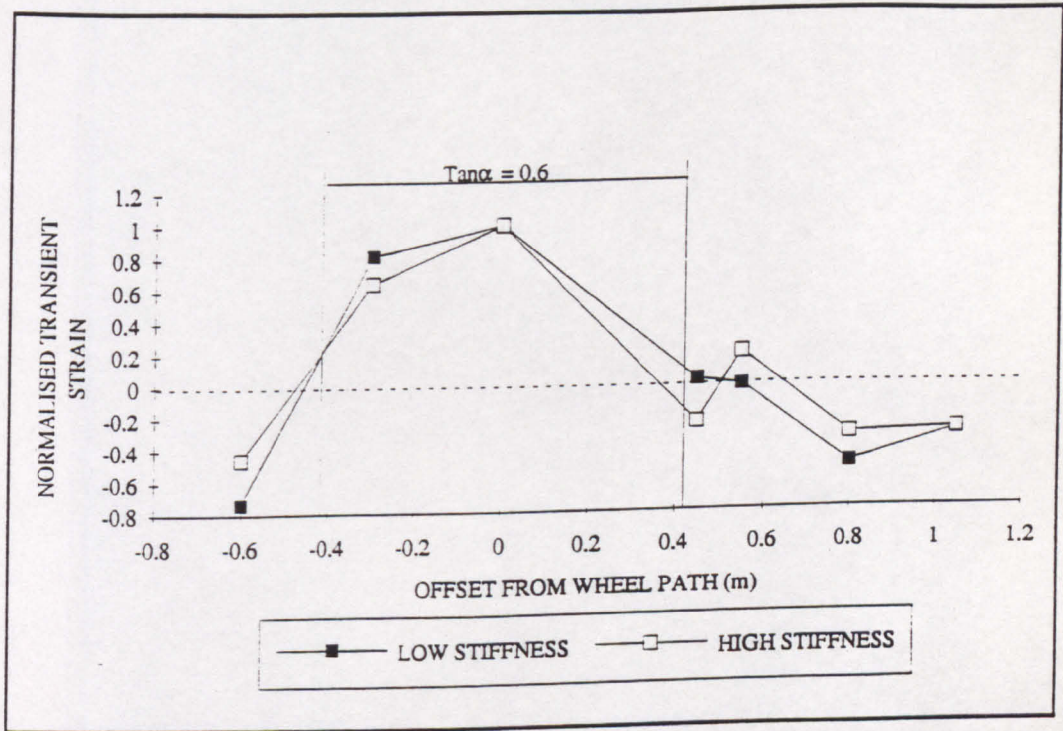
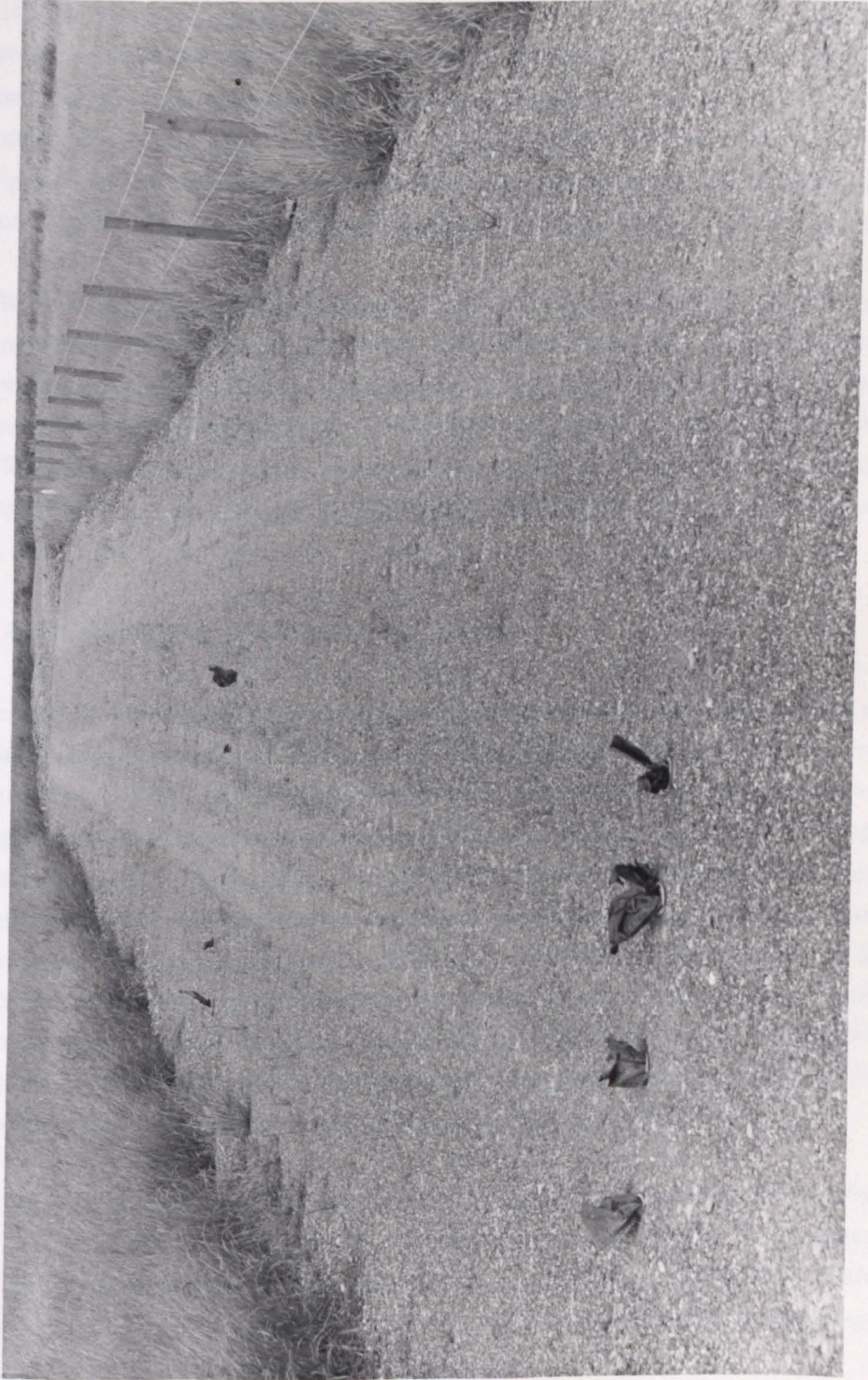


Figure 7.2 Normalised Strain Distribution  
Across the Geosynthetic



**Plate 7.1 - Pavements After a few Passes**

The high deformation in the first few passes is mirrored in the high deformations recorded in the first few cycles of repeated load triaxial testing of aggregates (Thom (1988)). When monotonic loading was undertaken, it was expected that large strains would occur as the load passed from zero to the equivalent of the axle load. If the material was then unloaded, the unloading stress/strain curve was steeper than the loading curve and, upon unloading, permanent deformation occurred, as shown in Figure 6.16. In subsequent cycles the stress path moved up and down the load/unload curve (albeit with a small amount of hysteresis) generating little permanent deformation.

The permanent strain on the first cycle is difficult to predict because it depends on the stress history of the sample. In theory, aggregates which have undergone the same construction and compaction processes should deform by the same amount in the first cycle. However, small variations in these processes appear to have a disproportionate effect on the properties of the aggregate layer in this first cycle. Thus it is difficult to predict how any one aggregate layer is likely to behave during the first cycle of loading.

#### **7.4.2 Comparison of Ultimate Rut Depth**

The rate at which rutting develops and the ultimate rut depth, are functions of many criteria. Not least of these functions are: the axle load and number of passes; the separation, filtration and reinforcement characteristics of the geosynthetics; the aggregate layer thickness, strength and stiffness; and the shear strength of the subgrade (Hausmann 1986). Thus, direct comparison between the performance of two sections is not truly valid, as many of these factors will vary between one section and another. To compare the performance of two different sections directly, the expected rut depth should be calculated, for each section, by a design method incorporating all of the above factors. The full-scale trials were planned so that all the sections should perform the same - according to each manufacturer's design methods - and that, as far as possible, the non-geosynthetic material characteristics remained constant.

Of the lower-bound pavements the ultimate rut depths varied between 24 and 49mm, for those sections that had not failed. As can be seen from Table 6.1 there appears to be little difference between sections whether the control, a medium/low stiffness geosynthetic or high stiffness geosynthetic section. As suggested above, the design of the experiment was such that this was to be expected.

### **7.4.3 Comparison of Rut Depth and Vertical Displacement**

The ratio of rut depth to vertical displacement was shown for each section in Table 6.2. For the upper-bound sections the rut depth to vertical displacement ratio was less than unity for the high stiffness geosynthetic reinforced pavements and for the Bidim Section (C). A ratio value of less than unity is difficult to explain as one might expect this to be the minimum value, ie all the rut depth is a result of vertical depression of the aggregate surface and no hogging occurs.

Of the lower-bound sections only the SS2 geogrid section (N) produced meaningful results out of the high stiffness group. The rut depth to vertical displacement on this section is the highest recorded at 1.88 indicating that a large amount of the rut depth is due to hog away from the wheel path.

### **7.4.4 Examination and Comparison of the Individual Elements Constituting a Rut**

As was shown in Figures 6.35 to 6.42 the surface rut depth is not usually mirrored precisely in the subgrade. Some internal aggregate deformation occurs producing a rut depth at the aggregate surface greater than at the aggregate subgrade surface.

Inspection of some of the figures mentioned above suggest that the aggregate thickness is increasing by more outside the wheel path than it is decreasing within it. This implies that the aggregate is dilating as it shears under the loading.

The high stiffness geosynthetic group indicate that for those excavated sections between 18% (Section N) and 20% (Section F) of the rut depth occurs within the aggregate layer. For the medium/low stiffness geosynthetics between 0% (Section M) and 28% (Section L) of the rut depth occurs within the aggregate layer and for the control 33% (Section K) occurs there.

#### **7.4.4.1 Control of Aggregate Deformation**

As was seen in Table 6.1. Sections A, B, C and D performed less well than their equivalent lower-bound counterparts. Indeed Section E may only have out-performed

Section J because of the much reduced thickness of Section J and Section F may only have out-performed Section I because the geogrid failed prematurely in Section I. It is possible that the increase in the upper-bound pavement deformation was caused by the lorry, as it came down off the hard standing area onto the pavements, inducing higher local stresses in the first section and continuing to bounce along the upper-bound pavements. Thus, Section A would be expected to have fared least well, with subsequent sections suffering progressively less severely. However, the speed of the lorry was, at most, 10m/s and it is felt that although the effects mentioned above might have had some bearing on the performance of Section A, it is unlikely that there would have been a continued affect further down the series. Examination of the longitudinal profile of Section A (Figure 6.17) shows that the vertical depression of the wheel path varies with a wavelength of 5m. Furthermore, a noticeable depression occurred before the start of Section A approximately 5m before the first measured depression. These observations are consistent with the lorry bouncing. Although there may be some evidence that this effect is still apparent in Section B (Figure 6.18), it is no longer evident in Section C (Figure 6.19) and so another explanation for the poor performance of the upper-bound sections must be found.

If the performance of these sections can not be attributed to the cause discussed above then another explanation may be that the aggregate layer is making a larger contribution to the overall rut depth by straining internally. In the thicker pavements of the upper-bound sections the geosynthetics are unable to work efficiently as they are too low in the pavement structure. Conventional wisdom for the reinforcement of static foundations implies that the reinforcement works at its most efficient when placed at approximately  $\frac{1}{3}$  of the footing width below the footing, as reviewed by Lee (1989). Assuming that the wheel print has an effective width of 600mm, geosynthetics will thus probably perform to their maximum advantage at a depth of 200mm into the pavement structure.

It would appear that there is a maximum appropriate thickness for singly reinforced pavements and that if the design dictates that larger thicknesses are required, then reinforcing inclusions within the fill should be considered.

Similarly, examination of the vertical strains monitored at the base of the aggregate layer shows that, although the transient strains are of a similar magnitude in the upper and lower-bound cases (Table 6.4), in the reinforced pavements; the permanent strains are higher in the upper-bound (Table 6.5). This unusual observation might be

explained by examining the vertical and horizontal strains. The transient vertical strains are probably of a similar order of magnitude because the differences in pavement thickness between the upper and lower-bound pavements are relatively small. In the thinner pavements however, the geosynthetic is in greater tension than in the thicker ones and this geosynthetic force increases the horizontal confining stress within the aggregate layer. Thus, in the thicker pavements the deviator stress at the base of the pavement, is greater than in the thinner one and it is known that, loosely, the permanent deformation is a function of the magnitude of this stress (Loach (1987), Thom (1988)).

#### **7.4.5 Geosynthetic Rupture**

Geosynthetic rupture occurred on three sections (I, J and O) during the trials at Bothkennar. Certainly in the case of Section I, the lightweight geogrid section, the rupture of the geosynthetic can be explained in terms of the observed deformations and geosynthetic properties.

It was shown from the geosynthetic testing at Strathclyde University (Yeo 1992) and summarised in Table 4.10, that the traffic damaged light weight geogrid (SS1) failed at a mean strain of 3.5%. As this is a mean value, geosynthetic rupture might reasonably be expected to commence at a lower strain level in situ at any weak points in the material.

The insitu strain of the geosynthetic can be estimated by reference to Giroud and Noiray (1981). From their calculations it is expected that for Section I the geosynthetic strain would have equalled 3.5% when the rut depth reached 124mm (below the failure criteria). Thus, it can be seen that geosynthetic rupture could be predicted to occur in these trials.

The geosynthetic rupture of Section O, the Polyfelt and Bamboo section, seemed to have been caused by a unique mechanism. Excavation of the post-failure pavement indicated that the bamboo poles had crushed, that is they had split in a longitudinal direction. The sharp edge of the bamboo had then cut the Polyfelt causing rupture and pavement failure.

The onset of the rupture was marked, it is supposed, by a noticeable change in gradient of the rut depth v passes plot. The rupture of the geosynthetic is catastrophic to the

serviceability of the pavement as the rate of rut depth development becomes very large. It was found that filling the ruts in a pavement where the geosynthetic had ruptured did not lead to a slowing in the rate of deformation. The marked increase in the rate of rut development occurred at around 40mm of rutting for Section I and 80mm for Section J and this compares to the value suggested by Tonus (undated) that the ruts should be filled when the depth reaches 90mm.

#### **7.4.6 Transverse Geosynthetic Permanent Strain**

The mean permanent transverse geosynthetic strains in the wheel path were shown in Table 6.5. The permanent strains in those coils away from the wheel path were, generally, too small to be measured with the instruments used. This observation supports the design method proposed by Milligan et al (1989a) in that the tension generated in the geosynthetic, as a result of permanent deformation, is not constant across the pavement but decays with distance from the wheel path.

### **7.5 THE RELATIONSHIP BETWEEN RUT DEPTH AND SUBGRADE STRESSES**

As can be seen from Figure 7.3 there would appear to be little correlation between rut depth and the subgrade surface stress. The stresses shown are the mean value of the peak stresses measured by the pressure cells for the 80kN and 126kN axle loads. It is possible that the variation in the readings of stress are a result of instrument variability but the range of values appears to be very high for any given rut depth.

One might conclude that subgrade surface transient stress is not a significant factor in the control of rut depth development. However that would appear to be contrary to the observation that the rut depth development increased with increased axle load and subgrade surface stress for any given pavement.

### **7.6 RUT DEPTH DEVELOPMENT AND GEOSYNTHETIC STIFFNESS**

The rut depth development, expressed in mm per pass, for each section was shown in Table 6.1. For the 80kN axle load the rate of rut depth development for the lower-bound section was found to be in the range of 0.009 to 0.019 mm/pass if Section J1 is

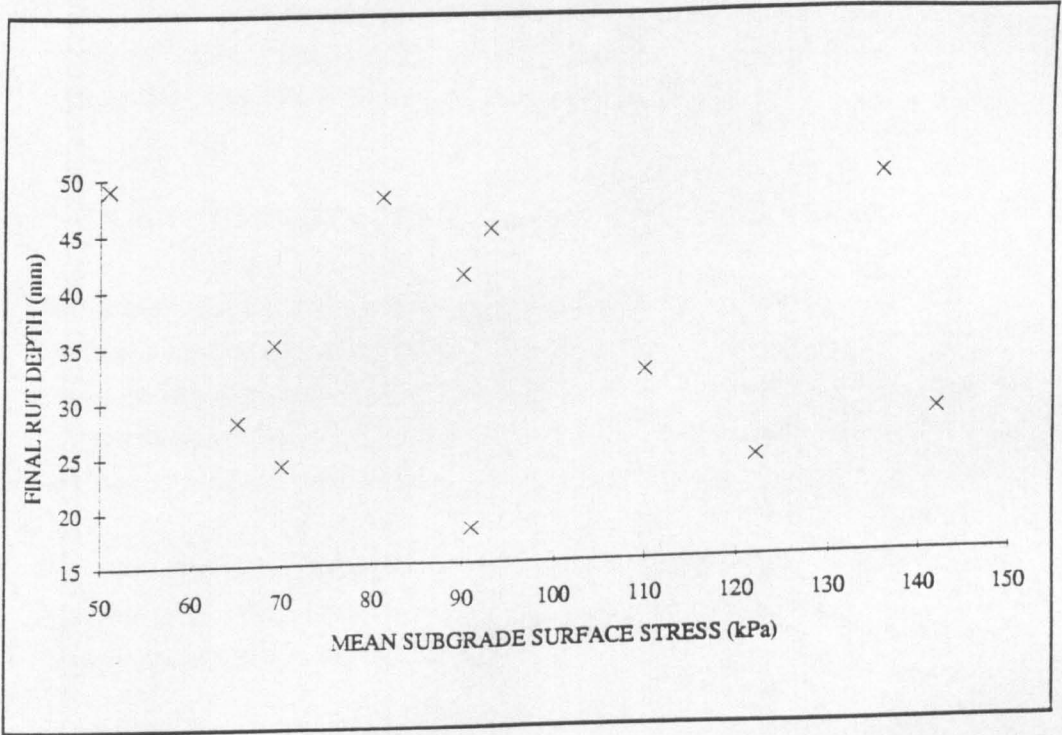


Figure 7.3 Comparison of Final Rut Depth and Mean Subgrade Stress

excluded. This rate appears to be "constant" for both the high stiffness and medium/low stiffness geosynthetic pavements as well as for the control pavements.

For the 126kN axle, the rate of rut depth development for the lower-bound pavements increased. Excluding the failed pavements, the rate varied from 0.008 to 0.025mm/pass and again no type of geosynthetic stiffness or the control sections excelled.

These observations could have been expected given that all of the pavements were designed to the same limiting deformation criteria. Therefore the rate at which deformation occurs should be equal on all types of pavement.

## 7.7 RELATIONSHIP BETWEEN PERMANENT AND TRANSIENT STRAINS

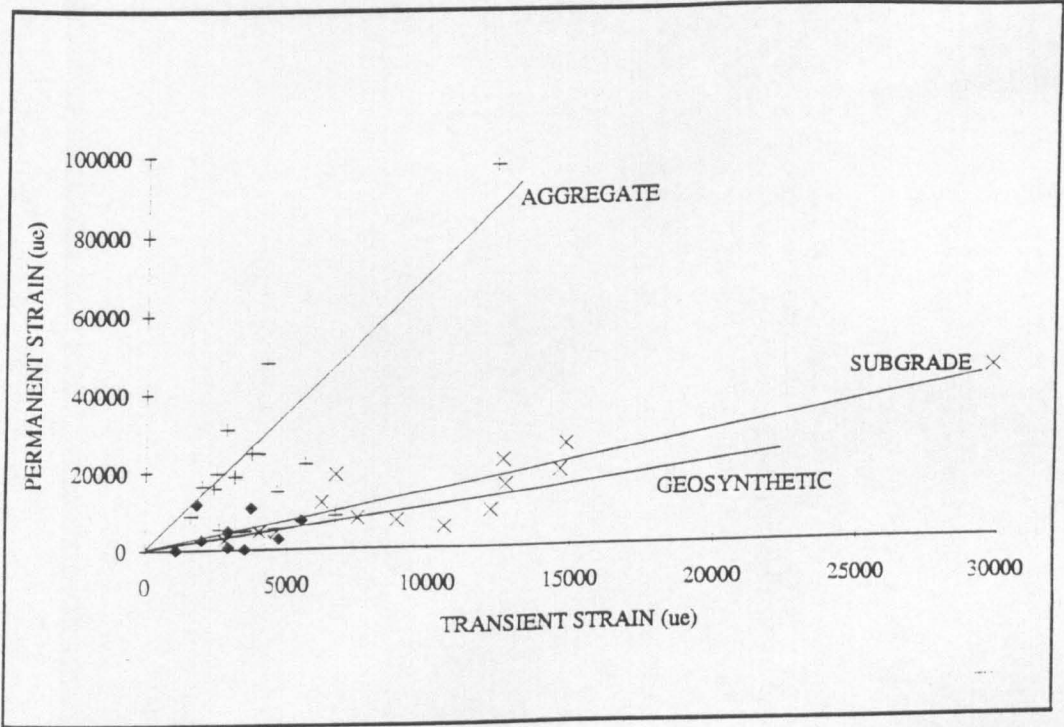
The mean transient strains read using the strain coils in pass 1 to 1000 have been plotted against the ultimate permanent strains obtained (Table 6.4 and 6.5 respectively). These results, shown in Figure 7.4, imply that there is a relationship between transient and permanent deformation in all three elements of the pavement. However, as can be seen from the figure, there is a good deal of scatter in the results.

This observation is encouraging for those design methods that are principally transient analyses as it implies that there is some correlation between the analysis and the permanent deformation that is of interest.

The slopes of the lines plotted on Figure 7.4 are dependent upon the number of load repetitions applied to produce the permanent strain. However, it can be seen that in this case the same value of transient strain in the aggregate and subgrade materials will produce proportionally more permanent deformation in the aggregate than in the subgrade.

## 7.8 NON-LINEAR BEHAVIOUR

The increase in the observed peak vertical stresses generated when the axle load increased from 80kN to 126kN was less than may have been expected from the multi-layered, linear-elastic analysis. The 58% increase in load led, on average, to an observed increase of 32% in the vertical stress at the base of the aggregate layer and a



20% increase in the vertical stress at the top of the subgrade. Furthermore, the increase in load also led to an average increase of 22% in the transient vertical aggregate strain, a 43% increase in the subgrade vertical transient strain and a 31% increase in the horizontal geosynthetic transient strain in the wheel path. The fact that the observed values did not increase by the amount predicted by multi-layered, linear elastic analysis is a result of the non-linear elastic behaviour of the aggregate and subgrade materials.

The change in the stiffness of the layers under the two axle loads can be computed from the measured stresses and strains. These are summarized in Table 7.1.

Section	80kN Axle Load		126kN Axle Load	
	Aggregate Stiffness	Subgrade Stiffness	Aggregate Stiffness	Subgrade Stiffness
	(MPa)	(MPa)	(MPa)	(MPa)
A	-	32	-	8
B	21	-	-	-
C	-	-	25	34
D	26	28	20	20
E	51	52	19	15
F	26	26	10	-
I	40	17	9	4
J	15	16	4	4
K	16	36	-	9
L	12	10	7	4
M	24	162	7	7
N	10	10	8	7
O	22	25	8	-
P	20	-	6	-

**Table 7.1 In-situ Measured Layer Stiffness**

The non-linear behaviour of clays and aggregates is a well-known phenomena, such as Hicks and Monismith (1971) or Brown (1979), and many models exist to predict the stress/strain relationships for both granular and cohesive materials. FENLAP is a finite element programme developed by Almeida et al (1991) primarily as a tool to calibrate the back-analysis programs which estimate the stiffness of pavement layers from falling weight deflectometer data. FENLAP was used with a "k theta model" (Hicks and Monismith (1971)) for the aggregate layer and a subgrade model described by Brown (1979) to analyse the non-linearity of the aggregate and subgrade. The constants required for the models were obtained by examining on-site FWD data using a non-linear approach (Almeida, in press). A FENLAP analysis predicts that the 58% increase in load applied at Bothkennar should generate a 37% increase in the vertical stress at the base of the aggregate layer and a 33% increase in the vertical stress at the top of the subgrade, which are closer to the observed values.

Therefore, the stresses and strains as measured in the pavement can be predicted, in the standard axle loading case, by the use of multi-layered, linear-elastic analysis provided that an appropriate stiffness for the aggregate and soil has been adopted. Changes in

the stress condition at the base of the aggregate layer and at the top of the subgrade due to a changing loading are not accurately modelled by linear-elastic analysis in which the same material stiffnesses are used. However non-linear analysis has produced some explanation for the stresses observed, giving some confidence that material non-linearity is having a significant effect.

## 7.9 LOAD EQUIVALENCY

### 7.9.1 Common Assumptions

The trials at Bothkennar incorporated the use of two axle loads (80 and 126kN). It is a common assumption that the data relating to different axle loads can be reduced to an equivalent number of standard axles. It is often assumed that some form of power relationship exists, relating non-standard axle loads to a standard one. For example:

$$\frac{N_s}{N_i} = \left( \frac{P_s}{P_i} \right)^\alpha \quad (7.1)$$

where:  $N$  = number of passes  
 $P$  = axle load  
 $s$  = standard axle  
 $i$  = non-standard axle  
 $\alpha = 3.95$  (Giroud & Noiray (1981))  
 or  $\alpha = 6.12$  (De Groot et al (1986))

It is also often assumed that a succession of non-standard and standard loadings may be treated as the sum of their equivalent loadings (using Equation 7.1) regardless of order of application. Mathematically, this is expressed as:

$$N_s = \Sigma \left[ N_i \left( \frac{P_s}{P_i} \right)^\alpha \right] \quad (7.2)$$

### 7.9.2 Examination of Assumptions

Assuming that damage is proportional to the logarithm of the number of passes and that a power law is appropriate, and that

$$P_i = 126\text{kN}$$

$$P_s = 80\text{kN}$$

$$\alpha = 4$$

$$\text{then } N_i = N_s \left( \frac{126}{80} \right)^4 = 6.1 N_s$$

Thus the damage done by one passage of the 126kN axle is equivalent to 6.1 passes of the 80kN axle. It can be seen from Table 6.1 that nearly all sections suffered a greater rate of rut depth development with the 126kN axle load. However, the relationships as suggested by Equation 7.1 and &.7.2 appear to significantly over-predict the observed behaviour.

## CHAPTER EIGHT

### EVALUATION OF DESIGN METHODS

#### 8.1 INTRODUCTION

The objective of this chapter is to critically examine each design method used and in particular to compare actual performance to that predicted by design. Where possible "as built" material properties are used as design inputs. However, where the "as built" properties exceed the limits proposed by the design method this is highlighted and solutions to circumvent the limitations are suggested.

Each design method is reviewed in the light of the pavement's performance and the strengths and weaknesses of each method summarised.

#### 8.2 UNREINFORCED PAVEMENTS (SECTIONS D, H & K)

##### 8.2.1 Unreinforced pavement design after Hammitt (1970)

###### 8.2.1.1 Summary of design method

Hammitt (1970) produced an empirical relationship for the thickness of aggregate required to produce a 75mm rut depth after N passes of a wheel load, P. This relationship was given in Equation 2.6.

$$h = (0.0236 \log N + 0.0161) \sqrt{\frac{P}{\text{CBR}} - 17.8A} \quad (2.6)$$

###### 8.2.1.2 Back analysis

The problem with attempting to use Equation 2.6 for any type of back-analysis is that the following variations occurred during the trials.

- 1) None of the three recorded control sections reached a rut depth of 75mm.

The results were:      Section D - 28mm (550mm Type 1 aggregate)  
                                  Section H - 34mm (400mm Sand and Gravel)  
                                  Section K - 24mm (400mm Type 1 aggregate)

- 2) P, the wheel load, varied from 40kN to 63kN and on doing so the contact area of the tyre, A, would have changed.
- 3) After 1229 passes the tyre pressure of the lorry was increased which, while not effecting P, would have changed A.
- 4) The quality of the aggregate employed is not recognised as being of any importance.

In order that the design proposed by Hammitt (1970) can be quantitatively examined some further assumptions will need to be made. Assuming that the wheel load was 40kN throughout and that the tyre pressure was 630kPa then the contact area would have been 0.06m<sup>2</sup>. The shear strength of the subgrade during the trials was found to be around 85kPa as was shown in Figure 3.14. If, as suggested by Giroud and Noiray (1981), a relationship of 30kPa shear strength is equivalent to 1% CBR then a shear strength of 85kPa is approximately 3% CBR. The thickness of aggregate on the lower-bound control sections was 400mm.

Thus from Equation 2.6 we can see that

$$0.400 = (0.0236 \log N + 0.0161) \sqrt{\frac{40}{3} - 17.8 \times 0.06}$$

therefore, according to Hammitt (1970) a rut depth of 75mm would occur after

$$\log N = 3.784$$

$$N = 6082 \text{ passes}$$

The rut depth after 1000 passes of an 80kN axle for the Type 1 Control Section (K) was 18mm and after 2115 passes of mixed traffic was 24mm.

Hammitt (1970) assumes that the rate of deformation is proportional to the logarithm of the number of passes applied. Thus as a 75mm rut depth is expected at log N = 3.784, at 1000 passes (log N = 3) one might expect the rut depth to be

$$\frac{3}{3.784} 75 = 60\text{mm.}$$

It would appear that Equation 2.6 is sensitive to changes in the CBR of the subgrade. Furthermore, of the elements contained within Equation 2.6 the CBR of the subgrade is the least well defined. The undrained shear strength of the subgrade was estimated to be 85kPa and it could be argued that this shear strength is closer to 4% CBR. Table 8.1 shows the predicted and measured rut depths for all of the control sections based upon Equation 2.6 with values of CBR at 3 and 4%.

	Measured Rut Depth at 1000 Passes	Predicted Rut Depth after 1000 Passes of 40kN Wheel Load 3% CBR	Predicted Rut Depth after 1000 Passes of 40kN Wheel Load 4% CBR
D	14	37	31
H	14	60	45
K	18	60	45

**Table 8.1 Predicted and Measured Rut Depths for the Control Sections**

This implies that the unreinforced pavements in the full-scale trials performed significantly better than Equation 2.6 would suggest. However, Hammitt's (1970) data was based around pavements where life expectancy was, at most, 300 passes (not 6,000) and so this example is operating beyond the empirical boundaries of Hammitt's work and so should be treated with caution.

## **8.2.2 Unreinforced Pavement Design After Giroud and Noiray (1981)**

### **8.2.2.1 Summary of design**

Several assumptions were made by Giroud and Noiray (1981) based upon the work of Hammitt (1970) and others and these were discussed in Chapter 2.

### **8.2.2.2 Back analysis**

Giroud and Noiray (1981) suggest that non-standard axle loading can be accommodated by the use of the "fourth power law". Using the fourth power law the 126kN axle load can be related to a standard axle load by using Equation 2.8. so, 1000 passes of the 126kN axle are equivalent to:

$$N_s = 1000 \left( \frac{126}{80} \right)^4 = 6,153$$

Thus, according to the fourth power law, a total of 7,153 equivalent standard axle loadings (6,153 equivalent passes by 126kN plus 1000 standard 80kN passes) were applied to the pavements at Bothkennar. From Equation 2.10 the thickness of aggregate required to resist a rut depth of 30mm (the mean of the two lower-bound control sections) is given by:

$$h = \frac{0.19 (\log 7153 - 2.34 (0.03 - 0.075))}{3^{0.63}} \quad (2.10)$$

$$h = 0.376\text{m}$$

Compared to an actual thickness of 0.4m. The equation appears to be very sensitive to the thickness of aggregate because if  $h = 0.4\text{m}$  is put in Equation 2.10, the expected rut depth after 7153 passes is minus 75mm. This is clearly nonsense and would suggest that the formula is being applied beyond the limits of the empirical base from which it was obtained.

In addition to this concern the use of a fourth power law must be questioned. As discussed in Chapter 7.9 it has not predicted the observed behaviour during the trials. The extensive trials on unreinforced, unpaved roads, undertaken by Hammitt (1970), produced a relationship which predicted the number of passes, of any given axle load which would generate a 75mm rut. Based on 59 sections and various axle loadings, Hammitt (1970) predicted that the number of passes was a function of  $\sqrt{\text{axle load} - \text{contact area}}$ . This appears to be based on a large number of sections and it appears that this leads to a sound basis for prediction. Thus, a relationship for non-standard axle loads is probably more correctly defined by reference to Hammitt (1970) than from more arbitrary use of a power law.

### 8.3 "BIDIM" REINFORCED PAVEMENTS (SECTIONS C & L)

#### 8.3.1 Summary of design for Section L

Bidim is a needle-punched polyester fabric and the grade used in the trials was Bidim B2. The polyester fabric was designed by reference to the publication of the Comité

Français des Geotextiles (1981) which specified that for 1,000 passes of HGV loading at 10-100 passes per day, good fill, an allowable rut depth of 150mm and a subgrade CBR between 2 and 5%, then 350 to 450mm of aggregate was required (350mm was suggested for the design of the lower-bound section (L) by Rhône Poulenc).

### 8.3.2 Back-Analysis of Section L

The actual thickness of the aggregate layer used in the pavement was shown in Table 5.2 as 354mm. The design method does not predict how the rut depth develops. The wide range of possible subgrade CBRs that are permitted for any one design does not fit with the observation that most analytical and empirical designs are sensitive to small changes in CBR. So, if the number of CBR intervals could be increased, the design method may have some useful function. This type of design method is very difficult to calibrate and to relate to the trials at Bothkennar. However, it was observed that the rut depth developed by the 2115 passes was 42mm, less than the 150mm expected for 1000 passes.

## 8.4 "POLYFELT" REINFORCED PAVEMENT (SECTION P)

### 8.4.1 Summary of Design

The Polyfelt section contained a needle-punched polypropylene geosynthetic (Polyfelt TS500) and was designed according to Polyfelt (undated). The thickness of aggregate required to resist failure, in this case static failure, was calculated and then adjusted to take account of trafficking and the acceptable rut depth.

The thickness of aggregate required to resist static failure, as shown in Figure 8.1, can be determined for two axle loads (90kN and 135kN) and although two qualities of fill,  $\phi' = 45^\circ$  and  $\phi' = 30^\circ$  are possible in the design method only one ( $\phi' = 45^\circ$ ) is shown here. The axle load 90kN is approximately equal to the lower axle load applied at Bothkennar, and the 135kN load nearer to the higher load applied. The aggregate at Bothkennar had an angle of friction of  $54^\circ$  and Figure 8.1 relates to aggregates with an internal angle of friction of  $45^\circ$ . For the case at Bothkennar, in order to approximately assess the method, it was assumed that the applied 80kN axle load and fill with an angle of internal friction of  $54^\circ$  was approximately equivalent to the 90kN axle load and  $45^\circ$  fill used in the design. Although these two assumptions act in the same direction

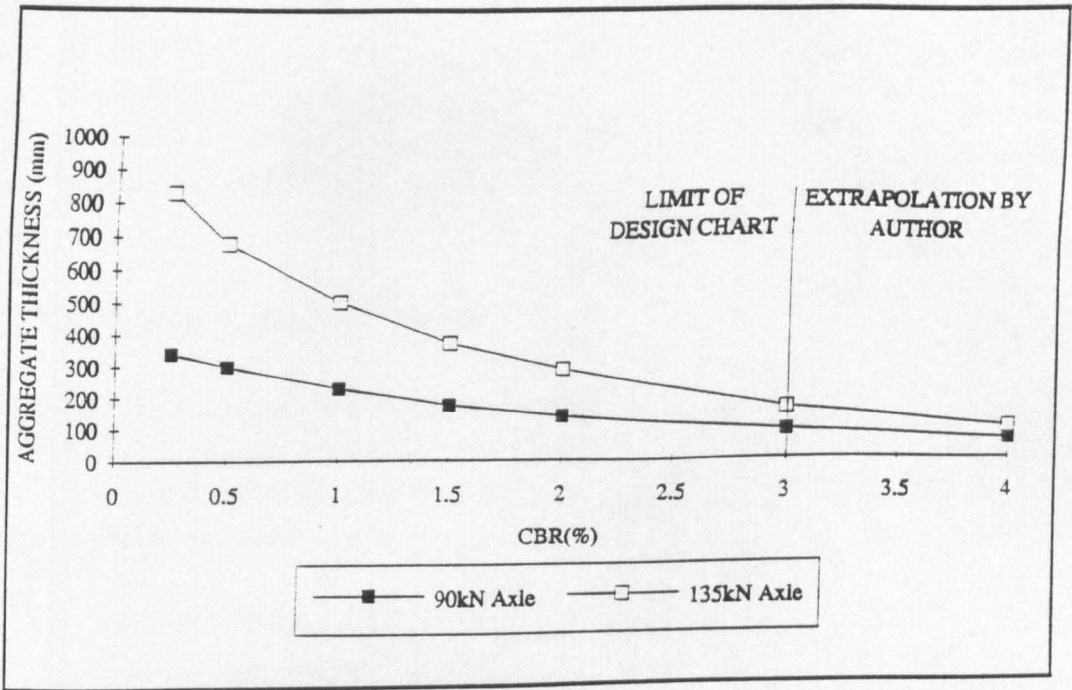


Figure 8.1 The Thickness of Aggregate Required to Resist Static Failure of 90kN & 135kN Axles - After Polyfelt (undated)

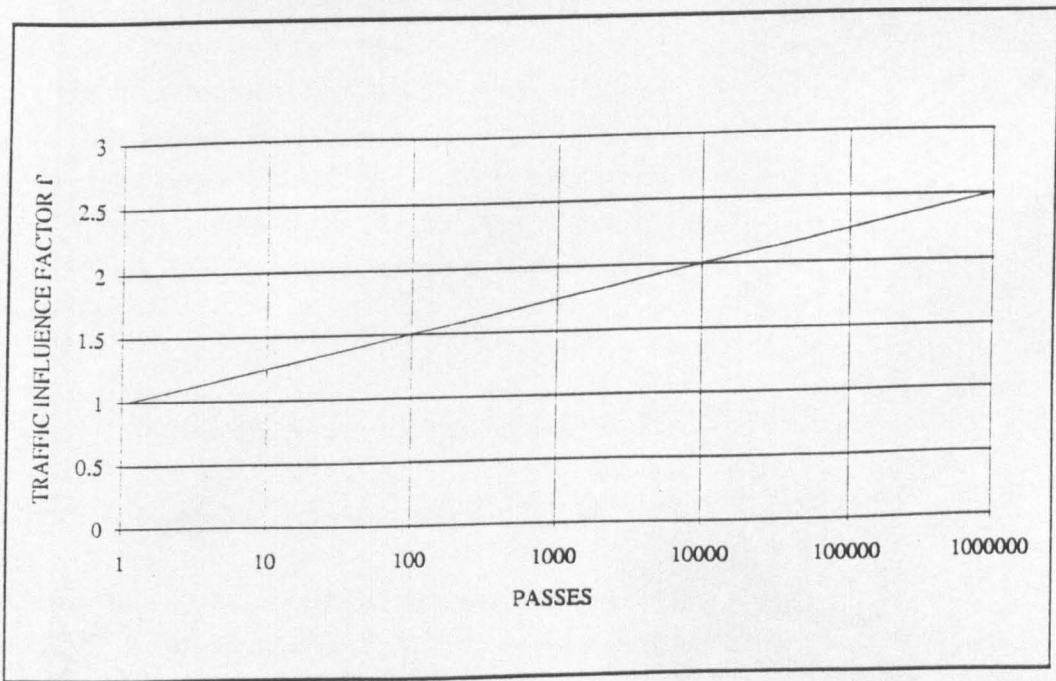


Figure 8.2 Traffic Influence Factor for a Rut Depth of 50mm - After Polyfelt (undated)

they were the best that were available from the design options. The design method is empirical and experimental data supporting such design methods cannot cover all eventualities. The design method gave a required aggregate layer thickness of 90mm, for a subgrade of 3% CBR, to resist static failure.

#### **8.4.2 Back analysis of Design**

The design, provided by Polyfelt Ges mbh, requested a design thickness of 350mm. The actual thickness of aggregate used in the trials was 360mm, as shown in Table 5.2 and a rut depth of 20mm occurred after approximately 1000 passes of an 80kN axle and the ultimate rut depth was 45mm after 2115 passes of mixed traffic.

The trafficking influence factor, which the design method uses to increase aggregate thickness from the static to the trafficked case, must be equal to  $\frac{360}{90} = 4$ . As can be seen from Figure 8.2 a rut depth of 50mm would be expected after many millions of passes. It appears that the design is over-optimistic as the predicted number of passes to produce a 50mm rut depth is much greater than the observed. The design method seems to be sensitive to CBR. If the CBR in-situ was indeed 2% not 3% then the design thickness of aggregate to resist static deformation increases from 90mm to 140mm. Thus, the trafficking influence factor decreases to  $\frac{360}{140} = 2.5$ . Thus a rut depth of 50mm would be expected to occur after 1 million passes, according to Figure 8.2. However, Figure 8.2 was extrapolated from the figure in Polyfelt (undated) and the pavement at Bothkennar was therefore outside the published limits of the design method. This highlights again one of the problems with empirical approaches to design.

### **8.5 TYPAR REINFORCED PAVEMENT (SECTIONS B & M)**

#### **8.5.1 Summary of Design for Section M**

The Typar section contained a heat-bonded polypropylene geosynthetic, namely Typar 3407. It was designed by Du Pont to the method proposed by Tonus (undated). The thickness of aggregate layer required to resist 1000 applications of an 80kN load is dependent upon the CBR of the subgrade and the geosynthetic inclusion. Such a thickness required versus CBR plot is shown in Figure 8.3 taken from Tonus (undated). The expected rut depth is one third of the thickness of the pavement, and

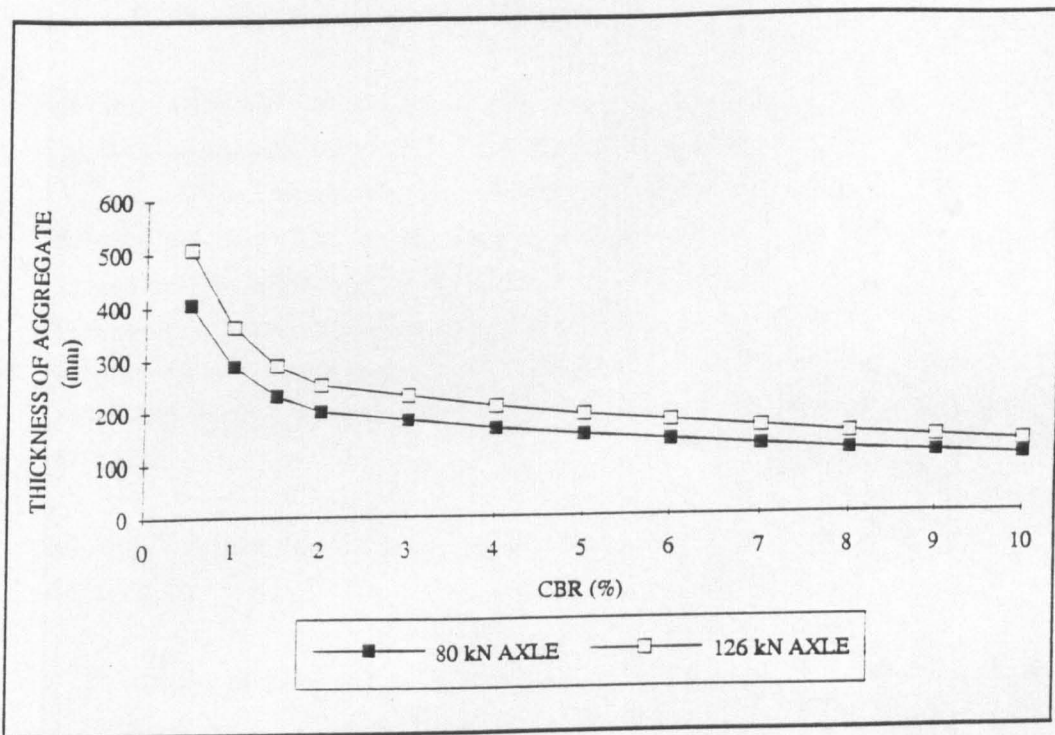


Figure 8.3 Thickness of Aggregate Layer to Resist 1,000 Passes of a 90kN Axle Load - After Tonus (undated)

therefore the design is a little inconvenient to the user, who tends to specify pavement performance by the rut depth which is permitted after a specified number and size of loadings. An analysis is possible using Tonus (undated), however, some assumptions, not mentioned in the method, have to be made and iteration is required. Similarly back calculation to compare actual and predicted performance requires some, unstated, assumptions to be made.

### 8.5.2 Back Analysis of Section M

For the trials at Bothkennar, the subgrade had an undrained shear strength of 85kPa. Figure 8.3 requires the subgrade to be characterised by CBR. The equivalency of CBR  $= \frac{S_u}{30}$  was used as suggested by Tonus (undated). Thus, 85kPa is equivalent to 2.8% CBR and therefore from Figure 8.3 it can be seen that the thickness of aggregate required to resist 1000 applications of the load is 200mm. Thus, for the lower-bound solutions it was expected that after these applications, the rut depth would be a third of the thickness of the pavement, 67mm. In reality the aggregate layer was 372mm thick in the lower bound case and the rut depth at this point, for the lower bound section (M), was 20mm.

The design method makes the following common assumptions about the effects of trafficking:

- a) that non-standard axles can be related to standard axles by the use of a "fourth power law",  $\left(\frac{N_s}{N_i}\right) = \left(\frac{P_i}{P_s}\right)^4$ , as discussed in Chapter 7.9.1.
- b) that a variety of axle loads can be expressed as the sum of their equivalent loads,  $N_s = \Sigma \left[ N_i \left(\frac{P_i}{P_s}\right)^4 \right]$

and

- c) that the trafficking damage is a function of the logarithm of the number of passes, as shown in Figure 8.4 where the traffic influence factor is derived from the work of Hammitt (1970) and is given in Equation 8.1.

$$f = 0.27 \log N + 0.19 \quad (8.1)$$

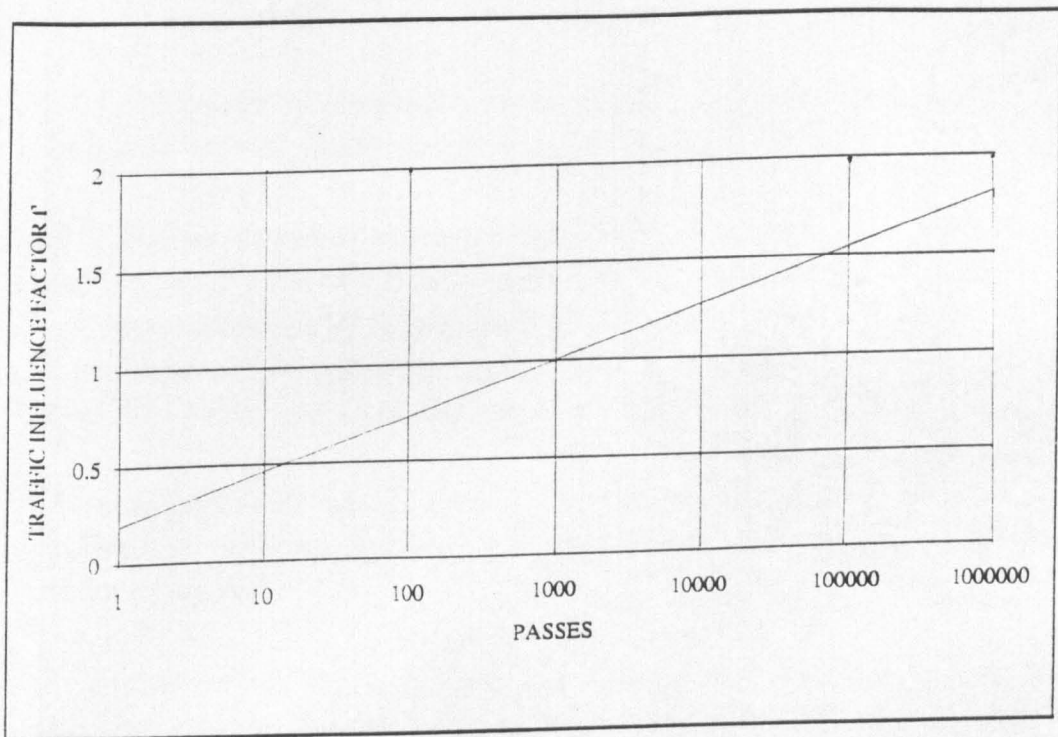


Figure 8.4 Traffic Influence Factor After Tonus (undated)

where  $f$  = the traffic influence factor

This differs from Equation 2.5 to take into account the beneficial effects of including Typar geosynthetics (Tonus (undated)). The design thickness of the pavement at Bothkennar was 350mm, as requested by Du Pont, and the actual thickness of 372mm implies that from Figure 8.4 the traffic influence factor,  $f$ , must be  $\frac{372}{200} = 0.27 \log N + 0.19$ .

$$\text{ie } \log N = 5.78$$

Using the assumptions made above, the variety of axle loadings can be reduced to an equivalency of 7,125 passes of an 80kN axle and  $\log 7,125 = 3.85$ .

Thus a 350mm thick pavement is expected to rut to one third of its depth, ie 117mm, after  $\log N = 5.78$  passes, ie after nearly 1 million passes. Continuing with the assumption in Equation 8.1, that rut depth development is dependent on the logarithm of the number of load applications, the rut depth expected at the end of trafficking is  $\frac{3.85}{5.78} \times 117 = 78\text{mm}$ . The actual, final rut depth was 24mm.

The design method does not attempt to predict any savings of aggregate that might be possible by incorporating the geosynthetic although comparison with Hammitt (1970) would be possible.

The prediction of rut depth development is compared to the actual in Figure 8.5. As can be seen from the figure, the design method overestimates the rut depth - in this case by a factor of about 2.

## 8.6 TENSAR REINFORCED PAVEMENT (SECTIONS A & N)

### 8.6.1 Summary of Design of Section N

The Tensar reinforced pavement contained a polypropylene geogrid made by Netlon, namely Tensar SS2. As was detailed in Chapter 2.3.3 the Tensar design approach is as proposed by Giroud & Noiray (1981). It consists of a comparison of static analysis of the unreinforced and reinforced cases to determine an aggregate saving. This saving is then applied to the thickness measured by an empirical design of an unreinforced pavement in order to obtain the thickness for the reinforced case.

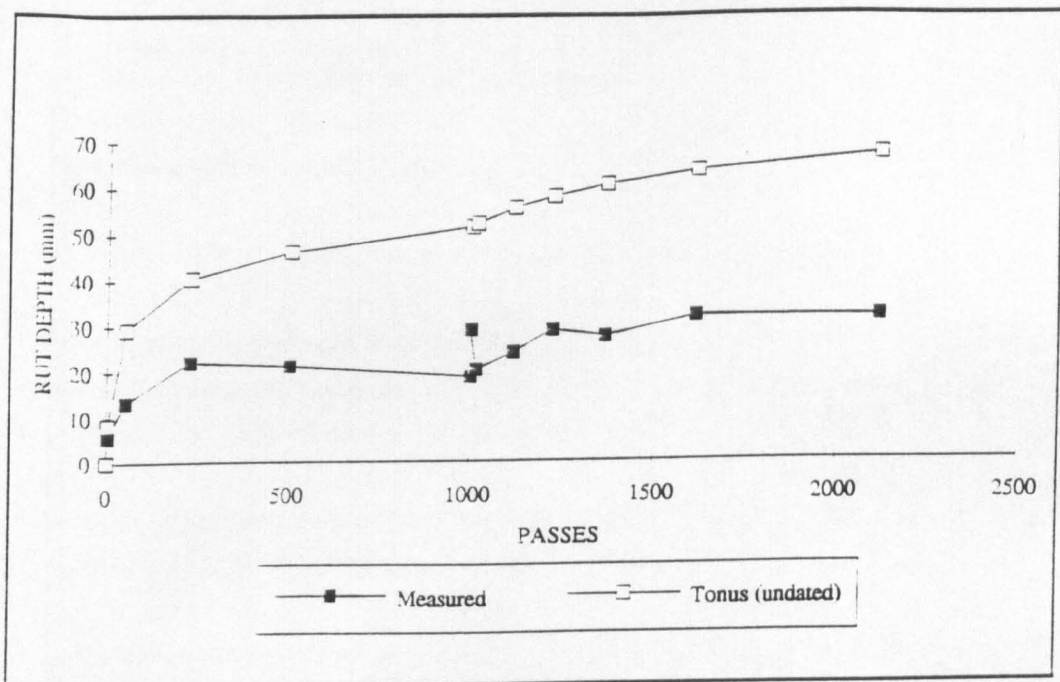


Figure 8.5 Measured and Predicted Deformation of the Section Designed According to Tonus (undated)

## 8.6.2 Back Analysis for Section N

### 8.6.2.1 Static Analysis - Unreinforced Case

In the unreinforced analysis, the vertical stress imposed upon the subgrade is taken to be limited by the elastic bearing capacity  $\pi S_u$ . Thus, the thickness of the pavement,  $h$ , required to resist an application of one pass of a wheel load in the unreinforced case is given by Equation 2.12:

$$\pi S_u = q \left( \frac{WL}{(W + 2h \tan \alpha)(L + 2h \tan \alpha)} \right) \quad (2.12)$$

For the case at Bothkennar, it is assumed that:-

$$S_u = 85 \text{ kPa}, W = 0.4 \text{ m}, L = 0.283 \text{ m}, \tan \alpha = 0.6, q = 350 \text{ kPa}$$

The concept of a load spread angle,  $\tan \alpha$  was discussed in Chapter 7 and it is assumed here to provide a fair approximation to the imposed vertical stress distribution on the subgrade. The value of  $\tan \alpha$ , as suggested by Giroud & Noiray, is 0.6.

By this means the thickness of aggregate layer to resist static loading in the unreinforced case can be found to be 0.04m.

It should be noted that  $h_0 = 0$  when  $S_u = 111 \text{ kPa}$ , that is direct static loading of the subgrade by a standard axle would be possible without exceeding the elastic bearing capacity. Hence, at shear strengths above 111kPa the design method is no longer valid.

### 8.6.2.2 Static Analysis - Reinforced Case

In the static analysis of reinforced pavements, as proposed by Giroud and Noiray (1981), the vertical stress which can be imposed on the subgrade is assumed to be limited by the plastic bearing capacity,  $(2 + \pi)S_u$ , rather than the elastic bearing capacity. This vertical stress is then modified by the contribution made by the geosynthetic due to the membrane effect. Under standard axle loading, the thickness of aggregate,  $h$ , required to resist the application of one pass of a wheel load in the reinforced case is given by Equation 2.19.

$$(2 + \pi)S_u = q \left( \frac{WL}{(W + 2h \tan \alpha)(L + 2h \tan \alpha)} \right) - p_r \quad (2.19)$$

where  $p_r$  is the reduction in vertical subgrade stress attributable to the membrane effect. If the contribution of the membrane effect is assumed to be ( $p_r = 0$ ) and the same values of parameters apply as in Section 8.6.1 then  $h = 0\text{m}$  when  $S_u = 60\text{kPa}$ .

This implies that direct static loading of the geosynthetics, by a standard axle, would be possible without exceeding the plastic bearing capacity of the subgrade.

At Bothkennar the subgrade shear strength was  $85\text{kPa}$  and therefore static analysis of the reinforced pavement, using the above approach, yields a negative requirement for the thickness of aggregate. Thus, the conclusion should be drawn that the method is not suitable for subgrade shear strengths above this level.

However, it could be argued that this type of analysis is somewhat arbitrary, in that it is the difference in aggregate thickness between the reinforced and the unreinforced cases that is of interest in the Giroud and Noiray (1981) method. This saving of aggregate is applied to an unreinforced, empirical design. Therefore, although negative thickness requirements at higher subgrade shear strengths may bring into question the applicability of the design, it is nevertheless possible to generate some form of design for the shear strengths as different thicknesses will still result. The use of questionable, negative required thickness is likely to generate more sensible answers than the alternative assumption which is that, at subgrade shear strengths above  $68.7\text{kPa}$ , the static, reinforced case thickness required equals zero because this does not take into account the effects of repeated loading.

The Vertical, Central Displacement of the Membrane (Section N) For the lower-bound geogrid pavement at Bothkennar,  $h = 0.33\text{m}$  and after 1000 passes of an  $80\text{kN}$  axle, a rut depth of  $0.018\text{m}$  had developed.

Therefore if  $\tan \alpha = 0.6$  and  $W = 0.4\text{m}$  then from Figure 2.7 the width,  $a$ , of the subgrade subject to vertical stress is given by :

$$a = \frac{W}{2} + h \tan \alpha = 0.39$$

and as the half axle width of the load was 0.95m then the width of the unloaded area,  $a'$ , is given as:

$$a' = 0.95 - 0.39\text{m} = 0.56\text{m}$$

As  $a' > a$ , Giroud and Noiray suggest that, if the subgrade is incompressible, volumetric equilibrium must occur during the deformation of the subgrade and so the vertical depression at the surface of the subgrade is given by Equation 8.2.

$$s = \frac{ra'}{a + a'} = 0.011\text{m} \quad (8.2)$$

The subgrade vertical depression under the wheel path is not the full rut depth, which depends, rather, on surface vertical depression plus surface heave away from the wheel path. Equation 8.2 predicts the contribution to the rut depth due to the vertical depression of the subgrade by making the assumption that the subgrade is incompressible and therefore the volume of material displaced from beneath the loaded area must be equal to that contributing to the area of heave. Equation 8.2 is formed by assuming that the convex and concave profiles of the post trafficking subgrade are parabolic and by equating the depression and heave areas (see Figure 2.7).

In this design case the theoretical vertical depression at the surface of the subgrade,  $s$ , is 60% of the rut at the surface of the aggregate and this ratio varies depending on  $a'$  and  $a$ . Thus, for any particular wheel loading, the ratio of  $s$  to  $r$  is related to the thickness of the aggregate layer and the load spread angle,  $\tan\alpha$ , considered applicable. For any given load spreading function,  $\tan\alpha$ , and rut depth,  $r$ , increasing the pavement thickness yields a smaller ratio of vertical subgrade depression,  $s$ , to the rut depth,  $r$ .

Because the analysis assumes that the aggregate layer deforms without changing its thickness, the subgrade vertical depression is assumed to be equal to the vertical depression of the surface of the aggregate. However, this is not the case because some deformation occurs within the aggregate layer and thus the actual vertical depression at the surface of the subgrade will be less than is calculated above.

It can be seen from Figure 8.6 that, at least for Bothkennar, the ratio of the surface rut depth to the surface vertical depression is approximately 0.70 for all sections regardless of the pavement thickness.

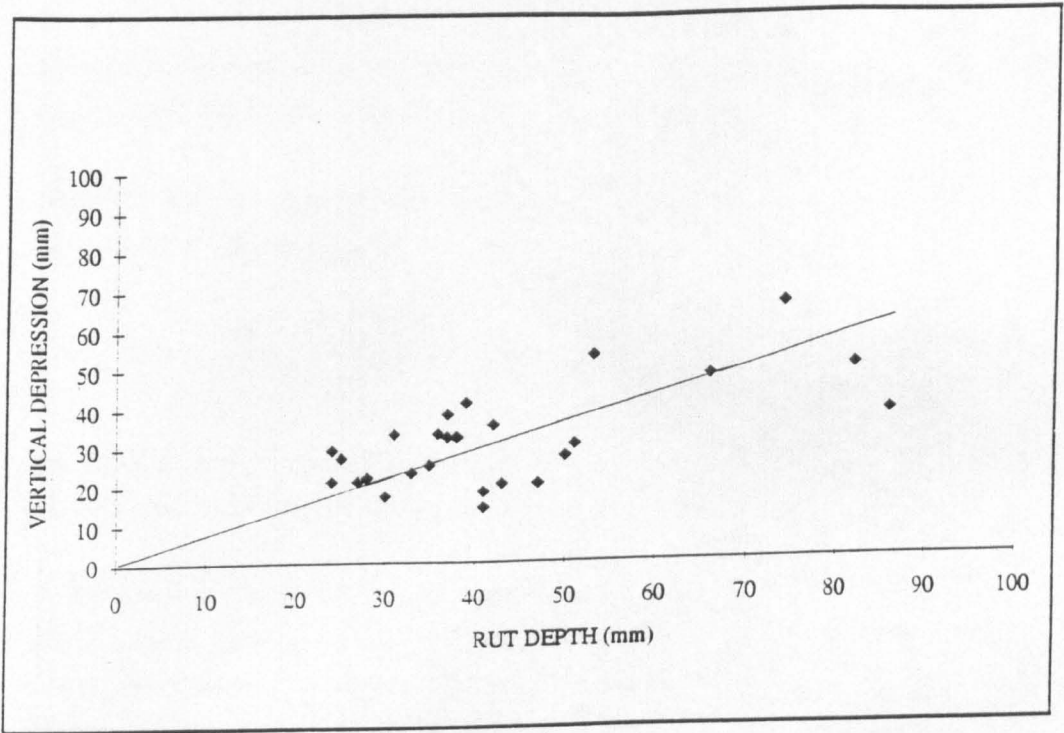


**Figure 8.6 Rut Depth and Vertical Depression  
for the Pavements at Bothkennar**

Geosynthetic Strains Assuming that the deformation of the subgrade is parabolic, and the length of the initial and final soil/aggregate interface profiles under the loaded area are  $a$  and  $b$  respectively, then the strain is given by the following equation presented by Giroud & Noiray (1981).

$$\frac{b}{a} - 1 = \frac{1}{2} \left[ \sqrt{1 + \left(\frac{2s}{a}\right)^2} + \frac{a}{2s} \ln \left( \frac{2s}{a} + \sqrt{1 + \left(\frac{2s}{a}\right)^2} \right) - 2 \right] \quad (8.3)$$

giving a linear strain in the loaded area of 0.07%. Therefore the length,  $b$ , of the final profile under the loaded area is 0.3803m.

The initial and final length of the subgrade profile between the loaded area,  $a'$  and  $b'$ , is given by the following equation

$$\frac{b'}{a'} - 1 = \frac{1}{2} \left[ \sqrt{1 + \left(\frac{2(r-s)}{a'}\right)^2} + \frac{a'}{2(r-s)} \ln \left( \frac{2(r-s)}{a'} + \sqrt{1 + \left(\frac{2(r-s)}{a'}\right)^2} \right) - 2 \right] \quad (8.4)$$

The initial length, of  $a'$ , was 0.57m and therefore the length of the final profile between the load area,  $b'$ , is 0.5701m giving a linear strain in the unloaded area of 0.02%.

As discussed in Chapter 2.3.3.3, the membrane effect assumes that the geosynthetic is pulled towards the wheel path as a result of the deformation. Furthermore, it assumes that the overburden vertical stress between the wheel path is insufficient to resist, by friction, the forces generated and so slipping occurs. Therefore, the strain is assumed to be constant across the pavement and is defined by this Equation 2.14:-

$$\epsilon = \frac{b + b'}{a + a'} - 1 = 0.05\% \quad (2.14)$$

where  $a + a'$  = initial geosynthetic roll width and  $b + b'$  = final geosynthetic roll width.

The validity of the assumption that the geosynthetic strain is even across the width of the pavement is common in many membrane effect design methods (Giroud & Noiray (1981), Neiuwenhuis (1977)) and indeed, if the geosynthetic is to transfer significant vertical forces to the area of the subgrade between the load areas, it is a pre-requisite that the strains induced in the geosynthetic out-side the load area are large. This has not been observed at Bothkennar where both the transient and permanent transverse

geosynthetic strain distributions are far from constant, reducing rapidly away from the wheel path and sometimes becomes compressive as shown in the examples in Figures 6.34 and 6.35. This observation confirms evidence from the Sandleheath trials (CIRIA (1986)), where the geosynthetics were seen to go into compression away from the wheel loads.

Vertical Subgrade Stress Reduction: The membrane effect of the design method predicts that there will be a reduction in the vertical stress applied to the subgrade. Again, assuming that the subgrade deformation is parabolic, the reduction in vertical stress is given by Equation 2.18.

$$p_r = \frac{E\varepsilon}{a\sqrt{1 + \left(\frac{a}{2s}\right)^2}} \quad (2.18)$$

Where  $k$  is the stiffness of the geosynthetic. Geosynthetics do not demonstrate linear stress/strain relationships and, although it is not specified within the design method, it appears to be sensible to assume a value for  $k$  at the strain level of interest. Also, geosynthetic stiffness is a function of the rate of loading and although some type of creep stiffnesses may be the most correct value to use, the BS 6906 part 1 (1987) test provided the most readily available data. Such a stiffness will thus tend to overestimate the vertical subgrade stress reduction as stress relaxation due to creep is unaccounted for.

For the example from Bothkennar, the strain induced in the geogrid by a surface rut depth of 0.018m is 0.05 percent. Results from Strathclyde University (Yeo (1992)) shown in Table 4.10 imply that at this strain level the force,  $E\varepsilon$ , that could be expected in the geogrid is

- 0.20 kN/m for the post compaction sample and
- 0.22 kN/m for the post trafficking sample

assuming that the stiffness is constant from 0 to 5% strain.

Thus after 1000 passes of an 80kN axle the value  $p_r$  can be calculated as 0.02kPa assuming a 0.22kN/m force at this strain level as recommended by Yeo (1992). This

may be compared with the estimated subgrade stress of 250kPa if the pavement is 0.4m thick (Equation 2.12) clearly the reinforcement effect due to the membrane effect is insignificant on this basis.

### 8.6.2.3 Aggregate Saving

The thickness of aggregate required to withstand the application of an 80kN axle load in this example is given by Equation.2.19:-

$$(2 + \pi) S_u = q \left( \frac{WL}{(W + 2htan\alpha) (L + 2htan\alpha)} \right) - p_r \quad (2.19)$$

with the data given in Section 8.6.1 (where  $h_0 = 0.040m$ ) and  $p_r = 0.02kPa$  as in Section 8.6.2.3, hence  $h = -0.028m$ .

As predicted  $h$  is negative however, the saving in aggregate may be considered as

$$\Delta h = h_0 - h = 0.040 - (-0.028) = 0.068m$$

### 8.6.2.4 Comparison of Design and Performance

The saving in the thickness of the aggregate, as calculated by the two phases of the quasi-static analysis, was applied to an unreinforced pavement design. For the purpose of calibration, the rut depth expected after 1,000 passes in the example above was calculated.

As shown above, the thickness reduction calculated as a result of the inclusion, was 0.070m. The actual thickness of the pavement constructed at Bothkennar was 0.300m. This implies that the pavement is equivalent to an unreinforced pavement of thickness 0.370m.

Giroud and Noiray (1981) suggest that unreinforced road design is governed by Equation 2.10

$$h = \frac{0.19 (\log N - 2.34 (r - 0.075))}{CBR^{0.63}} \quad (2.10)$$

where  $h = 0.370\text{m}$

$\log N = 3$

A CBR of 3.7% insitu was determined from Giroud and Noiray's recommendation that a shear strength of 23kPa = 1% CBR. Therefore the rut depth,  $r$ , as calculated by this method should be minus 540mm whereas it was found to be 3mm.

However, this design is sensitive to CBR of the subgrade. A CBR of 2% yields an expected rut depth of 69mm.

This comparison has produced answers that are beyond the limits of the design method. The large discrepancy between measured and predicted rut depth tends to confirm that for a subgrade CBR of 3.7% a direct comparison between expected and actual performance is not valid.

#### 8.6.2.5 Comments on the Design Method

The design method presented is, like many design methods, a static analysis and as such the controlling parameters relate to static failure. Rut depth development however, is not generally a single loading phenomenon, but the result of an accumulation of small plastic deformations caused by the repetition of vertical stresses well below the failure values. However, the analytical design method used relies on static analysis. It is generally accepted that designs be extrapolated on the basis of empirical data because simple repeated loading models, predicting permanent deformations within the system, have yet to be developed.

The low rut depths encountered in the trials have led to low geosynthetic strains and low computed stress reductions on the subgrade due to the membrane effect. Yet the design method predicts a reduction in aggregate thickness of 70mm for the case considered. It is apparent that the principal reason for this predicted improvement in performance is the change of the subgrade bearing capacity from elastic failure to general plastic failure. However, this change is not justified within the method. The vertical stresses imposed upon the subgrade are, at least at low rut depths, not affected by the inclusion of a geosynthetic because the membrane effect can only make significant contributions at high rut depths. Therefore, the vertical stress imposed on

the subgrade by each application of load is generally the same in both the reinforced and unreinforced cases and is well below the failure stress.

The assumption that the strain in the geosynthetic is constant across the pavement must be viewed critically. Experimental data from Bothkennar shows that the transient strains decay with distance away from the wheel path. This observation questions the validity of the membrane effect which assumes that the inclusion is pulled towards the wheel path as a result of the deformation. This would produce larger strains in the geosynthetic away from the loaded area than were observed. The membrane effect relies upon significant geosynthetic forces, and therefore strains, outside of the loaded area in order to transfer vertical loading to the area between the wheel paths.

In summary, the method proposed by Giroud and Noiray (1981) appears to be based on a membrane effect type of design but, in fact, generates most of the benefit by an arbitrary change in bearing capacity. This change in bearing capacity could be justified (Milligan et al (1989a)) for a fully reinforced analysis (see Section 8.8). However, static analysis is a poor model as, in fact, deformations are caused by multiple applications of stresses well below failure.

The concept of the membrane effect has not been supported by the experimental data. Even at reasonably large rut depths, the computed contribution it makes to the stress distribution is small and so is probably not worth considering. For standard wheel loadings the analysis requires a negative thickness of aggregate, to resist a single application, when the subgrade shear strength exceeds 68.7kPa and, as such, should be considered as a limitation of the design.

Giroud and Noiray (1981) provides an easy to follow method which, within limitations, may give reasonable results. However, it does so by making many assumptions that in many cases will be invalid.

## 8.7 BAMBOO REINFORCED PAVEMENT (SECTION O)

### 8.7.1 Summary of Design

The bamboo reinforced pavement (Section O) was designed by the team at Strathclyde University on the basis discussed in Chapter 2.3.6.

At 300mm spacing the poles covered around 20% of the formation which was the same percentage area covered by 4 poles in the experimental test tank used by McGown et al (1990). A standard wheel load is considered in some of the other design methods (eg Giroud & Noiray (1981)) as being 0.4m wide and the depth of aggregate on the Section was 0.35m which implies a width to depth to ratio,  $\left(\frac{W}{h}\right)$ , of 1.14 for the full-scale trials.

### 8.7.2 Back analysis

The ultimate vertical depression which occurred in Section O was 30mm and therefore the settlement ratio  $\left(\frac{S}{W}\right)$  can be given as 7.5%.

From the above information, tables presented by McGown et al (1990) imply that an improvement factor, over the unreinforced case, of around 1.4 might apply.

Direct comparisons with the unreinforced case in these trials would be inappropriate due to the differences in design thickness. However, the tables mentioned above imply that pavements reinforced with Polyfelt alone exhibited an improvement factor over the unreinforced case of around 1.2. As the design thicknesses were the same on the Polyfelt (P) and the Polyfelt bamboo sections (O), direct comparison of using the tables suggests that the Polyfelt/bamboo section should out-performs the Polyfelt section by a ratio of 1.4/1.2 or by 17%.

The final rut depth for the Polyfelt/Bamboo section (O) was 49mm and for the Polyfelt section (P) 45mm. This suggests that the included bamboo section did not improve the performance of the pavement. Exhumation of the section containing bamboo revealed that the trafficking had caused the bamboo to fail by crushing as shown in Plate 8.1. Some of the poles had split longitudinally and the sharp edges so exposed cut the geosynthetic. These probably provided stress localisation points which had a detrimental effect on the sub-grade.

It can be seen from Plate 8.2 that the aggregate depressed the subgrade in between the bamboo poles which would imply that the bamboo relieved the subgrade stresses directly under themselves. Thus, it could be argued, that the spacing of the bamboo was too great in this instance. However, this behaviour may have resulted from the age



Plate 8.1 - Bamboo Failure, Excavation After Trafficking

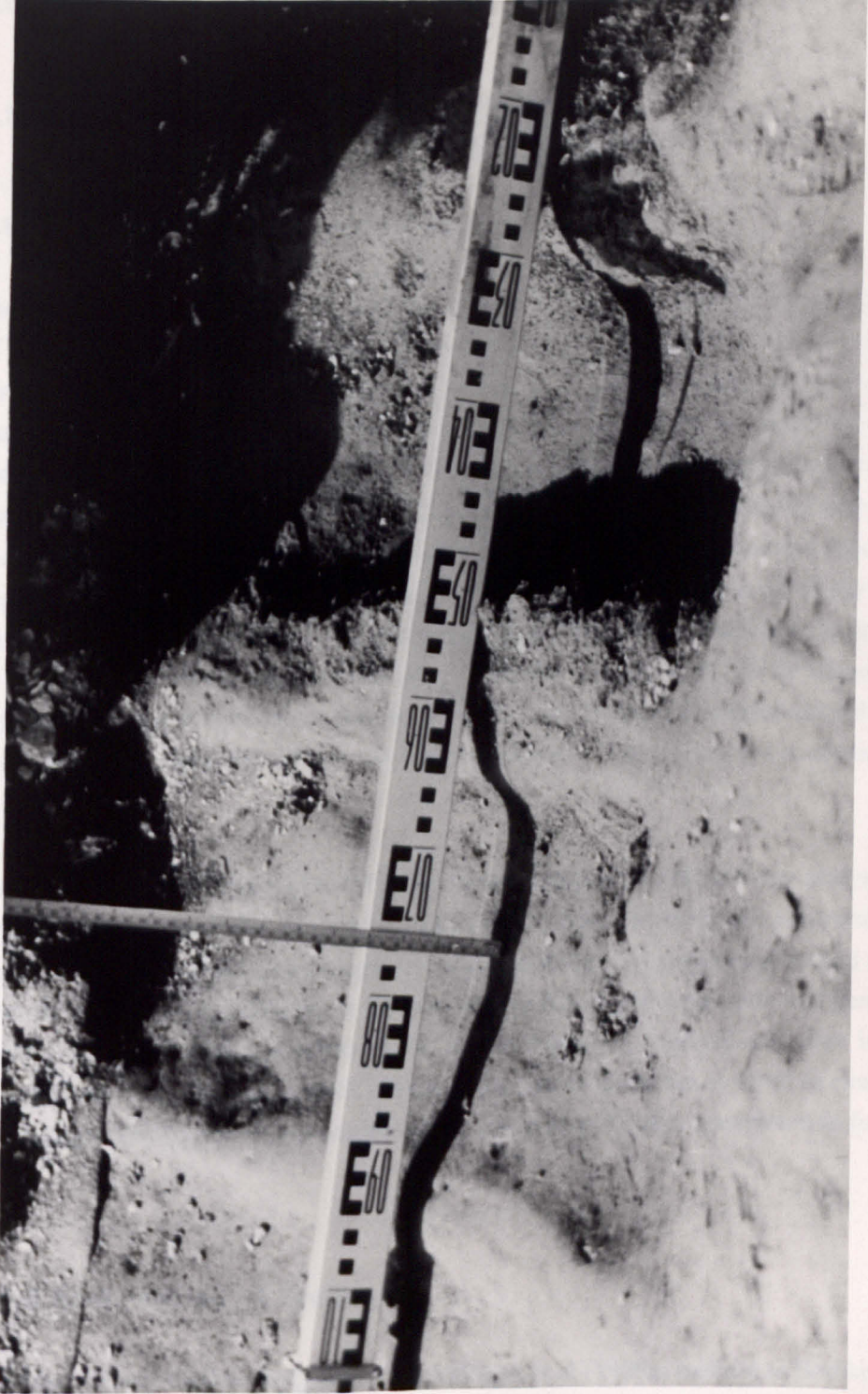


Plate 8.2 - Subgrade Deformation of the Post-Trafficked Polyfelt/Bamboo Section (O)

or variety of the bamboo used and so may not be representative of the design method in general, but if this is the case then it indicates further parameters need to be taken into account in the design procedure.

## 8.8 REINFORCED PAVEMENT ANALYSIS AFTER MILLIGAN ET AL (1989 A & B) (SECTIONS F & I)

### 8.8.1 Summary of Design for Section I

The design method proposed by Milligan et al (1989 a & b) considers the equilibrium of a block of aggregate below the wheel as was shown in Figure 2.9. Active forces within the aggregate under the wheel are resisted by passive forces away from the loaded area and because of the difference in vertical stresses in the two areas, the active forces are greater than the passive. Horizontal equilibrium of the aggregate block is made possible by inward shear forces acting at the base. In the unreinforced case equal and opposite shear forces are applied to the surface of the subgrade and can reduce its bearing capacity to as low as  $\left(1 + \frac{\pi}{2}\right) S_u$ . In the fully-reinforced case all of the shear forces are transferred to the geosynthetic, enabling purely vertical loading to be applied to the subgrade which enables a bearing capacity of  $(2 + \pi) S_u$  to be generated. However, a range of cases must exist between the fully-reinforced and the unreinforced cases depending upon the stiffness of the geosynthetic. This aspect is not considered by Milligan et al.

The analysis can be performed either as an axisymmetric or as a plain strain analysis. It is possible to perform the plane strain analysis by hand, whereas the axisymmetric analysis requires the aid of a computer. The distribution of stress (and strain) away from the centre will be different in the two cases and so the two methods will generate slightly different results in terms of the actual thickness required and thus in the aggregate saving. The plane strain case is more conservative but in order to examine the concepts behind the design method plane strain analysis was considered in further detail.

### 8.8.2 Back analysis of Section I

The lower-bound section designed by the Milligan et al (1989a) method at Bothkennar (Section I) consisted of a nominal 300mm of sand and gravel overlying a lightweight

polypropylene geogrid (Tensar SS1). If the loaded half footing width,  $\frac{W}{2}$ , is 0.2m and  $\tan\alpha = 0.6$  then the half width loaded area at subgrade level is:

$$\frac{W}{2} + h\tan\alpha = 0.38\text{m}$$

It was found in the 280mm diameter triaxial tests that the effective angle of internal friction of the sand and gravel was  $51^\circ$  as shown in Chapter 4.

Thus, the active earth pressure coefficient  $K_a$  is such that:

$$K_a = \frac{1 - \sin\phi'}{1 + \sin\phi'} = 0.12$$

and the passive earth pressure coefficient,  $K_p$ , is such that

$$K_p = \frac{1}{K_a} = 7.97$$

The non-dimensional parameter  $\psi \left( = \frac{\tau}{S_u} \right)$  is related to the bearing capacity,  $N_c$ , by Equation 2.26.

$$\psi = \frac{1}{2} (K_a - K_p) \frac{\gamma h^2}{S_u \left( \frac{W}{2} + h\tan\alpha \right)} + N_c \left[ \frac{K_a}{\tan\alpha} \ln \left( \frac{\left( \frac{W}{2} + h\tan\alpha \right)}{\frac{W}{2}} \right) \right]. \quad (2.26)$$

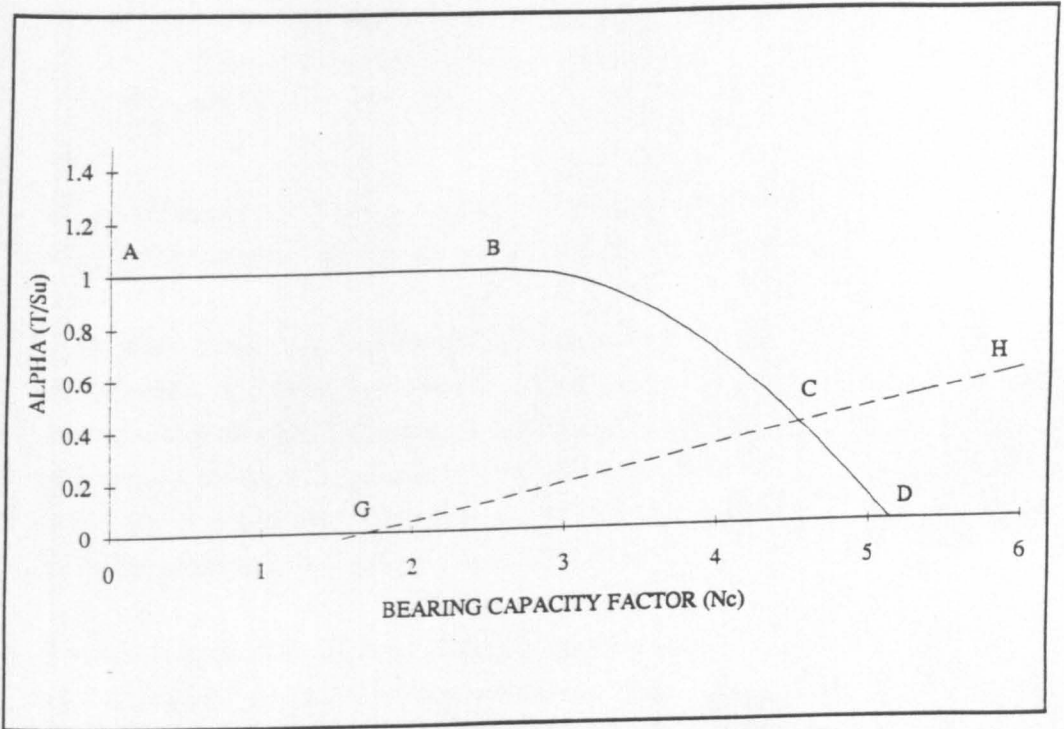
When  $h = 0.3\text{m}$ ,  $\tan\alpha = 0.6$ ,  $\gamma = 21\text{kN/m}^3$  and  $S_u = 85\text{kPa}$ , then

$$\psi = -0.230 + 0.134N_c$$

which is the line GCH in Figure 8.7.

The intercept of the line GCH with the available envelope yields the value  $N_c = 4.54$ .

Substitution of this value of  $N_c$  into Equation 2.27 gives:-



Line ABCE After Milligan et al (1989 a), Line GCH for Example Given in Text

**Figure 8.7 The Available and Required Bearing Capacities of a Loaded Subgrade - After Milligan et al (1989a)**

$$q_s = N_c S_u \left( \frac{\frac{W}{2} + \tan \alpha}{\frac{W}{2}} \right) = 7.33 \quad (2.27)$$

where  $q_s$  is the static stress required to induce soil failure.

The design also does not produce any predictions for the development of rut depth. Milligan et al (1989b) suggests that this static analysis be extended to the trafficking case by reference to De Groot et al (1982) who suggested that for reinforced roads:

$$\frac{q_s}{q_n} = N^{0.16} \quad (8.5)$$

The actual contact stresses,  $q_n$ , applied at Bothkennar were around 350 kPa and so  $\frac{q_s}{q_n} = \frac{733}{350} = 2.1$  and hence the number of passes to failure,  $N$ , = 101 passes.

In the plane strain case the permissible static stress  $q_s$  is thus only double the actual applied stress  $q_n$  and so, by reference to De Groot et al (1982), this appears to be an unsatisfactory design. However, if an unreinforced and reinforced analysis are compared, a saving in aggregate can be calculated which can then be applied to an unreinforced design such as Hammitt (1970). This approach would also yield a method of predicting the rut depth that is likely to develop.

This design consists mainly of a static analysis of failure, whereas pavements fail as a result of repeated loading at stresses well below failure. Although no model exists for accurately predicting subgrade deformation with passes, Brown and Dawson (1992) suggest that as long as a threshold value of deviator stress is not exceeded then gross deformations will not occur.

In the reinforced case the bearing capacity factor,  $N_c$ , = 5.14 (as shown in Figure 2.8) and so if the allowable surface contact stress remains constant in the two cases the contact stress 733kPa above equates to a thickness of aggregate by Equation 2.27.

$$733 = 5.14 S_u \left( \frac{\frac{W}{2} + h \tan \alpha}{\frac{W}{2}} \right) \quad (2.27)$$

which implies  $h = 0.226\text{m}$ .

This compares to the design thickness of 300mm.

Thus, a fully reinforced pavement will, in this case, generate an aggregate saving of 74mm.

The design would appear to be sensitive to changes in the aggregate shear strength. The Sand and Gravel used in the trials was found to have an angle of internal friction of 51°.

However, confidence in the determination is a little low due to the spread of the results. The effect of reducing the aggregate shear strength is shown in Figure 8.8. As can be seen the line GCH has risen from that shown in Figure 8.7.

$N_c$  is now shown to be 3.39 and from Equation 2.27  $q_s$  becomes 547kPa and from Equation 8.5 the number of passes to failure reduces to 16.

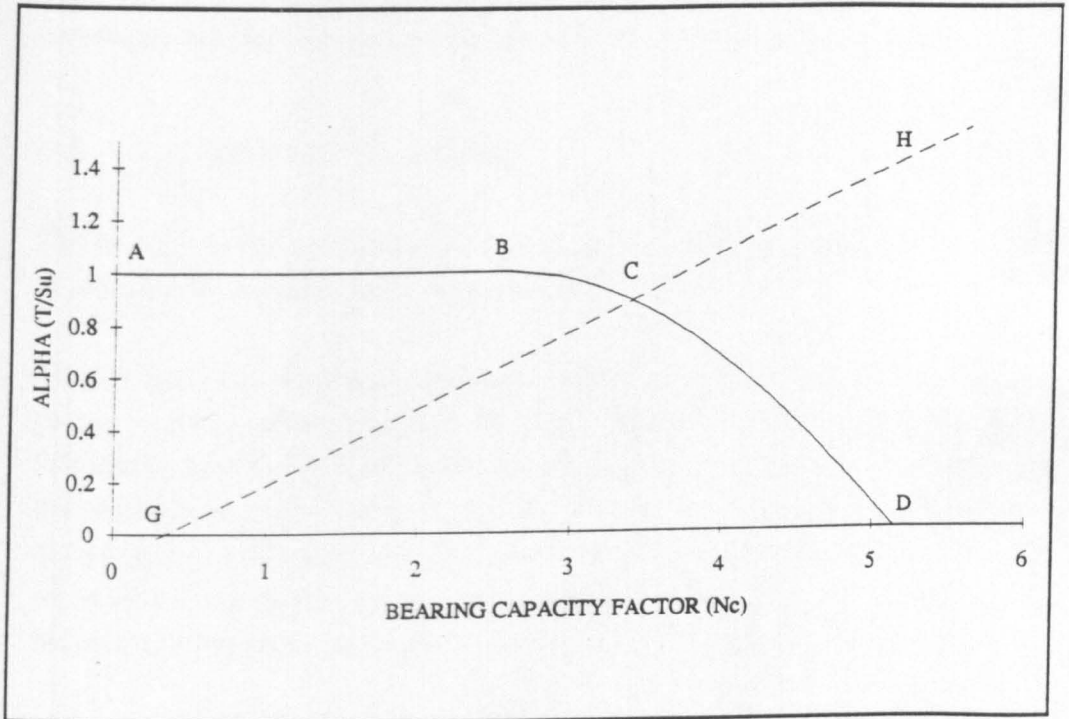
Although the number of passes to failure has reduced the potential saving in aggregate increases with lowering aggregate shear strength. Substitution of  $q_s = 547$  in Equation 2.27 implies  $h = 0.084$ , an aggregate saving of 216mm.

The axisymmetric analysis possible with the program "Roadsolver" (Houlsby and Jewell (1987)) generates permissible surface contact stresses of 1641kPa in the unreinforced case and 1722kPa in the reinforced case. These values are substantially above the contact stresses applied at Bothkennar.

### **8.8.3 Observations on the Design Method**

Milligan et al (1986b) suggest that the De Groot et al (1982) power law relationship (Equation 8.5) for varying axle loads, should be applied to determine how repeated, low contact stress loading can be converted to an equivalent load of a single axle application. However, the design method as such does not predict the rut depth that might be expected and, as Equation 8.5 is being used to allow for trafficking, it would appear more sensible to apply the work of Hammitt (1970) to both the axisymmetric and plain strain cases.

Apart from the modelling of the repeated loading however, the design method does predict the pattern of the observed transient and permanent strains generated in that they decay away from the wheel path.



Line ABCE After Milligan et al (1989 a), Line GCH for Example Given in Text

**Figure 8.8 The Available and Required Bearing Capacities of a Loaded Subgrade with Low Quality Aggregate Fill- After Milligan et al (1989a)**

## CHAPTER NINE

### DISCUSSION

#### 9.1 INTRODUCTION

This Chapter discusses the fundamental elements required for a design method and how these can be best obtained. Furthermore, some new concepts arising from the study of existing design methods and the full-scale trials, are introduced and discussed.

#### 9.2 RUT DEPTH DEVELOPMENT

The rut depth is the controlling factor in most serviceability considerations and as such is probably the most important design parameter.

Many of the design methods assume that the rate of rut depth development is linear with respect to the logarithm of passes. However, allowing for experimental scatter, the relationship between rut depth and passes would appear to be linear for each of the two axle loadings, as can be seen in Figures 6.1 to 6.15). This may change for sites where the subgrade is softer and a fuller range of the unpaved road's life is utilised. A change of gradient in the rut development versus passes curve also occurs at the point where the axle load was increased, which is more pronounced on some sections than others.

Furthermore, the experimental work of Webster and Watkins (1977) and Fannin (1986) can be re-plotted on a non-log cycles axis as shown in Figures 9.1 to 9.3. As can be seen from Figures 9.1 and 9.2 the full-scale trials of Webster and Watkins (1977) could demonstrate linearity of rut depth development with passes as could the model data of Fannin (1986) shown in Figure 9.3.

The assumption that deformation of unpaved roads is proportional to the logarithm of the number of passes arises from bituminous pavement design (Karkhovan and Dorman (1951)) where the life expectancy is often measured in millions of standard axles. Its application to unpaved road design is arbitrary given that haul road life expectancy is usually measured in hundreds or thousands of passes. Furthermore, the nature of deformation is different in paved and unpaved roads, the former being

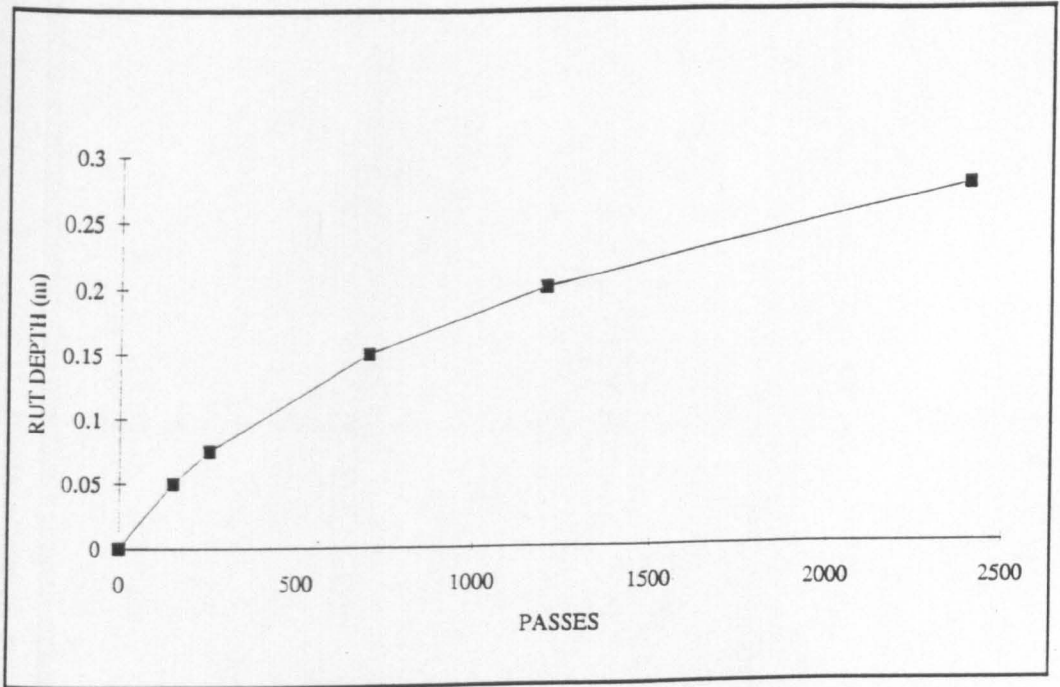


**Figure 9.1 Rut Depth Development  
After Webster and Watkins (1977) - Bidim Section**

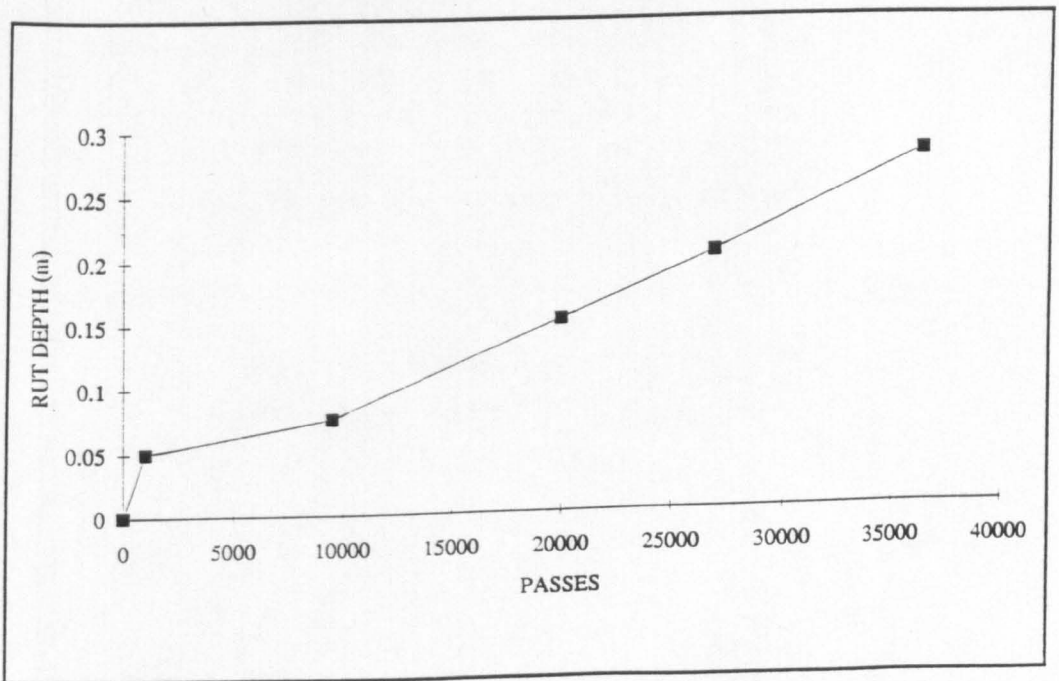


**Figure 9.2 Prediction of Rut Depth Development  
After Webster and Watkins (1977) - Woven Section**

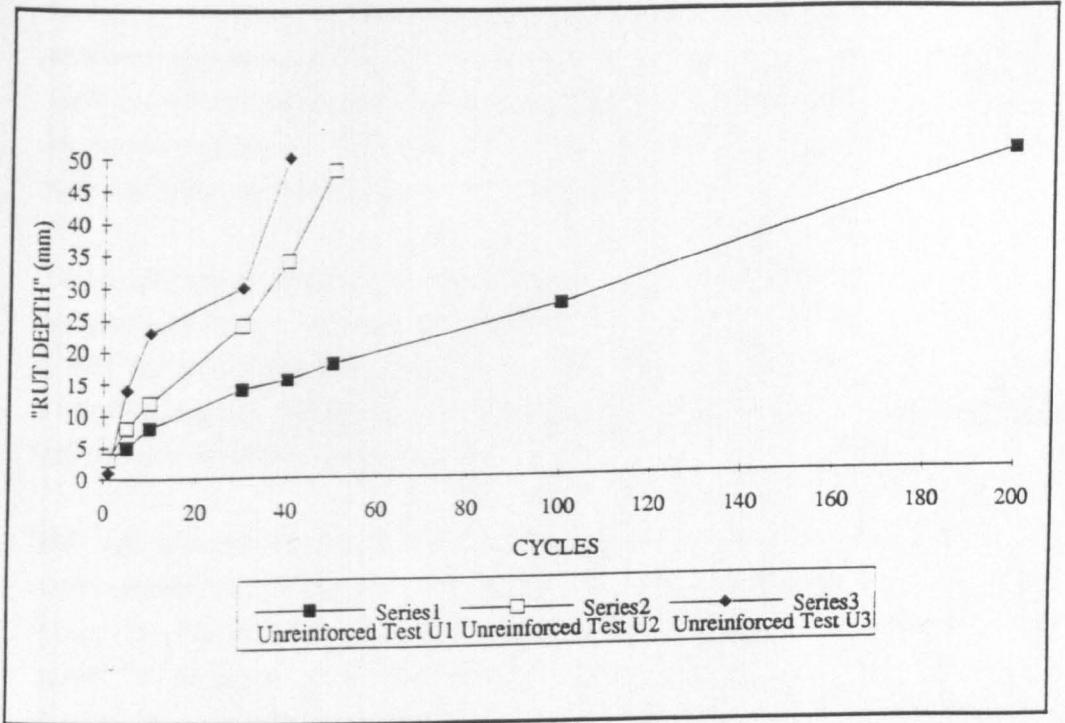


Figure 9.3 Model Data of Fannin (1986)  
Unreinforced Tests Plotted Against Cycles

principally a bitumen related problem and the latter deformation of the subgrade and internal aggregate shear.

X The rate at which the rut depth will develop is difficult to predict. However, the development of permanent deformation is loosely related to the proximity of the applied cyclic stress to the failure stress (Loach, 1987). Although the actual vertical stresses on the subgrade are likely to be the same for the unreinforced and reinforced cases at small rut depths (Table 6.3), the confining stresses in the reinforced case are probably higher as a result of tension within the geosynthetic (Table 6.4). Thus the development of permanent deformation may well be less in the reinforced case. Brown and Dawson (1992) introduced the idea of a threshold deviator stress beyond which gross permanent deformation will occur. They do not however, suggest how the actual rut depth can be predicted if this threshold value is not exceeded.

Models predicting permanent deformation of soils and granular materials as a result of repeated loading are not easily applicable to this type of analysis. Davies and Bridle (1990) appear to have had some success in this field by considering the work done within the system. However, it is beyond the scope of the research to propose or validate new models of this nature.

The lack of a reliable and easily applicable model for the permanent deformation characteristics of the aggregate layer and subgrade subjected to repeated loading makes it necessary to revert to empirical data to predict how rut depths will develop with passes. It has been observed at Bothkennar that a significant contribution to the rut depth occurs within the aggregate layer by shear deformation and compaction within the layer itself (see Figures 6.36 to 6.43). The proportion of deformation occurring within the aggregate layer may have been increased as a result of the stiff subgrade, but one might reasonably expect that at least some permanent deformation would occur within the aggregate layer even on soft subgrades. Thus a sophisticated model would require a deformation model for both the aggregate's and subgrade's contribution to the surface deformation.

The expected number of passes required to generate a rut depth of 75mm in an unreinforced pavement may be estimated from Hammitt (1970). It has been shown that the rate of development of rutting may well be linear with passes, at least for the relatively few cycles that a haul road is expected to be designed for. Thus, the number of passes required to generate rut depths not equal to the 75mm can be estimated in the

unreinforced case by extrapolation or interpolation of Hammitt's calculation. For the reinforced pavement design, the empirical data is rather sparse and, even so, the effect of wide variations in geosynthetic stiffness would hinder its interpretation in a manner similar to that of Hammitt (1970). It is therefore necessary to estimate the rut depth development rate for the reinforced pavements by examination of unreinforced data. It is an inherent assumption, in any "aggregate saving" method of reinforced road design, that a reinforced pavement consisting of, for example, 300mm of fill is "equivalent" to an unreinforced one consisting of, say, 350mm of fill. Therefore, the aggregate saving assumption implies that the thicker unreinforced pavement will deform at the same rate as the thinner reinforced one. However, there is little or no evidence for or against this assertion and further examples of reinforced pavement performance are required to validate this assumption.

### 9.3 DAMAGE FACTORS

The applicability of the "fourth power law" as a damage factor in unsurfaced roads was briefly discussed in Chapter 8.2.2. The fourth power law is normally considered to relate to surfaced pavements. Trials by De Groot et al (1986) on geosynthetic reinforced unsurfaced pavements suggested that the damage factor should be increased from 4 to 6.2 for this type of pavement.

An attempt was made to examine the damage power law for all of the sections in the trial and to determine if De Groot et al (1986) findings applied there. For each section a damage factor was chosen to produce a best fit between the observed and theoretical performance. An example is shown in Figure 9.4 which relates to the performance of Section P. The value of the damage factor has been adjusted in order to obtain the best 'least squares' fit. In order to get the best fit the damage factor is found to be 16 in this case.

In the analysis of the other sections, the fit between the predicted and measured deformations is not as good as for Section P. However, the analysis for the other sections shows that the best fit occurs for values of the damage factor in the range 8 to 20. Thus, the experimental data leads to values of damage factor that are not reasonable. To suggest that the power should be twenty means that doubling the axle load would yield an approximate equivalency of 4 million times which, in turn, would predict immediate pavement failure upon trafficking. Further doubt on the validity of

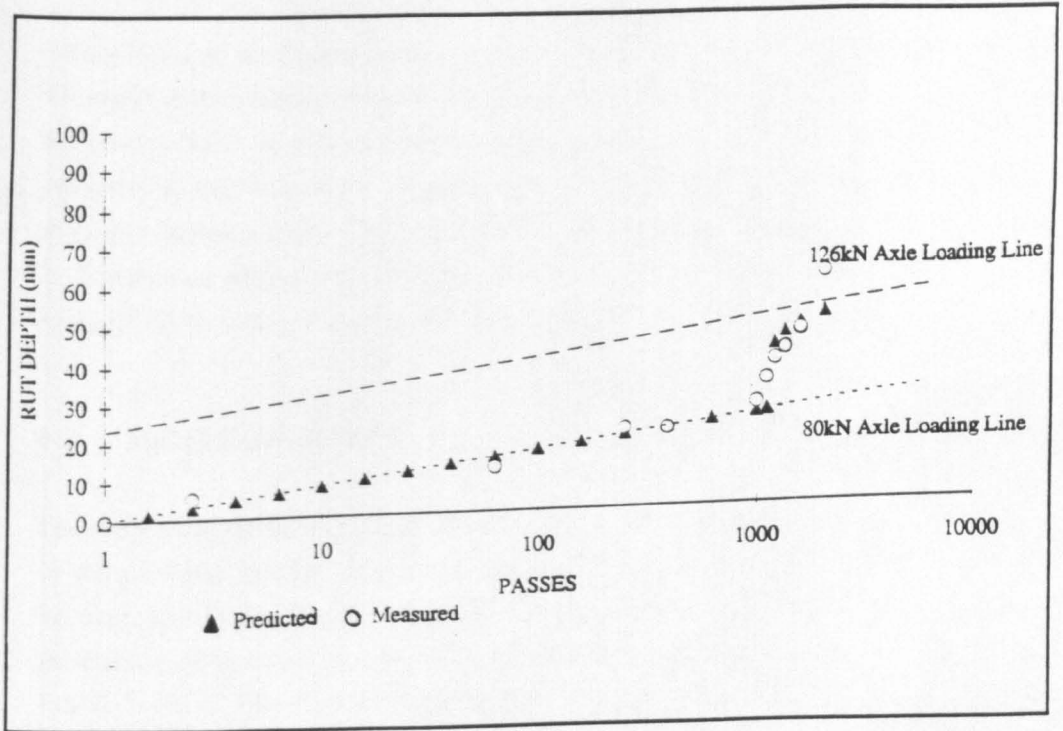


Figure 9.4 Predicted and Measured Deformation of Section P

this approach is raised in that there is a large degree of scatter in the results, especially when it is considered that only one aggregate and subgrade condition was considered.

So, although the approach suggested by Giroud and Noiray (1981) for unreinforced pavement design based on Hammitt (1970) and Webster and Watkins (1977) is workable, there are reservations about the use of power laws and the empirical nature of its basis. However, this method and the one described by Hammitt (1970) provide the only current analytical design methods for reinforced pavement design.

On the basis of the trials however, a fourth power law to describe load equivalency is not applicable to unpaved roads. De Groot et al (1986) based their recommendations for geosynthetic reinforced roads on the results of a few pavements. The trend observed at Bothkennar is, as noticed by De Groot, that the power (if appropriate) should be increased above the value 4 which is commonly assumed. The observations at Bothkennar suggest rather high and inconsistent power values. Therefore, the applicability to unbound pavements of any power law must itself be called in question.

#### 9.4 MEMBRANE EFFECT

The membrane effect, as discussed in Chapter 2.3.3, was considered for many years to be the principal mechanism behind the reinforcement of unpaved roads. However, calculations of the reduction in applied vertical stresses on the surface of the subgrade attributable to the membrane effect were made for a typical pavement after Giroud and Noiray (1981). The depth of aggregate was taken to be 350mm and  $\tan\alpha$ , the load spread angle, to be 0.6. The deformation of the subgrade was assumed to be parabolic in nature and the subgrade was incompressible. The calculated reduction in vertical subgrade stress for a range of rut depths up to 200mm is shown in Figure 9.5.

At low rut depths it can be seen that the predicted decrease in subgrade stress as a result of the membrane effect is small and that even at higher rut depths the decrease is not large. Therefore, because of the doubts expressed about the validity of the mechanism resulting from the inability of the method to predict the observed geosynthetic strain distribution, and because the decrease in applied vertical stress attributable to the membrane effect is small, it is almost certainly not the principal mechanism involved in the geosynthetic reinforcement of unsurfaced pavements to reduce rutting. Yet the final rut depths shown in Table 6.1 show that significant reinforcement was achieved as the

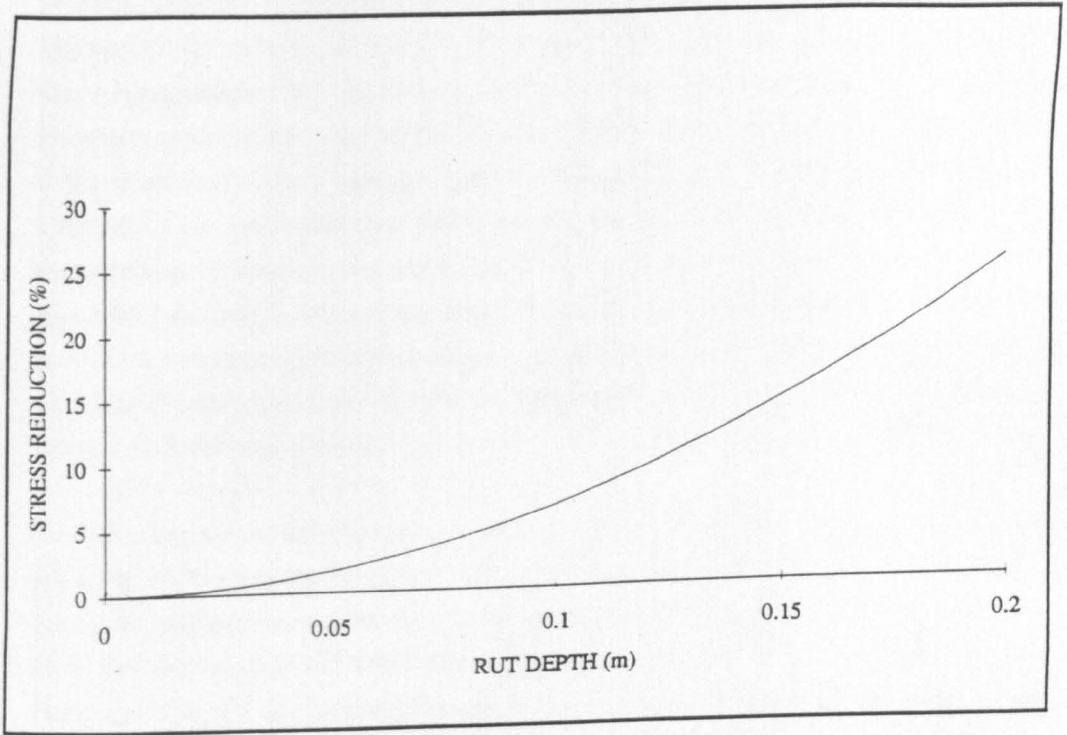


**Figure 9.5 The Calculated Reduction in Vertical Subgrade Stress as a Result of the Membrane Effect - After Giroud and Noiray (1981)**

thinner reinforced pavements have performed as well as the thicker unreinforced ones. Thus, other effects must be considered.

## 9.5 SLAB EFFECT

A slab effect basis for design such as that proposed by Sellmeijer (1990) and discussed in Chapter 2.4 might, on first inspection, appear to be promising. It is the only currently available design method which directly incorporates a stiffness property of the aggregate layer. It also recognises the fact that, unless slippage occurs at the interfaces, strain compatibility between the elements of the system must occur. The elastic deformations are predicted assuming that the applied load is resisted by the mobilization of the shear modulus of the aggregate, assisted by the plastic bearing capacity of the subgrade in the reinforced case and the elastic bearing capacity of the subgrade in the unreinforced. However, the elastic deformations are not helpful in determining the permanent deformations that are likely to occur. As with other methods, it may be possible to compute aggregate savings based on a comparison of the elastic deformation response of reinforced and unreinforced pavements and to apply these to an empirical permanent deformation model.

However, the slab effect design method is principally concerned with maintaining the integrity of the aggregate layer. The horizontal forces within the aggregate are calculated and great importance is placed on the maximum passive resistance (a function of  $\phi'$  the internal angle of frictional resistance of the aggregate not being exceeded. Plainly, within any one load application, it is undesirable for the aggregate layer to fail. However, this type of aggregate layer failure was observed during the full-scale trials after many passes of the load, principally in the Oxford section (I), and the Polyfelt/Bamboo section (O), where it was associated with geosynthetic rupture and bamboo failure respectively.

Passive failure of the aggregate is likely to occur at large strains and these will only occur at large rut depths. It is more likely that pavements will fail serviceability requirements before passive aggregate failure. Thus, both angle of frictional resistance and shear modulus are important aggregate parameters for the approach due to Sellmeijer (1990).

The slab effect relies upon the horizontal strains at the base of the aggregate layer being the same as that in the geosynthetic. This concept of strain compatibility between the

aggregate and geosynthetic is important. It determines the strain within the inclusion and, as such, the forces generated in the geosynthetic which are responsible for the reinforcement. However, because slipping between the aggregate and the geosynthetic is considered not to occur and because the geosynthetic stiffness is low in comparison to that of the aggregate (Sellmeijer 1990), the geosynthetic strain is governed by the aggregate strain.

## 9.6 AGGREGATE BASE RESTRAINT

An aggregate base restraint method such as proposed by Milligan et al (1989a), and discussed in Chapter 2.3.5, demonstrates the value of the geosynthetic in reducing the shear stress at the subgrade surface and thus improving the bearing capacity of the reinforced system. The low geosynthetic strains which were observed away from the wheel path in the experimental trials at Bothkennar imply that the assumption made by Milligan et al (1989a), that the aggregate pushes away from the loaded area is valid. Finite Element calculations (Brocklehurst (in press)) suggest that the improvement in the load carrying capacity of the system does not increase significantly when the geosynthetic is extended to an area that is normally considered as outside the load spread angle area of influence. The fact that little strain, either transient or permanent, was measured outside this area suggests that this analysis is more realistic than the constant-tension, membrane type of model which would predict non-decreasing strains in the geosynthetic away from the wheel path.

The method proposed by Milligan et al (1989 a & b) does not predict deformations, it considers only failure. A thickness saving of aggregate from the unreinforced case to the reinforced case can be calculated and applied to the empirical method of Hammitt (1970). This approach relies upon the assumption that, if the failure loadings suggest that an aggregate saving of, say, 100mm is possible, then a reinforced pavement can expect to perform as well as an unreinforced one 100mm thicker. This may not be the case as the mechanisms of static failure and of serviceability failure, caused by repeated loading, are different. However, it is a common assumption and, at present, it may be difficult to improve on this type of aggregate saving calculation.

The treatment of the subgrade properties in this method appears to be valid and the mechanism by which forces are dissipated within the structure appears to be sound. However, the method proposed by Milligan et al (1989 a & b) requires modification for partial reinforcement so as to be able to predict rut depths.

## 9.6 ESTIMATING TRANSIENT GEOSYNTHETIC STRAIN

Sellmeijer (1990) suggested that no slippage occurs between the components of the soil-aggregate-geotextile system. Giroud and Noiray (1981) also suggested that in the loaded area under the wheel path the vertical forces are sufficiently high to prevent the relative movement of aggregate and geosynthetic. Also, there was no evidence of any slippage of the various layers observed during the Bothkennar trials. Therefore Sellmeijer's assumption that there is strain compatibility at the system interfaces would appear reasonable.

The horizontal strain in the geosynthetic should therefore be the same as the estimate of the strain at the base of the aggregate layer. A first approximation to this strain could be obtained by considering the aggregate to be a linear elastic medium. Thus the transient horizontal strain within the layer is defined as given in Equation 9.1.

$$\epsilon_{\text{transient}} = \frac{1}{M_r} [\Delta\sigma_h - \nu(\Delta\sigma_v + \Delta\sigma_h)] \quad (9.1)$$

if it is assumed that the horizontal stress in the aggregate is equal in both directions and where  $\Delta\sigma_h$  and  $\Delta\sigma_v$  are the additional horizontal and vertical stresses imposed by the wheel load. The vertical transient stress,  $\Delta\sigma_v$ , can be calculated using the concept of a load spread angle in a semi-infinite layer and  $\Delta\sigma_h$  can be estimated from the expression

$$\Delta\sigma_h = \left( \frac{\nu}{1-\nu} \right) \Delta\sigma_v \quad (9.2)$$

where  $\nu$  = Poisson's Ratio.

The resilient modulus  $M_r$  can be determined by laboratory testing of aggregate samples, or a value of 100MPa might be assumed for a well compacted crushed rock (Brown and Pappin (1985)), although a higher value for directly trafficked aggregate might be applicable (Brown and Dawson (1992)). Assuming that Poisson's ratio is 0.35 and that  $M_r = 100\text{MPa}$ , and that the load spread angle,  $\alpha$ , is such that  $\tan\alpha = 0.6$ , Figure 9.6 shows some agreement between Equation 9.1 and the observed transient horizontal, geosynthetic strains. The value of the load spread angle,  $\alpha$ , such that  $\tan\alpha = 0.6$  is taken from Giroud and Noiray (1981) and as can be seen from Figure 9.6

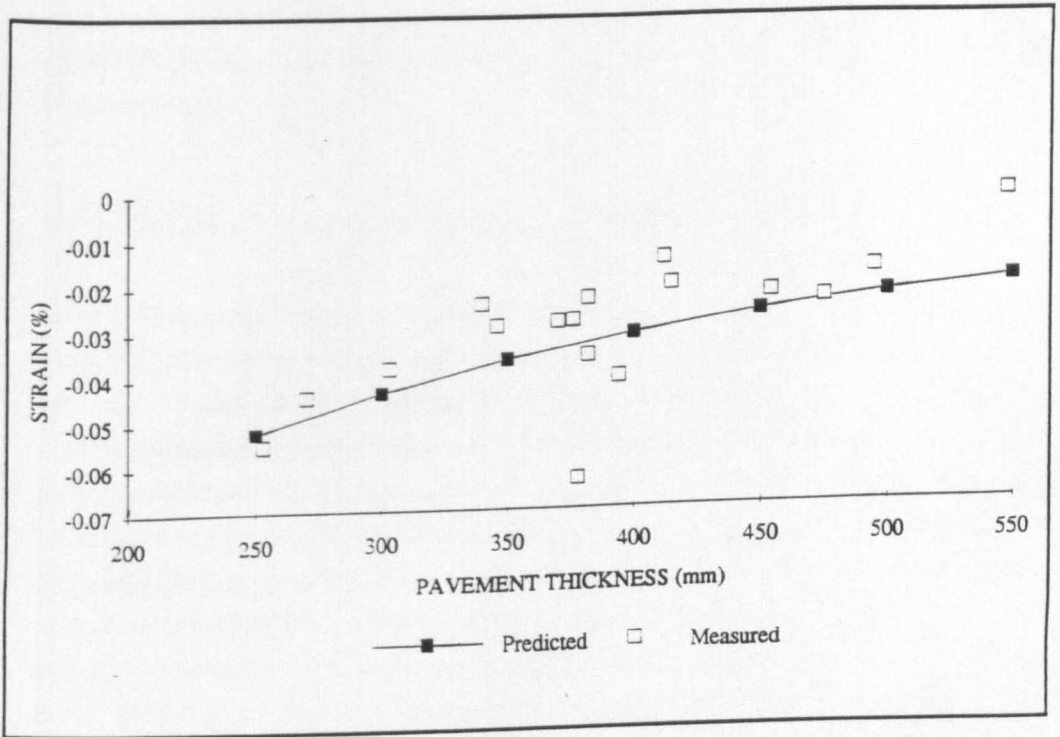


Figure 9.6 Predicted and Measured Horizontal Aggregate Strain

represents a sensible "average" value as it fits the experimental data reasonably well. However, it was shown in Figure 7.1 that the load spread angle changes with the stiffness of the geosynthetic. This might explain some of the scatter shown in the figure.

Equation 9.1 assumes that the aggregate acts in a linear elastic manner. This assumption, and that of load spreading in a semi-infinite layer, can be improved upon by computer programs which can calculate the effects of multi-layered elastic systems and/or incorporate some model for the non-linear elastic behaviour of the layers. FENLAP (Almeida et al (1991)) is one such program which would lead to a refinement of the estimate.

## 9.7 ESTIMATE OF GEOSYNTHETIC TENSILE FORCES

Since it is assumed that strain compatibility occurs, the geosynthetic will strain to the same degree as the aggregate layer. Therefore, knowing this strain, a first estimate of the forces being taken by the geosynthetic could be made by reference to the manufacturer's stiffness data. However, the actual forces in the geosynthetic are likely to be somewhat different. The rate of loading in the transient case is very fast which would result in higher stiffnesses and thus higher transient stresses in the geosynthetic than might be calculated by reference to the index tests. Permanent deformation of the system will lead to long term tension of the geosynthetic and creep induced stress relaxation would cause the forces in the geosynthetic to be over-estimated by reference to the index tests. To complicate the picture even further, the full-scale trials at Bothkennar and work done by Watts & Brady (1990) show that the properties of the geosynthetic change after installation and, from Bothkennar, that they change further during the trafficking process. No standard test covers these observed phenomena and so it is difficult to apply any index test to the stress/strain characteristics of the in-situ material. Thus, at present, an assumed stiffness based on index test results may be the best available approach.

It was shown in Table 4.10 that the geosynthetics generally became stiffer in service than in the British Standard index tests. This was particularly true of the needle punched materials and the increase in stiffness may have been due to fines within the the fabric "locking" the individual fibres into position. As was shown in Table 4.10 the ultimate strength of the geosynthetics was, generally, less than that of the control as was the strain to failure.

It is not possible, on the basis of one group of experimental results, to give any reliable design advice on the change in the in-service properties of the geosynthetics. Further studies are required to validate and quantify these observed changes.

## 9.8 PARTIAL REINFORCEMENT

The papers by Milligan et al (1989 a & b) and others such as Giroud and Noiray (1981) only consider either fully unreinforced or fully reinforced analyses. Plainly, there must be a range of cases between the two values depending, presumably, upon stiffness of the geosynthetic. Less stiff geosynthetics will relieve the subgrade of less of the shear forces at the interface so having some influence on the bearing capacity of the subgrade but not as much as in the fully reinforced case. Trials have shown (Sellmeijer et al (1982)) that the inclusion of stiffer fabrics results in continuing improvement in performance with stiffness. As a limiting geosynthetic stiffness has yet to be demonstrated, it is reasonable to conclude that all current geosynthetics perform a partial reinforcement of the system.

The treatment of the subgrade properties by Milligan et al (1989 a & b) best lend themselves to the concept of partial reinforcement as a range of subgrade bearing capacities exist depending upon the degree of reinforcement offered by the geosynthetic. As can be seen from Figure 2.18, the  $\psi/N_{ca}$  curve is steeper nearer to the fully reinforced condition than the unreinforced case. Therefore, small changes in the shear stresses imposed upon the subgrade, resulting from the change from the unreinforced to the partially reinforced, may have a more significant effect than the same amount of change from the partially reinforced to the fully-reinforced. Thus, even though the amount of shear stress relieved by the geosynthetic is proportional to its stiffness, the improvement in the bearing capacity of the system is not developed in the same proportion.

In the unreinforced case the bearing capacity of the subgrade is controlled by the shear stresses imposed at the aggregate/subgrade interface. The available bearing capacity curve is shown in Figure 9.7 and a typical required bearing capacity line,  $GCH$ , is shown which is calculated from Equation 2.26 as discussed in 2.3.5.

In the partially reinforced case, some of the applied shear stress at the interface is transferred to the geosynthetic, reducing the shear stress imposed upon the surface of the subgrade, and this reduces the value  $\psi$  ( $= \tau/S_u$ ). Thus, the reinforced case

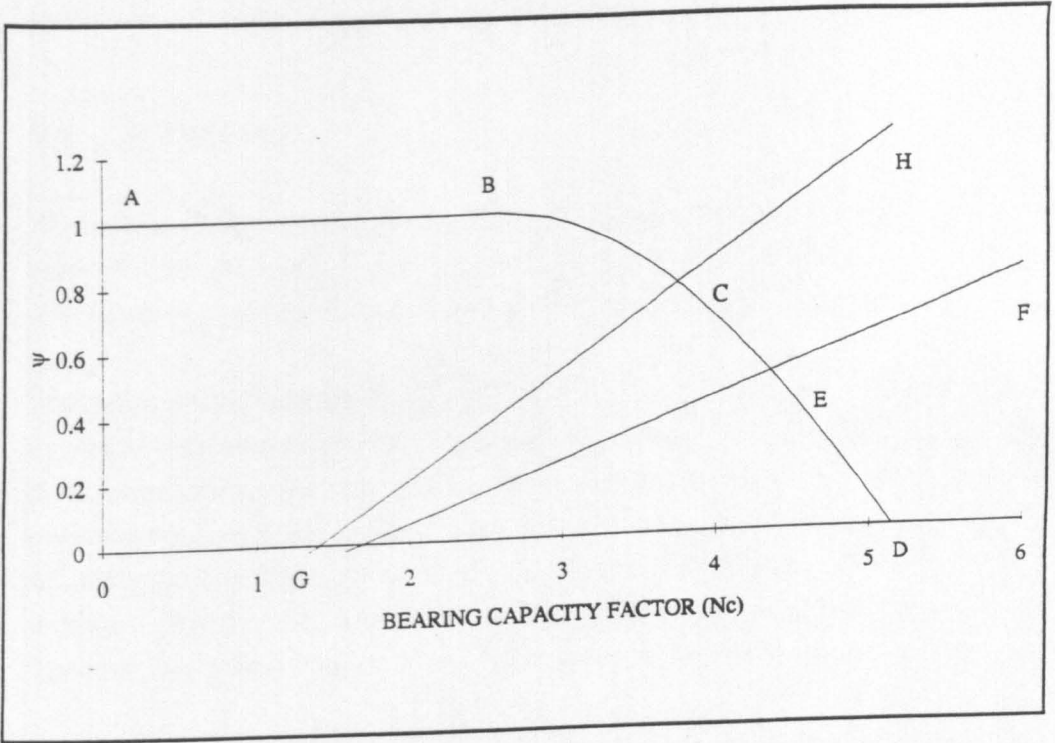


Figure 9.7 The Available and Required Bearing Capacity Factors of the Subgrade - After Milligan et al (1989a)

generates a change in bearing capacity because, as a result of the change in  $\psi$  caused by  $\Delta\tau$  (geosynthetic force (kN/m)), a new required bearing capacity line GEF is formed (Figure 9.7).

The changes in the bearing capacity of the system from the unreinforced to the reinforced case enables calculations of the permissible surface contact stress. In order for the contact stresses in the two cases to remain the same, the reinforced pavement must be constructed with a thinner layer of aggregate. Thus, from the bearing capacity calculations, a saving of aggregate, as a result of reinforcement, can be calculated.

## 9.9 SEPARATION

None of the design methods detailed in Chapters 2 and 8 place any analytical value on separation as shown in Figure 1.1 although the excavation of the post trafficked pavements showed that it was a noticeable effect as was shown in Chapter 6.6.1.

Separation could be defined as the ability of the geosynthetic to prevent the loss of aggregate into the soft subgrade. In pavements without geosynthetics, the aggregate particles are pushed into the formation during compaction and trafficking. Thus, for pavements including geosynthetics, the effective thickness of the aggregate layer is maintained and, as a consequence, its structural benefit to the pavement system remains constant. However, in a pavement without a geosynthetic separator, the amount of aggregate lost to the formation is, as yet, not calculated by any of the methods.

Van Den Berg and Kenter (1984) suggested that the geosynthetic properties important in the separation function were puncture strength and tear strength. Puncture strength is the ability of the geosynthetic to resist rupture, caused by the compaction of aggregate on its surface and the subsequent trafficking of the pavement, and tear strength is the ability to resist tearing once the material had been damaged in any way. Obviously, unless the geosynthetic remains complete throughout the compaction and trafficking process, it is not going to act as a separator.

For safe design the geosynthetic should continue to act as a separator within a post-failure pavement. The Prandtl (1920) theory of failure wedges suggests that large local strains are likely to occur during the failure of the subgrade. It is possible, but not certain, that high strength geosynthetics might alter the failure mechanism of the subgrade but, even so, high and low stiffness geosynthetics may have to undergo large

local strains if they are to avoid rupture. Therefore, geosynthetics which are designed to act as separators must either be extensible or, at pavement failure, the geosynthetic must slip with material being pulled in from the sides. However, it would appear that the option of mobilizing elongation in this manner is unlikely as the overburden stresses, coupled with aggregate/geosynthetic fictional interlock, will prevent the necessary slippage. Therefore it would appear that high-elongation-at-failure-geosynthetics are more likely to maintain the separation function in a post-failure pavement.

For pavements not including geosynthetics Dawson and Brown (1984) offered the following theory for a mechanism by which the aggregate is polluted by fines from the subgrade. As the traffic load is applied, the subgrade is stressed vertically at the points of aggregate/subgrade contact. Horizontal tensile strains develop at the interface with low vertical stresses between aggregate particles. The subgrade material, if soft enough, will tend to flow to these low stress points and as a result the aggregate sinks slightly. When the load is released the tensile strains are released too and the aggregate particles move together again. Subgrade material previously collected between them is forced up and down. When the next load cycle is applied the process is repeated and hence, the contamination slowly ratchets upwards.

The inclusion of a fabric at the subgrade/aggregate layer interface may help to prevent pumping action by acting as a barrier against the upward movement of the subgrade material. Other possible solutions are that the geosynthetic reduces the point stress on the subgrade and hence the depression of the aggregate particles or that lateral restraint prevents movement of the aggregate particles responsible for the mechanism described above.

Excavation of the post-trafficked pavements in the full-scale trials showed that the inclusion of geosynthetics in unpaved roads prevented the loss of aggregate particles into the subgrade as long as the geosynthetic survived the installation and trafficking processes. Excavation of the control sections showed that even a "stiff" subgrade, with a shear strength of 85kPa, some loss of aggregate thickness occurred due to the mechanism. The saving of aggregate attributable to separation may be significant, but unfortunately no current method exists to predict the amount of aggregate expected to be "lost" as a result of a specified number of load repetitions on a pavement founded upon a subgrade with a specified shear strength.

## CHAPTER TEN

### CONCLUSIONS & RECOMMENDATIONS FOR FUTURE WORK

The previous Chapters have shown that the study has brought some important findings to light. These are now summarized in the following sections.

#### 10.1 THE TRIALS AT BOTHKENNAR

The Bothkennar Soft clay Research site has superb office facilities equipped to a very high standard by the Science and Engineering Research Council. As time progresses, the engineering properties of the clay become better defined and the uniformity of the deposit makes it an ideal location for research into the behaviour of soft clays.

The site, however, has a firm crust (Figure 3.14) which was problematic for these trials. Pavement foundations are essentially controlled by shallow soil mechanics and so, although at depth the site was soft, geosynthetic reinforcement of unpaved roads is not normally considered to be economically viable for surface subgrade shear strengths of the magnitude encountered at Bothkennar. As a consequence it has been shown that, in this case, the possible savings of aggregate by including geosynthetics are small and hence the value of the products for the roads constructed was, in this instance, marginal. However, the instrumentation of the pavements was generally successful as it enabled a study of the mechanisms involved in this type of pavement which led to a new understanding of how geosynthetics perform in this application.

#### 10.2 RUT DEPTH DEVELOPMENT

At Bothkennar it was found that there was a relatively large amount of deformation which occurred in the first pass. Most of this initial deformation occurred within the aggregate layer, an observation also made by other authors in repeated triaxial tests on aggregates. It gives little, or no, indication as to the subsequent performance of the pavement. It was found that, as long as the geosynthetic did not rupture, the development of rutting, after the initial settling of the pavement, appeared to be linear with the number of passes of the axle. Other data (Webster & Watkins, 1977) and

(Fannin, 1986) was re-plotted on a linear scale and found to be in good agreement with a concept of a linear development of rut depth with passes.

The rate of the accumulation of rut depth with passes increased rapidly upon rupture of the geosynthetic as was seen in the three sections where the geosynthetic failed, namely the light-weight geogrid, the woven and the Polyfelt Bamboo lower-bound sections (Sections I, J and O respectively). Filling the ruts with extra material did not prevent further rutting developing. The failure was, in a sense, brittle. Rupture of the geosynthetic should therefore be avoided as, once this has occurred, the deterioration of the pavement is more rapid than if no geosynthetic was present.

No evidence was found to support the commonly held assumption that, for unpaved roads, non-standard loads can be related to the standard loads by the means of a fourth power law. An attempt to generate an estimate of the appropriate value led to high values in the range of 8 to 20 but with little or no consistency. This finding contradicted the proposal of De Groot et al (1986) for a power law of 6.2. In these trials the increase in axle load led to a small increase in the rate of development of rut depth and this is more in keeping with the earlier work of Hammitt (1977) than later, power law-type, calculations.

It can be seen from Table 6.1 that some of the thicker pavements in the trial had a higher rate of rut depth development than their thinner counterparts. One of the most important functions of the geosynthetic appears to be to reduce the horizontal outward shear stresses induced in the pavement by the wheel load. In thicker pavements the geosynthetic may be too low in the pavement structure, where the shear stresses are low, to be effective to the system. The maximum horizontal aggregate shear stress, in thick pavements, will occur within the aggregate layer and thus, in these pavements, internal aggregate deformation will contribute significantly to the overall rut depth. The evidence from the thinner pavements suggests that this internal shearing of the aggregate can be prevented by putting the geosynthetic higher in the pavement structure - in accord with the proposals of Bathurst et al (1986) - and this should be considered if the pavement thickness is to exceed 350mm.

It was found that even in pavements of approximately 350mm thickness a significant amount of the surface rut depth was caused by internal aggregate deformations. Excavation of the post-trafficking pavements (Figures 6.36 to 6.43) suggest that an average of 20% of the rut depth is generated by deformation within the aggregate layer.

The stiffness of the subgrade at Bothkennar may have affected the proportion of the rut depth development attributable to the aggregate layer.

### 10.3 MECHANISMS

Evidence was found to suggest that end restraint of geosynthetics was not required in order for them to be effective. The transient and permanent geosynthetic strains away from the wheel path, as shown in Figures 6.34 and 6.35, were found to be small and tending towards compression which agrees with finite element parametric studies undertaken by Brocklehurst (in press) and with earlier studies (CIRIA, 1986).

The transverse transient and permanent geosynthetic strain profiles shown in Figures 6.34 and 6.35 showed that the geosynthetic was not under constant tension across the pavement. Tensioned membrane design methods assume that constant tension exists, however, a non-constant tensioned membrane design could be developed. A membrane type of action, whether constant tensioned or not, could be a significant mechanism at large rut depths, >200mm, as suggested by Figure 9.5.

At low rut depths the principal mechanisms involved most closely matched those described by Milligan et al (1989 a & b). They predict the decay in transient strains away from the wheel path, as observed in Figure 6.34 and give an analytical solution for the improvement in bearing capacity between reinforced and unreinforced pavements observed by Werner & Resl (1986) and others.

It has been suggested in this thesis that "reinforced" pavements are, generally, only partially reinforced. This can be confirmed by calculating the forces required in the geosynthetics as suggested by Milligan et al (1989 a & b) and then comparing these forces to those available within the geosynthetic at strains calculated at the interface.

From the evidence of the excavation of the post-trafficked pavements separation would appear to be an important mechanism. Unfortunately no analytical method currently exists to predict the benefits of separation.

## 10.4 RECOMMENDATIONS FOR FUTURE WORK

The empirical nature of the prediction of permanent deformation is far from satisfactory. An analytical, permanent deformation model is required for the whole system of aggregate layer, subgrade and geosynthetic. It needs to be able to predict the increments of permanent deformation attributable to large and mainly elastic deformations. An analysis based on the work done by the system may be a possible avenue of exploration.

The value of separation may well be larger than the reinforcement value of the geosynthetic. A separation model would demonstrate a "base advantage" of using geosynthetics, with stiffer products enabling larger savings as a result of their higher reinforcement capabilities. The relative merits of different fabrics could then be assessed on the basis of commercial viability.

Non-linear analysis of the aggregate and subgrade components needs to be included within any new design method. Current methods utilise linear elastic theory to predict the strains that are expected at the interface, and this could be improved upon.

A new design method suitable for all geosynthetics could be developed. It should, in the authors opinion, be based upon the work proposed by Milligan et al (1989 a & b) modified by a concept of partial reinforcement, contain a realistic permanent deformation model, and should include allowances for separation.

## REFERENCES

- Almeida J, Brunton J M and Brown S F (1991), "Structural Evaluation of Pavements". Nottingham University, Second Progress Report Submitted to TRRL.
- Ahlvin R G (1959), "Developing a Set of CBR Design Curves". Instruction Report No 4, US Army Engineer Waterways Experimental Station, Vicksburg, Mississippi, USA.
- Bathurst R J and Raymond G P and Jarrett P M (1986), "Performance of Geogrid-Reinforced Ballast Railroad Track Support". Third International Conference on Geotextiles, Vienna, pp 43-48.
- Bender D A and Barenberg E J (1978), "Design and Behaviour of Soil-Fabric-Aggregate Systems". Transport Research Record 671 pp 64-67, TRB, Washington, USA.
- Boyce J R Cobbe M I and Fleming P R (1989), "Technical Note - Development of a Prototype Variable Impact Apparatus". Unbound Aggregates in Roads, Butterworths pp 397-407.
- Brocklehurst C (in print), "Finite Element Studies of Reinforced & Unreinforced Two-Layer Soil Systems". D.Phil, Oxford University.
- Brown S F (1977), "State-of-the-Art Report on Field Instrumentation for Pavement Experiments", Transport Research Record 640, Transport Research Board.
- Brown S F (1979), "The Characterisation of Cohesive Soils for Flexible Pavement Design". Proceedings of the 7th European Conference on Soil Mechanics and Foundation Engineering, Vol 2 pp 15-22.
- Brown S F and Brodrick B V (1973), "The Performance of Stress and Strain Transducers for use in Pavement Research", Nottingham University Report to the Science Research Council.
- Brown S F and Brodrick B V (1981), "Instrumentation for the Nottingham Pavement Test Facility", Transport Research Record 810, Transport Research Board.
- Brown S F and Dawson A R (1992), "Two Stage Mechanistic Approach to Asphalt Pavement Design". Seventh International Conference on Asphalt Pavements Nottingham.
- Brown S F and Pappin J W (1985), "Modelling of Granular Materials in Pavements". Transportation Research Record 1022 pp 45-51.

- Brunton J M and Ackroyd P M (1990), "Monitoring the Performance of a Full Scale Experimental Pavement". Third International Conference on the Bearing Capacity of Roads and Airfields. pp585-594.
- BS 812 (1975), "Methods for sampling and testing of mineral aggregates, sands and fillers". British Standards Institution.
- BS 1377 (1975), "Methods of Test for Soils for Civil Engineering Purposes". British Standards Institution.
- BS 6906 Part 1 (1987), "British Standards Methods of Test for Geotextiles. Determination of the Tensile Properties using a Wide Width Strip". British Standards Institution.
- BS 6906 Part 4 (1989), "British Standards Methods of Test for Geotextiles. Determination of the Puncture Resistance (CBR Puncture Test)". British Standards Institution.
- BS 6906 Part 6 (1990), "British Standards Methods of Test for Geotextiles. Determination for Resistance to Perforation (Cone Drop Test)". British Standards Institution.
- BS 6906 Part 8 (1991), "British Standards Methods of Test for Geotextiles. Determination of Sand-Geotextile Frictional Behaviour by Direct Shear". British Standards Institution.
- Chuang L-W and Dawson A R (1991), "Research to Improve Road Foundation Design (2nd Year Report)". Report No PR91040 submitted to TRRL.
- Comité Français des Géotextiles (1981), "Recommandations Pour L'emploi des Géotextiles dans les Voies de Circulation Brovisoire, les Voies à Faible Trafic et les Couches de Forme". Document du Ministère des Transports, Direction des Routes et de la Circulation Routière.
- Construction Industry Research & Information Association (1986), "The Construction and Performance Under Traffic of a Full-scale Experimental Road Incorporating Geotextiles". Technical Note 126.
- Davies M C R & Bridle R J (1990), "Predicting the Pavement Deformation of Reinforced Flexible Pavements Subject to Repeated Loading". Proceedings of the B.G.S. International Reinforced Soil Conference, Strathclyde University.
- Dawson A R, PhD Thesis submitted to the University of Nottingham, (in print).

- Dawson A R & Brown S F (1984), "Geotextiles in Road Foundations". Submitted to ICI Fibres, Geotextile Division. University of Nottingham, September 1984.
- Department of Transport (1986), "Specification for Highway Works, Part 3". HMSO.
- De Groot M, Janse E, Maagdenberg T A C & Van Den Berg C (1986), "Design Method and Guidelines for Geotextile Application in Road Construction". Third International Conference of Geotextiles, Vienna, pp 741-746.
- Fannin (1986), "Geogrid Reinforcement of Granular Layers on Soft Clay". PhD Thesis, Department of Engineering Science, Oxford University.
- Giroud J P & Noiray L (1981), "Geotextile Reinforced Unpaved Road Design". Proc ASCE Journal, Geotech. Eng. Div, No 1 107, No GT9, pp 1233-1254.
- Gostelow T P and Browne M A E (1986), "Engineering Geology of the Upper Forth Estuary". British Geological Survey, Vol 16 : No 8.
- Hammitt G M (1970), "Thickness Requirements for Unsurfaced Roads & Airfields Bare Base Support". Technical Report S-70-5, US Army Engineer Waterways Experimental Station, Vicksburg, Mississippi, USA.
- Hausmann M R (1986), "Fabric Reinforced Unpaved Road Design Methods - Parametric Studies", 3rd International Conference on Geotextiles 1986, Vienna.
- Hausmann M R (1987), "Geotextiles for Unpaved Roads - A Review of Design Procedures". Geotextiles & Geomembranes 5, pp 201-233.
- Hicks R G and Monismith C L (1971), "Factors Influencing the Resilient Responses of Granular Materials". Highway Research Record 345, Highway Research Board, Washington DC.
- Houlsby GT and Jewell RA (1989), "Road Solver - Design of Unreinforced and Reinforced Unpaved Roads on Soft Clay". Oxford Geotechnical Software.
- Jagielski K (1991), "Western European Geotextile Market Report". Geotextile Fabrics Report, October 1991, pp 24-25.
- Karkhoven R E and Dormon G M (1953), "Some Considerations on the Californian Bearing Ratio Method for the Design of Flexible Pavements". Shell International Petroleum Co Ltd, London.
- King G (1990), Personal Correspondence Relating to the Results from the ODIN Device at Bothkennar.

- Lee R G (1989), "Grid Reinforced Soil Foundations". Phd Thesis, University of Nottingham.
- Little P H (1990), "Construction of Experimental Haul Road at Bothkennar, Airth, Scotland". University of Nottingham Department of Civil Engineering, Report No PR90005.
- Little P H (1992), "Data Obtained from Full-Scale Trials at Bothkennar, Airth, Scotland". University of Nottingham Department of Civil Engineering, Report No PR92015, May 1992.
- Loach S L (1987), "Repeated Loading of Fine Grain Soils for Pavement Design". PhD Thesis Nottingham University.
- McGown A, Andrews K Z, Werner G and Yusuf Z (1990), "Bending and Tensile Reinforcement of Unbound Roads". Fourth International Conference on Geotextiles Geomembranes and Related Products, The Hague, pp 239-246.
- Milligan G W E, Jewel R A, Houlsby G T & Burd H J (1989a), "A New Approach to the Design of Unpaved Roads Part I". Ground Engineering, April 1989, pp 25-29.
- Milligan G W E, Jewel R A, Houlsby G T & Burd H J (1989b), "A New Approach to the Design of Unpaved Roads Part II". Ground Engineering, November 1989 pp 37-42.
- Nash D F T, Hawkins A B and Lloyd I (1985), "Location and Investigation of Test Bed Site on Soft Clay - Progress Report". University of Bristol, Department of Civil Engineering.
- Nieuwenhuis J D (1977), "Membranes and the Bearing Capacity of Roadbases". International Conference on the use of Fabrics in Geotechnics, Vol 1 pp 3-8.
- Paul M A, Peacock J D and Wood B F (1991), "The Engineering Geology of the Soft Clay at the National Soft Clay Research Site, Bothkennar". Heriot-Watt University.
- Peutz M G F, Von Kempem H P M and Jones A (1968), "Layered Systems Under Normal Surface Load - Computer Program BISTRO". Koninklijke/Shell-Laboratorium, Amsterdam.
- Polyfelt (undated), "Designing with Polyfelt", Polyfelt Ges mbh, 25 St Peters Strasse, Linz, Austria.

- Prandtl (1920), "Über die Harte Plastischer Körper". Nachr. Kgl. Ges. Wiss. Göttingen, Math-Phys. Kl.
- Resl S & Werner G (1980), "Influence of Non-Woven Needle Punched Geotextiles on Ultimate Bearing Capacity of the Subgrade". Third International Conference on Geotextiles, Vienna. pp 129-135.
- Sand & Gravel Association (undated), "Gravel Sub-base Materials : Type IG".
- Sellmeijer J B (1990), "Design of Geotextile Reinforced Paved Roads & Parking Areas". Fourth International Conference on Geotextiles, Geomembranes and Related Products, The Hague, Vol 1 pp 177-182.
- Steward J E, Williams R and Mahoney J (1977), "Guidelines for use of Fabrics in Construction and Maintenance of Low-Volume Roads". USDA Forest Serv, Portland, Oregon, USA. Report No FHWA-TS-78-205.
- Tam W S (1987), "Pavement Evaluation and Overlay Design". PhD Thesis, University of Nottingham.
- Tonus (undated), "Designing Aggregate Bases with "Typar" Spunbond Polypropylene", Du Pont Int. SA, PO Box 50, CH-1218 Le Grand-Saconnex, Geneva.
- Thom N H (1988), "Design of Road Foundations". Phd Thesis, University of Nottingham.
- Van Den Berg C, & Kenter C (1984), "Design Method and Guidelines for Geotextile Application in Unpaved Low Volume Roads". Geotextile Technology 1984.
- Watts G R A & Brady K C (1990), "Site Damage Trials on Geotextiles". Fourth International Conference on Geotextile Geomembranes and Related Products", The Hague, Vol 2, pp 603-607.
- Webster S L & Alford S J (1978), "Investigation of Construction Concepts of Pavements Across Soft Ground". Technical Report S-78-6, US Army Engineer Waterways Experimental Station, Vicksburg, Mississippi, USA.
- Webster S L & Watkins J E (1977), "Investigation of Construction Techniques for Tactical Bridge Approach Roads Across Soft Ground". Technical Report S-77-1, US Army Engineer Waterways Experimental Station, Vicksburg, Mississippi, USA.
- Yeo K (1992), "Results of Geosynthetic Index Testing of Samples from Bothkennar". Personal Correspondence.

## **APPENDIX 1**

### **DERIVATION OF EQUATIONS**

## SELLMIEJER (1990)

### - Derivation of Equations and Worked Example

#### Derivation of Equation 2.29

From Figure 2.10 it can be seen that:

$$d\tau = \{p - \tan\beta \, p \tan\Phi - q - \gamma h\} dx \quad (1)$$

$$dN = \{p \tan\beta + p \tan\Phi\} dx \quad (2)$$

$$dT = \{\sec\beta (S_u + h \tan\varphi + p \tan\Phi)\} dx \quad (3)$$

where  $\Phi$  = the aggregate/geosynthetic friction angle

$\varphi$  = the subgrade/geosynthetic friction angle.

If  $G$  is the shear modulus of the aggregate under the wheel imposed stress, then it is clear that the relationship between shear force and deflection is given by:

$$\frac{\tau}{h} = G \tan\beta \quad (4)$$

ie 
$$\frac{d\tau}{dh} = Gh \frac{d(\tan\beta)}{dx}$$

If the deflections are small then  $\tan\beta = 0$  and  $p = \sigma_v$

so re-writing Equations 1 to 4

$$\frac{ds}{dx} = S_u + \sigma_v (\tan\varphi + \tan\Phi) \quad (5)$$

$$\frac{dN}{dx} = \sigma_v \tan\Phi \quad (6)$$

$$Gh \frac{d(\tan\beta)}{dx} = \Delta\sigma_v - q \quad (7)$$

It can be seen that Equation 7 is the deformation equation. However, as  $\tan\beta$  is the rate of change of vertical displacement ( $y$ ) with respect to  $x$ ,  $\frac{dy}{dx}$ , then  $\frac{d\tan\beta}{dx}$  can be re-written  $\frac{d^2y}{dx^2}$ .

$$\text{Thus } Gh \frac{d^2y}{dx^2} = \Delta\sigma_v - q \quad (2.29)$$

### Derivation of Equation 2.31

The maximum horizontal stress can be calculated by examining the Mohr's circle as shown in Figure 2.13.

From Figure 2.13 it can be seen that:

$$x = \sqrt{\left(\frac{T}{h}\right)^2 + \left(\frac{1}{2} \left(\frac{1}{2} (\Delta\sigma_v + q) - \frac{\sigma_h}{h}\right)\right)^2} \quad (8)$$

$$y = \frac{1}{2} \left(\frac{1}{2} (\Delta\sigma_v + q) + \frac{\sigma_h}{h}\right) \quad (9)$$

$$\sin\phi' = \frac{x}{y} = \frac{\sqrt{4T_m^2 + \left(h\frac{1}{2}(\sigma_v + q) - \sigma_h\right)^2}}{\frac{1}{2}h(\Delta\sigma_v + q) + \sigma_h} \quad (10)$$

Re-arranging Equation 10 yields:

$$\sigma_h = (\sec^2\phi' - \frac{1}{2})(\sigma_v + q)h - \sec\phi' \sqrt{\{(\sigma_v + q)h\}^2 \tan^2\phi' - (\Delta\sigma_v^2 - (b-W)^2)} \quad (2.31)$$

### Calculation of Geosynthetic Forces

The geosynthetic force ( $T$ ) is a maximum under the wheel load and reduces away from it. The force  $T$  can be described as:

$$T = T_m \quad \text{- in Section 3} \quad (10)$$

$$T = T_m + (x - \frac{1}{2}(b-W)) (S_u + \sigma_v(\tan\phi + \tan\Phi)) \quad \text{- in Section 2} \quad (11)$$

$$T = T_m - \frac{1}{2}(b-W) (S_u + \sigma_v(\tan\phi + \tan\Phi)) + x\gamma h (\tan\phi + \tan\Phi) \quad \text{- in Section 1} \quad (12)$$

where Sections 1, 2 and 3 are as shown in Figure 2.11

$$T_m = \sigma_{hmax} - \sigma_h + \frac{1}{2}((B-A)-b) (S_u + \gamma h \tan\phi) + \frac{1}{2} (b-W) (S_u + \sigma_v \tan\phi) \quad (13)$$

The length over which T acts is controlled by:

$$\frac{T_m - \frac{1}{2} (b - W) (S_u + \Delta\sigma_v (\tan\phi' + \tan\Phi))}{- (S_u + \gamma h (\tan\phi' + \tan\Phi))} \quad (14)$$

### Derivation of the Strain Compatibility Equations - after Sellmijer (1990)

$$\epsilon_{agg} = \sigma_v h \frac{(1 - \nu)\sigma_h}{2Gh} \quad (15)$$

$$2Ghu = \int_0^{\frac{B}{2}} \nu \sigma_v h dx - \int_0^{\frac{B}{2}} (1 - \nu) \sigma_h dx \quad (16)$$

$$\int_0^{\frac{B}{2}} \sigma_v h dx = \nu h \left( \frac{B}{4} \gamma h + Wq \right) \quad (17)$$

$$(1-\nu) \int_0^{\frac{B}{2}} (1-\nu) \left[ \frac{1}{8} \{ (B-A-W)^2 + (A-W)^2 \} \sigma_v \tan\Phi - \frac{1}{2} B \sigma_{hmax} - \frac{1}{8} \{ (B-A-b)^2 + (A-b)^2 \} (\sigma_v - \gamma h) \tan\Phi \right] \quad (18)$$

Therefore:

$$2Ghu = vh \left( \frac{B}{4} \gamma h + Wq \right) + \left[ \frac{1}{8} \{ (B-A-W)^2 + (A-W)^2 \} \sigma_v \tan \Phi - \frac{1}{2} B \sigma_{hmax} - \frac{1}{8} \{ (B-A-b)^2 + (A-b)^2 \} (\sigma_v - \gamma h) \tan \Phi \right] \quad (19)$$

$$\epsilon_{\text{geotextile}} = \frac{T}{E}$$

$$Eu = \int T \, dx \quad (20)$$

$$Eu = \frac{1}{2} B T_{\max} - \frac{1}{8} \{ (B-A-W)^2 + (A-W)^2 \} \{ S_u + \sigma_v (\tan \Phi + \tan \phi) \} + \frac{1}{8} \{ (B-A-b)^2 + (A-b)^2 \} (\sigma_v - \gamma h) (\tan \Phi + \tan \phi) \quad (21)$$

Equating Equations 19 and 21 the elongation,  $u$ , required can be calculated, and hence  $E$ .

## EXAMPLE CALCULATION - AFTER SELLMIEJER (1990)

### Assumptions

The aggregate/geosynthetic friction angle, $\Phi$	= 45°
The subgrade/geosynthetic friction angle, $\phi$ ,	= 0°
The angle of internal aggregate friction, $\phi$ ,	= 45°
Poissons ratio	= 0.35
Road width, $B$ ,	= 4.5m
Distance between the wheels, $A$ ,	= 1.9m
Width of the loaded area, $W$ ,	= 0.32
Contact stress, $q$ ,	= 500kPa
Undrained shear strength of subgrade, $S_u$ ,	= 45kPa
Thickness of the aggregate layer, $h$ ,	= 0.4m
Density of the aggregate, $\gamma$ ,	= 21kN/m <sup>3</sup>
Shear modulus of the aggregate, $G$ ,	= 35MPa
Max permissible vertical subgrade stress, $\sigma_v$ ,	= $(2 + \pi) S_u = 231\text{kPa}$

Therefore the width of the subgrade mobilising plastic bearing capacity,

$$b = \frac{Wq}{\Delta\sigma_v} = 0.693m$$

### Deflection

The deflections under the wheel load  $\Delta w = (b-W)^2 \frac{q}{8Gh} \frac{\Delta\sigma_v}{q - \Delta\sigma_v} = 0.5mm$  (2.30)

### Aggregate Stresses

$$\sigma_h = \frac{1}{2} (b - W) \Delta\sigma_v \tan\Phi + \frac{1}{2} \gamma h^2 \frac{1+\sin\phi}{1-\sin\phi} \quad (2.32)$$

= 52.87kPa (maximum permissible horizontal aggregate force, controlled by passive failure.)

$$\sigma_{h \max} = (\sec^2\phi' - \frac{1}{2}) (\sigma_v+q) - \sec\phi' \sqrt{\{\sigma_v+q\}^2 \tan^2\phi' - \Delta\sigma_v^2 \left(\frac{b-W}{h}\right)^2} \quad (2.31)$$

$$\sigma_h = \frac{\nu}{(1-\nu)} \gamma h = 4.52kPa$$

Equation 2.31 suggests that the horizontal forces should decay to  $\sigma_h$  in Section 1. However, in this case  $\Delta\sigma_v$  is large (due to the high shear strength) and thus the forces will decay to  $\sigma_h$  at a point in Section 2.

$$\sigma_{h\max} - \sigma_h - x \Delta\sigma_v \tan\Phi = 0$$

$$x = 0.16$$

And thus the length of geosynthetic required to dissipate these forces,  $\frac{1}{2} (B-A)_{\text{new}}$  is:

$$\frac{1}{2} (B-A)_{\text{new}} = \frac{W}{2} + x = 0.32m.$$

## Geosynthetic Stresses

$$T_m = \sigma_{hmax} - \sigma_h + \frac{1}{2} ((B-A)-b) (S_u + \gamma \tan \phi) + \frac{1}{2} (b-W) (S_u + \Delta \sigma_v \tan \phi) \quad (13)$$

But  $\phi = 0$  and  $\frac{1}{2} (B-A)_{new} - b = 0$  as the geosynthetic stops working in Section 2. Furthermore, as the term  $\frac{1}{2} (b-W)$  relates to section 2 it should be replaced by  $x$  and so

$$T_m = \sigma_{hmax} - \sigma_h + x S_u = 44.84 \text{ kN/m.}$$

These geosynthetic stresses dissipate over the length,  $A = \frac{W}{2} + x$

where  $x$  is 0.16m

## Strain Compatibility

By Equating 19 and 21 as shown below

$$\begin{aligned} & \frac{2Gh}{E} \{ (B-A-W)^2 + (A-W)^2 \} \{ S_u + \Delta \sigma_v (\tan \Phi + \tan \phi) \} \\ & \quad + \frac{1}{8} \{ (B-A-b)^2 + (A-b)^2 \} (\Delta \sigma_v - \gamma h) (\tan \Phi + \tan \phi) \\ & = \nu h \left( \frac{B}{4} \gamma h + Wq \right) + \left[ \frac{1}{8} \{ (B-A-W)^2 + (A-W)^2 \} \Delta \sigma_v \tan \Phi \right. \\ & \quad \left. - \frac{1}{2} B \sigma_{hmax} - \frac{1}{8} \{ (B-A-b)^2 + (A-b)^2 \} (\Delta \sigma_v - \gamma h) \tan \Phi \right] \end{aligned}$$

Thus  $E$  can be found to be 37kN/m and by knowing that:

$$\tan \phi = 0 \quad (B-A-b) = 0 \quad \text{and} \quad A-b = 0.$$

Thus, for a 40kN wheel load acting on a 0.43m thick aggregate layer, overlying a subgrade of shear strength 45kPa, a tensile force of 45kN/m is developed in the geosynthetic and the required stiffness of the geosynthetic is 37kN/m per cent strain.

## **APPENDIX 2**

### **CONSTRUCTION DATA SUMMARY**

## SECTION A

### Materials

Constructed with Tensar SS2 and 400mm of Type1 aggregate.

### Dates Constructed

11/7/89 - 14/7/89

### Shear Vane Readings (kPa)

Depth (mm)	Reading Location 1			Reading Location 2		
30	Off-scale	Off-scale	114	74	Off-scale	Off-scale
200	89	78	72	80	87	86
300	69	79	58	95	102	96
400	67	68	62	75	81	82
500	51	58	53	55	70	76
800	42	53	45	62	65	69

### Clegg Hammer Subgrade Readings

Reading Location 1 Average Value = 11.6

Reading Location 2 Average Value = 13.1

### Cone Penetrometer Subgrade Readings

Reading Location 1 Average Value = 6.86 = 143 kPa

Reading Location 2 Average Value = 7.36 = 154 kPa

### Subgrade Moisture Content (%)

Depth (mm)	Reading Location 1	Reading Location 2
surface	14.8	7.4
200	27.0	31.1
350	31.9	32.9

## SECTION B

### Materials

Constructed with Typar 3407 and 450mm of Type1 aggregate.

### Dates Constructed

17/7/89 - 19/7/89

### Shear Vane Readings (kPa)

Depth (mm)	Reading Location 1			Reading Location 2		
30	118	94	Off-scale	Off-scale	88	Off-scale
200	98	52	102	Off-scale	114	88
300	98	78	88	Off-scale	119	92
400	77	59	74	122	82	64
500	58	48	70	76	74	54
800	42	43	44	61	43	48

### Clegg Hammer Subgrade Readings

Reading Location 1 Average Value = 9.7

Reading Location 2 Average Value = 14.8

### Cone Penetrometer Subgrade Readings

Reading Location 1 Average Value = 6.13 = 128kPa

Reading Location 2 Average Value = 6.70 = 140 kPa

### Subgrade Moisture Content (%)

Depth (mm)	Reading Location 1	Reading Location 2
surface	17.6	17.3
200	33.6	25.9
350	32.4	40.4

## SECTION C

### Materials

Constructed with Bidim B2 and 500mm of Type 1 aggregate.

### Dates Constructed

19/7/89 - 20/7/89

### Shear Vane Readings (kPa)

Depth (mm)	Reading Location 1			Reading Location 2		
30	Off-scale	95	126	Off-scale	Off-scale	Off-scale
200	Off-scale	105	93	Off-scale	Off-scale	Off-scale
300	115	96	102	Off-scale	107	106
400	102	69	80	97	87	65
500	92	64	57	60	88	40
800	42	52	53	50	56	43

### Clegg Hammer Subgrade Readings

Reading Location 1 Average Value = 13.8

Reading Location 2 Average Value = 12.1

### Cone Penetrometer Subgrade Readings

Reading Location 1 Average Value = 6.02 = 126kPa

Reading Location 2 Average Value = 6.01 = 126kPa

### Subgrade Moisture Content (%)

Depth (mm)	Reading Location 1	Reading Location 2
surface	20.8	9.6
200	32.8	27.6
350	37.5	34.1

## SECTION D

### Materials

Control section constructed with 550mm of Type1 aggregate.

### Date Constructed

21/7/89

### Shear Vane Readings (kPa)

Depth (mm)	Reading Location 1			Reading Location 2		
30	Off-scale	110	122	Off-scale	102	Off-scale
200	Off-scale	110	Off-scale	Off-scale	112	110
300	118	106	124	Off-scale	95	86
400	94	82	91	92	77	68
500	62	70	72	66	61	50
800	54	62	45	54	53	45

### Clegg Hammer Subgrade Readings

Reading Location 1 Average Value = 13.5

Reading Location 2 Average Value = 11.0

### Cone Penetrometer Subgrade Readings

Reading Location 1 Average Value = 5.15 = 108kPa

Reading Location 2 Average Value = 4.66 = 94kPa

### Subgrade Moisture Content (%)

Depth (mm)	Reading Location 1	Reading Location 2
surface	20.8	24.3
200	30.2	38.6
350	33.4	28.0

## SECTION E

### Materials

Constructed with a woven Geosynthetic and 490mm of Type 1 aggregate.

### Dates Constructed

5/9/89 - 6/9/89

### Shear Vane Readings (kPa)

Depth (mm)	Reading Location 1			Reading Location 2		
30	46	Off-scale	126	81	102	124
200	62	85	90	82	104	106
300	66	96	118	78	94	104
400	51	64	76	67	73	72
500	45	54	66	58	60	58
800	38	54	48	49	49	50

### Clegg Hammer Subgrade Readings

Reading Location 1 Average Value = 7.6

Reading Location 2 Average Value = 7.6

### Cone Penetrometer Subgrade Readings

Reading Location 1 Average Value = 4.86 = 102kPa

Reading Location 2 Average Value = 4.30 = 90kPa

### Subgrade Moisture Content (%)

Depth (mm)	Reading Location 1	Reading Location 2
surface	21.7	33.3
200	43.9	35.0
350	36.4	35.4

## SECTION F

### Materials

Constructed with Tensar SS1 and 400mm of Sand and Gravel.

### Dates Constructed

8/9/89 - 12/9/89

### Shear Vane Readings (kPa)

Depth (mm)	Reading Location 1			Reading Location 2		
30	Off-scale	102	89	Off-scale	113	107
200	121	112	87	112	113	122
300	121	102	84	Off-scale	Off-scale	117
400	75	70	61	80	77	84
500	72	60	62	72	64	59
800	45	58	46	53	46	41

### Clegg Hammer Subgrade Readings

Reading Location 1 Average Value = 8.2

Reading Location 2 Average Value = 9.9

### Cone Penetrometer Subgrade Readings

Reading Location 1 Average Value = 5.82 = 122kPa

Reading Location 2 Average Value = 7.53 = 157kPa

### Subgrade Moisture Content (%)

Depth (mm)	Reading Location 1	Reading Location 2
surface	29.0	19.0
200	28.7	31.4
350	37.5	39.4

## SECTION I

### Materials

Constructed with Tensar SS1 and 400mm of Sand and Gravel.

### Dates Constructed

12/9/89 - 14/9/89

### Shear Vane Readings (kPa)

Depth (mm)	Reading Location 1				Reading Location 2	
30	78	62	63	76	61	72
200	96	83	98	90	104	78
300	100	118	108	110	115	108
400	95	89	94	106	94	86
500	82	93	81	78	65	72
800	65	72	62	54	62	55

### Clegg Hammer Subgrade Readings

Reading Location 1 Average Value = 6.8

Reading Location 2 Average Value = 4.6

### Cone Penetrometer Subgrade Readings

Reading Location 1 Average Value = 3.81 = 80kPa

Reading Location 2 Average Value = 3.45 = 72kPa

### Subgrade Moisture Content (%)

Depth (mm)	Reading Location 1	Reading Location 2
surface	35.8	32.8
200	38.1	34.3
350	31.7	32.3

## SECTION J

### Materials

Constructed with a woven geosynthetic and (notionally) 340mm of Type1 aggregate.

### Dates Constructed

11/9/89 - 12/9/89

### Shear Vane Readings (kPa)

Depth (mm)	Reading Location 1			Reading Location 2		
30	72	94	80	74	82	86
200	80	82	88	88	76	94
300	96	88	102	106	91	110
400	82	77	76	92	80	90
500	66	58	62	74	72	75
800	58	69	52	60	62	65

### Clegg Hammer Subgrade Readings

Reading Location 1 Average Value = 4.9

Reading Location 2 Average Value = 6.0

### Cone Penetrometer Subgrade Readings

Reading Location 1 Average Value = 2.68 = 56kPa

Reading Location 2 Average Value = 3.41 = 71kPa

### Subgrade Moisture Content (%)

Depth (mm)	Reading Location 1	Reading Location 2
surface	32.1	30.5
200	32.4	32.4
350	33.5	32.0

## SECTION K

### Materials

Control section constructed with 400mm of Type 1 aggregate.

### Dates Constructed

2/10/89 - 3/10/89

### Shear Vane Readings (kPa)

Depth (mm)	Reading Location 1				Reading Location 2	
30	78	80	81	108	84	83
200	95	89	102	94	94	106
300	100	108	Off-scale	116	123	112
400	98	100	116	106	92	105
500	78	78	85	74	70	75
800	62	65	70	74	65	60

### Clegg Hammer Subgrade Readings

Reading Location 1 Average Value = 7.9

Reading Location 2 Average Value = 7.3

### Cone Penetrometer Subgrade Readings

Reading Location 1 Average Value = 5.00 = 105kPa

Reading Location 2 Average Value = 5.47 = 114kPa

### Subgrade Moisture Content (%)

Depth (mm)	Reading Location 1	Reading Location 2
surface	28.0	25.1
200	37.2	32.3
350	31.9	31.0

## SECTION L

### Materials

Constructed with Bidim B2 and 350mm of Type1 aggregate.

### Dates Constructed

26/9/89 - 27/9/89

### Shear Vane Readings (kPa)

Depth (mm)	Reading Location 1			Reading Location 2		
30	60	68	68	38	54	60
200	86	100	104	76	86	66
300	112	108	118	73	90	84
400	74	84	94	71	77	64
500	60	75	72	66	56	56
800	62	58	56	56	64	55

### Clegg Hammer Subgrade Readings

Reading Location 1 Average Value = Clegg Hammer Faulty  
Reading Location 2 Average Value = No Readings Available

### Cone Penetrometer Subgrade Readings

Reading Location 1 Average Value = 2.83 = 59kPa  
Reading Location 2 Average Value = 2.13 = 45kPa

### Subgrade Moisture Content (%)

Depth (mm)	Reading Location 1	Reading Location 2
surface	34.1	34.7
200	38.5	33.3
350	36.0	38.8

## SECTION M

### Materials

Constructed with Typar 3407 and 350mm of Type1 aggregate.

### Dates Constructed

28/9/89 - 29/9/89

### Shear Vane Readings (kPa)

Depth (mm)	Reading Location 1				Reading Location 2		
30	81	82	105	92	76	78	
200	83	87	78	94	94	96	
300	104	104	94	102	94	90	
400	76	72	74	74	74	69	
500	61	58	60	55	60	58	
800	70	60	54	62	52	64	

### Clegg Hammer Subgrade Readings

Reading Location 1 Average Value = 6.9

Reading Location 2 Average Value = 6.4

### Cone Penetrometer Subgrade Readings

Reading Location 1 Average Value = 4.43 = 93kPa

Reading Location 2 Average Value = 4.27 = 89kPa

### Subgrade Moisture Content (%)

Depth (mm)	Reading Location 1	Reading Location 2
surface	30.8	33.0
200	36.8	29.3
350	38.1	37.5

## SECTION N

### Materials

Constructed with Tensar SS2 and 300mm of Type 1 aggregate.

### Dates Constructed

4/10/89 - 5/10/89

### Shear Vane Readings (kPa)

Depth (mm)	Reading Location 1			Reading Location 2		
30	78	99	95	72	108	93
200	84	98	88	104	102	88
300	76	79	75	75	99	85
400	64	60	62	62	71	71
500	52	55	47	54	62	54
800	45	44	60	47	42	53

### Clegg Hammer Subgrade Readings

Reading Location 1 Average Value = 9.3

Reading Location 2 Average Value = 8.0

### Cone Penetrometer Subgrade Readings

Reading Location 1 Average Value = 6.02 = 126kPa

Reading Location 2 Average Value = 6.88 = 144kPa

### Subgrade Moisture Content (%)

Depth (mm)	Reading Location 1	Reading Location 2
surface	27.5	26.3
200	31.6	34.2
350	41.7	41.3

## SECTION O

### Materials

Constructed with Polyfelt TS500, 60/65mm diameter bamboo and 350mm of Type 1 aggregate.

### Dates Constructed

23/10/89 - 25/10/89

### Shear Vane Readings (kPa)

Depth (mm)	Reading Location 1			Reading Location 2		
30	126	78	92	86	112	72
200	61	66	74	87	86	77
300	68	70	73	82	76	83
400	54	64	59	69	68	66
500	47	46	52	66	58	64
800	46	44	44	56	48	38

### Clegg Hammer Subgrade Readings

Reading Location 1 Average Value = 7.0

Reading Location 2 Average Value = 5.7

### Cone Penetrometer Subgrade Readings

Reading Location 1 Average Value = 5.92 = 124kPa

Reading Location 2 Average Value = 4.02 = 84kPa

### Subgrade Moisture Content (%)

Depth (mm)	Reading Location 1	Reading Location 2
surface	31.7	29.1
200	34.1	44.6
350	44.8	42.2

## SECTION P

### Materials

Constructed with Polyfelt TS500 and 350mm of Type1 aggregate.

### Dates Constructed

26/10/89 - 28/10/89

### Shear Vane Readings (kPa)

Depth (mm)	Reading Location 1			Reading Location 2		
30	62	83	70	32	13	36
200	94	100	108	48	52	69
300	102	100	96	71	58	69
400	74	84	72	50	49	66
500	68	74	74	55	43	52
800	54	44	46	42	35	43

### Clegg Hammer Subgrade Readings

Reading Location 1    Average Value = 7.2

Reading Location 2    Average Value = 4.7

### Cone Penetrometer Subgrade Readings

Reading Location 1    Average Value = 3.66 = 76kPa

Reading Location 2    Average Value = 1.28 = 27kPa

### Subgrade Moisture Content (%)

Depth (mm)	Reading Location 1	Reading Location 2
surface	42.2	38.1
200	30.1	34.7
350	37.3	39.2

## **APPENDIX 3**

### **MISCELLANEOUS TESTING**

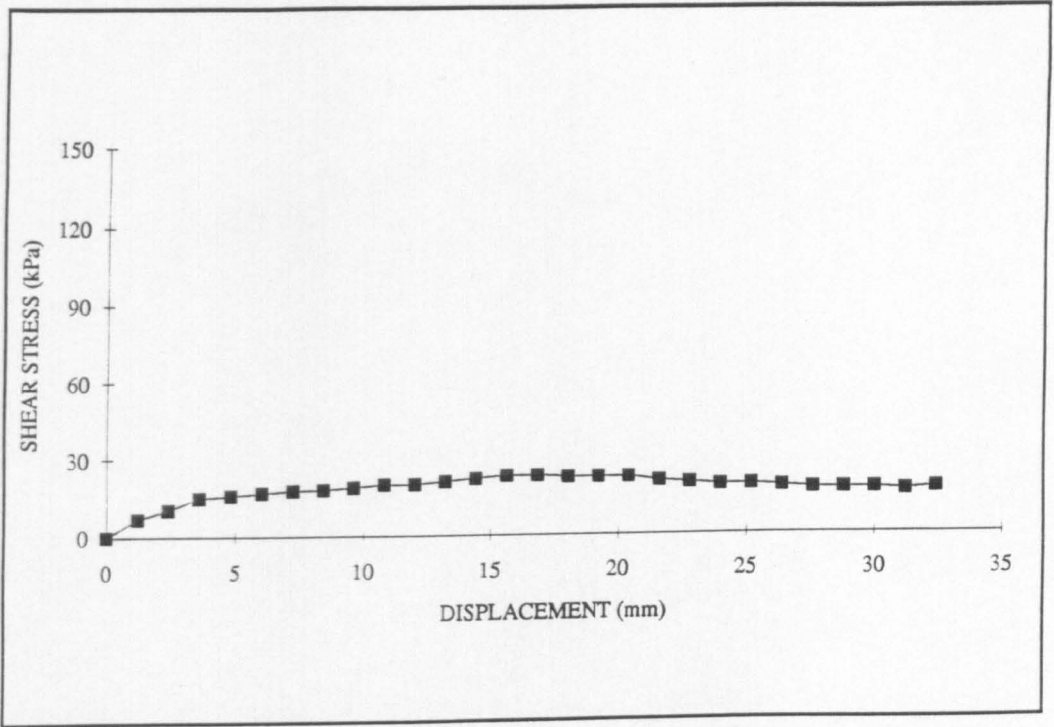


Figure 1 Aggregate/Typar Shear Box Test - Confining Stress 11kPa

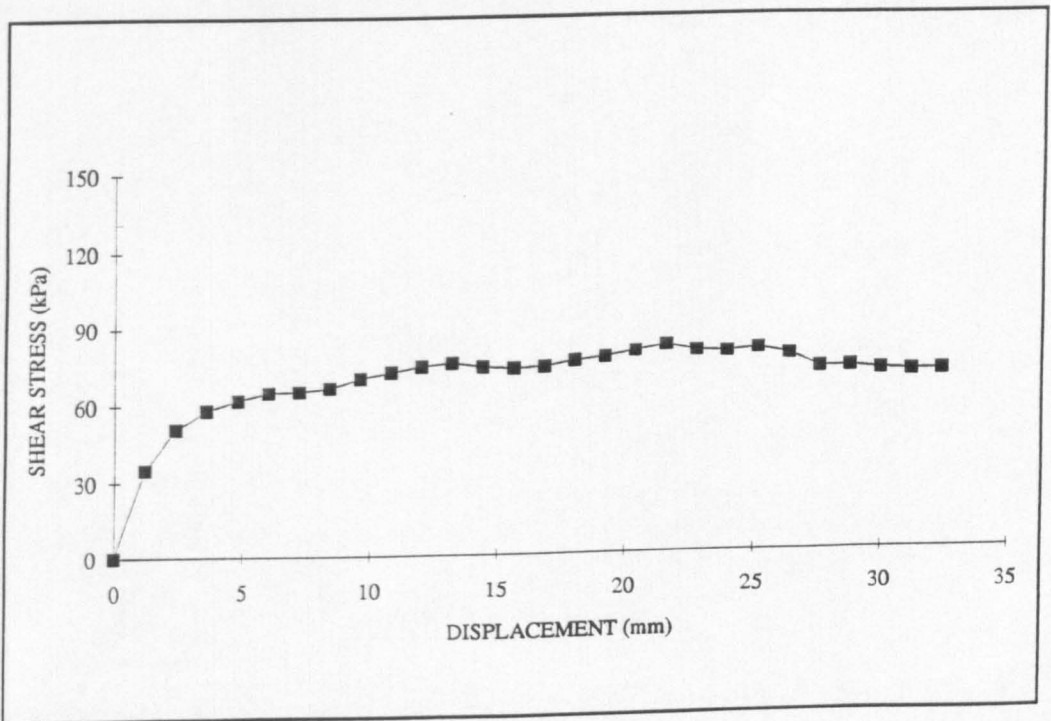


Figure 2 Aggregate/Typar Shear Box Test - Confining Stress 54kPa

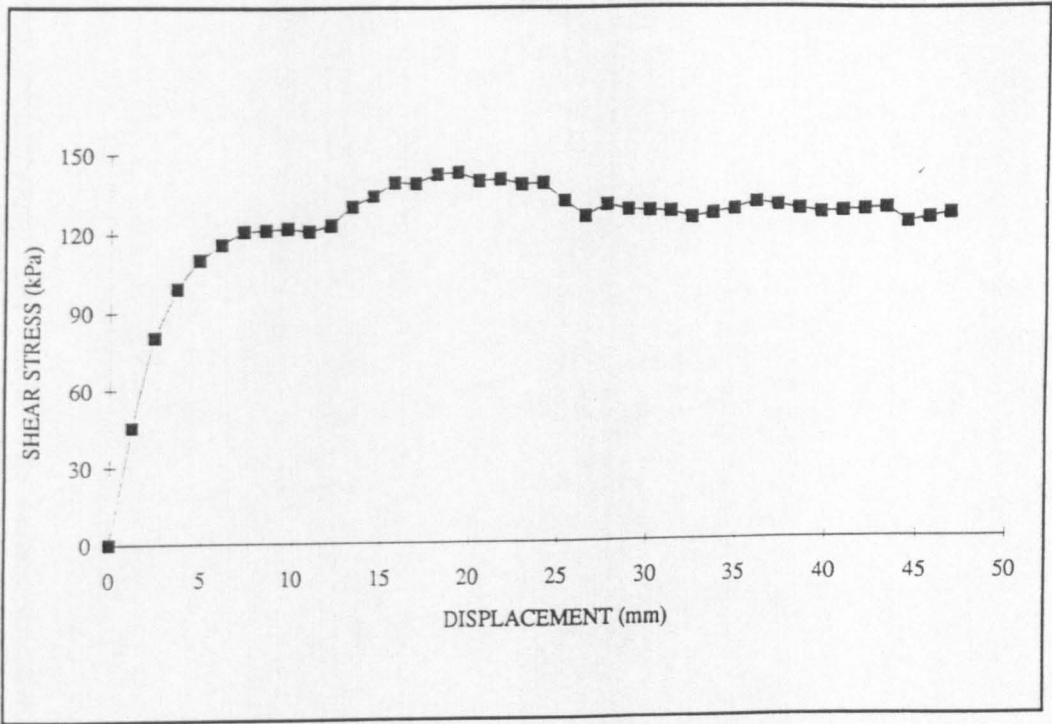


Figure 3 Aggregate/Typar Shear Box Test - Confining Stress 103kPa

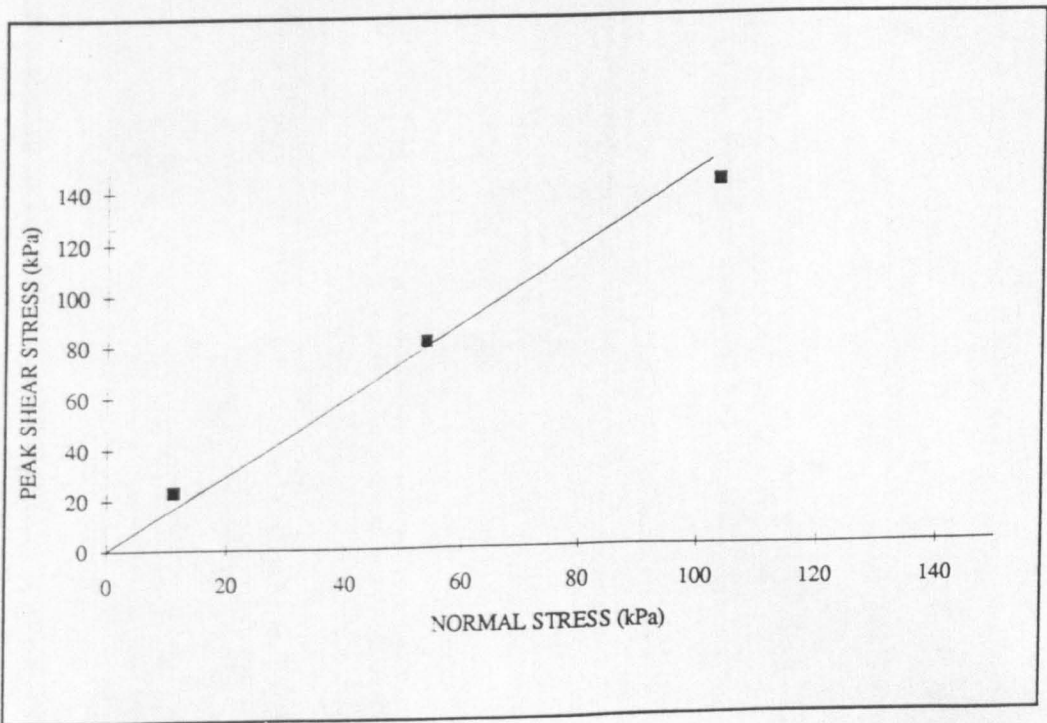


Figure 4 Angle of Frictional Resistance - Aggregate/Typar

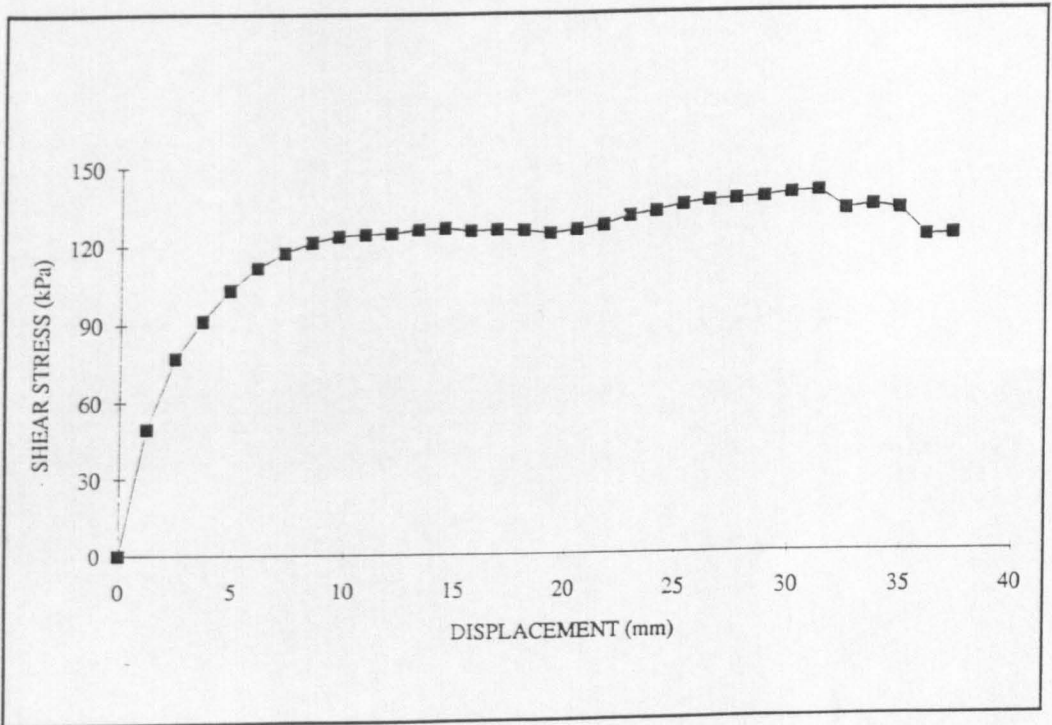


Figure 5 Aggregate/Bidim Shear Box Test - Confining Stress 103kPa

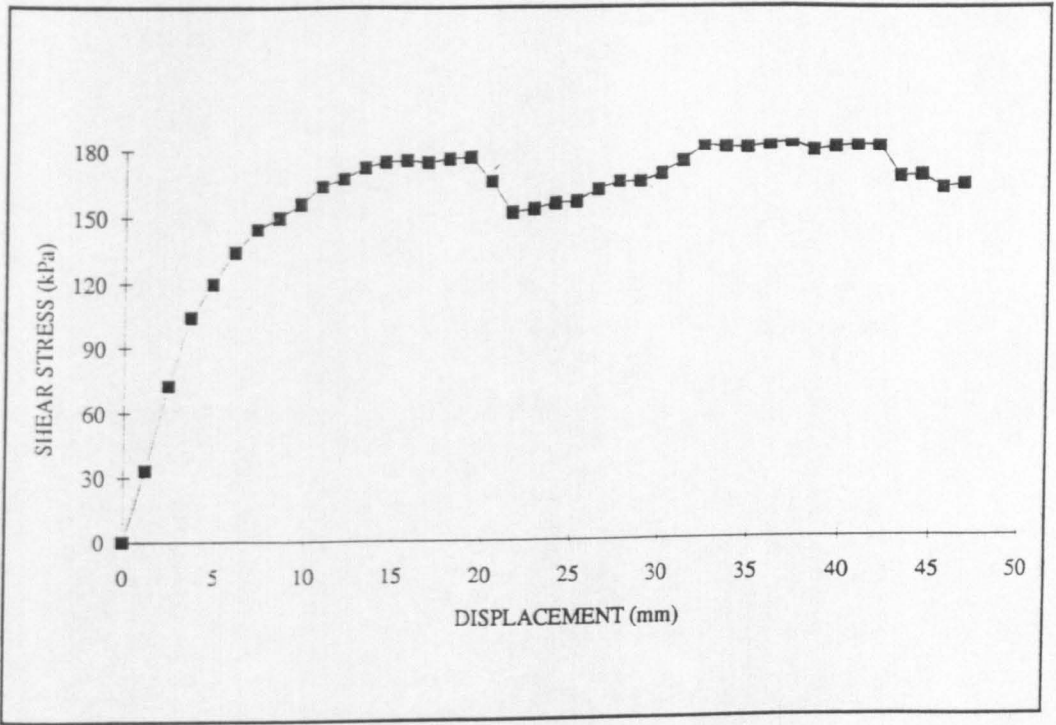


Figure 6 Clay Sheared over Aggregate - Confining Stress 100kPa

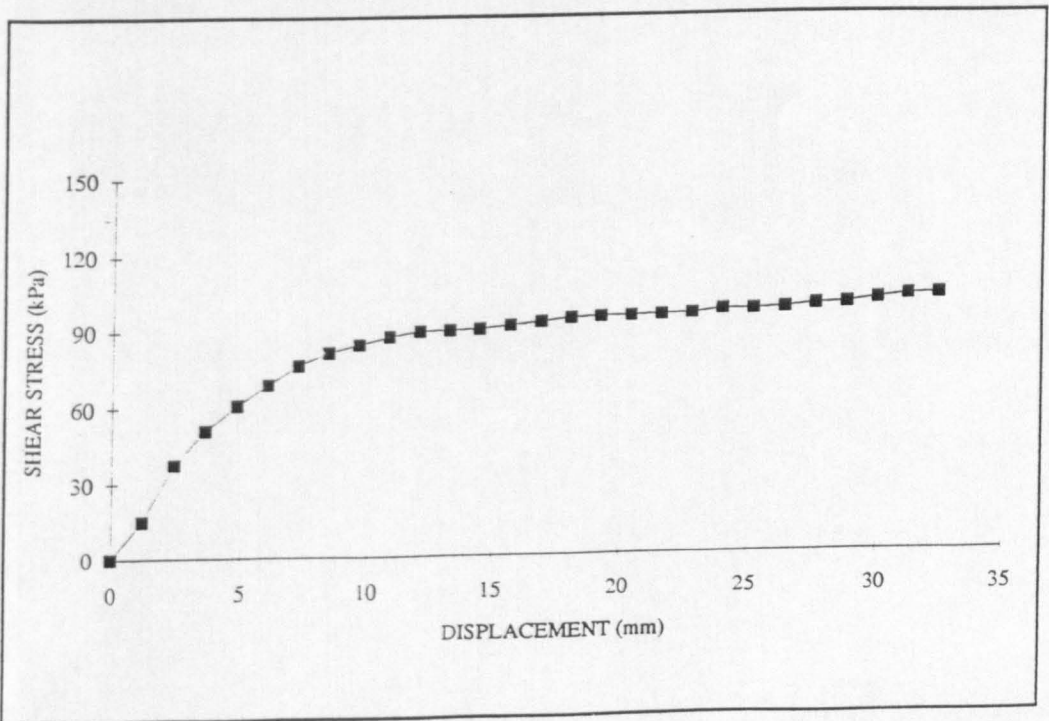


Figure 7 Clay Sheared over Bidim - Confining Stress 100kPa

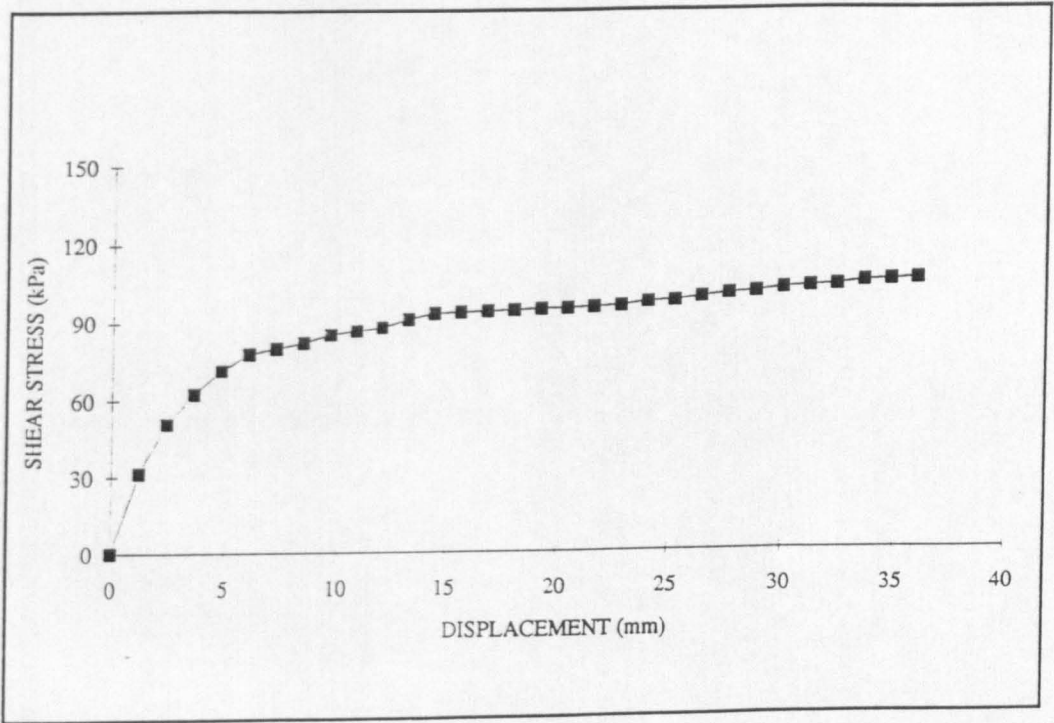


Figure 8 Clay Sheared over Typar - Confining Stress 100kPa

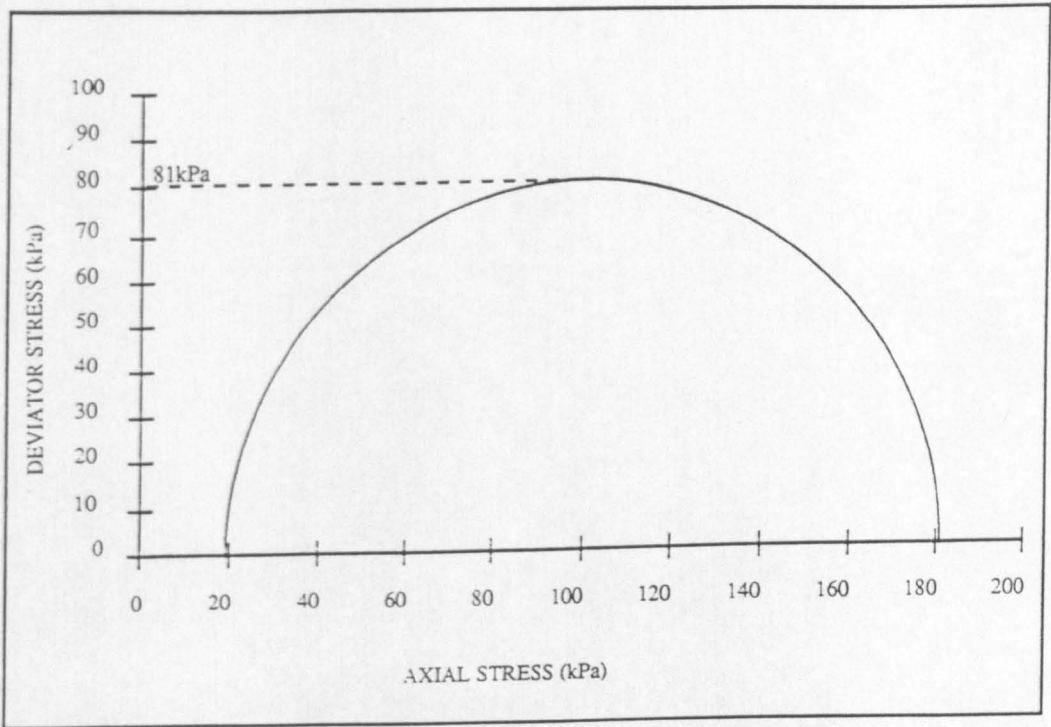


Figure 9 Quick Undrained 76mm Diameter Triaxial Test - Section H

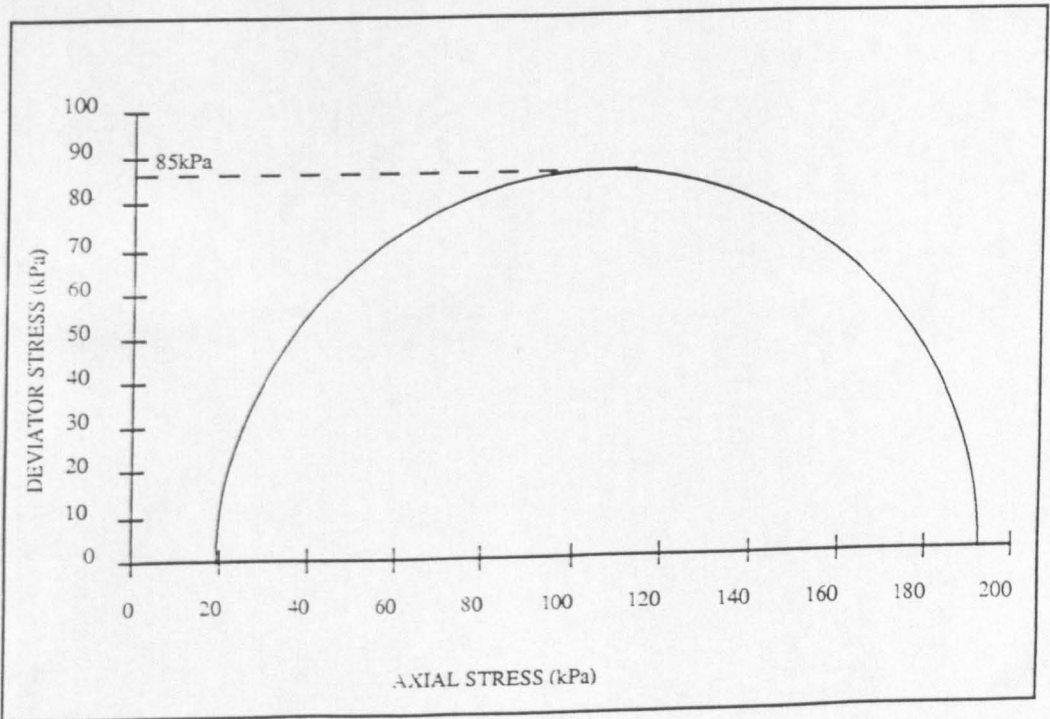


Figure 10 Quick Undrained 76mm Diameter Triaxial Test - Section L

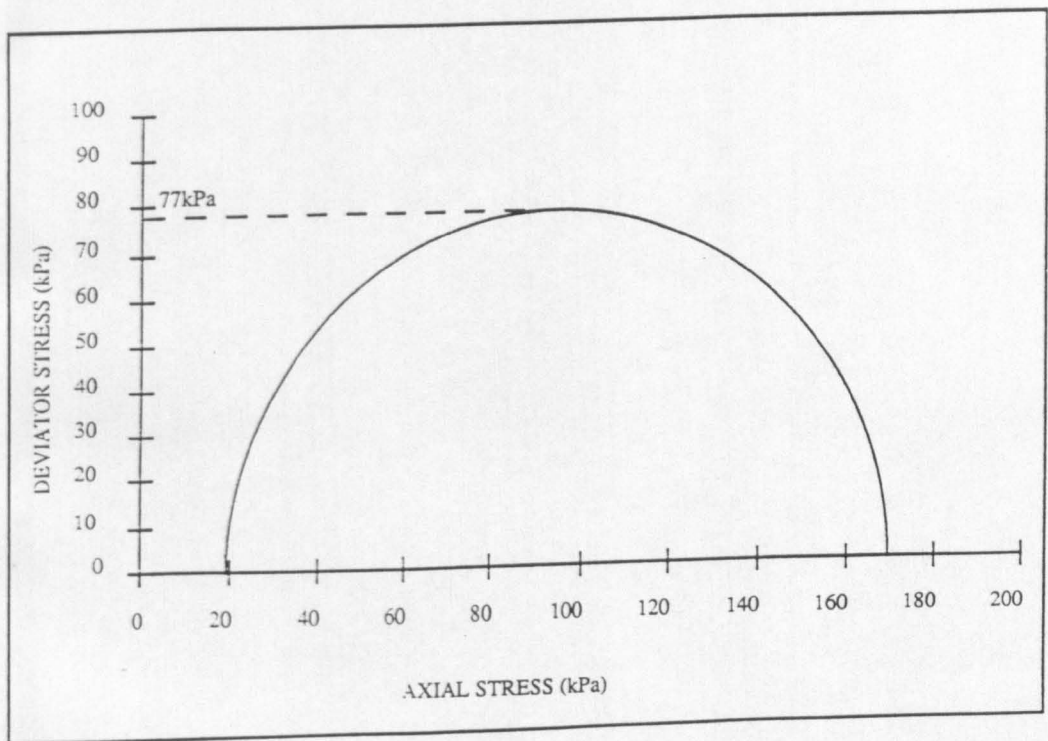


Figure 11 Quick Undrained 76mm Diameter Triaxial Test - Section P